NEUTRON DOSIMETRY BY REACTION RATE MEASUREMENTS IN STANDARD FAST NEUTRON FIELDS

A thesis submitted for the award of the degree of Doctor of Philosophy of the University of London.

by

ABUL HUSSAIN MOHAMMAD ABDUL HANNAN

M.Sc.(Dacca), M.Sc.(London), Dip.Q.M.C.

University of London Reactor Centre
Department of Mechanical Engineering
Imperial College of Science and Technology
LONDON, SW7 2AZ.

October 1976

ABSTRACT

Integral reaction rates have been measured in well established standard fast neutron fields. The standard fast neutron fields chosen in this work are: NISUS, MOL-ΣΣ and $\chi_{25}(E)$. Absolute reaction rates of non fissile materials were determined by foil activation technique. Fission rates of various fissile materials were measured by fission chamber and foil activation techniques.

Interlaboratory comparison of measured reaction rates and their ratios were performed for NISUS, ΣΣ and $\chi_{25}(E)$ neutron fields to provide accurate integral reaction rates and their ratios, to investigate the variation of spectrum in these three fast neutron fields and also to identify any discrepancy in measurement techniques.

The absolute reaction rates measured in the NISUS standard neutron field were used to evaluate simultaneously cross section data, integral reaction rates and spectrum by the SIMMM code. Calculated reaction rates have agreed well with the measured reaction rates within ± 3%. This confirms the consistency and reliability of the SIMMM code and the data used.

The NISUS central neutron spectrum unfolded by multiple foil spectrometry was compared with the results of the other experimental techniques (proton recoil counter and ^{6}Li sandwich spectrometer).

An interlaboratory comparison of spectra of fast neutron fields (NISUS and ΣΣ) was made.

ACKNOWLEDGMENTS

The author wishes to express his sincere gratitude to his supervisor, Dr. J.G. Williams, for his expert guidance, help, advice, criticism, correction of the manuscript and close interest during the course of this research.

The author acknowledges with gratitude the advice, encouragement and support throughout the work of Mr. M. Kerridge, Director of the University of London Reactor Centre, specially for the financial support to visit C.E.N./S.C.K., Mol, Belgium.

The author wishes his gratitude to Dr. A. Fabry, C.E.N./S.C.K., Mol, Belgium, for his help, advice, criticism and encouragement during this project and also for the arrangement of the visit to C.E.N./S.C.K., Mol, Belgium. The author acknowledges, with sincere thanks, the help and good cooperation of Dr. J. Debrue, Head of the Reactor Physics Section, Mr. F. Cops and other members of staff of C.E.N./S.C.K., Mol, Belgium during the author's visit to Mol, Belgium.

The author gratefully acknowledges the advice and generous encouragement received from Dr. C.B. Besant and Professor P.J. Grant of the Nuclear Power Section, Imperial College.

The author acknowledges the assistance and support of all members of staff of the University of London Reactor Centre. Sincere thanks are due to Dr. T.D. Mac Mahon for valuable discussions and his assistance during the work, Mr. G.D. Burholt, Reactor Manager, for his cooperation and interest in the work, Mr. T.C. Jones, Design Engineer, for his assistance in design work, Mrs. S.J. Parry for her assistance in the Library matters, Mr. A.G. Haylett for his assistance in maintaining the electronic equipment, Mr. J.G. Sanderson in providing the required materials and Mr. J.H. Roberts for general assistance during the stay at U.L.R.C.

The author acknowledges his sincere thanks to Mrs. W. Carder for her help, advice and assistance on computer programming specially on the SIMMM code and also to Mr. J.A. Mason for his help, interest and encouragement during this project.

Special thanks to Mr. E.A.Y. Caesar, Reactor Supervisor, for his skilful help and assistance during the experimental work in the reactor and Mr. J.W. Brown for his precise manufacturing of experimental components. Special thanks also to Messrs. E. Ansell and B.N. Edwards, Reactor Operators, for their cooperation and help during the experiments in the reactor.

The author is indebted to the authority of the University of Dacca, Bangladesh, for awarding the scholarship and for permission to study at the University of London.

The author acknowledges with sincere thanks the patient effort of Mrs. J. Vine, Mrs. M. Ryman, Mrs. M.R. Jones and Miss S. Martin in the typing of his manuscript into a legible and presentable form, specially of Mrs. J. Vine.

Last, but not least, the author acknowledges the support and sacrifices of his wife, Syeda, during this period.

TABLE OF CONTENTS

	Page
TITLE	
ABSTRACT	1
ACKNOWLEDGMENTS	3
TABLE OF CONTENTS	6
LIST OF FIGURES	12
LIST OF TABLES	19
1. INTRODUCTION	26
1.1 Relevance of the study of fast reactors	26
1.2 Role of integral measurements in fast reactors	28
1.3 Objectives of this work	30
1.4 Justification of activation method	32
2. EXPERIMENTAL TECHNIQUES	34
2.1 Neutron detectors	34
2.1.1 Activation detectors	34
2.1.2(a) β-particle measurement	37
2.1.2(b) γ-radiation measurement	38
2.1.3 Fission chambers	39

Page

2.2 Gamma spectrometers 40

2.2.1 Ge(Li) detector 44

2.2.1(a) Determination of peak areas 45

2.2.1(b) Peak detection efficiencies 47

2.2.1(c) Counting stability 53

2.2.2 NaI(Tl) detector 55

3. STANDARD FAST NEUTRON FIELDS 57

3.1.1 Review of the need for standard fast neutron fields 57

3.1.2 Fast benchmark reactor core experiments 59

3.1.3 Intermediate energy standard neutron field 61

3.2 Description of the NISUS facility 62

3.3 Description of the MOL-ΣΣ facility 67

3.4 Description of the ^{235}U thermal fission neutron spectrum facility 69

4. REACTION RATE MEASUREMENTS IN NISUS 74

4.1 Choice of activation detectors 74

4.2 Specifications of non fission and fission foils 75

4.3 Correction for external- and self-absorption of gamma rays, self-shielding and flux perturbation of foils 78

		Page
4.3.1	External- and self-absorption of gamma rays	78
4.3.2	Neutron flux perturbation corrections	80
4.3.2(a)	Neutron self shielding effect	80
4.3.2(b)	Flux density depression	82
4.4	Specification of fission sources for fission chamber measurements	84
4.5	Streaming of neutrons through access plug and access hole	84
4.5.1	Perturbation due to access plug	86
4.5.2	Perturbation due to access hole	86
4.6	Detector responses in the NISUS spectrum	98
4.7		
4.7.1	Reaction rate measurements in the NISUS neutron field	99
4.7.2	Calculation of reaction rates	105
4.7.3	Uncertainties in absolute reaction rates	107
4.7.4	Reactor power monitoring	111
4.7.5	Reaction rate traversing in NISUS	118
4.8	Fission rate and fission ratio measurements at the centre of NISUS	138
4.8.1	Fission rates and fission ratio by fission chamber technique	139
4.8.2	Absolute fission rates and fission ratio by fission foils (^{140}La technique)	142

Page

4.8.3 Weighted average of fission rates and fission ratio of ^{235}U and ^{238}U 150

4.8.4 Fast fission ratio ($^{238}U/^{235}U$) measurement by total integral counting technique 150

4.8.4(a) Irradiation of foils and counting procedure 150

4.8.4(b) Determination of the γ-activity ratio 153

4.8.4(c) Measurement of calibration factor P(t) in NISUS 157

4.8.5 Final fission rate and fission ratio measurements at the centre of NISUS 167

4.9 NISUS central reaction rate measurements 170

5. MEASUREMENT OF REACTION RATES IN MOL-ΣΣ AND $\chi_{25}(E)$ AND COMPARISON OF REACTION RATE RATIOS IN NISUS, MOL-ΣΣ AND $\chi_{25}(E)$ NEUTRON FIELDS 175

5.1 Reaction rate measurements in MOL-ΣΣ and $\chi_{25}(E)$ neutron fields 175

5.2 Comparison of experimental reaction rate ratios in NISUS, MOL-ΣΣ and $\chi_{25}(E)$ fields 181

6. CROSS SECTION DATA 191

6.1 Evaluated energy dependent cross sections 191

6.2.1 Fission spectrum averaged cross section 194

6.2.2 Group collapsing 197

6.3 NISUS spectrum weighted cross sections 199

Page

7. COMPARISON OF MEASURED AND CALCULATED REACTION RATES IN NISUS AND INTERLABORATORY COMPARISON OF THE EVALUATED CENTRAL NEUTRON SPECTRUM (NISUS AND ΣΣ) 208

7.1 Comparison of measured and calculated reaction rates in NISUS 208

7.2 Comparison of unadjusted and adjusted cross sections and spectrum in NISUS 213

7.3 NISUS unfolded spectrum 223

8. COMPARISON OF NISUS SPECTRUM UNFOLDED BY MULTIPLE FOIL SPECTROMETRY WITH OTHER SPECTROMETER TECHNIQUES 234

9. SUMMARY AND CONCLUSIONS 242

REFERENCES 253

APPENDICES

A. 262

A.I. Standardisation of ^{110m}Ag gamma source 263

A.II. Dead time and pulse pile up effects 269

A.III. Correction for finite source area of activation foils 272

Page

B. Unadjusted and adjusted cross section data for threshold and non threshold reactions 276

C. Correction for coincidence summation effects in ^{58}Co absolute activity measurement 283

D. List of the SIMMM program 288

Page

LIST OF FIGURES

2.1.(a)	Ge(Li) – NaI(Tl) spectrometers with automatic disc sample changer	42
2.1.(b)	Ge(Li) - NaI(Tl) detector assembly and counting system	42
2.2	Aluminium foil tray design	43
2.3	Block diagram of Ge(Li) counting system	46
2.4	A typical gamma ray spectra peak measured with a Ge(Li) detector	46
2.5	Absolute photopeak efficiency measured for a 43-cm^3 coaxial Ge(Li) detector at ULRC	52
2.6	Schematic diagram of a scintillation detector	56
3.1	Cross sectional sketch of the NISUS facility	65
3.2	A view of NISUS with the top half removed. Foils are shown in position within the central cavity. The foil holder is mounted on the end of a composite loading plug.	66
3.3	Cross sectional sketch of the ΣΣ facility	70
3.4	Experimental configuration in the spherical cavity of the BR-1 thermal column	70

		Page
4.1	Neutron self-shielding for three typical dosimetry reactions in the ΣΣ central neutron field.	83
4.2(a & b)	Cross sectional sketch of the NBS fission chamber for fission rate measurements in NISUS	88
4.3	Cross sectional sketch of the ULRC fission chamber with modification to the access hole for fission rate measurements in NISUS	91
4.4	Threshold and non-threshold detector responses in the NISUS spectrum	100
4.5	Threshold detector responses in the NISUS spectrum	101
4.6	Activation foil detectors inside the NISUS facility	103
4.7	Block diagram of the position details of the Au foil monitors	112
4.8	Block diagram of the position details of fission chamber monitors	113
4.9(a)	Reaction rate traverses in NISUS for $^{55}Mn(n,\gamma)^{56}Mn$ reaction	124
4.9(b)	Reaction rate traverses in NISUS for $^{197}Au(n,\gamma)^{198}Au$ reaction	124
4.10	Reaction rate traverses in NISUS for $^{115}In(n,\gamma)^{116m}In$ reaction	125

		Page
4.11(a)	Reaction rate traverses in NISUS for $^{115}In(n,n')^{115m}In$ reaction	127
4.11(b)	Reaction rate traverses in NISUS for $^{58}Ni(n,p)^{58}Co$ reaction	127
4.12(a)	Reaction rate traverses in NISUS for $^{64}Zn(n,p)^{64}Cu$ reaction	130
4.12(b)	Reaction rate traverses in NISUS for $^{56}Fe(n,p)^{56}Mn$ reaction	130
4.13(a)	Reaction rate traverses in NISUS for $^{27}Al(n,p)^{27}Mg$ reaction	133
4.13(b)	Reaction rate traverses in NISUS for $^{27}Al(n,\alpha)^{24}Na$ reaction	133
4.14	Reaction rate traverses in NISUS for $^{24}Mg(n,p)^{24}Na$ reaction	135
4.15	Most probable energy response of multiple foil detector in the NISUS central neutron spectrum	137
4.16	Block diagram of the dual triple-scaler counting system	143
4.17	Decay scheme of ^{140}La	146
4.18	Variation of γ activity ratio with time measured by two uranium foils without fission chamber	156
4.19	The enlarged cross sectional view of the ULRC double fission chamber	158

		Page
4.20	Variation of γ activity ratio with time measured by two uranium foils with fission chamber	163
4.21	Calibration factor as a function of time P(t) measured by fission chamber and uranium foils for the NISUS neutron spectrum	165
5.1(a)	Schematic diagram of an aluminium foil holder with activation foils position inside	176
5.1(b)	Schematic diagram of an aluminium tube with aluminium foil holder position inside	176
5.2(a)	Cross section in-pile view of the $\Sigma\Sigma$ facility with activation foils mounted at the centre	177
5.2(b)	Schematic diagram of ^{235}U fission spectrum cavity with activation foils mounted at the centre	177
5.3	Measured spectral indices for NISUS and $\Sigma\Sigma$ neutron fields relative to the ^{235}U fission neutron spectrum in the present work	190
6.1	Simpson's rule	196
6.2	Group conversion for cross sectional data	196
6.3	$^{55}Mn(n,\gamma)^{56}Mn$ and $^{115}In(n,\gamma)^{116m}In$ cross sections	201
6.4	$^{197}Au(n,\gamma)^{198}Au$ cross section	202

		Page
6.5	$^{235}U(n,f)$ and $^{239}Pu(n,f)$ cross sections	203
6.6	$^{237}Np(n,f)$ cross section	204
6.7	$^{115}In(n,n')^{115m}In$ and $^{238}U(n,f)$ cross sections	205
6.8	$^{58}Ni(n,p)^{58}Co$, $^{64}Zn(n,p)^{64}Cu$ and $^{27}Al(n,p)^{27}Mg$ cross sections	206
6.9	$^{56}Fe(n,p)^{56}Mn$, $^{24}Mg(n,p)^{24}Na$ and $^{27}Al(n,\alpha)^{24}Na$ cross sections	207
7.1	Residual discrepancy between calculated and measured reaction rate relative to the uncertainty in the measurement without and with adjustment of the data of threshold reactions	216
7.2	Comparison of calculated and measured reaction rate ratios of threshold reactions in the NISUS central neutron field	217
7.3	Residual discrepancy between calculated and measured reaction rate relative to the uncertainty in the measurement without and with adjustment of the data of non-threshold and threshold reactions	220
7.4	Comparison of calculated and measured reaction rate ratios of non-threshold and threshold reactions in the NISUS central neutron field	221

		Page
7.5	The NISUS central neutron spectrum unfolded by multiple foil (threshold reactions) spectrometry (using the ΣΣ spectrometry evaluated central neutron spectrum as the starting spectral form)	225
7.6	Comparison of the NISUS central neutron flux spectrum unfolded by threshold foil detectors and the ΣΣ spectrometry evaluated central neutron flux spectrum for the energy range ∿15 MeV - ∿60 KeV	226
7.7	The NISUS central neutron spectrum unfolded by multiple foil (non threshold and threshold reactions) spectrometry (using the ΣΣ spectrometry evaluated central neutron spectrum as the starting spectral form)	229
7.8	Comparison of the NISUS central neutron flux spectrum unfolded by non threshold and threshold detectors and the ΣΣ spectrometry evaluated central neutron flux spectrum for the energy range ∿15 MeV - ∿50 eV	230
8.1	Comparison of the NISUS central neutron spectrum unfolded by multiple foil spectrometry and measured by proton recoil and ^{6}Li spectrometers. The ΣΣ evaluated central neutron spectrum is used as the reference spectrum	236

		Page
8.2	Comparison of the NISUS central neutron flux spectrum unfolded by multiple foil spectrometry and measured by proton recoil and ^{6}Li spectrometers. The ΣΣ spectrometry evaluated central neutron flux spectrum is used as the reference spectrum	237
A.1.	Absolute photopeak efficiency measured for the Ge(Li) detector at 0.662 -, 0.835 - and 0.898 - MeV by standard gamma sources used to obtain absolute efficiency at 0.658 -, 0.818 - and 0.885 - MeV	265
A.2.	Dimensions of activation foil in mm	272

LIST OF TABLES

		Page
2.1	Specifications of Ge(Li) detector	44
2.2	Specifications of standard gamma-ray emitting sources	48
2.3	Absolute photopeak efficiency of Ge(Li) detector for gamma sources	51
2.4	Absolute efficiency values used in reaction rate calculation	54
3.1	List of zero-power reactors available in the world	60
3.2	Material and geometrical data of NISUS configuration 1b	68
3.3	ΣΣ detailed material and geometrical data	71
3.4	Specification of ^{235}U fission spectrum facility	73
4.1	Specification and dimension of non-fission and fission foils	76
4.2	Self absorption corrections applied to activation foils	81
4.3	Fissionable deposits exposed at the centre of NISUS standard neutron field	85

		Page
4.4	Effects of thermal neutron streaming through the access hole in the fission ratio measurements in the NBS fission chamber	89
4.5	Effect of access hole perturbation and fission chamber body for non-threshold and threshold reactions in ULRC fission chamber in NISUS	92
4.6	Effect of epicadmium access hole perturbation and fission chamber body for non-threshold reactions inside NISUS facility	94
4.7	Effect of epicadmium access hole perturbation and fission chamber body for threshold reaction in NISUS facility	95
4.8	Correction for epicadmium access hole perturbation and ULRC fission chamber body to non-threshold and threshold reactions in fission chamber in NISUS	96
4.9	Energy response of neutron detectors in the NISUS spectrum	102
4.10	Summary of the estimate of error contributions to the total error in absolute reaction rates	108
4.11	Day-to-Day reactor power monitoring by means of activation foils (reactor power 100 kW) (February - June, 1975)	115

		Page
4.12	Day-to-Day reactor power monitoring by fission chambers and Gold foils for fission rate measurement by NBS chambers (reactor power 100 kW) (June 14-20, 1975)	116
4.13	Day-to-Day reactor power monitoring by fission chambers and Gold foils for NISUS central reaction rate measurement (reactor power 100 kW) (December, 1975 and February - May, 1976)	117
4.14	$^{55}Mn(n,\gamma)^{56}Mn$ Absolute reaction rates	121
4.15	$^{115}In(n,\gamma)^{116m}In$ Absolute reaction rates	121
4.16	$^{197}Au(n,\gamma)^{198}Au$ Absolute reaction rates	122
4.17	$^{115}In(n,n')^{115m}In$ Absolute reaction rates	122
4.18	$^{58}Ni(n,p)^{58}Co$ Absolute reaction rates	128
4.19	$^{64}Zn(n,p)^{64}Cu$ Absolute reaction rates	128
4.20	$^{27}Al(n,p)^{27}Mg$ Absolute reaction rates	132
4.21	$^{56}Fe(n,p)^{56}Mn$ Absolute reaction rates	132
4.22	$^{24}Mg(n,p)^{24}Na$ Absolute reaction rates	134
4.23	$^{27}Al(n,\alpha)^{24}Na$ Absolute reaction rates	134
4.24	Corrections of the pulse rates to isotopic unperturbed fission rates of NBS and ULRC fission chambers	141
4.25	Average isotopic fission/monitor ratio for the exposure of NBS fission chambers at NISUS centre	144

		Page
4.26	NISUS central fission rates of ^{235}U and ^{238}U by fission activation detectors	149
4.27	Weighted average of fission rates and fission ratio of ^{235}U and ^{238}U by fission chamber and ^{140}La technique in NISUS centre	151
4.28	Result of gamma activity fission ratio $(F8/F5)_\gamma$ as a function of time with uranium foils without fission chamber	155
4.29	Absolute fission ratio (F8/F5) measurement by ULRC chamber in NISUS centre	160
4.30	Result of the calibration factor P(t) obtained from fission chamber and uranium foils measurement for NISUS	161
4.31	Result of true fission ratios (F8/F5) obtained from calibration factor P(t) and gamma activity fission ratio F8/F5 and the weighted mean of true fission ratio	166
4.32	Result of fast fission ratio (F8/F5) measurement by total integral technique and weighted mean of fission chamber and ^{140}La technique	168
4.33	Final results of fission rates and fission ratios of ^{235}U, ^{239}Pu, ^{238}U and ^{237}Np at the centre of NISUS	169

		Page
4.34	Results of NISUS central reaction rate measurement of various neutron dosimeters	171
5.1	Data relative to joint irradiations in ΣΣ and the fission spectrum at MOL	179
5.2	Day-to-Day reactor power monitoring by means of indium activation detector (reactor power 600 kW)	179
5.3	Central reaction rate measurements in ΣΣ and $\chi_{25}(E)$ benchmark neutron fields at MOL, Belgium	182
5.4	Comparison of experimental reaction rate ratios in NISUS and ΣΣ neutron fields between present measurements in NISUS and ΣΣ and Fabry's measurement in ΣΣ	184
5.5	Comparison of experimental reaction rate ratios in $\chi_{25}(E)$ neutron field at MOL between present measurement and Fabry's measurement	186
5.6	Comparison of reaction rate ratios in NISUS, ΣΣ and $\chi_{25}(E)$ neutron fields between present measurements	189
6.1	Dosimetry reactions and source and specification of cross section data set used	192
7.1	Details of measured reaction rates used in nuclear data unadjustment and adjustment runs	215

		Page
7.2	Calculated reaction rates (threshold) without and with adjustment of data and measured reaction rates and their ratios. The value of the minimisation function F	218
7.3	Calculated reaction rates (non threshold and threshold) without and with adjustment of data and measured reaction rates and their ratios. The value of the minimisation function F	222
7.4	NISUS unfolded neutron fluxes and ΣΣ input neutron fluxes and their ratios over energy ranges for threshold reactions	227
7.5	NISUS unfolded neutron fluxes and ΣΣ input neutron fluxes and their ratios over energy ranges for non threshold and threshold reactions	231
8.1	NISUS spectrum unfolded by multiple foil spectrometry and comparison with other experimental results	235
A.1	Gamma ray energy and branching ratio of ^{110m}Ag source	267
A.2	Absolute efficiencies of ^{110m}Ag source at 0.658 -, 0.818 - and 0.885 MeV	267
A.3	Activities of ^{110m}Ag source at 0.658 -, 0.818 - and 0.885 - MeV and the weighted mean of activity of ^{110m}Ag source	268

		Page
A.4	Pulse pile up corrections applied to the count rate of standard gamma sources	271
A.5	Absolute efficiency of Ge(Li) detector for 0.658 MeV at different radial distances	274
A.6	Absolute efficiency of Ge(Li) detector at 0.658 MeV	274
B.1	Unadjusted and adjusted cross section data for $^{197}Au(n,\gamma)^{198}Au$ and $^{235}U(n,f)$ reactions	277
B.2	Unadjusted and adjusted cross section data for $^{237}Np(n,f)$ and $^{115}In(n,n')^{115m}In$ reactions	278
B.3	Unadjusted and adjusted cross section data for $^{238}U(n,f)$ and $^{58}Ni(n,p)$ reactions	279
B.4	Unadjusted and adjusted cross section data for $^{27}Al(n,p)^{27}Mg$ and $^{56}Fe(n,p)^{56}Mn$ reactions	280
B.5	Unadjusted and adjusted cross section data for $^{24}Mg(n,p)^{24}Na$ and $^{27}Al(n,\alpha)^{24}Na$ reactions	281
B.6	Unadjusted cross section data for $^{55}Mn(n,\gamma)^{56}Mn$ $^{115}In(n,\gamma)^{116m}In$, $^{239}Pu(n,f)$ and $^{64}Zn(n,p)^{64}Cu$ reactions	282
C.1	The photopeak efficiency and the photofraction for the gamma ray of energy $E_{\gamma i}$	286

1. INTRODUCTION

1.1 Relevance of the study of fast reactors

Cheap and plentiful energy leads to industrial progress and better living standards. Much of this energy is used directly in the burning of gasoline in a motor car or oil in a central heating plant, but an ever increasing share of the total is turned into electricity. Electricity production is rising more rapidly than that of other forms of energy. In 1970, in most countries, electricity production was increasing with a doubling time of about ten years; in many, especially in the developing countries the doubling time was as short as five or seven years. Energy consumption in the year 2000 were projected as about four times as high as in 1970[1]. Recent trends have slowed this rise and made forecasting difficult, but large increases in consumption will undoubtedly occur. Enormous effort will clearly be needed to provide the energy, and particularly the electrical energy, required to meet the demand of the industrialised countries.

There are also long-term considerations. Reserves of coal, oil and natural gas are not unlimited. These "fossil" energy resources represent valuable raw materials for industries - plastics manufacture, drugs, dye stuffs and so on. Technology is also turning to new sources of energy like geothermal, tidal, hydro, wind and solar energy. But by far the most important and readily usable new source in the near future is nuclear energy.

The only option currently available on a commercial scale to meet the world's demand of electricity is nuclear fission. Most reactors at present in operation are thermal reactors. ^{235}U makes up only 0.7% of the total uranium reserves and the existing thermal reactors use principally ^{235}U as fuel. The breeding ratio of thermal reactors is smaller than unity (it is then called conversion ratio) and these reactors actually burn fissile material plus a small fraction of ^{238}U. This fraction can be increased through ^{239}Pu recycling, but it can never exceed a few per cent of ^{238}U[(2)], which constitutes 99.3% of natural uranium. Moreover, reserves of fuel for nuclear power in the form of uranium ore are also limited. So mankind is compelled to exploit available energy sources more effectively until fusion power plants which will meet the world's energy requirements for indefinite future are put into operation.

Meanwhile, the fast breeder reactor is thought to be an alternative solution at the threshold of the world energy crisis. A great advantage of the breeder reactor and the incentive for developing it lies in its fuller utilisation of nuclear fuels. An appreciable fraction of much more abundant ^{238}U of natural uranium can be converted into ^{239}Pu by the breeding process (breeding ratio exceeds unity in the case of fast reactors) and this also can be used as a fissile fuel. The uranium utilisation remains near 1% for low conversion ratio reactors and reaches about 70% when the conversion ratio exceeds unity. Consequently one would expect an increase in the utilisation of fissile fuel reserves by a factor of 70 if high conversion ratio reactors are

used[3]. As the utilisation of uranium is increased, it becomes economic to mine even lower grade deposits of which the total reserves are estimated to be appreciably large[3].

It seems clear that nuclear power can play a significant part in our long term energy programme only if we use predominantly high breeder ratio reactors.

1.2 Role of integral measurements in fast reactors

The development of fast reactor physics has been undertaken rapidly by extensive measurement programs in fast critical assemblies in a number of laboratories in the world since 1960 when thermal reactors became competitive with conventional electric power plants.

The neutron reactions in fast reactors are not confined to particular regions of the neutron energy spectrum as in thermal systems. In fast reactors, there is a need for nuclear data in a much broader energy range and for a variety of neutron nuclear reactions to predict the reactor performance. The availability of fast digital computers with big storage capacity has stimulated the development of sophisticated reactor-theory computer programs allowing very detailed prediction of reactor-physical properties. As a result, the errors due to defects in reactor calculational methods have become smaller than the errors introduced by the uncertainties in nuclear data of the important reactor materials (such as ^{239}Pu, ^{238}U, ^{235}U, Na, Fe and O).

Neutron dosimetry measurements play an important role for the development of fast reactor fuels and materials because there is an invariant need of accurate prediction of fission rates, burn up and neutron exposure for neutron-induced property changes. Appropriate emphasis has to be and is increasingly placed onto the establishment of consistent and reliable dosimetry cross section files for the dosimetry nuclear reactions.

The sensitivity of fast reactor performance to nuclear data uncertainties has been studied thoroughly and it is concluded that the differential nuclear data requires very considerable improvement. The target accuracies proposed from such studies can be met in two ways:

(a) by the development of improved measurement technique and at the same time increased effort by experimentalist and evaluators in understanding the source and magnitude of the systematic errors in the existing measurements[4].

(b) The second method is based on the use of both evaluated differential data and integral information. The integral data such as reaction rate, neutron spectrum and critical quantities are measured in clean geometry fast lattices. The evaluated differential data is adjusted by least square fitting process to this measured integral data[5] & [6].

As the first method is time consuming and expensive, the second method is preferred for the timely development of fast breeder reactors. Reaction rate measurement is one of the most important sources of integral information. A consistent set of measured reaction rates and ratios can be used for flux spectral analysis and data testing of the evaluated dosimetry cross section data files. Present accuracy for dosimetry cross sections is in the10 - 20% range at 68% confidence level[7]. This accuracy can be improved if the sources of existing inconsistencies between calculated integral - averaged cross sections using current evaluated energy dependent cross sections $\sigma(E)$ and measured values are identified and effectively eliminated. Fuels and materials development programs require ever-increasing accuracy because obtaining fission rates is an important step in the overall process of obtaining accurate heat output of fuel and total burn up[8].

1.3 Objectives of this work

Accurate prediction of reaction rates related to the reactor materials and fuels is an essential requirement for the development and operation of nuclear power plants. A major goal of reactor dosimetry involves the specification of neutron flux spectrum data from integral reaction rates induced in an appropriate number of selected dosimeters, e.g. activation foils. The aim of this project is to perform a series of reaction rate measurements in standard fast neutron fields using activation foils. The following well established fast neutron fields are used in the present work:

(a) NISUS - Neutron intermediate spectrum Uranium Source at the University of London Reactor Centre, Imperial College, England[9].

(b) MOL-ΣΣ - Natural Uranium Secondary Standard Neutron Field at CEN-SCK, MOL, Belgium[10].

(c) $\chi_{25}(E)$ - U-235 thermal neutron induced fission spectrum at CEN-SCK, MOL, Belgium[11].

To determine reliable and well documented values of experimental reaction rates and their ratios, necessary steps for this objective to be met are:

(i) to intercompare reaction rates measured in different laboratories. The overall consistency of reactor dosimetry is best insured by calibration of reaction rate measurement technique through irradiations in reference neutron fields.

(ii) to establish through intercomparison a capability for measuring reaction rates from non-fissile materials with an accuracy of $< \pm 5\%$ ($1\ \sigma$ level)[12] and from fissile materials the accuracy approaching $< \pm 2.5\%$ ($1\ \sigma$ level)[8].

(iii) to obtain accurate sets of reaction rate values for important dosimetry reactions measured in fast neutron reactor environments. These reaction rates would then be of use in testing and evaluating energy dependent cross section sets.

(iv) to predict reaction rates after adjustment of the evaluated cross section sets and spectrum with the measured reaction rates.

(v) to unfold the neutron spectrum of the fast neutron field by multiple foil method and make an interlaboratory comparison of the spectrum with another fast neutron field (NISUS unfolding spectrum is compared with the ΣΣ spectrometry evaluated central neutron spectrum in this work).

(vi) to compare the unfolded spectrum with the spectra measured by proton recoil proportional counter and Li^6 sandwich spectrometer for the NISUS neutron field.

1.4 Justification of activation method

The use of activation detectors represents the most convenient technique[13] to determine integral reaction rates from which the neutron energy spectrum and flux can be computed. Activation detectors have the following advantages:

(a) the detectors are not sensitive to the intense gamma radiation in the reactor.

(b) the response of the detectors is not dependent on temperature.

(c) the detectors are normally small in size and can therefore be applied in laboratories where the available space is limited (e.g. in coolant channels, between fuel plates). The flux perturbations can be minimised if the detectors are sufficiently thin.

(d) the detectors do not require external connections with cables during irradiation.

(e) the counting techniques are in general not too complicated.

(f) by careful selection of the detectors, it is possible to obtain highly sensitive detectors for low fluxes.

(g) it is possible to select detectors sensitive to different neutron energies and thus detect a particular group of neutrons.

(h) the detector materials normally used are not expensive.

The abovementioned advantages and the simplicity of the activation detectors are the main reasons for their extensive use in research organisations.

2. EXPERIMENTAL TECHNIQUES

2.1 Neutron detectors

Since the neutron is an electrically neutral particle, it does not interact with the usual detectors employed for ionising radiation, it is detected indirectly using nuclear reactions that produce charged secondary particles or radiations[14]. There are two different kinds of reactions:

(a) the ionising radiations are produced instantaneously, as for examble, in the $^{10}B(n,\alpha)^{7}Li$ or $^{3}He(n,p)^{3}H$ reactions. The promptly indicating neutron detectors depend on these reactions.

(b) the second kind of nuclear reaction forms the basis of the radioactive indicators which are particularly important for measurements in neutron fields. These indicators are based on reactions that lead to the production of radioactivity (β^{+}, β^{-} or γ-radiation). These indicators are known as activation detectors.

2.1.1 Activation detectors

It occurs quite frequently that transmutations induced by neutrons have radioactive species as product nuclides. The activity of the product radioisotope can often be used for the measurement of the amount and energy distribution of the neutron flux which induced the radioactivity. A detector employing this principle is referred to as a neutron activation detector. The neutron activation detectors may be in any form. A common

form, particularly for metallic materials, is in a thin foil. Such detectors are often referred to as foil detectors.

In neutron measurements by induced activity, the stable material is exposed to the neutron flux for a measured period of time. Following the irradiation, the material is removed from the neutron field and the activity is measured which has been induced in it. A thin foil is used in order that the neutron flux shall not be appreciably disturbed and also that the flux shall be uniform throughout the absorber.

When a target material is exposed to a flux ϕ of neutrons, the rate at which its concentration increases with time is given by:

$$\frac{dN_B}{dt} = \sigma_A \phi N_A - \lambda_B N_B \qquad (2.1.1)$$

where N_B is the number of atoms of radioactive nuclide B which decays with its characteristic disintegration constant λ_B, N_A is the number of atoms in the target material A and σ_A is the activation cross section of A.

By integration of equation (2.1.1) the number of radioactive atoms present at the end of irradiation time, t_a, will be given by

$$N_B^{t_a} = \frac{\sigma_A \phi N_A}{\lambda_B} \left|1 - \exp(-\lambda_B t_a)\right| \qquad (2.1.2)$$

The number of disintegrations per second of N_B radioactive nuclei represented as the activity $A_B^{t_a}$ after an irradiation time of t_a sec is

$$A_B^{t_a} = N_B^{t_a}\lambda_B = \sigma_A\phi N_A|1 - \exp(-\lambda_B t_a)| \qquad (2.1.3)$$

The activity that will be detected, $A_B^{t_d}$, will therefore depend on the decay time after the end of irradiation and on the half life of the active species. If t_d is the decay time:

$$A_B^{t_d} = A_B^{t_a}\exp(-\lambda_B t_d) = \sigma_A\phi N_A|1 - \exp(-\lambda_B t_a)|\ |\exp(-\lambda_B t_d)| \qquad (2.1.4)$$

The "saturation" activity is attained when the irradiation time is long compared to the half life of the product radionuclide and rate of formation is equal to the rate of disintegration. $|1-\exp(-\lambda_B t_a)|$ approaches unity and

$$A_B^{t_a}(S) = N_B^{t_a}\lambda_B = \sigma_A\phi N_A$$

the activity of B at the time of counting will be

$$A_B^{t_a}(S) = \sigma_A\phi N_A \exp(-\lambda_B t_d)$$

Thus the saturation activity is

$$A_B^{t_a}(S) = \sigma_A \phi N_A = \frac{A_B^{t_d}}{|1-\exp(-\lambda_B ta)|\ |\exp(-\lambda_B td)|} \qquad (2.1.5)$$

This saturated activity together with the cross section $\sigma(E)$ for a particular neutron induced reaction is used for the measurement of the amount and energy distribution of flux

$$A_{Sat} = \int_o^\infty N\sigma(E)\ \phi(E)\ dE \qquad (2.1.6)$$

Most of the radioactive nuclides emit both β and γ-radiation and these radiations are detected by Geiger counter, proportional, and scintillation and solid state counters or ionisation chambers. Both types of radiations are described below. Choice has been made by considering advantages and disadvantages of both radiations.

2.1.2 β-particle measurement

(a) β-particles from the radioactive nuclides are counted by the detector which has a high beta efficiency and a low gamma response. The most reliable and simple detector generally used for β-counting is the Geiger-counter. The distinguishing feature of Geiger-Muller tubes for use in the counting of beta particles is the thin wall or

window in the tube. The necessity of this region for admitting the particles arises from the relatively short range of the beta particles which are emitted by most radioisotopes. Many radioactive nuclides do not emit any usable γ-rays. In this case, β-counting is preferred.

The β-spectrum from an active source is usually degraded in energy as a result of absorption of the β-particles in the sources, the source holder and the counter window. As the majority of the β-particles emitted originate from the outer layers of the source, the count rate will change as a function of the surface area of the active source. Slight variations in shape and surface conditions will cause large changes in counting efficiency. These effects are much smaller when counting γ-rays and except for low energy γ-rays, there is a uniform contribution from the whole volume of the source. Also if the source is used as flux monitor and in reaction rate measurement repeatedly, any deterioration in the quality of the source will thus have a smaller effect on the counting efficiency of γ-rays than of β-rays[15].

Considering the above facts, γ-radiation is counted to determine the saturated activity of each foil.

2.1.2 γ-radiation measurement

(b) Foils of various materials of importance in neutron dosimetry measurements were irradiated in different standard fast neutron fields

(NISUS at Imperial College, England, MOL-ΣΣ and ^{235}U Fission Spectrum Source at MOL, Belgium) for an adequate period of time. The gamma ray spectrum of each irradiated foil was measured by a calibrated Ge(Li) detector and in some cases by a NaI(Tl) detector and thereby gamma ray emission rates were determined. Reaction rate (saturated activity) of each foil was computed based on these gamma ray emission rates. The reaction rate values determined by these techniques have an accuracy of better than ± 5.0% (at the 1σ level). Gamma ray spectrum is described in detail in section 2.2.

2.1.3 Fission chambers

In the fission of a heavy nucleus, the fission fragments have a total kinetic energy of the order of 160 MeV. It is therefore possible to make extremely γ-insensitive fission chambers for neutron detection. Such detectors are important for neutron measurements in reactors (where there is a high γ-background) as threshold and non-threshold detectors.

A number of factors contribute to the utility of fission chambers. The wide choice of fissionable materials allows the selection of the energy dependence and of the efficiency. Fission chambers clad with fissionable isotopes are frequently used with fast neutrons as threshold detectors. The thermally fissionable isotopes ^{233}U, ^{235}U and ^{239}Pu also serve as spectral indicators in thermal neutron fields.

Generally double fission chambers are in common use. The double fission chamber contains two independent fast ionisation chambers. The

backings of the fissionable deposits are positioned back-to-back and serve as the common grounded electrode between the chambers. The electrodes parallel to the fissionable deposits serve as the anodes. To reduce neutron absorption and scattering effects, the electrodes and structural elements are made up of aluminium and the insulators are made up of a hydrogen-free polymer. The double chamber is designed to allow easy and repeated access for exchange of the fissionable deposits. Fission chambers can be operated with continuous gas flow or tight gas seals. Either pure methane or P-10 gas (90% argon - 10% methane) works well[16].

The absolute fission rates were determined from the absolute counting of the fissions occurring in a known quantity of fissile material after applying corrections due to (a) perturbation of the flux introduced from the fission chamber material, (b) shielding of the access hole for electronic cables and gas tubing against the thermal and epithermal neutron streaming.

Absolute accuracies for the fission rates per nucleus of ^{235}U, ^{239}Pu, ^{238}U and ^{237}Np measured are in the range of $< \pm 1.5 - 2.5\%$.

2.2 Gamma spectrometers

The study of nuclear radiation detection requires an understanding of the interaction of radiation with matter. The interaction of gamma radiation with matter is primarily through three mechanisms,

namely, the photoelectric effect, Compton scattering and pair production. As a result of interaction of electromagnetic radiation with matter, energetic electrons are released.

When a stable isotope is irradiated in a nuclear reactor or accelerator, radioactive products are formed and these radio nuclides are measured by the detection of gamma rays. Gamma ray spectroscopy is generally classified into two classes: (a) semi conductor detectors and (b) scintillation detectors.

Ge(Li) detector and NaI(Tl) detector were used in this work. Ge(Li) detector was used for a number of experiments which would require the distinct resolution of certain gamma rays amongst fission products or other activation gammas. Both counting systems have an automatic sample changer (shown in Fig. 2. 1a and b). The sample changer has space for a loading of eight samples which are held in suitable aluminium trays within the recessed holes of a 24" dia. brass disc. The aluminium trays are covered with $\sim$ 1.4 mm thick aluminium to shield the detectors from β-particles. A diagram of an aluminium tray with cover is shown in Fig. 2.2. The brass disc rotates in a vertical plane, carrying the appropriate sample to a point on the longitudinal axis of both Ge(Li) and NaI(Tl) detectors. Ge(Li) detector was placed on one side of the sample changer and NaI(Tl) detector on the other side of the changer as shown in Fig. 2.1 a and b. The sample wheel was driven by a step motor which is controlled by the

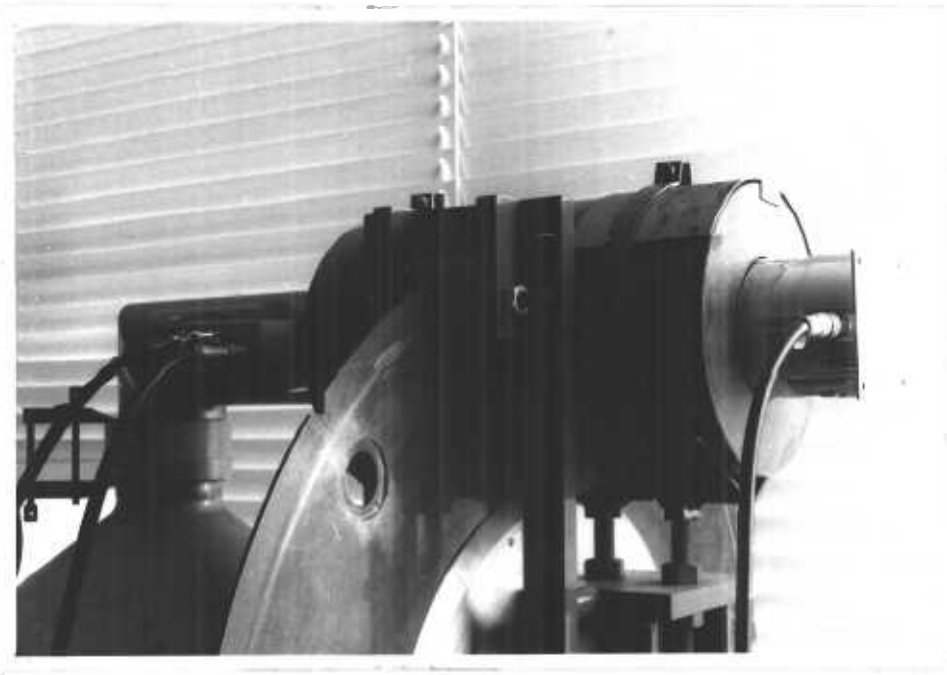


Fig.2.1(a). Ge(Li)-NaI(Tl) spectrometers with automatic brass disc sample changer.

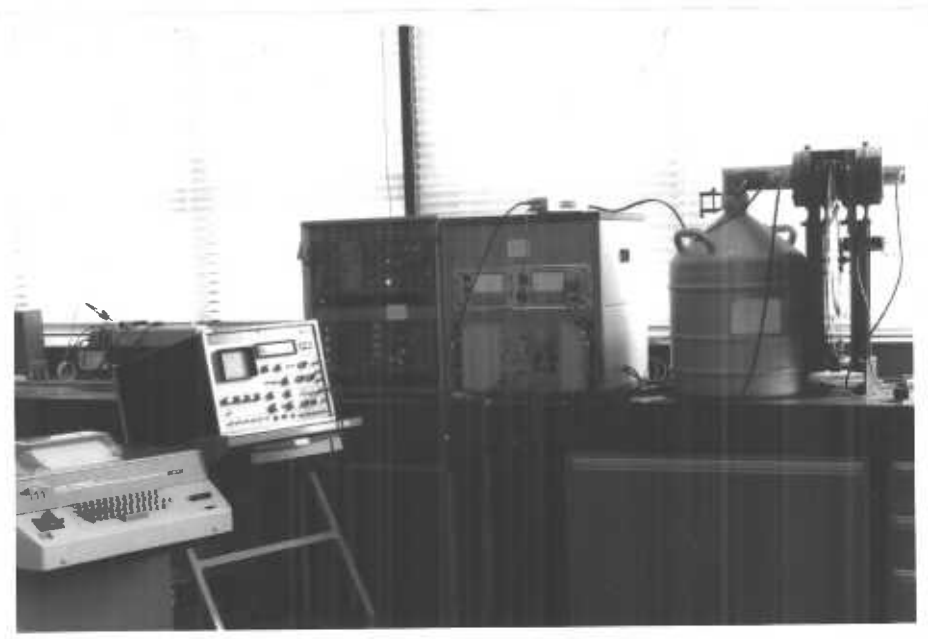


Fig.2.1(b). Ge(Li)-NaI(Tl) detector assembly and counting system.

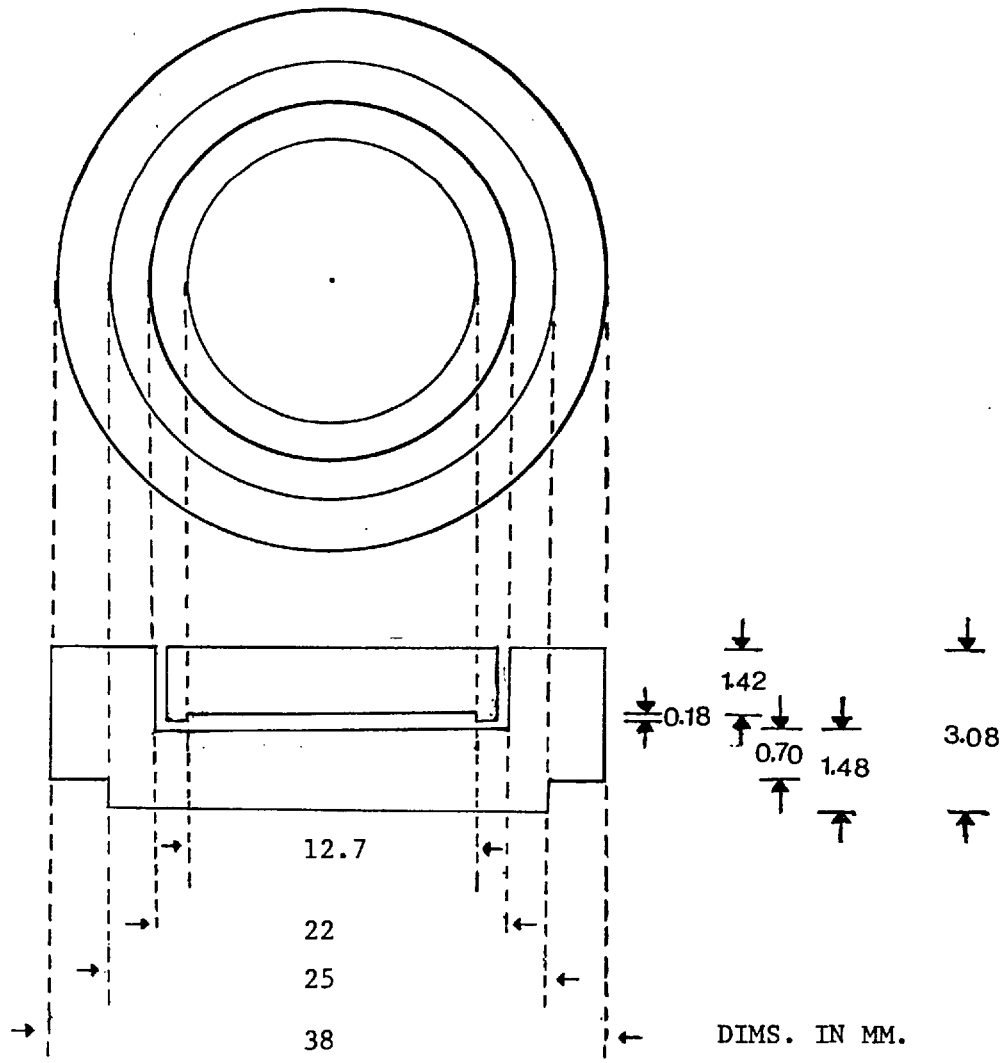


Fig.2.2. Aluminium foil tray design.

counting system itself. Each sample was counted for a preset time and while the data was being printed out, the sample wheel moved to the next position.

2.2.1 Ge(Li) Detector

Lithium drifted Germanium detectors are being widely used for gamma ray spectroscopy primarily because of their superior resolution compared with NaI(Tl) detectors.

The counting time, the automatic sample changer and the read out unit (Harwell 95/2140-3/6) were controlled by the multichannel analyser. The specifications of the Ge(Li) detector are given in Table 2.1.

Table 2.1

Specifications of Ge(Li) detector

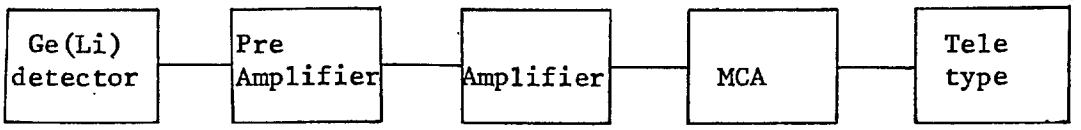
Type	True Coaxial
Sensitive volume	43 cm^3
Manufacturer	Canberra, U.S.A.
FWhm at 1.332 MeV of ^{60}Co source	2.21 Kev
Source - Crystal Separation distance	1.772 cm

The Ge(Li) detector has been used to measure gamma ray spectra from the decay of radioactive products and reaction rates have been determined from these gamma emission rates. A block diagram of the Ge(Li) counting system is shown in Fig. 2.3. To determine absolute gamma ray emission rates with a Ge(Li) detector, it is necessary to measure the spectrum for a known counting time, determine the peak areas and apply the appropriate corrections for dead time, pulse pile up (explained in Appendix AII), finite source area (explained in Appendix AIII) and peak detection efficiencies.

2.2.1 Determination of Peak areas

(a) Considering the problem of accurately determining peak areas, Fig. 2.4 illustrates a typical peak obtained in a gamma ray spectrum measured with a Ge(Li) detector system.

A classical peak method[17] was used to measure the peak area. 40 channels corresponding to 8.224 KeV were selected on either side of the Photo peak channel and this symmetry is maintained always in determining the Peak area. A line is drawn from the 40th channel at one side of the Photo peak (low energy side) to the 40th channel of the other side of the Photo peak (high energy side). These points determined the limiting channels within which the total counts are summed and a trapezoidal area is subtracted as indicated in Fig. 2.4 (A B C D). The choice of background function and peak area finding procedure are not, however, critical to accurate measurement of gamma ray emission rates provided that consistency was maintained in all



1.	Ge(Li) detector	-	Canberra 7219 Model
2.	Pre Amplifier	-	Canberra 1408C
3.	Research Amplifier	-	Canberra 1412
4.	Multichannel Analyser	-	ECON 1000 Channel
5.	Teletype	-	Data Dynamics 90

Fig. 2.3 Block diagram of Ge(Li) counting system

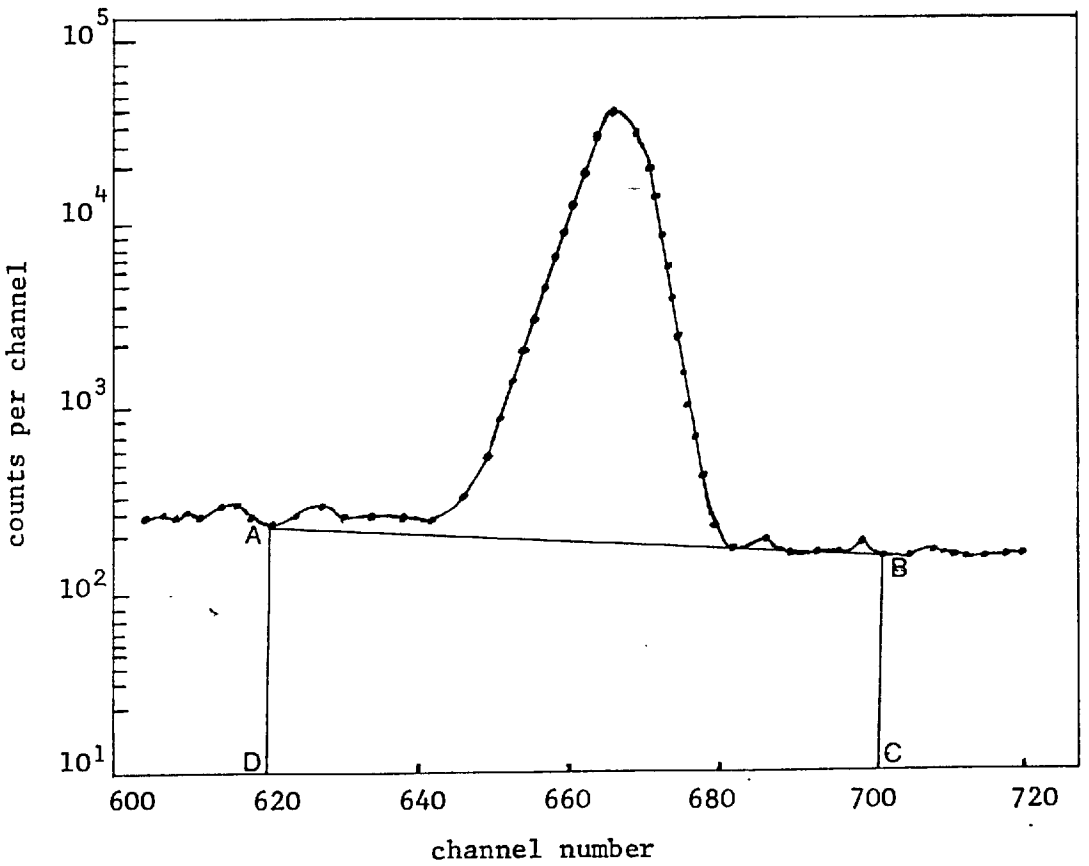


Fig. 2.4 A typical gamma ray spectra peak measured with a Ge(Li) detector

phases of measurements (i.e. the same functions were used both to measure the peak efficiencies and gamma emission rates from the foil).

2.2.1 Peak detection efficiencies

(b) Peak detection efficiencies were determined for Ge(Li) detector by measuring the spectra from gamma emitting sources. Calibrated gamma ray emitting sources were available from the Radiochemical Centre, Amersham, England. One ^{110m}Ag gamma emitting source was made at the University of London Reactor Centre (ULRC) and standardised to obtain more complete efficiency calibration data (explained in detail in Appendix AI). Specifications of gamma sources are given in Table 2.2. The efficiency of Ge(Li) counting system is defined as

$$\eta = \frac{C_\gamma}{C_T} \qquad (2.2.1)$$

Where C_γ is the measured count rate and C_T is the true gamma emission rate of the sample. If the activity of the sample and its half life are known, its disintegration rate at any time can be calculated.

Each standard gamma source was counted several times. The peak area of a particular gamma ray energy of the gamma source is determined as described in Section 2.2.1(a). Thus knowing the

TABLE 2.2

Specifications of standard gamma-ray emitting sources

Isotope	Form	Manufacturer	Half-life	Gamma-ray energy (MeV)	Gamma-ray intensity (%)	Activity (μCi)	Error in Activity (%)
^{203}Hg	Solid	Amersham[a]	46.6d	0.279	81.50	1.201	1.6
^{110m}Ag	Solid	ULRC[b]	253.0d	0.447	3.46	0.1700	1.7
^{110m}Ag	Solid	ULRC[b]	253.0d	0.620	2.81	0.1700	1.7
^{110m}Ag	Solid	ULRC[b]	253.0d	0.658	94.30	0.1700	1.7
^{137}Cs	Solid	Amersham[a]	30.1y	0.662	85.10	2.191	1.9
^{110m}Ag	Solid	ULRC[b]	253.0d	0.707	16.57	0.1700	1.7
^{110m}Ag	Solid	ULRC[b]	253.0d	0.818	7.42	0.1700	1.7
^{54}Mn	Solid	Amersham[a]	312.5d	0.835	100.00	0.987	1.7
^{110m}Ag	Solid	ULRC[b]	253.0d	0.885	73.98	0.1700	1.7
^{88}Y	Solid	Amersham[a]	106.6d	0.898	93.20	1.673	2.3
^{60}Co	Solid	Amersham[a]	5.26y	1.173	99.86	1.195	1.4
^{60}Co	Solid	Amersham[a]	5.26y	1.332	99.98	1.195	1.4
^{110m}Ag	Solid	ULRC[b]	253.0d	1.384	26.07	0.1700	1.7
^{110m}Ag	Solid	ULRC[b]	253.0d	1.476	4.38	0.1700	1.7
^{88}Y	Solid	Amersham[a]	106.6d	1.836	99.40	1.673	2.3

(a) Half-lives, Gamma-ray energies and intensities, Activities and their errors of standard sources are quoted from Refs. 18 and 22.

(b) Half-lives, Gamma-ray energies and intensities for ^{110m}Ag source are quoted from Ref. 19.

activity, half life, decay time, number and energy of gammas and measured count rate, the efficiency for each gamma ray energy was determined using the equation:

$$\eta = \frac{C_\gamma}{A_C \times 3.7 \times 10^{10} \times \exp(-\lambda t_d) \times b} \qquad (2.2.2)$$

Where A_C Activity of standard source in Curies at the time of standardisation.

λ Decay constant.

t_d Decay time since standardisation.

b Gamma ray branching ratio.

Total errors (random and systematic errors) on η are calculated using the equation from Ref. 20:

$$(\Delta\eta)^2 = \left(\frac{\delta\eta}{\delta C_\gamma}\right)^2 \cdot (\Delta C_\gamma)^2 + \left(\frac{\delta\eta}{\delta A_c}\right)^2 \cdot (\Delta A_c)^2 + \left(\frac{\delta\eta}{\delta b}\right)^2 \cdot (\Delta b)^2 \qquad (2.2.3)$$

A computer program E02ABF[21] was used in fitting the peak efficiency data points. This program calculates a weighted least squares polynomial approximation to a set of data points. If the given points are (E_i, η_i), i = 1,.....M where M is the number of data points and each point has a positive weight W_i (the weight is inversely proportional to the square of the standard error of each observation) associated with it, the procedure computes the coefficients of the polynomial P(E) of degree N which minimises the expression

$$\sum_{i=1}^{M} Wi\left|P(E_i) - \eta_i\right|^2 \qquad (2.2.4)$$

over the set of polynomials of degree N.

The Program E02ABF fitted the peak efficiency data with the polynomial of degree 8 and the coefficients are:

P_o = 2.08686 E-01, P_1 = -1.42624 E+00

P_2 = 4.64551 E+00, P_3 = -8.66299 E+00

P_4 = 9.89089 E+00, P_5 = -7.03132 E+00

P_6 = 3.03502 E+00, P_7 = -7.27830 E+00

P_8 = 7.43644 E+00.

The peak efficiency data points and the corresponding fitted points are given in Table 2.3. It can be seen from Table 2.3 that the peak efficiency data points agree very well within~± 2.0% with the fitted efficiency points. An efficiency curve has been drawn by hand through the peak efficiency data points and is shown in Fig. 2.5. Efficiency values used in reaction rate calculations have been determined in two different ways:

(a) efficiency values obtained from the hand drawn efficiency curve by interpolation (Fig. 2.5)

(b) efficiency values computed by the program E02ABF with experimental efficiency points of different standard gamma sources (Table 2.3) as input data.

TABLE 2.3

Absolute peak efficiency of Ge(Li) detector for gamma sources

Gamma emission energy (MeV)	Peak efficiency (Experimental Points)	Error in [(a)] experimental efficiency values (%)	Peak efficiency (Fitted points)
0.279	0.3362 E-01	1.8	0.3362 E-01
0.447	0.1681 E-01	2.3	0.1682 E-01
0.620	0.1138 E-01	2.7	0.1125 E-01
0.658	0.1043 E-01	2.0	0.1048 E-01
0.662	0.1027 E-01	1.9	0.1038 E-01
0.707	0.9490 E-02	2.2	0.9568 E-02
0.818	0.7842 E-02	2.4	0.7864 E-02
0.835	0.7780 E-02	2.3	0.7648 E-02
0.885	0.7130 E-02	2.0	0.7089 E-02
0.898	0.7000 E-02	2.4	0.6945 E-02
1.173	0.4980 E-02	1.5	0.5110 E-02
1.332	0.4350 E-02	1.5	0.4363 E-02
1.384	0.4210 E-02	2.2	0.4130 E-02
1.475	0.3760 E-02	2.3	0.3765 E-02
1.836	0.2972 E-02	2.1	0.2915 E-02

(a) Errors quoted at 1σ confidence level.

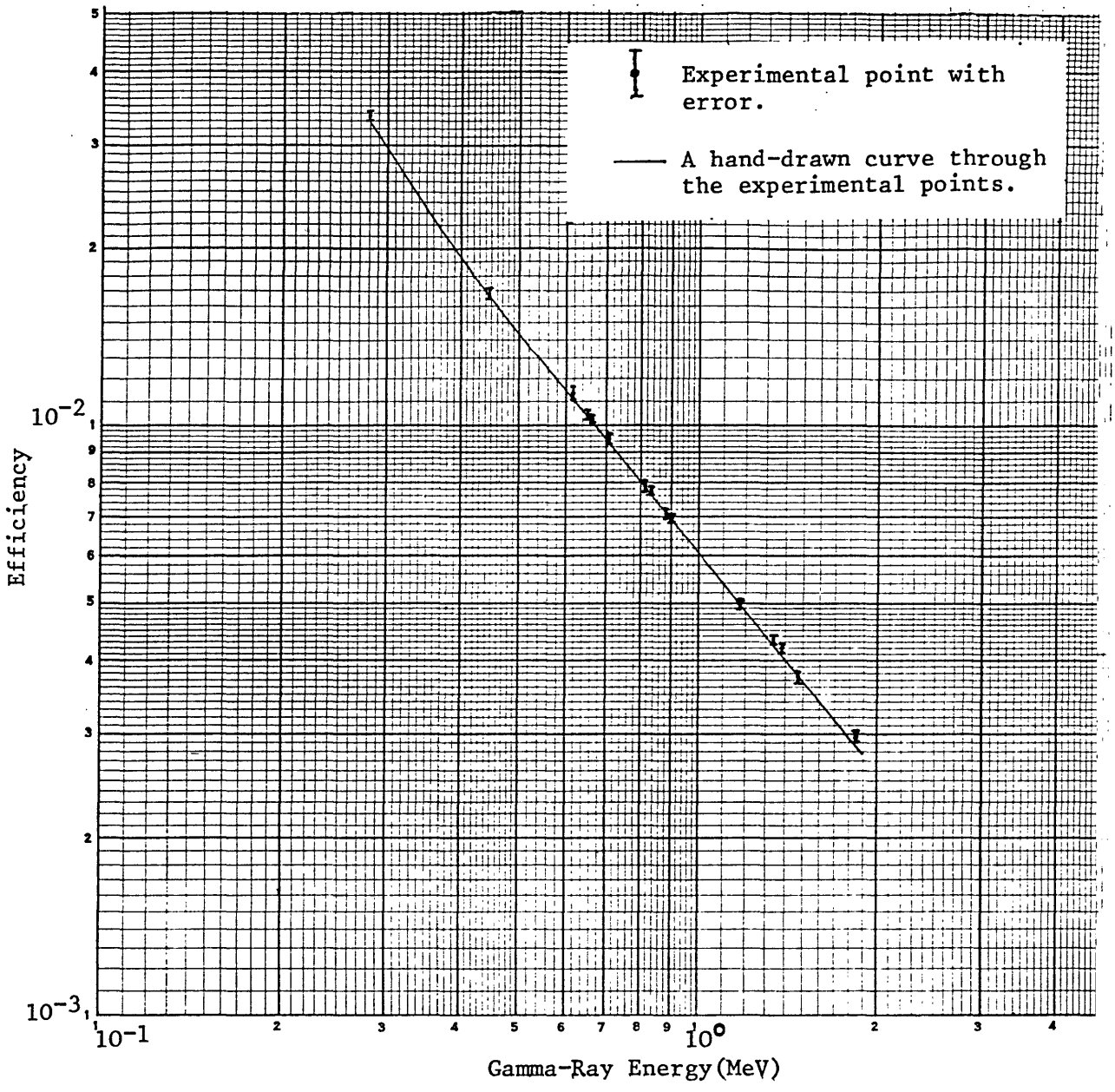


Fig.2.5. Absolute photo-peak efficiency measured for a 43-cm^3 co-axial Ge(Li) detector at ULRC. A hand-drawn curve is shown through the experimental points.

Efficiency values obtained from Fig. 2.5 and by the program are given in Table 2.4. It can be seen from Table 2.4 that both efficiency values agree well within $\sim \pm 2.0\%$. So the efficiency values obtained from Fig. 2.5 were used in reaction rate calculations with ± 2.0% error for gamma ray energy ranging from 0.336 MeV to 1.596 MeV.

2.2.1 Counting stability

(c) Reaction rate measurements were performed during a period of fifteen months and so it was necessary to maintain steady reproducible conditions of the counting system. The counting stability was checked weekly with a standard ^{137}Cs source. (Source number A0906,Activity: 10.70μci ± 1.60%, Standardised on 1.2.1973at 1200 Noon G.M.T.[75]. The system was also checked by counting the ^{137}Cs source before and after measurement of gamma ray spectra from each irradiated foil. This standard ^{137}Cs source (No. A0906) was used as reference source. To determine peak area, 100 channels was chosen i.e. 50 channels on either side of the photopeak channel. Net photopeak area was determined in the same way as described in Section 2.2.1. (a). Consistency was checked after making decay time correction every time. The reference peak area count rate used was 2811.68 on 5.2.1975. A maximum variation of $\sim \pm 1.0\%$ was observed during the whole period of measurement. Correction was applied to gamma ray spectra where necessary.

TABLE 2.4

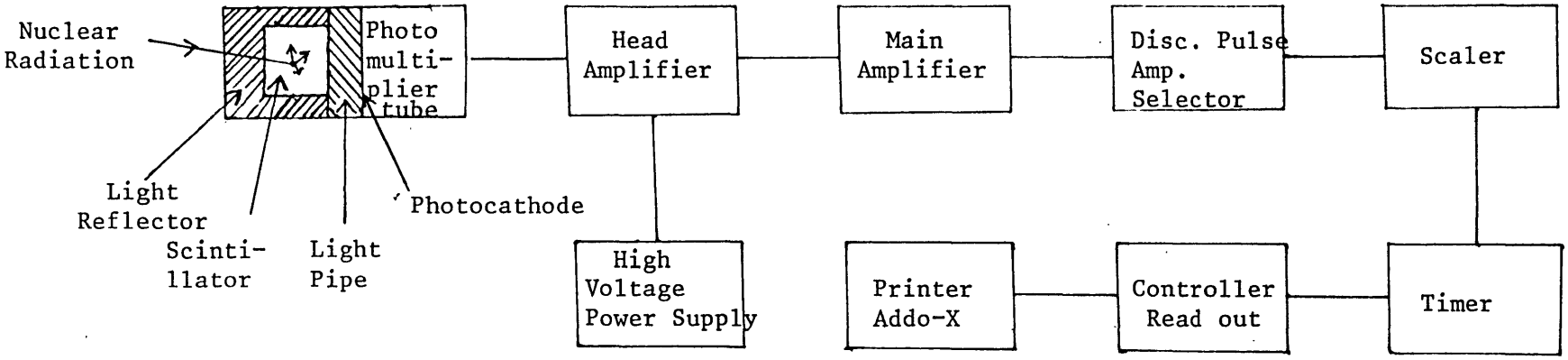
Absolute efficiency values used in reaction rate calculation

Gamma ray energy (MeV)	Efficiency points obtained from Fig. 2.5	Efficiency points (fitted)	Error (%)
0.336	0.0250	0.0253	2.0
0.412	0.0186	0.0187	2.0
0.511	0.0140	0.0142	2.0
0.810	0.00790	0.00797	2.0
0.844	0.00755	0.00754	2.0
0.847	0.00750	0.00750	2.0
1.293	0.00442	0.00454	2.0
1.368	0.00414	0.00420	2.0
1.596	0.00340	0.00342	2.0

2.2.2 NaI(T1) Detector

The wide scale use of scintillation detectors as gamma ray spectrometers has been made possible by the availability of large single crystals of NaI(T1) and the development of end window photomultiplier tubes with high resolution. Gamma rays interact with NaI(T1) crystals by three mechanisms: photoelectric effect, Compton effect and pair production. Fig. 2.6 is a schematic diagram of a scintillation detector used in the counting system. Harwell 2000 Series electronic unit was used namely: a head amplifier which supplied E H T to the photomultiplier tube, a main amplifier, a discriminator pulse amplitude selector, a scaler and a timer. A controller read out unit was used in conjunction with the scaler and the timer. The counts from the scaler was printed out by ADDO-X printer on paper tape.

The NaI(T1) detector was used only for integral counting as the scintillation detector does not have distinct resolution which is required for certain gamma rays amongst fission products or activation foils in this work. The NaI(T1) detector was used for integral counting to obtain the fission rate of ^{238}U relative to that of ^{235}U (F_8/F_5).



1. NaI(Tl) Scintillation Crystal Harwell P1132 dia. 4.5 cm by 5 cm.
2. Photomultiplier tube Type No. 1653/B Cat. No. 94/35107/6 Serial No. 2185.
3. Head Amplifier 95/0045 - 1/6
4. Main Amplifier 95/0045 - 1/6
5. Discriminator Pulse Amplitude Selector 95/2133 - 1/6 Serial No. C139.
6. Scaler
7. Timer
8. Controller Read out unit
9. Printer Addo-X
10. Power Supply 95/2147 - 2/6 Serial No. C193

Fig. 2.6 Schematic diagram of a scintillation detector

3. STANDARD FAST NEUTRON FIELDS

3.1.1 Review of the need for standard fast neutron fields

The design, development and operation of nuclear reactors from economic and safety considerations require accurate predictions of the major reaction rates and safety coefficients related to the reactor constituents. These integral parameters cannot be computed reliably owing to uncertainties in calculational models and approximations as well as in basic nuclear data. It is therefore necessary to make accurate integral and differential microscopic measurements in zero power mock-up and benchmark assemblies.

Several research groups throughout the world are devoted to the improvement of nuclear data and methods for reactor design using zero-power mock-up and benchmark assemblies. It is desirable to standardise all these results with each other but the standardisation of measuring techniques between different laboratories in fast reactor physics has not been easy due to the lack of any standard neutron source which could fulfil the requirements of fast reactor physics. Building fast reactor cores in different laboratories is an enormously expensive method and, in fact, is limited to a very few research organisations in the world.

Thus the need emerges for the creation of a fast neutron standard field which would be inexpensive and so could be adopted by a large number of laboratories and universities as an international standard. The standard should simulate the neutron spectrum of the core and breeder of a fast reactor. To enable interlaboratory comparison the standard should be permanent and easy to be reproduced in different laboratories.

The concept of the intermediate energy standard neutron field[23] has been promoted by CEN-SCK, MOL, Belgium, since 1967 within the framework of the tripartite German-Dutch-Belgian fast breeder program. In 1969, the MOL-ΣΣ facility was proposed as an international intermediate-energy secondary standard neutron field and was put into operation in early spring of 1970[10]. As a result of the work of Fabry et al[23] at MOL and collaboration between CEN/SCK, Belgium, UKAEA and Imperial College, a general purpose neutron intermediate standard uranium source (NISUS)[9 & 24] was built in a graphite thermal column on the CONSORT[25] reactor of the University of London in December 1971. The basic idea of NISUS design was to build an assembly for generating a neutron spectrum covering the energy range from about 50 eV to 5 MeV which is important for the study of fast breeder reactors[26].

3.1.2 Fast benchmark reactor core experiments

Experiments in fast reactor physics may be classified into two kinds. The "mock-up" experiment is the first kind where the object is to simulate a given power reactor design as closely as possible. The "mock-up" experiment is used to estimate the errors in the predictions, by a particular data set and a given calculation model, of the properties of the power reactor being simulated. It is of minor use in identifying errors in nuclear data because of the complex geometry of the system, though of great assistance in predicting the performance of the simulated reactor.

The "benchmark" assemblies are the second type of experiments used in fast reactor studies. They are geometrically simple assemblies for which errors from the calculational methods are small and which focus attention on the nuclear data. From the analysis of a series of such clean geometry integral experiments, over a wide range of energy spectra, it becomes possible to improve, by adjustment, the nuclear data used in theoretical predictions[27, 28 & 29].

There is a continuing programme of work directed towards the understanding of the physics of fast reactors. The data and methods used for making performance predictions are being revised to take account of new differential measurements and integral checks on zero-power reactors.

A list of zero-power reactors[30 & 31] available in the world is given in Table 3.1.

TABLE 3.1

Zero-Power Reactor	Country
Zebra	U.K.
Vera	U.K.
Z P R	U.S.A.
Sefor	U.S.A.
Big Ten	U.S.A.
C F R M F	U.S.A.
Suak	Germany
Sneak	Germany
Masurca	France
Tapiro	Italy

List of Zero-Power reactors available in the world.

3.1.3 Intermediate-energy standard neutron field

The essential requirements for a primary standard neutron field are:

(i) The neutron field should produce a moderately intense intermediate energy neutron spectrum encompassing the energy range 1 KeV to 5 MeV appropriate for the measurement of neutron reaction rates important for the design, safety and economic operation of fast breeder reactors.

(ii) The system must be optimised for reliable calculation of the neutron spectrum so that the calculation is more reliable than for any existing fast neutron field. This is possible only if materials with the most completely and accurately known cross sections are employed in creating the field.

The concept for a primary intermediate energy standard neutron field (ISNF)[32] at NBS (Washington) is a spherically symmetric arrangement consisting of small fission spectrum sources, partial moderation in graphite and a low energy cut off with ^{10}B. The relevant cross sections for the ISNF spectral shape are ^{235}U fission, carbon scattering and ^{10}B absorption, which are known to the degree of accuracy of primary standard cross sections. The spectrum shape in NISUS and MOL-ΣΣ type systems is dominated by ^{238}U inelastic scattering cross sections which are not known to standard cross section accuracy, so NISUS and MOL-ΣΣ neutron fields are known as secondary standard neutron fields.

No integral measurements from the primary standard ISNF at NBS have been reported yet. It is believed that careful fission and capture reation rate results for this facility will give very useful information on reactor dosimetry cross section data testing and improvement[31].

3.2 Description of the NISUS facility

The NISUS facility consists of two concentric spherical shells, the outer driver shell of natural uranium and an inner shell of boron carbide (B_4C). The shells are supported in the centre of the air filled spherical cavity of 50 cm diameter hollowed out of a 60 cm cube of graphite. To reduce the effect of thermal flux decreasing with distance from the core, the shells are mounted at the centre of the spherical cavity. The thermal neutrons entering the outer cavity will not all enter the shells directly but scatter around the cavity wall to give a more uniform thermal neutron source surrounding the natural uranium. The shells' support is manufactured from aluminium and its height is adjustable using aluminium spacers. The graphite cube is mounted in an extension of a thermal column of CONSORT reactor.

The mechanism of spectrum generation in NISUS is that neutrons, originating from the reactor core, are moderated in the thermal column and provide a well thermalised source that impinges on the natural uranium shell. This gives rise to a fission source distribution which is a maximum at the outer shell edge owing to the attenuation

of the thermal flux through the driver shell (uranium shell). Inelastic scattering of fission neutrons in the inner region of the driver shell degrades the spectrum to a characteristic fast neutron shape above 10 KeV. The inner boron carbide absorbing shell is used to suppress any unwanted thermal and epithermal neutron response in the detectors which are located inside an inner air filled cavity at the centre of the shells.

The graphite of the thermal column acts as a reflector to the fission neutrons from the natural uranium shell. The central spectrum, inside the boron carbide sphere, has two main components, a direct contribution which penetrates inwards from the driver shell and a wall return contribution that has a larger $\frac{1}{E}$ component due to scattering in the graphite. This wall return component, although small above 100 KeV, is the main contributor to the central spectrum below 50 KeV. An increase of the size of the outer cavity with respect to the diameter of the uranium shell decreases the wall return component but increasing the thickness of graphite reflector surrounding the outer cavity increases the wall return component of the central spectrum. Computations using discrete ordinate methods[33] have shown that for graphite thicknesses of greater than 35 cm no changes are observed in the central spectrum. The graphite is then essentially an "infinite" reflector and the wall return is constant to within a few per cent.

The NISUS facility can be effectively isolated from the reactor core by a remote controlled cadmium shutter with a closed/open operation time of 46 seconds.

The loading of neutron detectors into the inner cavity is done through an access hole on the central axis of the thermal column at the rear of the facility. The neutron detectors are mounted on a composite plug and are loaded into the central cavity via an access hole of diameter 85.5 mm on the central axis of the thermal column extension. The composite plug consists of a removable piece of boron carbide shell 17 mm thick connected to a part of uranium shell 80 mm long. The diameter of the boron carbide and the uranium parts is 45.75 mm matching the diameter of a hole in the shells, so that when the plug is fully loaded, the NISUS sphere is complete. The uranium part of the plug is connected to a 990 mm long graphite plug by an aluminium stem. Figure 3.1 shows the cross sectional view of the NISUS facility with the composite plug in the full "in" position with the activation foil holder secured to its extremity. A view of NISUS, with the top half removed is shown in Fig. 3.2. A set of foils is shown, positioned within the central cavity by means of a foil holder (Reproduced from Ref.9).

The NISUS assembly allows the installation of concentric spherical shells of different thicknesses so that it is possible to generate spectra with different degrees of hardness. There are available in

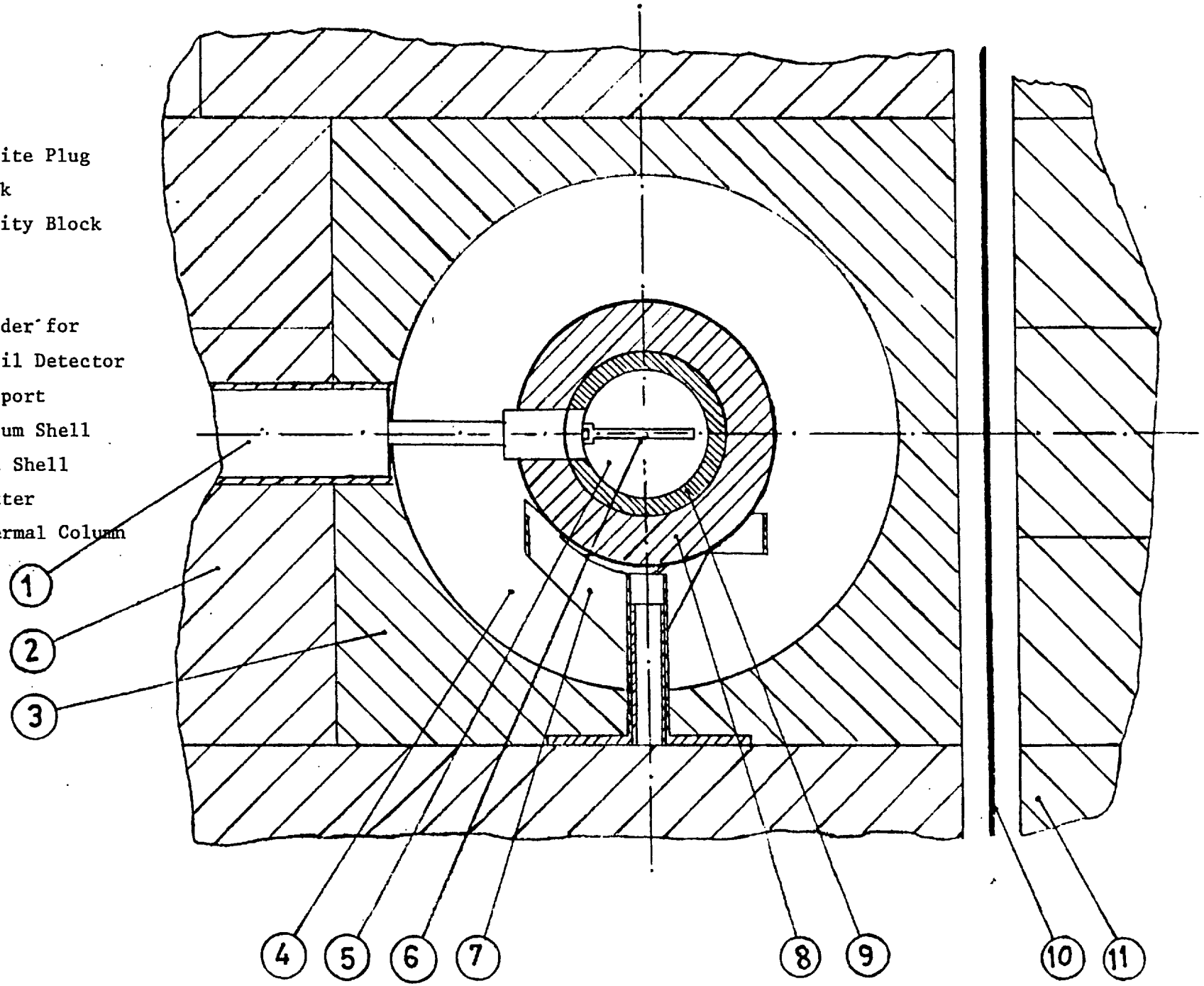


Fig. 3.1. Cross sectional sketch of the NISUS facility.



Fig.3.2. A view of NISUS with the top half removed . Foils are shown in position within the central cavity. The foil holder is mounted on the end of a composite loading plug.

total eight natural uranium shells, two B_4C shells with different dimensions and densities and one iron shell which can be accommodated in the assembly in different combinations. The specification for the NISUS configuration employed in this work, is given in Table 3.2.

A one dimensional discrete ordinates transport code, ANISN, is used for spectrum prediction in the inner cavity of the NISUS facility. The design of the NISUS facility is described extensively in Ref. 33.

3.3 Description of the MOL-ΣΣ facility

ΣΣ is a thermal-fast coupled spherical source assembly located within a horizontal graphite thermal column of the Belgian reactor BR1. The spherical source shell of natural uranium is embedded at the centre of a 50 cm diameter spherical cavity in graphite, surrounding a 15 mm thick aluminium-clad concentric natural boron carbide shell at the centre of which fast flux is generated. The ΣΣ uranium shell is supported by an aluminium holder ring which is fixed to a moveable graphite and shielding plug. The entire assembly on its plug can be pulled out of the graphite cavity for inserting neutron detectors inside the ΣΣ cavity.

Like NISUS the natural uranium shell acts as a thermal-fast converter; the bulk of the fission neutrons is created within the outer edge of this source and undergoes appreciable energy degradation

TABLE 3.2

Material and geometrical data of NISUS configuration 1b[a]

Natural Uranium		
Uranium Shell number 2	outside diameter	198.12 ± 0.1 mm
	internal diameter	157.48 ± 0.1 mm
Uranium Shell number 3	outside diameter	238.76 ± 0.1 mm
	internal diameter	198.12 ± 0.1 mm
Uranium Shell number 4	outside diameter	254.0 ± 0.1 mm
	internal diameter	238.76 ± 0.1 mm
Uranium	density	18.9 g/cm^3
Uranium Shell	thickness	48.26 ± 0.1 mm
Boron Carbide		
Boron Carbide Shell[b] No:B_4C2	outside diameter	157.4 ± 0.1 mm
	internal diameter	123.4 ± 0.1 mm
	density	1.58 g/cm^3
	thickness	15.0 ± 0.1 mm
Graphite Reflector		
	cavity diameter	500 mm
	density[c]	1.722 ± 0.001 g/cm^3

(a) All data quoted are obtained by Private Communication with T.C. Jones of ULRC.

(b) Thickness of aluminium cladding of B_4C shell is 1 mm.

(c) The graphite density value is quoted from Ref. 34.

through elastic and inelastic scattering in the inner layer of the driver shell. The inner boron carbide shell is used for shaping the low energy tail of the ΣΣ central flux spectrum.

The loading of neutron detectors inside the ΣΣ central spectrum is done through different standard access holes for activation foils and solid state track recorders which are inserted inside the ΣΣ facility without access hole. A cross sectional view of the ΣΣ facility is shown in Fig. 3.3 (Reproduced from Ref. 10.) The material and geometrical data of the ΣΣ configuration are given in Table 3.3.

A one dimensional discrete ordinates transport theory calculation using the ENDF/BIII nuclear data file is used to derive a recommended ΣΣ central-neutron spectrum $\phi(E)$. ΣΣ has been selected by CSEWG as one of the five benchmarks for Phase-II data testing of the ENDF/B dosimetry file. Most recently ΣΣ has also been identified as an IAEA benchmark for the validation of nuclear data for reactor neutron dosimetry[10]. The design and description of the ΣΣ facility are given more elaborately in Refs. 23, 10 & 35.

3.4 Description of the ^{235}U thermal fission neutron spectrum facility

Fission neutron spectra are generated by means of various arrangements in a 1 meter diameter spherical cavity within the vertical graphite thermal column of the Belgian BR1 reactor. A cylindrical geometry of the fission source was selected for the irradiation of activation foils in the present work.

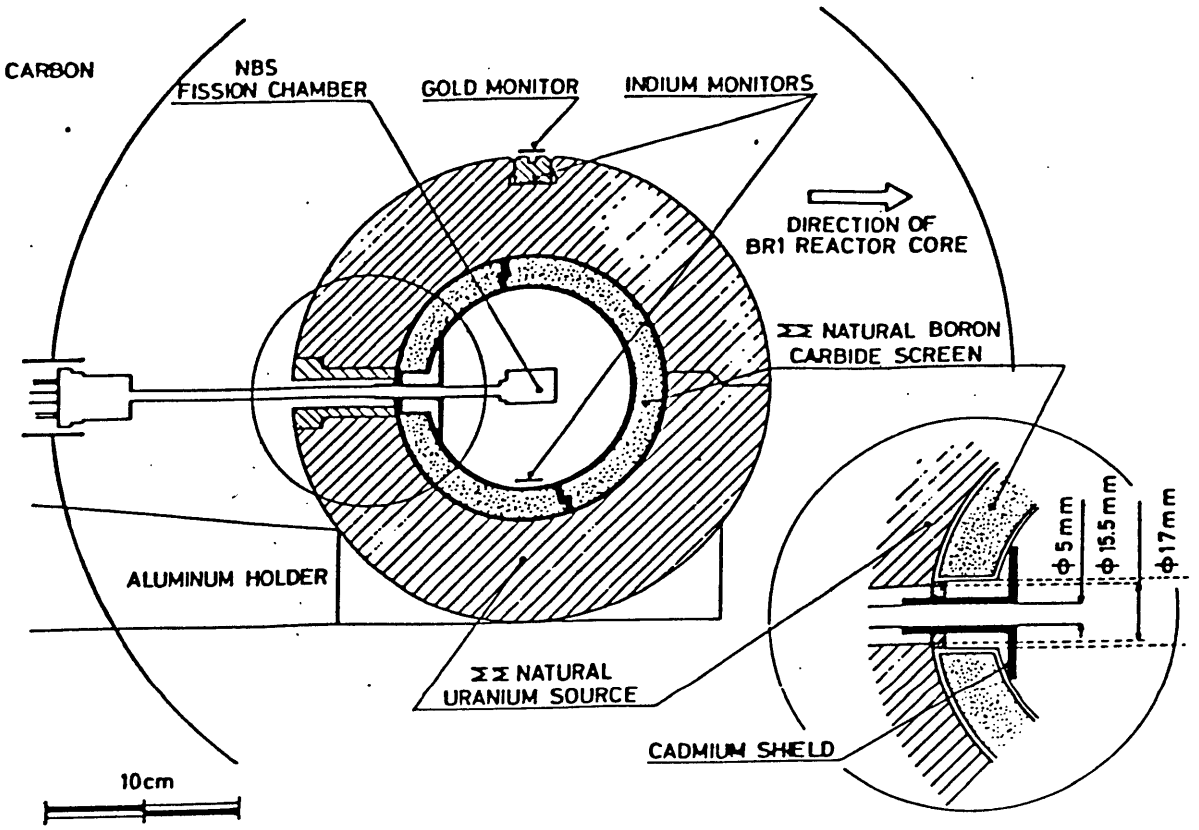


Fig.3.3. Cross-sectional sketch of the ΣΣ facility.

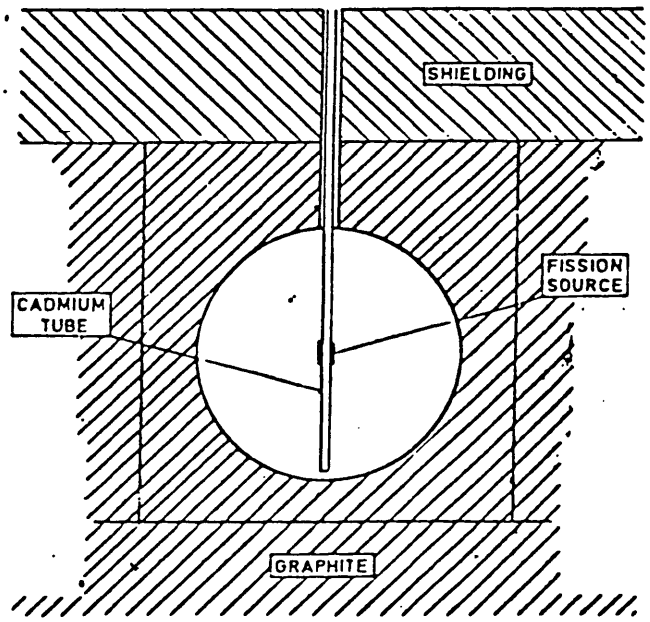


Fig.3.4. Experimental configuration in the spherical cavity of the BR-1 thermal column.

TABLE 3.3

ΣΣ detailed material and geometrical data[a]

Natural Uranium		
Shell	outside diameter	245 ± 0.2 mm
Shell	thickness	50 ± 0.1 mm
Uranium	density	18.92 ± 0.03 g/cm^3
Boron carbide		
Boron carbide shell[b]	thickness	15 ± 0.1 mm
Boron carbide	density	1.499 ± 0.005 g/cm^3
Graphite reflector		
Graphite	cavity diameter	500 mm
Graphite	density	1.60 ± 0.02 g/cm^3

(a) All these data quoted from Ref. 10.

(b) Thickness of aluminium cladding of B_4C shell is 1 mm.

In the experimental set up, the exposure zone is constituted by a 1 mm thick cadmium tube of inner diameter 3.1 cm and about 2 meters long. The tube is placed vertically along the polar axis of the spherical cavity in the BR1 thermal column. The bottom of this tube is tightly closed by a cadmium plate while the top is closed by a reactor shielding block. The fission source is simply a 93% enriched, 0.1 mm thick and 7.7 cm long metalic uranium sheet. The uranium sheet is fixed coaxially around the cadmium tube at the cavity centre. This uranium converter is protected by a very thin (<0.02 mm) aluminium wrapping[11]. Figures 3.4 (Reproduced from Ref. 11) presents a sketch of this experimental configuration.

A stack of non fissile threshold foils was placed inside a small aluminium tube. This small tube was connected to a long aluminium tube by an aluminium stem and then inserted vertically inside the cadmium tube in such a way that the activation foils were placed at the centre of the spherical cavity. The specification of the ^{235}U fission spectrum facility at MOL is given in Table 3.4.

The design, implementation and use of a one meter diameter ^{235}U fission neutron spectrum field are discussed extensively in an annual report Blg-481 (1972) of CEN/SCK MOL. The ^{235}U fission neutron spectrum field in BR1 reactor at MOL, Belgium is one of the few benchmarks identified by CSEWG for the phase II data testing of the EDNF/B-IV dosimetry file and also selected for similar purposes at the IAEA panel on nuclear data for reactor neutron dosimetry[11].

TABLE 3.4

Specification of ^{235}U fission spectrum facility[a]

Uranium		
Uranium metallic sheet[b]	length	7.7 cm
Uranium	thickness	0.01 cm
Uranium	enrichment	93.0%
Cadmium		
Cadmium tube	length	∿ 200 cm
Cadmium tube	intermal diameter	3.1 cm
Cadmium tube	thickness	0.1 cm
Graphite reflector		
Graphite	cavity diameter	100 cm

(a) All these data quoted from Ref. 11.

(b) Uranium metallic sheet wrapped by aluminium of thickness < 0.002 cm.

4. REACTION RATE MEASUREMENTS IN NISUS

4.1 Choice of activation detectors

To determine reaction rate experimentally in fast neutron spectra materials sensitive to different energy neutrons are selected. A systematic list has been made of all aspects which influence the selection of activation detectors:

(1) Materials whose sensitivity to the neutron field span the range of spectra encountered in fast neutrons.

(2) Cross section for the reaction under consideration should be well known.

(3) The half life of the product nuclide should not be too short compared with counting and waiting time.

(4) The product nuclide must have possibilities for simple activity determination, preferably with gamma counting or coincidence counting technique (gamma counting technique is used in this work).

(5) The material should be available with as high purity as possible in order to minimise perturbing reactions with impurities.

(6) The material should contain only one or predominantly one stable isotope, so that possibilities for competing reactions with isotopes in the materials are minimised.

(7) The detector material should preferably be a rigid structure.

(8) Gamma abundance and gamma energy should be known correctly.

(9) The detectors should be chemically stable.

(10) The thickness of the detector should be chosen in such a manner that flux density depression due to the presence of detector is minimum.

(11) The material should be commercially available, not too expensive, simple to handle and safe to use.

(12) The material can be used repeatedly.

Due to this long list of requirements the number of neutron detectors used are limited. Those materials which cover the energy range of NISUS (Fast neutron spectrum) are used in this work. A list of materials used in reaction rate measurement in NISUS is given in Table 4.1.

4.2 Specifications of non fission and fission foils

Non fission and fission foils which cover the energy range of the NISUS spectrum are considered in this work. Most of the non fission foils and ^{238}U fission foils were obtained from Reactor Experiments Inc., California, U.S.A. Purity, thickness, weight, diameter were supplied by Reactor Experiments Inc.[36]. Gold foils were prepared at the University of London Reactor Centre by J. Petr[47]. ^{235}U fissile foils were on loan from UKAEA, Aldermaston, U.K. The specifications of all these foils are given in Table 4.1. Purity and uncertainty in gamma ray branching ratio of some foils are not quoted because the data is not available.

TABLE 4.1

Specification and dimension of non-fission and fission foils

Target nucleus (type of reaction)	Reaction product	Abundance (%)	Half life	Emitted radiation	Energy of Emitted radiation (Mev)	Branching ratio (%) (g)	Foil thickness (mm)	Foil diameter (mm)	Irradiation time (hour)	Material purity (%)
$^{55}Mn(n,\gamma)$	^{56}Mn	81.30 (c)	2.580h (b)	γ	0.8470 (b)	98.80 (b)	0.0508 (a)	12.70 (a)	7.0	99.90 (a)
$^{115}In(n,\gamma)$	^{116m}In	95.72 (c)	54.03 min (d)	γ	1.293 (d)	83.40(15) (d)	0.2540 (a)	12.70 (a)	7.0	99.90 (a)
$^{197}Au(n,\gamma)$	^{198}Au	100.0 (c)	2.696d (d)	γ	0.4118 (d)	95.48(10) (d)	0.0508 (e)	9.00 (e)	7.0	99.99 (e)
$^{235}U(n,f)$	F.P(^{140}La)	95.60 (c)	12.79d (d)	γ	1.596 (d)	95.33(16) (d)	0.0635 (f)	10.16 (f)	7.0	99.54 (j)
$^{115}In(n,n')$	^{115m}In	95.72 (c)	4.500h (d)	γ	0.3362 (d)	45.9(1) (h)	0.254 (a)	12.70 (a)	7.0	99.90 (a)
$^{238}U(n,f)$	F.P(^{140}La)	99.96 (c)	12.79d (d)	γ	1.596 (d)	95.33(16) (d)	0.0381 (a)	12.70 (a)	7.0	99.90 (a)
$^{58}Ni(n,p)$	^{58}Co	67.88 (c)	70.78d (i)	γ	0.8108 (i)	99.45(1) (i)	0.254 (a)	12.70 (a)	7.0	99.90 (a)
$^{64}Zn(n,p)$	^{64}Cu	48.89 (c)	12.70h (d)	γ	0.5110 (d)	36.80(16) (d)	0.254 (a)	12.70 (a)	7.0	99.90 (a)
$^{27}Al(n,p)$	^{27}Mg	100.0 (c)	9.460min (d)	γ	0.8437 (d)	71.40(5) (d)	1.170 (e)	12.70 (e)	7.0	-
$^{56}Fe(n,p)$	^{56}Mn	91.66 (c)	2.580h (b)	γ	0.8470 (b)	98.80 (b)	2.997 (e)	12.70 (e)	7.0	-
$^{56}Fe(n,p)$	^{56}Mn	91.66 (c)	2.580h (b)	γ	0.8470 (b)	98.80 (b)	0.381 (a)	12.70 (a)	7.0	99.90 (a)
$^{24}Mg(n,p)$	^{24}Na	78.70 (c)	15.00h (d)	γ	1.369 (d)	99.99(2) (d)	0.127 (a)	12.70 (a)	7.0	99.90 (a)
$^{24}Mg(n,p)$	^{24}Na	78.70 (c)	15.00h (d)	γ	1.369 (d)	99.99(2) (d)	0.381 (a)	12.70 (a)	7.0	99.90 (a)
$^{27}Al(n,\alpha)$	^{24}Na	100.00 (c)	15.00h (d)	γ	1.369 (d)	99.99(2) (d)	1.170 (e)	12.70 (e)	7.0	-

(a) These values are taken from the certificate of vendor (Reactor Experiment inc.), Ref. 36.

(b) These data are taken from Ref. 37.

(c) Handbook of Chemistry and Physics (CRC), Ref. 38.

(d) Evaluated decay scheme data, Ref. 39.

(e) These foils were made at the University of London Reactor Centre. Foil thickness, diameter and material purity obtained from Ref. 47.

(f) These foils were on loan from UKAEA, Aldermaston, Berks, U.K.
Foil thickness and diameter measured at ULRC.

(g) The numbers in parenthesis indicate uncertainty (1σ) in the last digit(s), Ref. 39.

(h) Branching ratio of ^{115}In (n,n') and its uncertainty (1σ level) are taken from Ref. 46.

(i) Gamma ray energy, branching ratio and half life of ^{58}Ni (n,p) ^{58}Co reaction are taken from Ref.46.

(j) Material purity obtained from J.G.Williams (ULRC) by Private Communication.

4.3 Correction for external- and self-absorption of gamma rays, self-shielding and flux perturbation of foils

4.3.1 External- and self-absorption of gamma rays

After irradiation in NISUS, the neutron dosimeters were counted using a Ge(Li) detector for gamma ray emission rates to compute the reaction rate of each activation detector. The foils counted require several corrections to the Ge(Li) data. Gamma rays were attenuated in the samples itself and the ∿ 1.50 mm aluminium foil tray. The "external-absorber" corrections for aluminium foil tray can be determined from the equation:

$$A = A_o \exp\left|- \mu(E)d\right| \qquad (4.3.1)$$

where A = observed gamma intensity

A_o = unattenuated gamma intensity

$\mu(E)$= linear absorption coefficient for the material of interest

d = aluminium foil tray thickness

The external absorber correction was not done because the thickness of aluminium tray used for standard source was ∿ 1.12 mm and the standard source was sealed between 0.5 mm polystyrene windows. Linear attenuation in source capsule (point source sealed between 0.5 mm polystyrene windows[18] and 1.12 mm standard source aluminium tray) relative to 1.48 mm aluminium tray used for foils is:

Difference in aluminium tray between foil and standard source,

$$d = (1.48 - 1.12)\text{mm} = 0.36 \text{ mm}$$

$$= 0.036 \text{ cm}$$

linear absorption coefficient for aluminium for 0.800 MeV,

$$\mu(E) = 0.1844 \text{ cm}^{-1}(40).$$

correction due to 0.036 cm for aluminium

$$= \exp(-\mu(E)d) = 0.993$$

Transmission factor certified by vendor for 0.5 mm polystyrene windows = 0.995.

Net external absorber correction to be performed for foils relative to standard source

$$\simeq 0.995 - 0.993 \simeq 0.002 \simeq (0.2 \pm 0.5)\%$$

the correction for external absorber used in standard source and foils is negligible $\sim(0.2 \pm 0.5)\%$, so no external absorber correction has been applied.

Self absorption correction has been applied to all materials because the thickness of different foils varies from $\sim$ 3.0 to $\sim$ 0.4 mm as shown in Table 4.1. The self absorption correction was determined from the first order approximation(8).

$$A_o = \frac{A\,\mu(E)d}{\{1 - \exp|-\mu(E)d|\}} \qquad (4.3.2)$$

where A_o = uattenuated gamma intensity

A = observed gamma intensity

$\mu(E)$ = linear absorption coefficient for the material of interest

d = foil thickness

Linear absorption coefficient data for different materials was obtained from Ref. 41 and is shown in Table 4.2. Self absorption correction is important because it is another means of improving interlaboratory precision.

4.3.2 Neutron flux perturbation corrections

The intrinsic neutron field perturbation caused by measuring instruments requires careful consideration. In this work the effect of neutron self shielding and flux depression was considered.

4.3.2 Neutron self shielding effect

(a) The thickness of aluminium foil holder ($\sim$ 0.4 mm), thickness of activation foils ($\sim$ 3.0 to $\sim$ 0.4 mm) and arrangements adopted for irradiation of foils inside NISUS were made in such a way that the neutron field perturbation was negligible. However, such is generally not the case for neutron self shielding within non-threshold detectors. Self shielding corrections for some capture reactions are non trivial. Self shielding measurements for non threshold reactions were not performed in NISUS. These corrections were applied for several NISUS neutron dosimetry reactions from self shielding measurements in MOL-ΣΣ

TABLE 4.2

Self absorption corrections applied to activation foils

Reaction	Gamma-ray energy (MeV)	Foil thickness (cm)	Absorption coefficient $\mu(E)$ cm^{-1}	Self absorption correction factor applied to foils in this work
$^{55}Mn(n,\gamma)^{56}Mn$	0.8470	0.00508	0.45863	1.00117
$^{115}In(n,\gamma)^{116m}In$	1.293	0.0254	0.37454	1.00476
$^{197}Au(n,\gamma)^{198}Au$	0.4118	0.00508	4.0070	1.01021
$^{235}U(n,f)F.P.$	1.596	0.00635	1.0110	1.00321
$^{115}In(n,n')^{115m}In$	0.3362	0.0254	1.0395	1.01326
$^{238}U(n,f)F.P.$	1.596	0.00381	1.0110	1.00193
$^{58}Ni(n,p)^{58}Co$	0.8108	0.0254	0.60832	1.00774
$^{64}Zn(n,p)^{64}Cu$	0.5110	0.0254	0.59596	1.00759
$^{27}Al(n,p)^{27}Mg$	0.8437	0.1170	0.18026	1.01058
$^{56}Fe(n,p)^{56}Mn$	0.8470	(0.2997[a]	0.51239	(1.07875
		(0.0381		(1.00980
$^{24}Mg(n,p)^{24}Na$	1.369	(0.0127[a]	0.09454	(1.00060
		(0.0381		(1.00180
$^{27}Al(n,\alpha)^{24}Na$	1.369	0.1170	0.14302	1.00839

(a) Foils of different thicknesses were used for $^{56}Fe(n,p)^{56}Mn$ and $^{24}Mg(n,p)^{24}Na$ reaction rate measurements

because NISUS and MOL-ΣΣ are two similar fast neutron fields. Self shielding correction has been made only for $^{197}Au(n,\gamma)^{198}Au$ reaction because the correction for $^{115}In(n,\gamma)^{116m}In$ reaction is negligible[10] shown in Fig. 4.1. No correction has been done for $^{55}Mn(n,\gamma)^{56}Mn$ reaction because no self shielding data is available. The values for this reaction are therefore not used in any subsequent discussion of consistency of the integral data.

4.3.2 Flux density depression

(b) Flux density depression due to foil-to-foil shadowing effects was checked by Azad[42] with Indium foils inside NISUS. She made three experiments with indium foils. The first experiment was the irradiation of one ^{115}In foil at the centre of NISUS. The second experiment had three ^{115}In foils and the third one had five ^{115}In foils. Each ^{115}In foil was placed at a distance of 2 cm from each other. Reaction rates of $^{115}In(n,\gamma)^{116m}In$ and $^{115}In(n,n')^{115m}In$ were reproduced within experimental errors in these three experiments. This shows that a separation of 2 cm is sufficient to prevent flux depression by neighbouring foils. These experiments imply that measurements of In(n,γ) and In(n,n') can be performed in five positions inside NISUS without flux density depression correction. Such may not be the case for other reactions, however, particularly those which show greater self shielding effects than In(n,γ) and In(n,n'). For this reason only, those reaction rates measured using a single foil will be considered in the discussion (Section 4.9 in this chapter

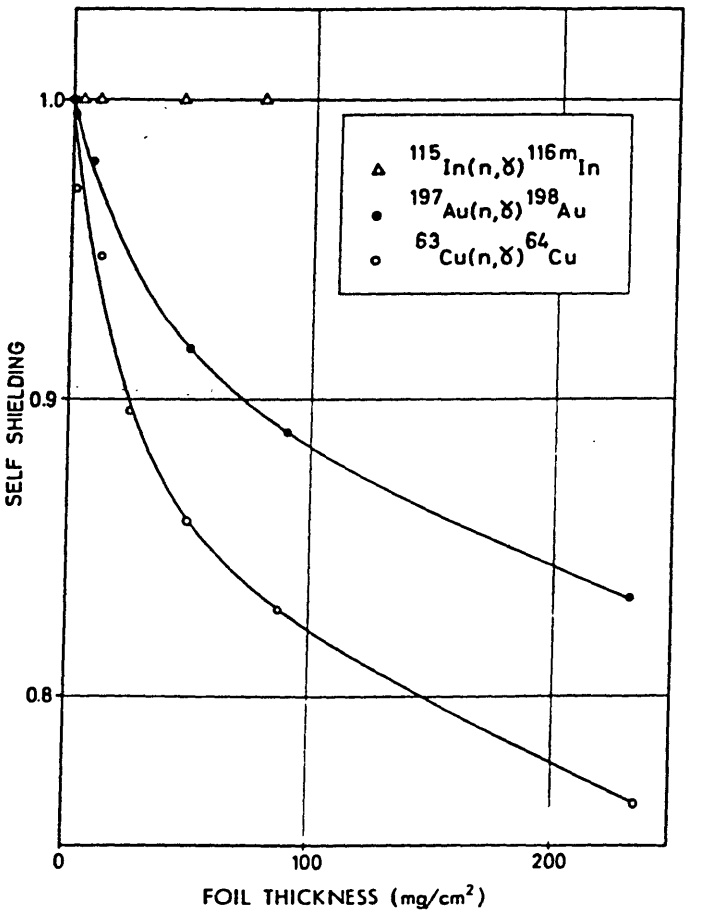


Fig.4.1. Neutron self-shielding for three typical dosimetry reactions in the ΣΣ central-neutron field (Reproduced from Ref.10)

and section 7.1 in chapter 7), of the consistency of the NISUS measurements with each other and with values from ΣΣ and calculated from differential data. Data obtained from simultaneous irradiations of more than one foil provide useful information, however, on flux gradients within NISUS.

4.4 Specification of fission sources for fission chamber measurements

Measurements of the absolute fission rates have been performed by using NBS-type fission chambers and ULRC-type fission chambers. Fissionable deposits were exposed at the centre of NISUS standard neutron field. Five of these fissionable deposits came from National Bureau of Standards (NBS), Washington. The deposits were 12.7 mm diameter fissionable oxides prepared by vacuum evaporation. Deposit backings were 19.0 mm diameter polished platinum 0.13 mm thick disks. The remaining two deposits were prepared for the University of London Reactor Centre (ULRC) at AERE, Harwell. These two deposits were 20 mm diameter vacuum evaporated or painted in the case of the two thickest fissionable oxides on the backings of 42.0 mm diameter polished platinum. A full list of fissionable deposits[34] exposed at the centre of NISUS is given in Table 4.3.

4.5 Streaming of neutrons through access plug and access hole

The perturbation of the NISUS neutron field by the access plug and access hole should be found correctly - most importantly for reliable inter-comparisons of fission rate measurements by means of fission chamber and activation foils. The access plug is used to

TABLE 4.3

Fissionable deposits exposed at the centre of NISUS standard neutron field

Foil identification and principal isotope	Deposit diameter (mm)	Isotopic concentration (atom per cent)	Mass of principal isotope	
			µgm.	µgm/cm^2
NBS 49 I-1-1 ^{239}Pu	12.7	^{239}Pu : 99.11; ^{240}Pu : 0.0880; ^{241}Pu : 0.010; ^{242}Pu : 0.005	105.1±1.3%	83.0
NBS 28 N-5-2 ^{238}U	12.7	^{238}U : 99.275; ^{235}U : 0.72	686±1.4%	541.5
NBS 25 S-2-3 ^{235}U	12.7	^{235}U : 99.748; ^{238}U : 0.1261; ^{234}U : 0.0608; ^{236}U : 0.0652	222±1.2%	175.2
NBS 37 S-5-2 ^{237}NP	12.7	^{237}NP : 99.3; ^{239}Pu : 0.68	630±1.8%	497.3
NBS 28 HD-5-1 ^{238}U	12.7	^{238}U : 99.999; ^{235}U : ~ 0.0001	651±1.5%	513.9
ULRC -3 ^{238}U	20.3±0.2	^{238}U : 99.965; ^{235}U : 0.035	780.6±1.9%	241.2
ULRC -6 ^{235}U	20.0±0.1	^{235}U : 93.0; ^{238}U : 7.0	326.3±1.3%	102.8

measure fission and non-fission reaction rates by activation foils and the access hole is used to measure fission rates by fission chambers.

4.5.1 Perturbation due to access plug

It has been observed from NISUS reaction rate traverses (explained in detail in Section 4.8) for $^{197}Au(n,\gamma)^{198}Au$ and $^{55}Mn(n,\gamma)^{56}Mn$ reactions with the access plug that there may exist some streaming of neutrons through the access plug. This streaming effect is found only at the reaction rate closest to the access plug though the effect is small. Reaction rate traverses for these two reactions in the present work are compared with the reaction rate traverses for NISUS by Azad[42] (shown in Fig. 4.9 in section 4.7.5). Azad did not find any streaming effect for these two reactions using the same access plug as used in the present work. Fabry determined reaction rate traverses for these two reactions experimentally and theoretically for MOL-ΣΣ neutron field[10]. No streaming effect for MOL-ΣΣ was observed when there was no access hole. The streaming effect due to the access plug is considered negligible for foil exposed at the centre of NISUS and no correction has been made for this effect in reaction rate measurements.

4.5.2 Perturbation due to access hole

Fission rate measurements have been performed by NBS fission chambers. The chamber is held within a natural uranium plug so that the access hole diameter is 17 mm, the same as in ΣΣ and is shielded

by 1 mm thick cadmium screens (Fig. 4.2.(a)). But the hole in the Boron carbide shell has a diameter of 45 mm in NISUS instead of 15.5 mm in ΣΣ which may cause streaming of epithermal and thermal neutrons through the access hole. In order to confirm thermal neutron leakage, three runs were performed for ^{235}U, ^{239}Pu, ^{238}U and ^{237}Np deposits:

(i) by bare fission chamber,

(ii) by surrounding fission chamber with a 1 mm thick cadmium box,

(iii) by moving the inner cadmium screen (umbrella) closer to NISUS centre (at ∿ 2 cm from NISUS centre) (Fig. 4.2.(b)).

From these three measurements it was found that bare ^{235}U and ^{239}Pu had a ∿ 1% higher fission rate than cadmium covered ^{235}U and ^{239}Pu fission rates due to thermal neutron stremaing through the access hole. The thermal neutron streaming effect has been shown in Table 4.4[34].

Epicadmium access hole correction for ^{235}U and ^{239}Pu fission rates in ΣΣ has been determined as (0.5 ± 0.5)% by Fabry et al[44]. This figure cannot be applied straight away to NISUS because the hole in the boron carbide shell is much bigger than in ΣΣ while the hole in the uranium shell is identical. A separate measurement has been performed by means of activation foils. NBS chambers were not available during these experiments so ULRC chambers were used after fixing an annular piece of cadmium around the inner edge of access hole on the boron carbide shell and cadmium cover on the inner surface of

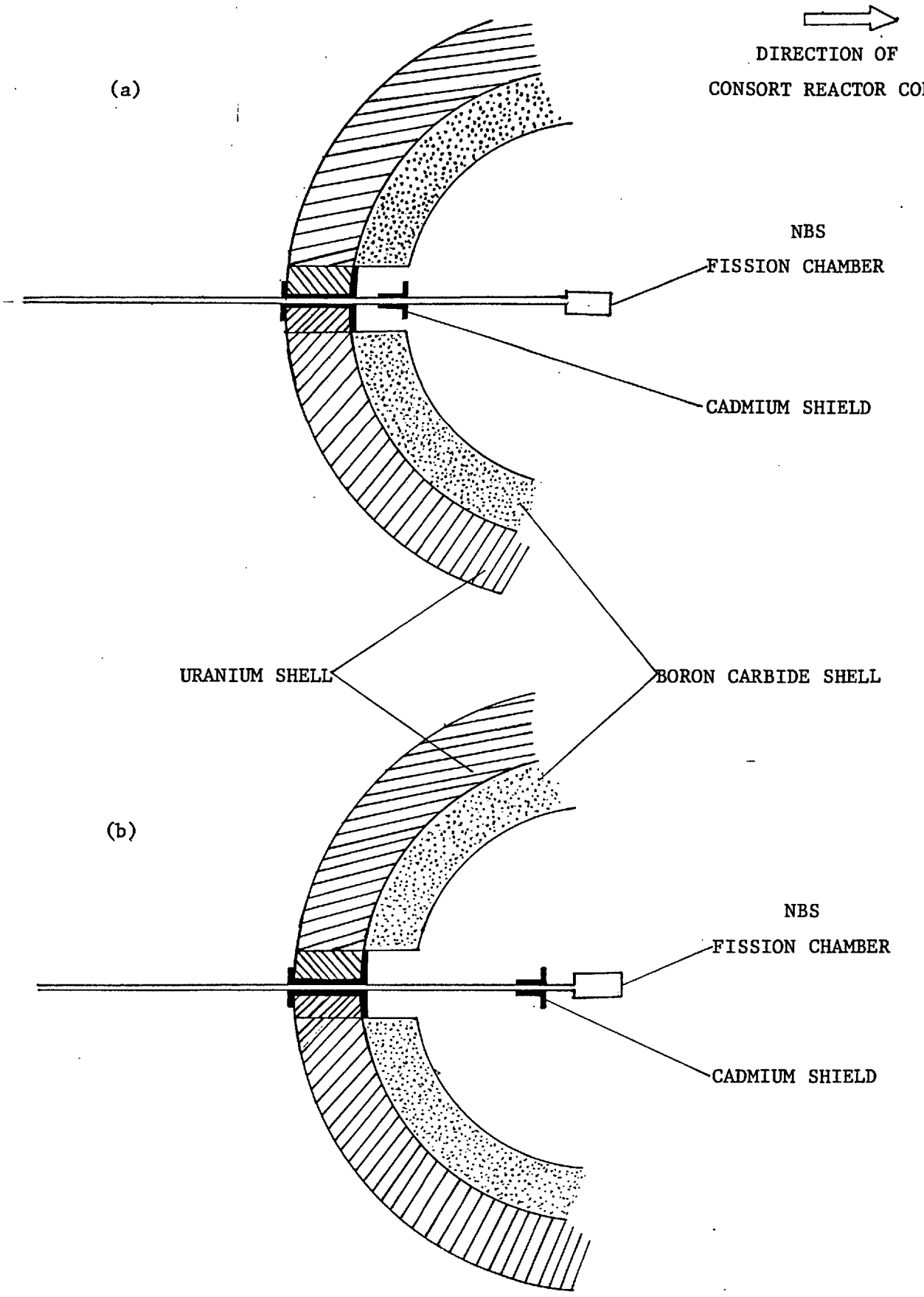


Fig.4.2(a&b). Cross-sectional sketch of the NBS fission chamber for fission rate measurements in NISUS.

TABLE 4.4

Effects of thermal neutron streaming through the access hole in the fission ratio measurements in the NBS fission chamber

Fission ratio	NISUS			ΣΣ
	Bare chamber	Cadmium umbrella	Cadmium Box	
$^{239}Pu/^{238}U$	21.29	20.90	20.72	20.85
$^{239}Pu/^{235}U$	1.197	1.186	1.177	1.175
$^{237}Np/^{235}U$	0.3783		0.3805	0.380
$^{238}U/^{235}U$	0.05669		0.05735	0.05636

the uranium plug so that thermal neutron streaming is kept to a minimum (Fig. 4.3.)

In the first experiment two uranium foils (one enriched and one depleted) each wrapped by 0.0254 mm thick aluminium catcher foil were sandwiched between the two ULRC deposits (^{235}U and ^{238}U). The ULRC chamber was then inserted inside NISUS and irradiated for a few hours. In the second experiment two uranium foils each wrapped by aluminium catcher foil were irradiated with the solid access plug only. The fission rates of ^{235}U and ^{238}U as a function of decay time were determined by total integral counting method (explained in Section 4.8). The ratio of fission rate of ^{235}U without fission chamber and with fission chamber was determined for several runs and the average value with error is given in Table 4.5. Similarly the average value of the fission rate of ^{238}U was determined and is shown in Table 4.5. These ratios will show the effect of epicadmium access hole perturbation and scattering in the ULRC chamber. To check the consistency of the measurements of fission foils for epicadmium access hole perturbation, four more experiments were performed in the following way:

(a) Indium foil was sandwiched between two ULRC deposits in the chamber and irradiated.

(b) Indium foil was irradiated with access plug only (without fission chamber).

(c) Indium foil was irradiated with uranium access plug but no boron carbide plug.

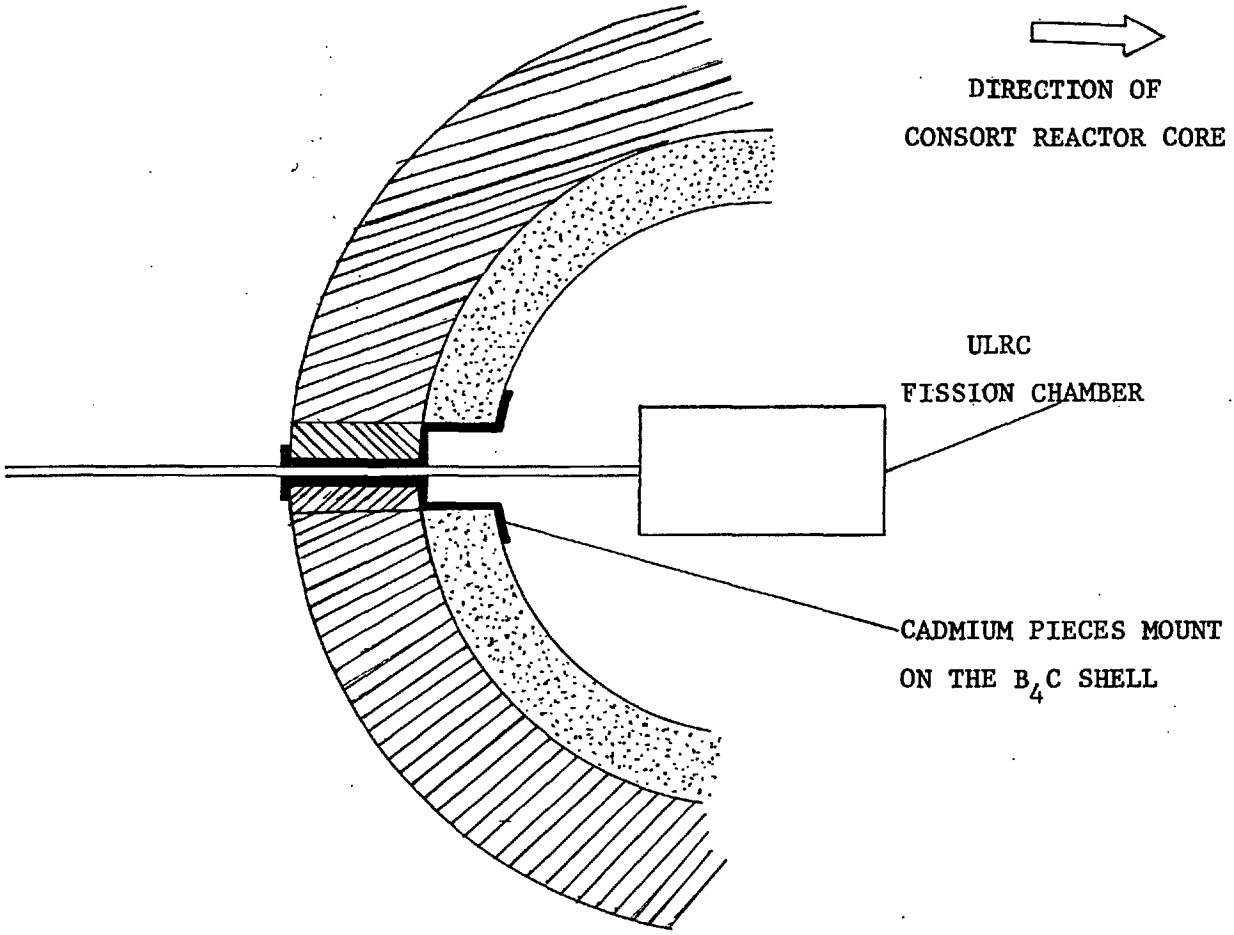


Fig.4.3. Cross-sectional sketch of the ULRC fission chamber with modification to the access hole for fission rate measurements in NISUS.

TABLE 4.5

Effect of access hole perturbation and fission chamber body for non threshold and threshold reactions[(a)] in ULRC fission chamber in NISUS

Fission rate of ^{235}U without fission chamber per F.C. monitor	Fission rate of ^{238}U without fission chamber per F.C. monitor
Fission rate of ^{235}U with fission chamber per F.C. monitor	Fission rate of ^{238}U with fission chamber per F.C. monitor
0.995 ± 0.5%	1.007 ± 0.9%

(a) Random error with 1 σ confidence level.

(d) Indium foil was irradiated with access plug only (without fission chamber).

Indium foil was used because the energy responses of $^{115}In(n,\gamma)^{116m}In$ and $^{115}In(n,n')^{115m}In$ reactions are similar to $^{235}U(n,f)$ and $^{238}U(n,f)$ reactions. The ratio of $^{115}In(n,\gamma)^{116m}In$ reaction rate without fission chamber and with fission chambers was determined. In the same way, the ratio of $^{115}In(n,n')$ reaction rate was determined. Similarly the ratio of $^{115}In(n,\gamma)^{116m}In$ and $^{115}In(n,n')^{115m}In$ with boron carbide and without boron carbide in the access plug were determined.

The ratio of fission rates of fission foils and Indium reaction rates with fission chamber and without fission chamber and the ratio of Indium reactions rates with and without B_4C shell in the access plug are given in tables 4.6 and 4.7. By comparing the ratio of fission rates and reaction rates in table 4.6 and 4.7, the correction for epicadmium access hole perturbation for non threshold fission reaction is $(0.5\pm0.5)\%$ for NISUS given in Table 4.8. Epicadmium access hole correction for $\Sigma\Sigma$ is $(0.5\pm0.5)\%$ for non threshold fission reaction[43] and negligible for threshold fission reaction[44]. It is found that the epicadmium access hole perturbation for non threshold fission reaction is the same for these two neutron fields. But in the case of threshold fission detector, the correction is $(1.1\pm0.4)\%$ for NISUS whereas this is negligible for $\Sigma\Sigma$. So further investigation is required to resolve the discrepancy for non threshold fission reactions in these two neutron fields. It must be noted,

TABLE 4.6

Effect of epicadmium access hole perturbation and fission chamber body for non-threshold reactions inside NISUS facility.

$\frac{\text{Fission rate of } ^{235}U \text{ without F.C.}}{\text{Fission rate of } ^{235}U \text{ with F.C.}}$ (a,d)	$\frac{\text{In } (n,\gamma) \text{ reaction rate without F.C.}}{\text{In } (n,\gamma) \text{ reaction rate with F.C.}}$ (a,b,e)	$\frac{\text{In } (n,\gamma) \text{ reaction rate with } B_4C \text{ in access plug}}{\text{In } (n,\gamma) \text{ reaction rate without } B_4C \text{ in access plug}}$ (a,c,f)
0.995 ± 0.5%	0.985 ± 2%	0.553 ± 1.3%

(a) Random error with 1 σ confidence level.

(b) Agrees with ^{235}U fission foil measurement, but poor precision.

(c) This ratio is not considered because no cadmium shielding was used in this measurement.

(d) Fission rate normalised by fission chamber monitor for power monitoring.

(e) Reaction rate normalised by Au monitor because fission chamber monitor was not used.

(f) Average value of reaction rate normalised by both fission chamber monitor and Au monitor.

TABLE 4.7

Effect of epicadmium access hole perturbation and fission chamber body for threshold reaction in NISUS facility.

$\frac{\text{Fission rate of } ^{238}U \text{ without F.C.}}{\text{Fission rate of } ^{238}U \text{ with F.C.}}$ (a,c)	$\frac{\text{In (n,n') reaction rate without F.C.}}{\text{In (n,n') reaction rate with F.C.}}$ (a,b,d)	$\frac{\text{In (n,n') reaction rate with } B_4C \text{ shell in access plug}}{\text{In (n,n') reaction rate without } B_4C \text{ shell in access plug}}$ (a,b,e)
1.007 ± 0.9%	1.013 ± 0.4%	1.011 ± 0.4%

(a) Random error with 1 σ confidence level.

(b) Agreed with ^{238}U fission rate measurement.

(c) Fission rate normalised by fission chamber monitor for power monitoring.

(d) Reaction rate normalised by Au monitor for power monitoring because fission chamber monitor was not used at that time.

(e) Average value of reaction rate normalised by both fission chamber monitor and Au monitor is taken.

TABLE 4.8

Correction for epicadmium access hole perturbation and U L R C fission chamber body to non threshold and threshold reactions in fission chamber in NISUS

Correction factor	
Non threshold fission reaction	Threshold fission reaction
0.995±0.5%	1.011±0.4%

however, that this figure is due to a combination of scattering in the fission chamber body and perturbation due to the access hole. The correction found for $\Sigma\Sigma$ with an NBS chamber and attributed to the chamber only is $(0.6\pm0.3)\%$ [43].

4.6 Detector responses in the NISUS spectrum

The response of a detector or its activation by neutrons, is proportional to the product of the differential activation cross section, $\sigma(E)$ and the differential flux spectrum $\Phi(E)$:

$$I = k \int_0^\infty \sigma(E)\Phi(E)\, dE \qquad (4.6.1)$$

where I = Integral response of a detector

k = Normalisation constant

$\sigma(E)$ = Energy dependent cross section for a particular detector.

$\Phi(E)$ = Fast neutron flux density per unit energy interval. In this case ΣΣ evaluated spectrum [10] is considered as NISUS and ΣΣ are two similar fast neutron fields.

Activation detectors are chosen in such a manner that their energy response should cover the entire range of the NISUS spectrum. The fractional response per unit lethergy as a function of neutron energy of threshold and non threshold detectors used in NISUS for reaction rate measurements is shown in Fig. 4.4. Threshold detectors have been shown separately again in Fig. 4.5 in a different scale as fractional response per unit energy (MeV) in order to show their responses more prominently in the high energy region.

The response of the detectors is also characterised by the energy range causing the bulk of the activation. Assuming ΣΣ evaluated spectrum, calculations show that the central 90% of the

activity induced in the detectors generally used for fast neutron measurements is caused by neutrons with the energy ranges listed in Table 4.9. The energy range covered by the neutron detectors for ~90% response in NISUS is 50ev - 12.50 MeV (shown in Table 4.9) which is essentially the fast neutron energy range. Energy response for the same activation detectors used in ΣΣ is similar to NISUS and ~90% energy response range for the ΣΣ spectrum is ~60.0eV - ~12.2 MeV [7].

Differences in the response function of detectors are the basis for methods developed to determine spectra from activation data.

4.7.1 Reaction rate measurements in the NISUS neutron field

Foils of various materials of importance in neutron dosimetry measurements were used for irradiation in NISUS standard neutron field. The specifications of the foils are given in Table 4.1. A set of five foils of the same material were mounted on the aluminium holder at the distance of 2cm from each other. The holder was designed to have the minimum amount of aluminium (thickness ~0.4mm) to reduce the spectrum perturbation. After loading the foils, the holder was screwed to the last section of the access plug and the plug was inserted into the NISUS facility. When the access plug is inside NISUS, the middle foil is at the centre of NISUS cavity (Fig. 4.6). Five foils of one material in each experiment were irradiated for a period of 7 hours at full reactor power (100kW) and the irradiation

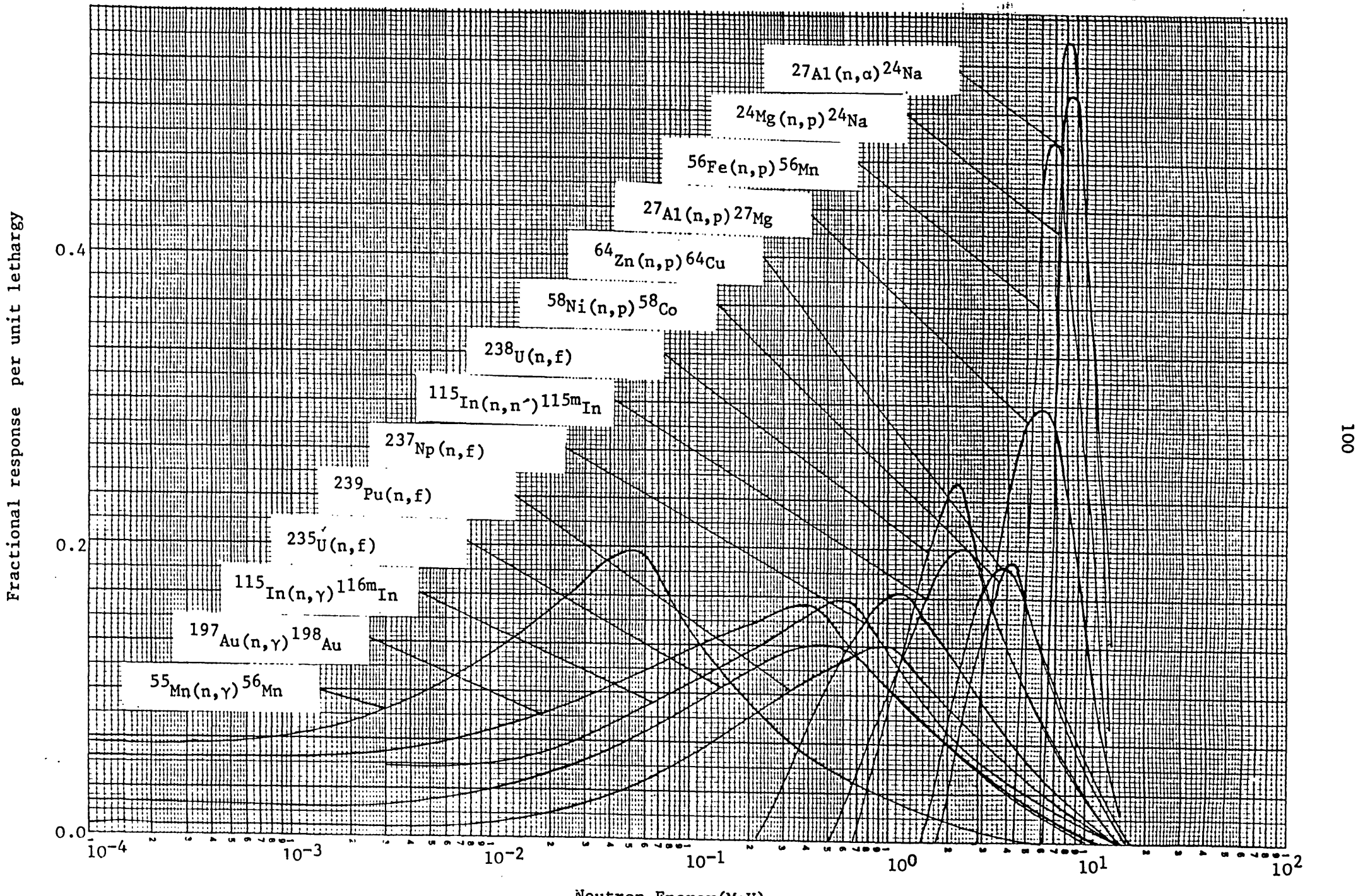


Fig.4.4. Threshold and Non-thresholddetector Responses in the NISUS spectrum.

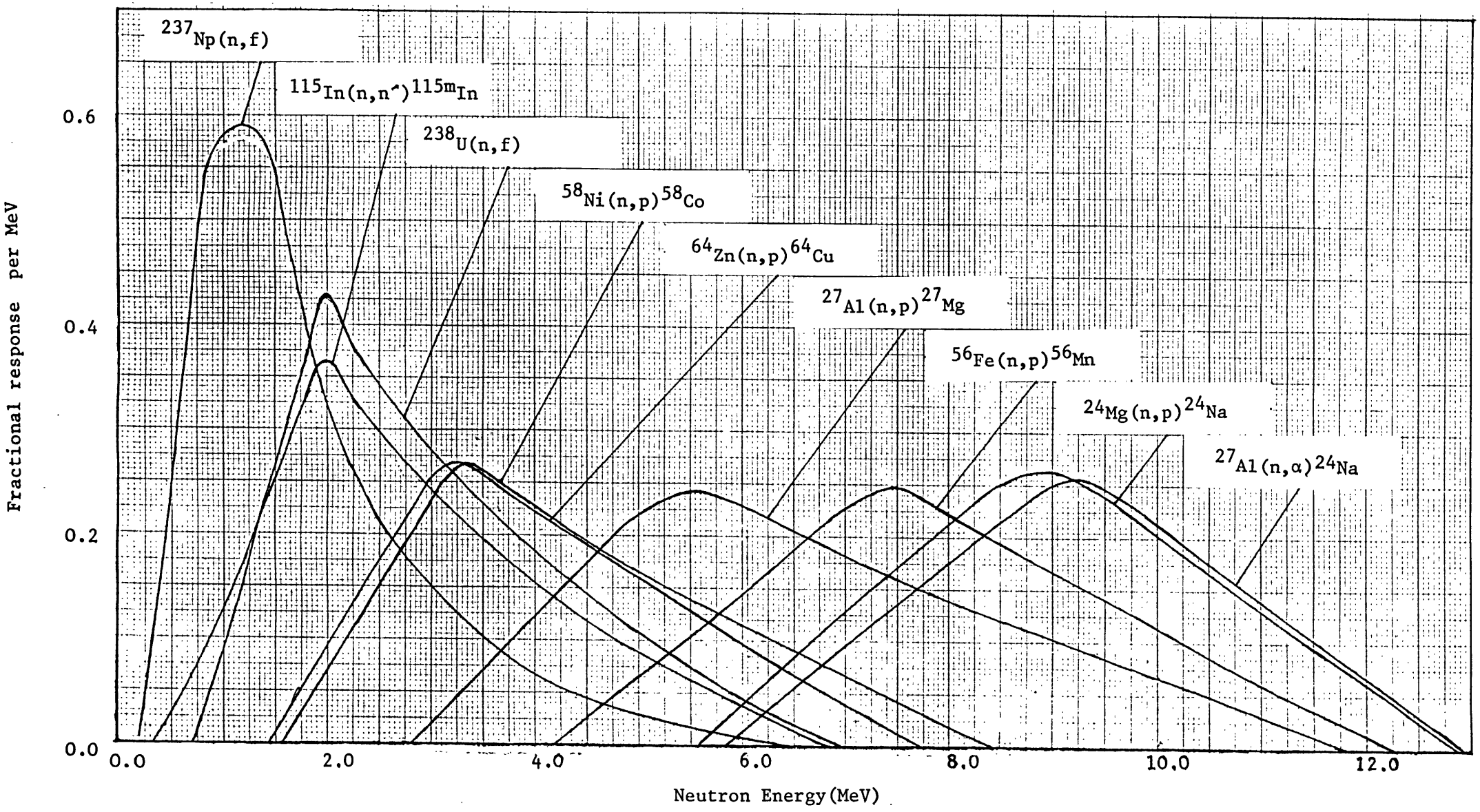


Fig.4.5. Threshold detector Responses in the NISUS spectrum.

TABLE 4.9

Energy Response of neutron detectors in the NISUS Spectrum

Reaction	Energy Response Range (a) (MeV)	
	E_L	E_u
^{197}Au (n,γ) ^{198}Au	5.0×10^{-5}	0.850
^{55}Mn (n,γ) ^{56}Mn	3.0×10^{-4}	1.30
^{115}In (n,γ) ^{116m}In	4.0×10^{-4}	1.60
^{235}U (n,f) F.P.	6.0×10^{-4}	3.00
^{239}Pu (n,f) F.P.	5.0×10^{-2}	3.60
^{237}NP (n,f) F.P.	0.45	4.60
^{115}In (n,n') ^{115m}In	0.85	5.80
^{238}U (n,f) F.P.	1.40	7.00
^{58}Ni (n,p) ^{58}CO	2.00	7.45
^{64}Zn (n,p) ^{64}Cu	2.23	7.50
^{27}Al (n,p) ^{27}Mg	3.30	9.00
^{56}Fe (n,p) ^{56}Mn	5.00	11.00
^{24}Mg (n,p) ^{24}Na	6.50	12.00
^{27}Al (n,α) ^{24}Na	6.40	12.50

(a) The lower (E_L) and upper (E_u) energy limits within which the central ~ 90% of the detectors energy response falls for the NISUS spectrum.

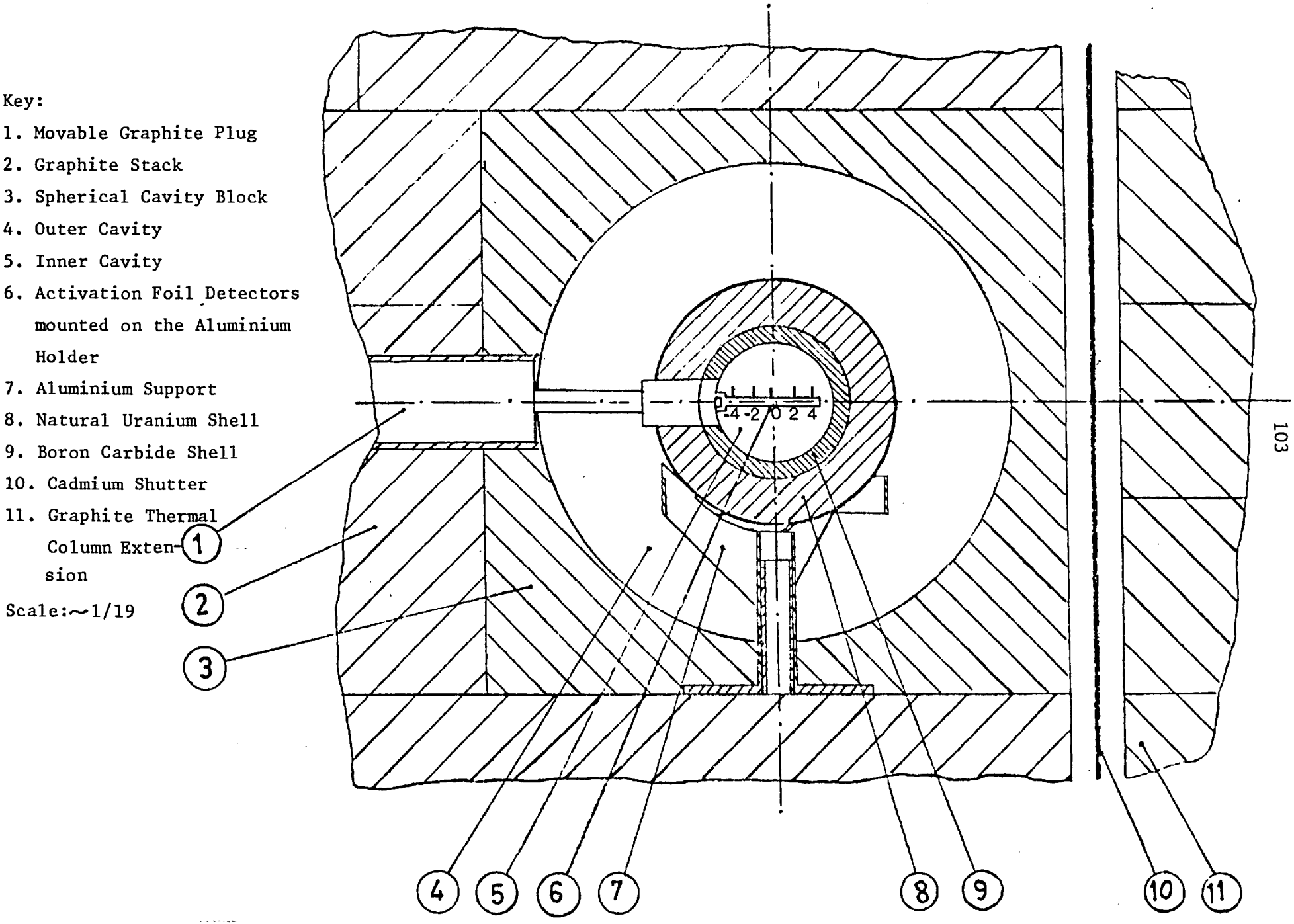


Fig. 4.6. Activation foil detectors inside the NISUS facility.

period was controlled by the cadmium shutter. Background counting of each foil was performed before irradiation.

After irradiation the foils were transfered to the counting room. Each foil was mounted on ~1.5mm thick aluminium foil tray and covered by aluminium to shield the detectors from β particles and the foils were placed in different positions of the sample changer. The gamma ray spectrum of each foil was measured by Ge(Li) detector. The positioning of five foils of the same material at different positions in the automatic sample changer was checked several times by measuring the reference ^{137}Cs source (No. A0906) at different positions of the sample changer. The positioning correction in the wheel was determined relative to the NISUS centre foil positioning in the wheel. The correction was found to be ~$\pm$1%. This correction was applied to the gamma ray spectrum of each foil where necessary. The block diagram of Ge(li) detector and the counting system is given in Fig. 2.3 chapter 2. Absolute gamma emission rates with Ge(Li) detector were determined after measuring the gamma spectrum at a standard source - detector distance for a preset counting time to give sufficient high count rate, determining the peak areas, applying appropriate corrections for external and self absorption, self shielding and peak detection efficiency. The peak area was determined by the classical method [17] (explained in section 2.2chapter 2). Since the count rates were low in all cases the dead time was within ~7% recorded by the analyser. All foils were counted in live time in the analyser so the dead time

was corrected automatically by the analyser itself. External absorber and self absorption corrections of gamma rays were performed according to section 4.3.1. Self shielding corrections were applied to the activation detectors where necessary according to section 4.3.2(a). Peak detection efficiency of the Ge(Li) detector was obtained from Chapter 2. Then these absolute gamma ray emission rates have been used to compute reaction rates. It was thought from the decay scheme of the activated foils[22] used in this work that the gamma rays of different energies considered for reaction rate measurements would not have appreciable coincidence summing effects. So no correction was done for this effect. An error of a few per cent[52] may arise in the results for $^{58}Ni(n,p)^{58}Co$ due to the omission of such a correction. However, the correction for coincidence summing effect for $^{58}Ni(n,p)^{58}Co$ reaction has been determined according to Ref. 74. and the correction determined was 2.9% (explained in Appendix C).

4.7.2 Calculation of reaction rates

The saturation activity is given by the expression (2.1.7):

$$A_B^{ta}(s) = \frac{A_B^{td}\{\exp(\lambda_B td)\}}{\{1-\exp(-\lambda_B ta)\}}$$

$$= \frac{\lambda_B N_B\{\exp(\lambda_B td)\}}{\{1-\exp(-\lambda_B ta)\}} \qquad (4.7.1)$$

Where N_B is the number of activation product nuclides at the start of counting.

$$N_B = \frac{C}{b\ \eta\left|1-\exp(-\lambda_B\ t_c)\right|} \qquad (4.7.2)$$

Where C = Peak area due to gamma spectrum.

b = Gamma ray branching ratio.

η = Ge(Li) detector efficiency.

Thus the absolute reaction rate becomes

$$A_s = A_B^{ta}(S) = \frac{C}{b\ \eta}\ \frac{\left|\exp\ (\lambda_B\ t_d)\right|\ \lambda_B}{\left|1-\exp(-\lambda_B\ t_a)\right|\ \left|1-\exp(-\lambda_B\ t_c)\right|}$$

The absolute activity per atom of the foil can be calculated if the number of atoms in the foil is known:

$$N = \frac{m\ p\ N_o}{a}$$

Where m = Foil mass.

p = Fraction of foil mass for isotope of interest.

N_o = 6.022×10^{23}

a = Atomic mass of isotope of interest.

Therefore the absolute activity per atom of the foil per second is given by

$$A = \frac{C}{b\,\eta}\ \frac{\exp(\lambda_B\, t_d)\lambda_B}{|1-\exp(-\lambda_B\, t_a)|\ |1-\exp(-\lambda_B\, t_c)|}\ \frac{a}{m\ p\ N_o}\ \frac{1}{f_1 f_2 f_3} \qquad (4.7.3)$$

Where f_1 = Correction for gamma ray self shielding.

f_2 = Correction for attenuation of gamma ray in external absorber.

f_3 = Correction for attenuation of gamma ray in the sample itself.

4.7.3 Uncertainties in absolute reaction rate

Table 4.10 lists the components that contribute to the total uncertainties in the measured reaction rates. It is not necessary to deal with all quantities mentioned in Table 4.10, because some of them contribute relatively very little to the total error on the saturation activity.

The weight of the foils were measured to 10^{-5}gm which gives uncertainty in the foil weight < 0.3%.

The diameter of activation foils is ≈ 12.7 mm but point sources were used for the efficiency calibration of the Ge(Li) detector. Correction

TABLE 4.10

Summary of the estimate of error contributions to the total error in absolute reaction rates

Source of Error	Estimate of Error
Net Peak area (C)	$\sigma_C = \pm \left[(\sigma)^2_{\text{Total counts}} + (\sigma)^2_{\text{Background counts}} \right]^{\frac{1}{2}} \times 100\%$ / C
Radiation Intensity(b)	$\sigma_b = \pm \frac{\Delta b}{b} \times 100\%$ Table 4.1 Section 4.2
Peak efficiency (η)	$\sigma_\eta = \pm \frac{\Delta \eta}{\eta} \times 100\%$ ($\sim \pm 2\%$ for ~ 300 Kev $< E_\gamma < 2$ Mev)
Foil mass (m)	$\sigma_m = \pm \frac{\Delta w}{w} \times 100\%$ ($< 0.3\%$)
Self shielding(f_1)[a]	σ_{f1} Not applied.
External absorber(f_2)[b]	σ_{f2} Not applied.
Radiation self absorption (f_3)	σ_{f3} = negligible.
Monitor consistency and positioning	Applied according to Sections 4.7.4 & 5.1.
Counting stability	$\sim \pm 1\%$
Positioning in wheel[c]	$\sim \pm 1\%$

(a) Self shielding correction is applied only to $^{197}Au(n,\gamma)$ reaction. Error in the self shielding is not available from Ref.10.

(b) This correction is very small and not applied to the reaction rate measurement. So, this uncertainty is not accounted in the total uncertainty evaluation.

(c) This error is applied to the total error when Reaction-rate-traversing was considered.

has not been applied for the finite source area of activation foils (explained in detail in Appendix A II).

In general, quantities in equation (4.7.3) are conventionally separated into two types, those contributing to the random errors and those which are associated with the systematic errors. The random and systematic errors can be expressed using the equation as:

$$(\Delta A)^2 = \pm (\frac{\delta A}{\delta X})^2 \Delta x^2 + (\frac{\delta A}{\delta Y})^2 \Delta Y^2 \pm (\frac{\delta A}{\delta Z})^2 \Delta Z^2 \qquad (4.7.4)$$

Where A is a function of X, Y, Z etc., and ΔA, ΔX, ΔY, ΔZ are the absolute errors in A, X, Y, Z etc., and $(\frac{\delta A}{\delta X})$, $(\frac{\delta A}{\delta Y})$, $(\frac{\delta A}{\delta Z})$ are the partial deriviatives at A with respect to X, Y, Z etc., respectively.

Each foil was counted several times. The weighted mean of the absolute activity can be determined[45] from:

$$\bar{A} = \frac{\sum_{i=1}^{n} A_i W_i}{\sum_{i=1}^{n} W_i} \qquad (4.7.5)$$

Where $W_i = \frac{1}{(\Delta A_i)^2_{random}}$ (4.7.6)

and n is the number of counting runs. The average random error in $\bar{A}$ is given by $(\Delta\bar{A})_{random}$ and can be computed from the following equation:

$$\frac{1}{(\overline{\Delta A})^2_{random}} = \sum_{i=1}^{n} \frac{1}{(\Delta A_i)^2_{random}} \quad (4.7.7)$$

The total error in reaction rate measurement is expressed in the form:

$$(\Delta A) = \left| (\Delta\bar{A})^2_{random} + (\Delta A)^2_{sys} \right|^{\frac{1}{2}} \quad (4.7.8)$$

Such a combination of errors is only valid if there is no correlation between the components.

A computer program SAT ACT was written to calculate the reaction rate and error of each foil. All the information about the foil, its irradiation time, decay time, count rate and the detector specifications are read into the program as data.

4.7.4 Reactor power monitoring

Before mentioning the absolute reaction rate data, it is necessary to make day-to-day reactor power monitoring of each irradiation. The reaction rates of each foil were measured relatively to a specific NISUS monitoring scheme essentially based on the activation reactions $^{115}In(n,n')^{115m}In$ and $^{197}Au(n,\gamma)^{198}Au$. This has been backed by using two pulse fission chambers during the time of fission rate measurements by NBS double fission chambers[43] and subsequent central reaction rate measurements to check reproducibility. The activation monitors and fission chamber monitors are placed as follows:

(1) Indium foil at a distance of 3 cm (towards the core) from the centre of NISUS within the central exposure zone as shown in Fig. 4.6.

(2) Gold foils are placed in NISUS thermal column extension. Fig. 4.7 shows a schematic diagram of the position details of the foil-monitors. The foils are placed in the positions A and B of the square graphite plug and loaded in the hole 1 of the NISUS thermal column. Hole No. 1 is chosen because it is far enough from NISUS to be uninfluenced by its presence and also not close to the edge of the graphite stack to avoid too much thermal flux gradient effect.

(3) Two pulse fission chambers type FC4A/1000/235 with sensitivity of 3×10^{-3} cps/nV (Fission chamber monitor 1 and Fission chamber monitor 2) have been positioned in the graphite stack 1 with different distances with respect to the cadmium shutter. Details are shown in Fig. 4.8.

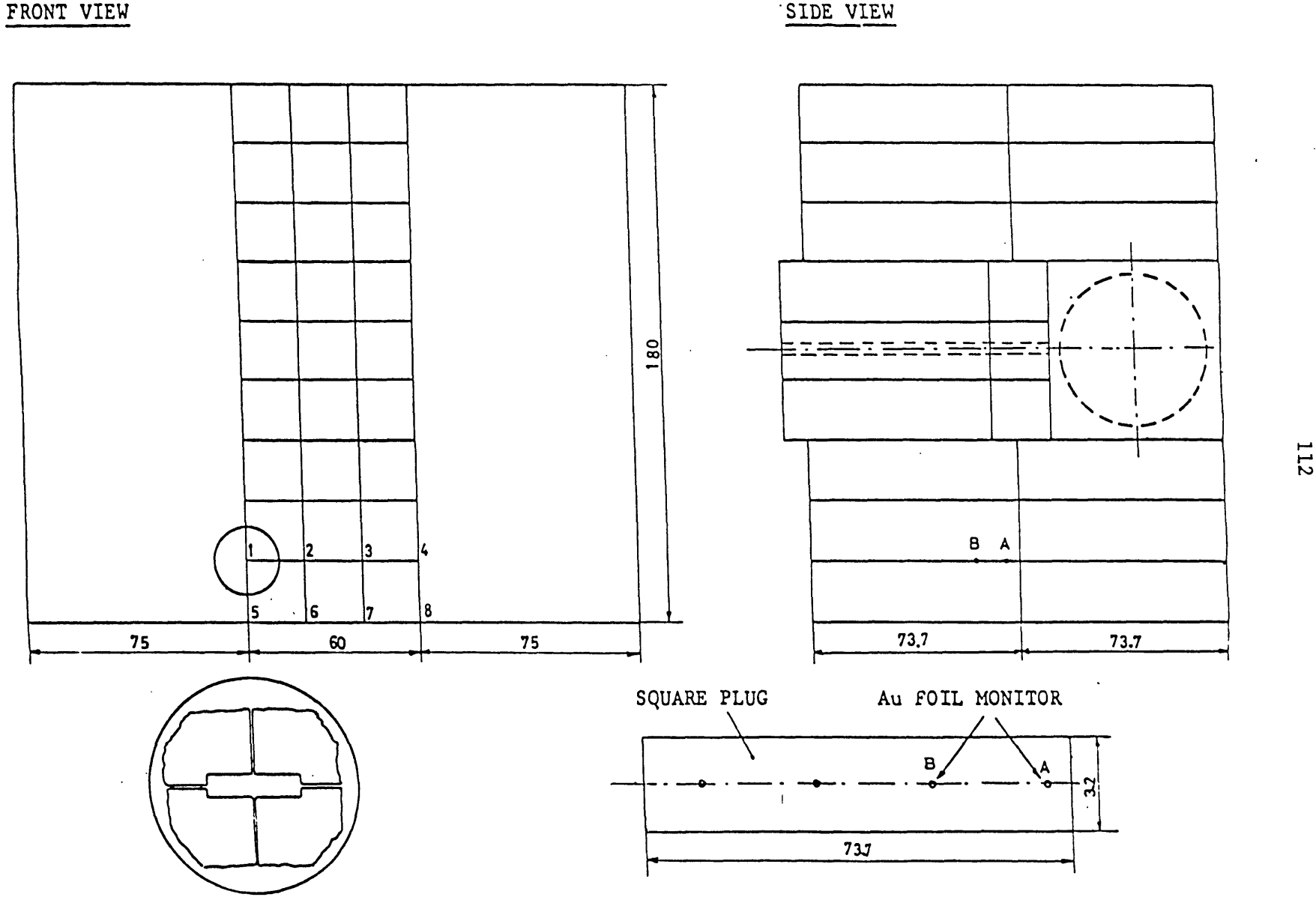


Fig. 4.7. Block diagram of the position details of Au foil monitors.

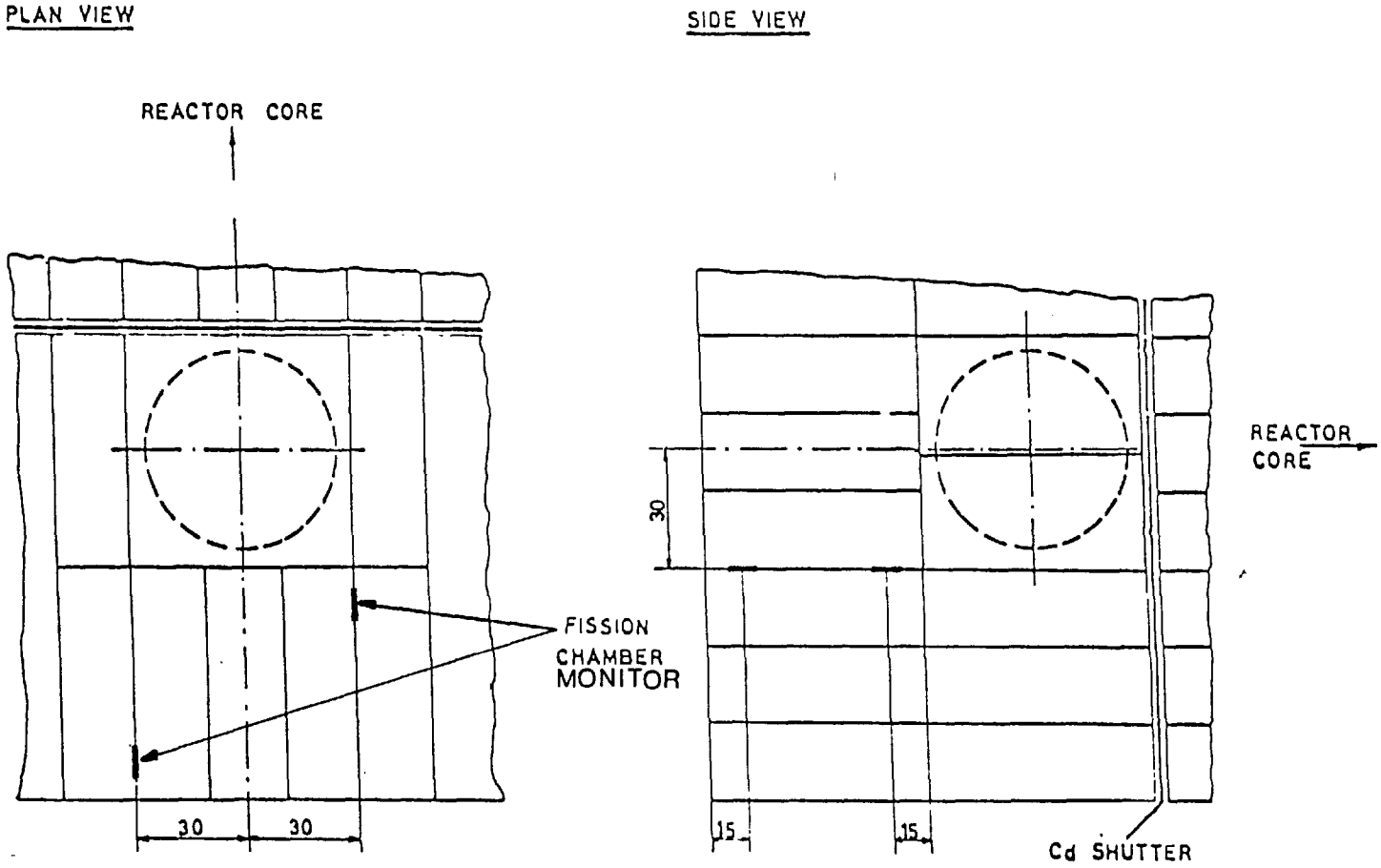


Fig.4.8. Block diagram of the position details of Fission chamber monitors.

The saturated activity per atom of $^{115}In(n,n')^{115m}In$ and $^{197}Au(n,\gamma)$ reactions is calculated using equation(4.7.3) and program SAT ACT.No self shielding correction is made for $^{197}Au(n,\gamma)^{198}Au$ reaction because reaction rate of various activation detectors is measured relative to monitor saturated activity. The monitor chambers are connected to the dual triple scalar counting system to get monitor counts at short intervals[34].

Table 4.11 shows the reproducibility and linearity of day-to-day reactor power monitoring by activation foils for a period of five months for reaction rate measurements of activation detector in five positions inside the inner cavity of NISUS. The variation in $^{115}In(n,n')^{115m}In$ reaction is $\sim$ 1.7% (1σ) and in $^{197}Au(n,\gamma)^{198}Au$ reaction position A is $\sim$ 1.1% (1σ) and in position B is $\sim$ 1.2% (1σ).

Table 4.12 shows the reproducibility of day-to-day reactor power monitoring by fission chambers and gold foils during fission rate measurements by NBS fission chambers in NISUS for a period of one week. Monitor Indium foil could not be used with NBS fission chambers inside the inner cavity of NISUS. The variations in fission chamber monitor 1 is $\sim$ 0.4% (1σ) and while that of monitor 2 is $\sim$ 0.13% (1σ). In the case of Au foil monitors the variations in position A is $\sim$ 1.3% (1σ) and in position B is $\sim$ 1.3% (1σ).

TABLE 4.11

Day-to-Day Reactor Power monitoring by means of activation detectors (a) (Reactor Power 100 KW) (February-June, 1975)

Run	Reaction	$^{115}In(n,n')^{115m}In$ reaction rate/atom $\times 10^{-18}$	$^{197}Au(n,\gamma)^{198}Au$	
			Position A $\times 10^{-15}$	Position B $\times 10^{-16}$
1	$^{55}Mn(n,\gamma)^{56}Mn$	7.4267± 0.44%	1.0476± 0.16%	6.5493± 0.18%
2	$^{115}In(n,\gamma)^{116m}In$	7.5061± 0.31%	1.0439± 0.17%	6.4036± 0.19%
3	$^{197}Au(n,\gamma)^{198}Au$	7.5693± 0.36%	1.0529± 0.17%	6.4894± 0.20%
4	$^{235}U(n,f)$ F.P.	7.6252± 0.25%	1.0631± 0.18%	6.5493± 0.21%
5	$^{115}In(n,n')^{115m}In$	7.5959± 0.29%	1.0807± 0.16%	6.5325± 0.23%
6	$^{238}U(n,f)$ F.P.	7.3062± 0.18%	1.0796± 0.15%	6.3163± 0.24%
7	$^{58}Ni(n,p)^{58}CO$	7.8358± 0.19%	1.0716± 0.16%	-
8	$^{64}Zn(n,p)^{64}Cu$	7.4684± 0.20%	1.0683± 0.18%	6.5224± 0.24%
9	$^{27}Al(n,p)^{27}Mg$ Pos 1	7.6358± 0.31%	1.0649± 0.17%	6.5128± 0.29%
10	$^{27}Al(n,p)^{27}Mg$ Pos 2	7.5563± 0.31%	1.0548± 0.18%	6.4327± 0.22%
11	$^{27}Al(n,p)^{27}Mg$ Pos 3	7.6190± 0.30%	1.0629± 0.16%	6.5237± 0.23%
12	$^{27}Al(n,p)^{27}Mg$ Pos 4	7.6593± 0.32%	1.0737± 0.17%	6.6453± 0.25%
13	$^{27}Al(n,p)^{27}Mg$ Pos 5	7.7202± 0.37%	1.0734± 0.16%	6.6051± 0.24%
14	$^{56}Fe(n,p)^{56}Mn$	7.4959± 0.37%	1.0513± 0.16%	6.4922± 0.25%
15	$^{24}Mg(n,p)^{24}Na$	7.4992± 0.29%	1.0522± 0.20%	6.4723± 0.26%
16	$^{27}Al(n,\alpha)^{24}Na$	7.5343± 0.19%	1.0732± 0.17%	6.5436± 0.23%

(a) Quoted uncertainties statistical only (1σ level).

TABLE 4.12

Day-to-Day Reactor Power monitoring[(a)] by fission chambers and Gold foils for fission rate measurement by NBS chambers

(Reactor Power 100 KW) (June 14-20, 1975)

Run	Foil identification	Fission chamber		$^{197}Au(n,\gamma)^{198}Au$	
		Monitor 1 (CPS)	Monitor 2 (CPS)	Position A $x10^{-15}$	Position B $x10^{-16}$
1	^{235}U	1323.0±0.06%	548.4±0.07%	1.0438±0.24%	6.4350±0.30%
2	^{239}Pu	1313.3±0.05%	546.8±0.07%	1.0351±0.31%	6.4121±0.40%
3	^{237}NP	1323.1±0.05%	548.1±0.09%	1.0643±0.20%	6.5936±0.30%
4	^{238}U	1323.9±0.05%	547.8±0.09%	1.0596±0.20%	6.4616±0.45%

(a) Quoted uncertainties statistical only (1^{σ} level).

TABLE 4.13

Day-to-Day Reactor Power monitoring by fission chambers and Gold foils for NISUS central reaction rate[a] measurement (Reactor Power 100 KW) (December, 1975 and February-May, 1976)

Run	Reaction	Fission chamber		$^{197}Au(n,\gamma)^{198}Au$	
		Monitor 1 (CPS)	Monitor 2 (CPS)	Position A $x10^{-15}$	Position B $x10^{-16}$
1	$^{55}Mn(n,\gamma)^{56}Mn$	1368.20±0.02%	542.63±0.03%	1.0605±0.22%	6.5184±0.30%
2	$^{115}In(n,\gamma)^{116m}In$ & $^{115}In(n,n')^{115m}In$	1355.07±0.04%	560.53±0.04%	1.0611±0.22%	6.5810±0.29%
3	$^{197}Au(n,\gamma)^{198}Au$	1357.97±0.02%	- [b]	1.0755±0.22%	6.5844±0.29%
4	$^{58}Ni(n,p)^{58}CO$	1337.97±0.02%	552.08±0.12%	1.0432±0.22%	6.5591±0.30%
5	$^{64}Zn(n,p)^{64}Cu$	1340.38±0.02%	550.22±0.09%	1.0560±0.23%	6.4164±0.29%
10	$^{27}Al(n,p)^{27}Mg$	1288.32±0.38%	- [b]	1.0408±0.22%	6.3170±0.30%
7	$^{56}Fe(n,p)^{56}Mn$	-	-	1.0402±0.22%	6.4457±0.28%
8	$^{56}Fe(n,p)^{56}Mn$	1353.55 0.04%	564.06±0.04%	1.0549±0.25%	6.5543±0.31%
9	$^{24}Mg(n,p)^{24}Na$	- [b]	587.35±0.06%	1.0297±0.23%	5.9569±0.31%
6	$^{27}Al(n,\alpha)^{24}Na$	1361.23±0.08%	562.93±0.33%	1.0768±0.24%	6.4326±0.29%

(a) Quoted uncertainties statistical only (1σ level).

(b) Fission chamber monitor did not work properly.

Table 4.13 gives the reactor power monitoring by fission chambers and gold foils for NISUS central reaction rate measurement of various activation detectors for a period of four months. It was found that the long term monitoring consistency may not be achieved by fission chambers due to the drifting in electronic system (gain and/or discrimination level)[34] as shown in run 9 Table 4.13. The variations in fission chamber monitor 1 is $\sim$ 1.9% (1σ) and in chamber monitor 2 is $\sim$ 2.6% (1σ). The variations in Au foil monitors in position A is $\sim$ 1.5% (1σ) and in position B is $\sim$ 3.0% (1σ).

By comparing Table 4.11, 4.12 and 4.13 it may be concluded that for long term monitoring in NISUS Au foil monitor in position A is more consistent than any other monitor in the present work. So all reaction rate data of fission and non fission detectors are normalised relative to the saturated activity of $^{197}Au(n,\gamma)^{198}Au$ monitor in position A.

4.7.5 Reaction rate traversing in NISUS

Reaction rates across the diameter of the inner cavity of NISUS assembly in the plane parallel to the thermal column axis of the CONSORT reactor core have been determined for various activation detectors. The reaction rate in five positions across a distance of 8 cm through the centre of NISUS was measured for each activation foil. The five positions inside NISUS are denoted as +4 cm and +2 cm (in the direction of reactor core), 0 (centre of NISUS), -2 cm and -4 cm (away from the core) (Fig. 4.6). Absolute reaction rates with

their errors for different detectors are given in Tables 4.14 - 4.23. Total uncertainties are estimated at 1σ confidence level. Reaction rate traverses are formed relative to central reaction rate in NISUS for each foil. Reaction rate traverses are fitted by least squares line except $^{55}Mn(n,\gamma)^{56}Mn$ and $^{197}Au(n,\gamma)^{198}Au$ reaction rates. The decrease across the diameter of the NISUS cavity is determined from the fitted line. Reaction rate traverses in NISUS for different activation foils are shown in Figs. 4.9 - 4.14. Errors shown in Figs. 4.9 - 4.14 are only statistical (1σ).

(1) $^{197}Au(n,\gamma)^{198}Au$ reaction

$^{197}Au(n,\gamma)$ reaction rates with their errors in five positions inside the NISUS cavity are given in Table 4.16. The reaction rates are corrected for self shielding effect according to section 4.3.2(a). Reaction rate traverses across the distance of 8 cm through the centre of NISUS are shown in Fig. 4.9(b). Only statistical error is considered for reaction rate traversing. Comparison of present reaction rate traversing has been made with those determined by Azad[42] as shown in Fig. 4.9(b). It is found that the reaction rate at a distance of -4 cm is higher than that of distance of -2 cm in the present work. Azad found lower value of the reaction rate at a distance of -4 cm than that of -2 cm. Fabry determined theoretical and experimental reaction rate traverses for $^{197}Au(n,\gamma)$ reaction in ΣΣ for both standard access hole and no access hole. He found that the reaction rate at -5 cm in ΣΣ is higher when there is an access hole and the reaction

rate is lower when there is no access hole[10]. By comparing the curves obtained by reaction rate traverses in NISUS (present work), NISUS (previous work[42]) and ΣΣ (reaction rate traverses data are not available at present) it is found that the present reaction rate traverses in NISUS do not agree with the previous measurements in NISUS but agree with those of ΣΣ when there is no access hole except that the reaction rate at -4 cm in NISUS should be lower but inspite it is higher which proves that there exists some streaming of neutrons through the access plug in NISUS though the effect may be small. As the access plug perturbation is affecting only the reaction rate at -4 cm and the effect is small, no correction has been made to the central reaction rate value.

(2) $^{55}Mn(n,\gamma)^{56}Mn$ reaction

$^{55}Mn(n,\gamma)$ reaction rates inside NISUS are given in Table 4.14. These reaction rates are not corrected for self shielding effect because no correction factor is available for this reaction. The experimental errors are ∿ 3.0%. Reaction rate traverses are shown in Fig. 4.9(a) and compared with reaction rate traverses determined in Ref. 42. Reaction rate traverses in NISUS agree both for present and previous measurement except reation rate at -4 cm is higher in the present work but lower in the previous work as shown in Fig. 4.9(a). Fabry also found higher value for reaction rate at -5 cm when there is an access hole[10]. The present reaction rate traverses confirms the streaming of neutrons through the access plug as observed in $^{197}Au(n,\gamma)$ reaction rate traverses in Fig. 4.9(b). No correction has been made for this access hole perturbation as the correction may be small and it affects only the reaction rate at -4 cm.

TABLE 4.14

^{55}Mn (n,γ) ^{56}Mn Absolute reaction rates

Position (cm)	Reaction-rate/atom[(a)] x 10^{-3}	Error[(b)] (%)
4	3.5058	±3.0
2	3.5646	±3.0
0	3.7408	±2.8
-2	3.5619	±3.1
-4	3.6048	±3.1

(a) Normalised to monitor ^{197}Au (n,γ) reaction rate per atom.

(b) All uncertainties are 1 σ estimates.

TABLE 4.15

^{115}In (n,γ) ^{116m}In Absolute reaction rates

Position (cm)	Reaction-rate/atom[(a)] x 10^{-3}	Error[(b)] (%)
4	31.255	±2.9
2	30.773	±2.9
0	29.688	±2.8
-2	29.754	±3.0
-4	27.925	±3.0

(a) Normalised to monitor ^{197}Au (n,γ) reaction rate per atom.

(b) All uncertainties are 1 σ estimates.

TABLE 4.16

$^{197}Au(n,\gamma)$ ^{198}Au Absolute reaction rates

Position (cm)	Reaction-rate/atom (a) x 10^{-3}	Error (b) (%)
4	49.867	± 2.8
2	50.377	± 2.8
0	50.355	± 2.8
-2	48.416	± 2.8
-4	48.785	± 2.8

(a) Normalised to monitor $^{197}Au(n,\gamma)$ reaction rate per atom.

(b) All uncertainties are 1 σ estimates.

TABLE 4.17

$^{115}In(n,n')$ ^{115m}In Absolute reaction rates

Position (cm)	Reaction-rate/atom (a) x 10^{-3}	Error (b) (%)
4	7.4826	± 2.8
2	7.1110	± 2.8
0	6.8803	± 2.8
-2	6.4099	± 2.8
-4	6.3681	± 2.8

(a) Normalised to monitor $^{197}Au(n,\gamma)$ reaction rate per atom.

(b) All uncertainties are 1 σ estimates.

(3) $^{115}In(n,\gamma)^{116m}In$ reaction

$^{115}In(n,\gamma)^{116m}In$ reaction rates for different positions in NISUS are given in Table 4.15. No self shielding correction has been made for this reaction because the correction is found negligible as shown in Fig. 4.1. The foils were counted after a decay of two half lives (∿ 2 hours) of the reaction product nuclide in order to bring the dead time in the analyser within ∿ 5%. The gamma spectrum is determined from 1.293 MeV gamma rays for $^{115}In(n,\gamma)^{116m}In$ reaction. Reaction rate traverses are shown in Fig. 4.10. The reaction rates are fitted by the least squares line. The reaction rate decreases by ∿ 10% across the NISUS cavity in the direction away from the core. Reaction rate traverses in Ref. 42 has been shown in Fig. 4.10 but these do not show a systematic decrease as observed in the present measurement. The fitted line does not agree with the experimental points in Azad's work.

(4) $^{115}In(n,n')^{115m}In$ reaction

The foils are counted after a decay of one half life (∿ 5 hours) of the product nuclide so that the gamma radiation from 0.336 MeV for $^{115}In(n,n')^{115m}In$ reaction is not interefered due to $^{115}In(n,\gamma)^{116m}In$ activity at 0.417 MeV. The reaction rates at different positions in NISUS are shown in Table 4.17. The experimental errors are within ∿ 3%. Reaction rate traverses are given in Fig. 4.11(a). The fitted reaction rate decreases by ∿ 17% across the distance of 8 cm through the centre of NISUS. This agrees with the ∿ 18% decrease given by

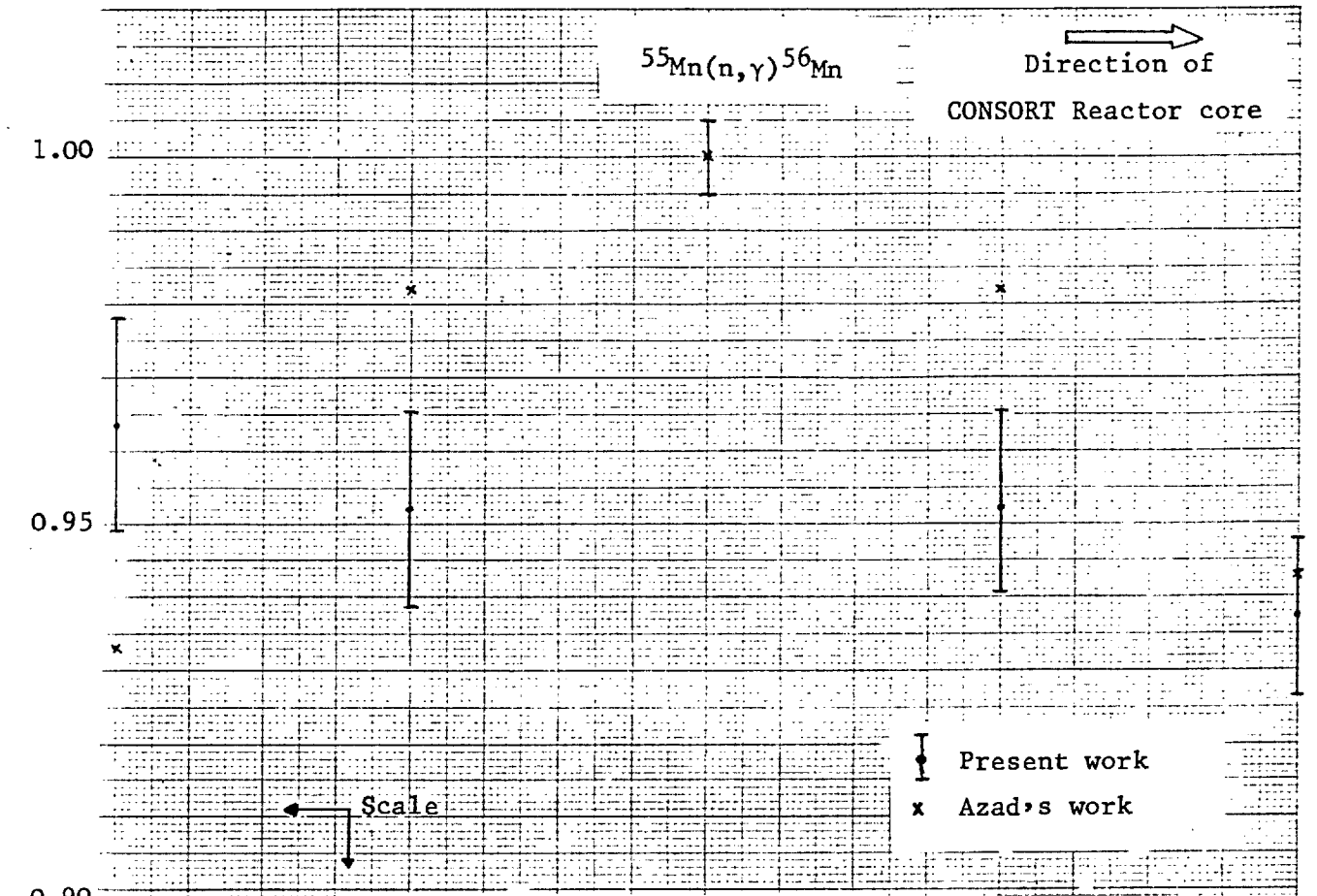


Fig.4.9(a). Reaction rate traverses in NISUS for $^{55}Mn(n,\gamma)^{56}Mn$ reaction.

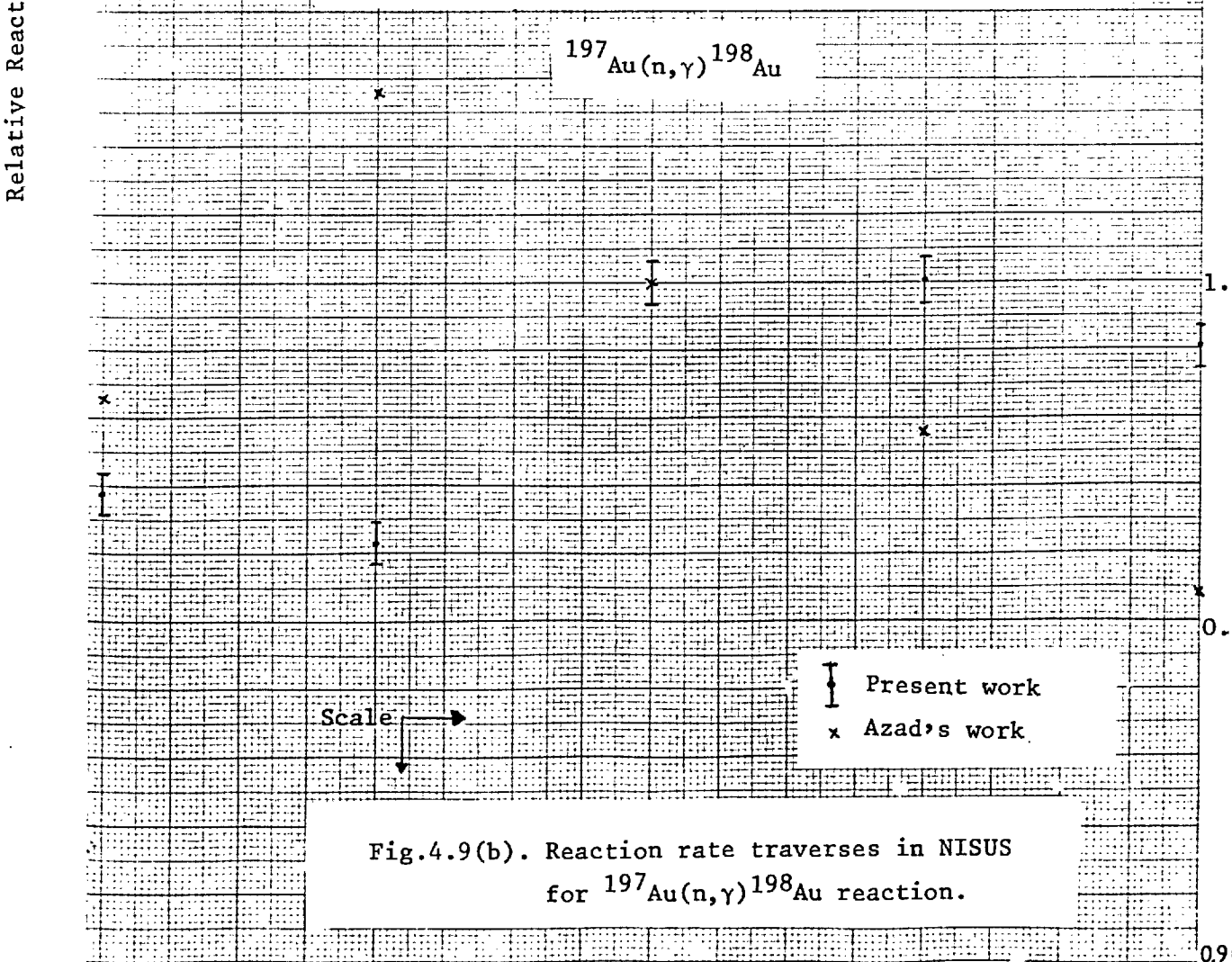


Fig.4.9(b). Reaction rate traverses in NISUS for $^{197}Au(n,\gamma)^{198}Au$ reaction.

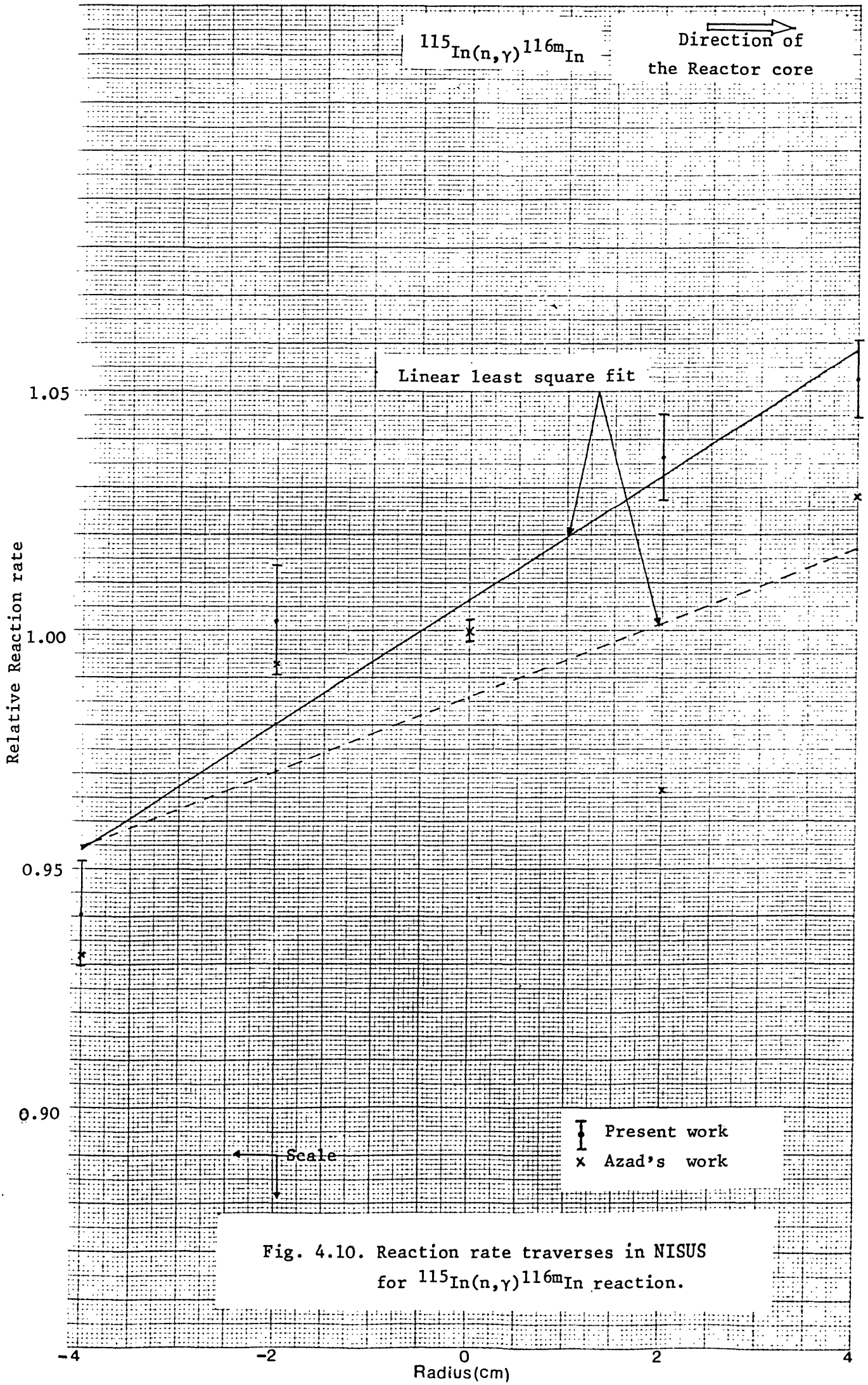


Fig. 4.10. Reaction rate traverses in NISUS for $^{115}In(n,\gamma)^{116m}In$ reaction.

Fabry for high energy reaction rate traverses in ΣΣ for a distance of 10 cm through the centre of ΣΣ[10]. Reaction rate traverses determined by Azad are shown in Fig. 4.11(a) but the decrease is not systematic across the diameter of the cavity and the decrease is ∿ 8%.

(5) $^{58}Ni(n,p)^{58}Co$ reaction

The foils were counted after a decay time of 3 days so that short life Isomer ^{58m}Co (9.1 h) has decayed and only ^{58}Co is left for counting. The foils are counted for a long time to get good statistics of the counting. Reaction rates with their errors are given in Table 4.18. Reaction rate traverses are shown in Fig. 4.11(b) which decrease by ∿ 20% away from the core. Nearly the same trend of decrease (∿ 20%) is observed for reaction rate traverses away from the core for NISUS by Azad[42] as shown in Fig. 4.11(b) and also by Fabry for ΣΣ[10].

(6) $^{64}Zn(n,p)^{64}Cu$ reaction

$^{64}Zn(n,p)^{64}Cu$ reaction rates in five positions are given in Table 4.19. The experimental errors are ∿ 3%. Reaction rate traverses for this reaction are shown in Fig. 4.12(a). The reaction rate decreases by ∿16% across the NISUS cavity. Reaction rate traverses given by Azad[10] decrease by ∿14% across the inner diameter of the cavity. The present work and Azad's work agree well for this reaction rate traversing.

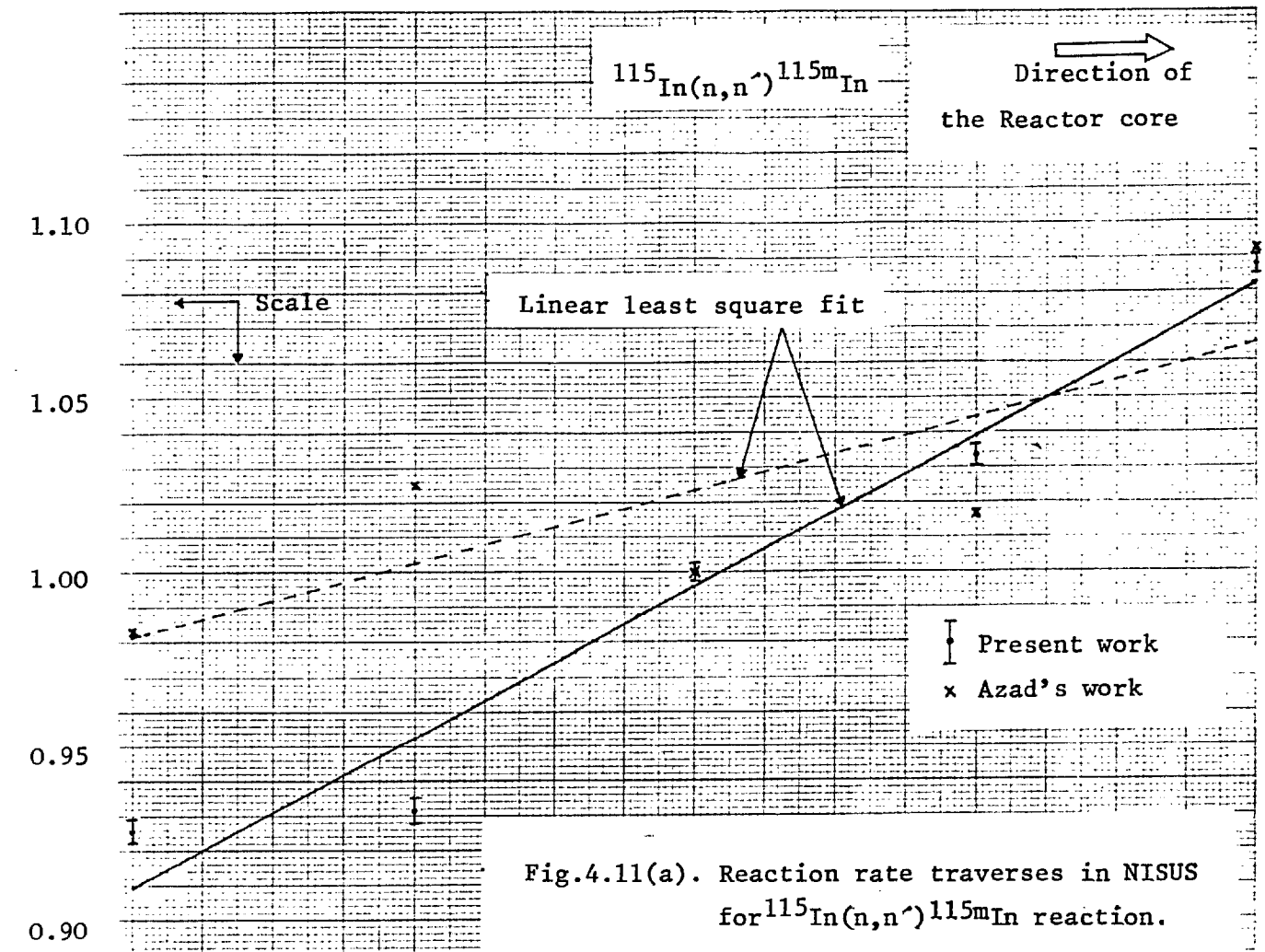


Fig.4.11(a). Reaction rate traverses in NISUS for $^{115}In(n,n')^{115m}In$ reaction.

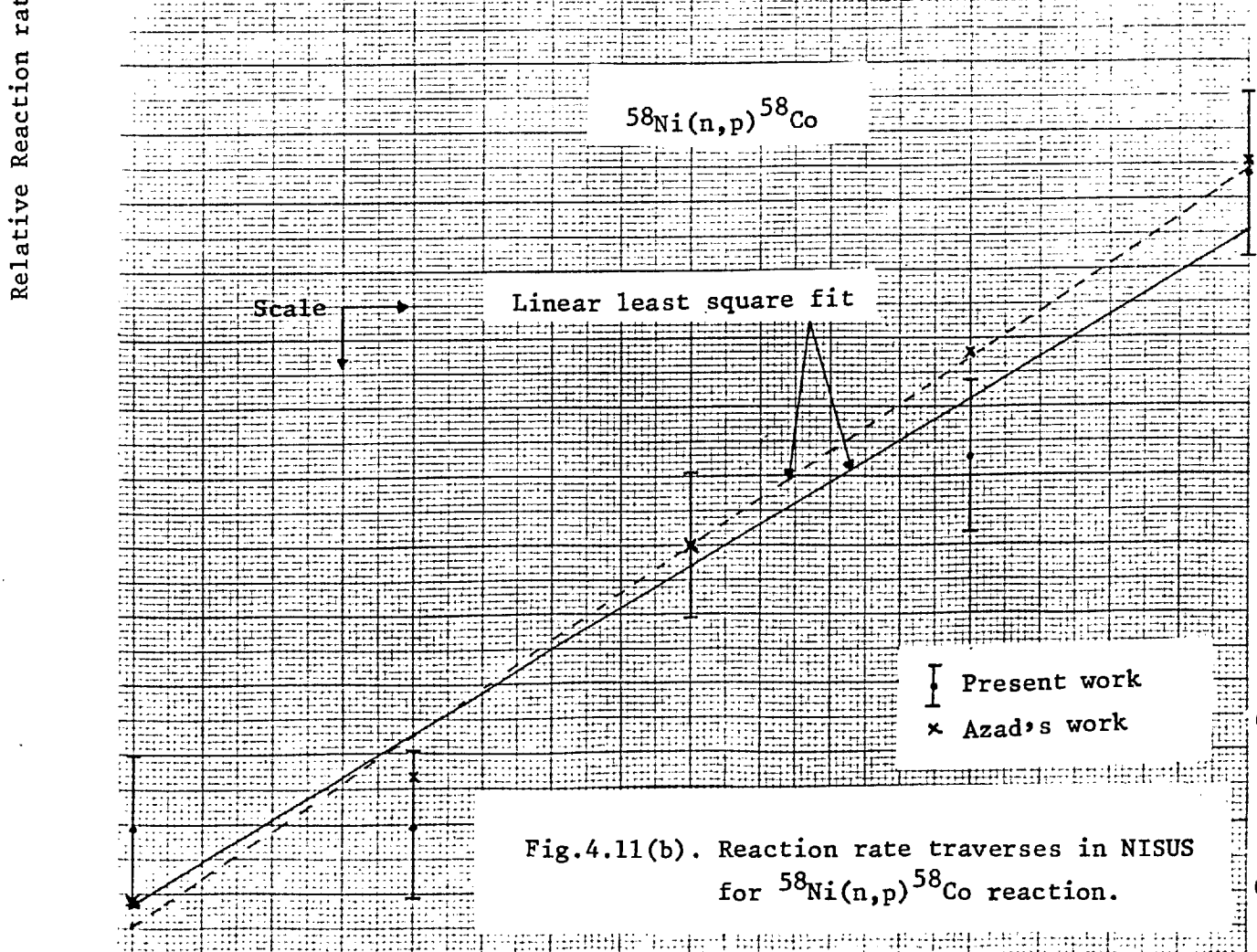


Fig.4.11(b). Reaction rate traverses in NISUS for $^{58}Ni(n,p)^{58}Co$ reaction.

TABLE 4.18

^{58}Ni (n,p) ^{58}CO Absolute reaction rates

Position (cm)	Reaction-rate/atom (a,c) x 10^{-3}	Error (b) (%)
4	3.6814	± 3.6%
2	3.4112	± 3.6%
0	3.3250	± 3.6%
-2	3.0581	± 3.7%
-4	3.0531	± 3.7%

(a) Normalised to monitor ^{197}Au (n,γ) reaction rates per atom.

(b) All uncertainties are 1 σ estimates.

(c) 2.9% correction has been made for coincidence summing effect according to Ref.74.

TABLE 4.19

^{64}Zn (n,p) ^{64}Cu Absolute reaction rates

Position (cm)	Reaction-rate/atom (a) x 10^{-3}	Error (b) (%)
4	1.0508	± 3.1
2	0.9677	± 3.2
0	0.9462	± 3.2
-2	0.8926	± 3.2
-4	0.8853	± 3.2

(a) Normalised to monitor ^{197}Au (n,γ) reaction rate per atom.

(b) All uncertainties are 1 σ estimates.

(7) $^{56}Fe(n,p)^{56}Mn$ reaction

The iron foil has two reactions when activated in a fast neutron flux. These reactions are $^{54}Fe(n,p)^{54}Mn$ and $^{56}Fe(n,p)^{56}Mn$ reactions. The half life of $^{54}Fe(n,p)$ reaction is $\sim$312 days whereas the half life of $^{56}Fe(n,p)$ reaction is 2.58 hours. The gamma rays emitted by these two reactions are at 0.835 MeV and 0.847 MeV. High resolution (FWHM is $\sim$2.2 KeV at 1.332 MeV) Ge(Li) detector is used and also the analyser is calibrated at 0.206 KeV/channel for a conversion gain of 8192 so the gamma spectrum from these two reactions are resolved easily. To subtract the activity of $^{54}Fe(n,p)$ from the activity of $^{56}Fe(n,p)$ reaction, the foils were counted immediately after irradiation for $^{56}Fe(n,p)$ reaction due to its short half life. Then after a decay of 5 days the foils were counted again for $^{54}Fe(n,p)$ reaction for the same time as in $^{56}Fe(n,p)$ reaction but no appreciable amount of activity of $^{54}Fe(n,p)$ reaction was observed due to its low isotopic abundance and short counting time. Fe foils ($\sim$ 3 mm thickness) were used for $^{56}Fe(n,p)$ Mn reaction rate traversing measurement. Gamma self absorption correction has been done for each foil according to section 4.3.1.

Reaction rates in five positions in NISUS are given in Table 4.21. The experimental errors are $\sim$ 3.5%. Reaction rate traverses are shown in Fig. 4.12(b). The measured reaction rates do not agree well with the fitted line in this work. The reaction rates decrease by $\sim$24% across the diameter of the NISUS cavity. It is observed during NISUS central reaction rate measurement alone that the central reaction rate

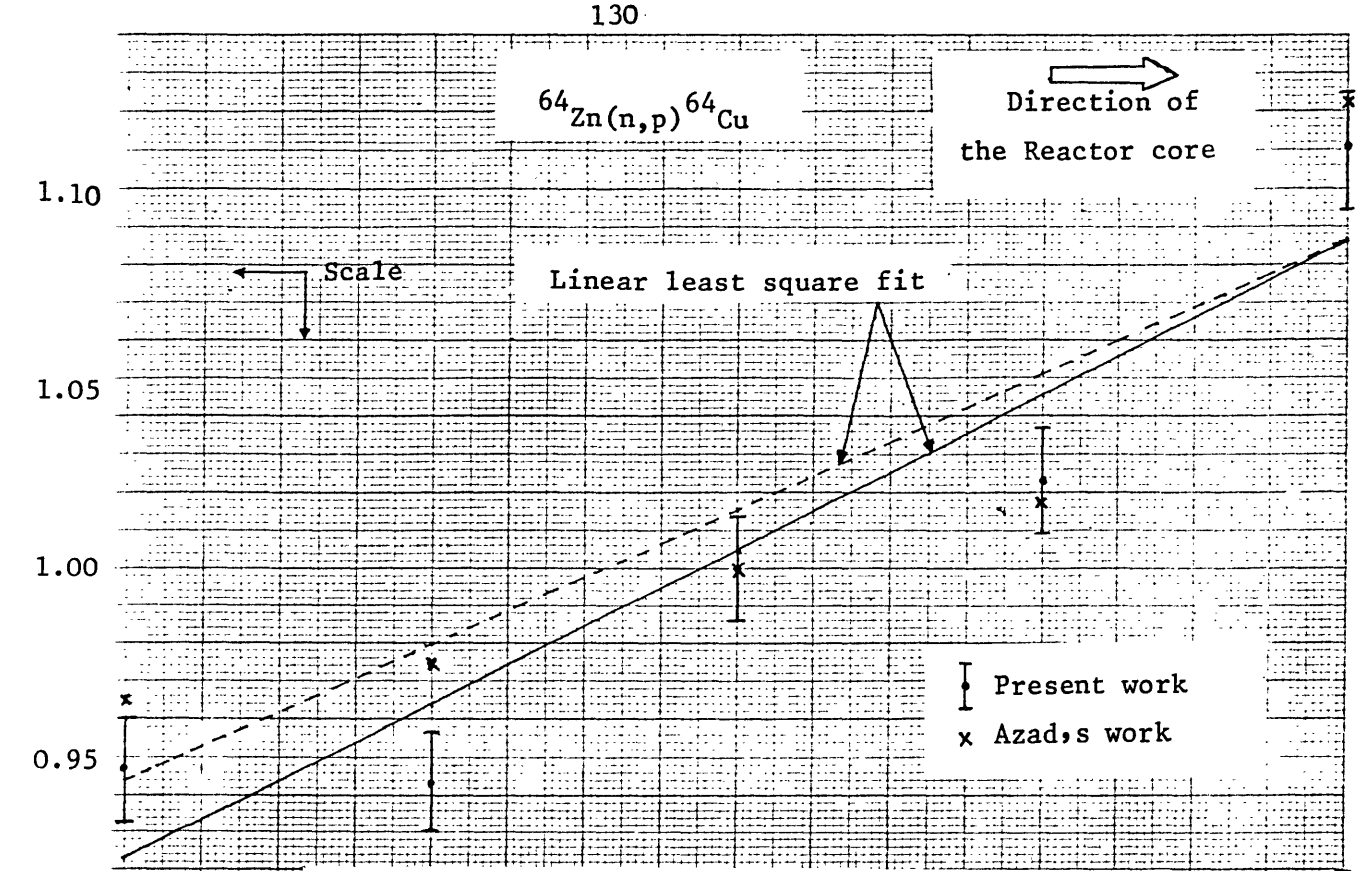


Fig.4.12(a). Reaction rate traverses in NISUS for $^{64}Zn(n,p)^{64}Cu$ reaction.

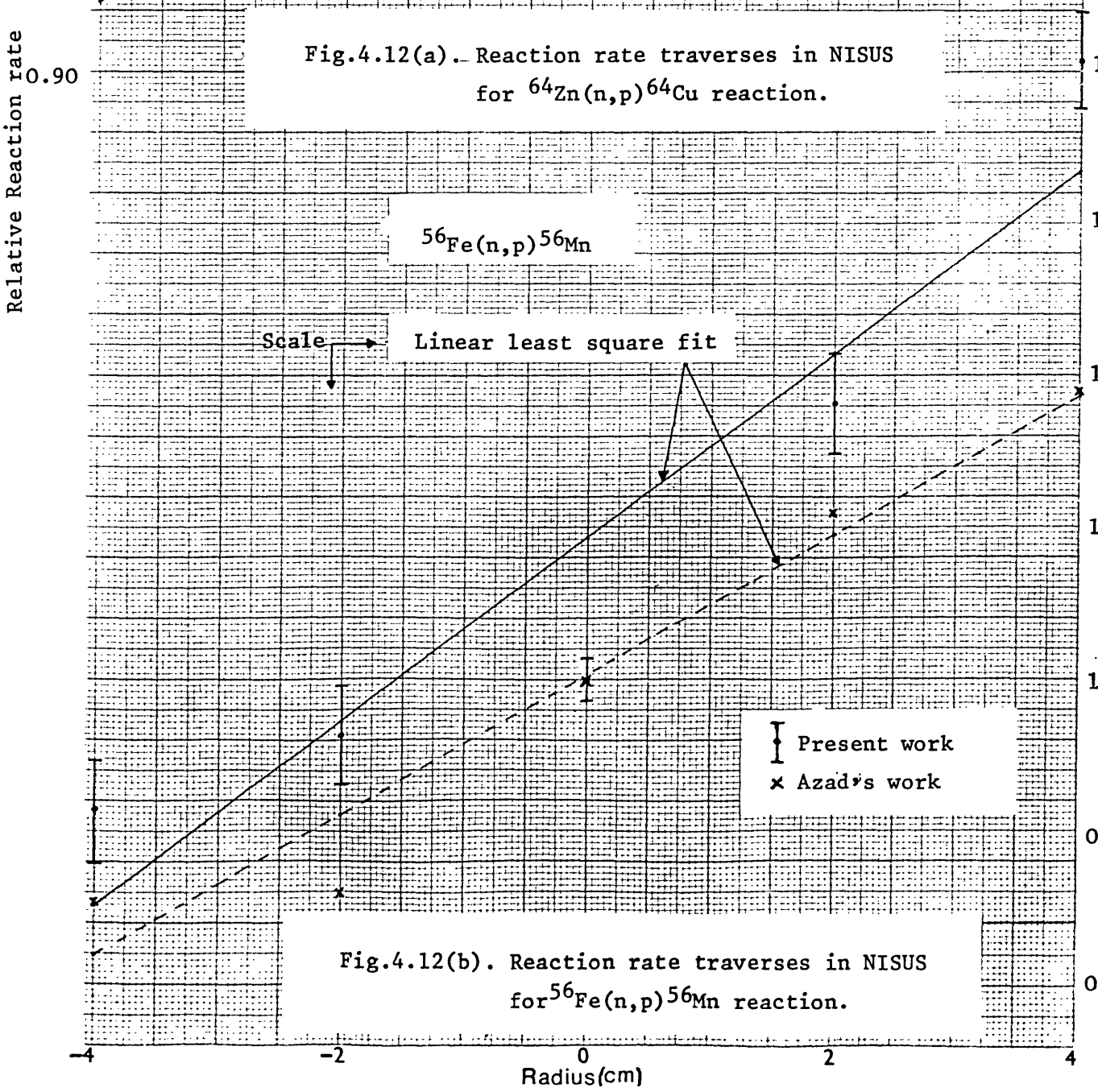


Fig.4.12(b). Reaction rate traverses in NISUS for $^{56}Fe(n,p)^{56}Mn$ reaction.

measurement of $^{56}Fe(n,p)^{56}Mn$ reaction obtained from reaction rate traversing is in error. This value is ∿12% lower than the value obtained from central reaction rate measurement alone (described in section 4.9 and shown in Table 4.34). It is found that Azad's reaction rates agree very well with the fitted line. The decrease in reaction rates across the distance of 8 cm in Azad's work is ∿ 18% and agress with ΣΣ [10].

(8) $^{27}Al(n,p)^{27}Mg$ reaction

This reaction has got very short half life of 9.46 min. so it is not possible to measure the reaction rate traverses in one day irradiation. One foil was irradiated for every position in NISUS for each day and was counted immediately after the removal of the foil from the reactor which takes at least 15 minutes after the end of irradiation. Due to its short half life, the foil could not be counted for a long time and for several times. The statistical error in each foil was found ∿4.0%. Thick Al foils (∿1.2 mm thickness) were used for reaction rate measurement. Correction for gamma self absorption has been performed according to section 4.3.1. Reaction rates are given in Table 4.20. Reaction rate traverses are given in Fig. 4.13(a). The reaction rate decreases by ∿20% across the diameter of the cavity. Azad's reaction rate traverses do not show systematic decrease and do not agree with the fitted line. There is no decrease observed in reaction rate traverses in Azad's work. The present reaction rate traverses agree with the ΣΣ reaction rate traverses.

TABLE 4.20

^{27}Al (n,p) ^{27}Mg Absolute reaction rates

Position (cm)	Reaction rate/atom[a] x 10^{-3}	Error[b] (%)
4	0.1321	±5.2
2	0.1239	±5.8
0	0.1178	±5.6
-2	0.1090	±5.6
-4	0.0974	±5.5

(a) Normalised to monitor ^{197}Au (n,γ) reaction rate per atom.

(b) All uncertainties are 1σ estimates.

TABLE 4.21

^{56}Fe (n,p) ^{56}Mn Absolute reaction rates

Position (cm)	Reaction-rate/atom[a] x 10^{-3}	Error[b] (%)
4	0.0331	±3.0
2	0.0300	±3.1
0	0.0275	±2.8
-2	0.0270	±3.2
-4	0.0263	±3.3

(a) Normalised to monitor ^{197}Au (n,γ) reaction rate per atom.

(b) All uncertainties are 1σ estimates.

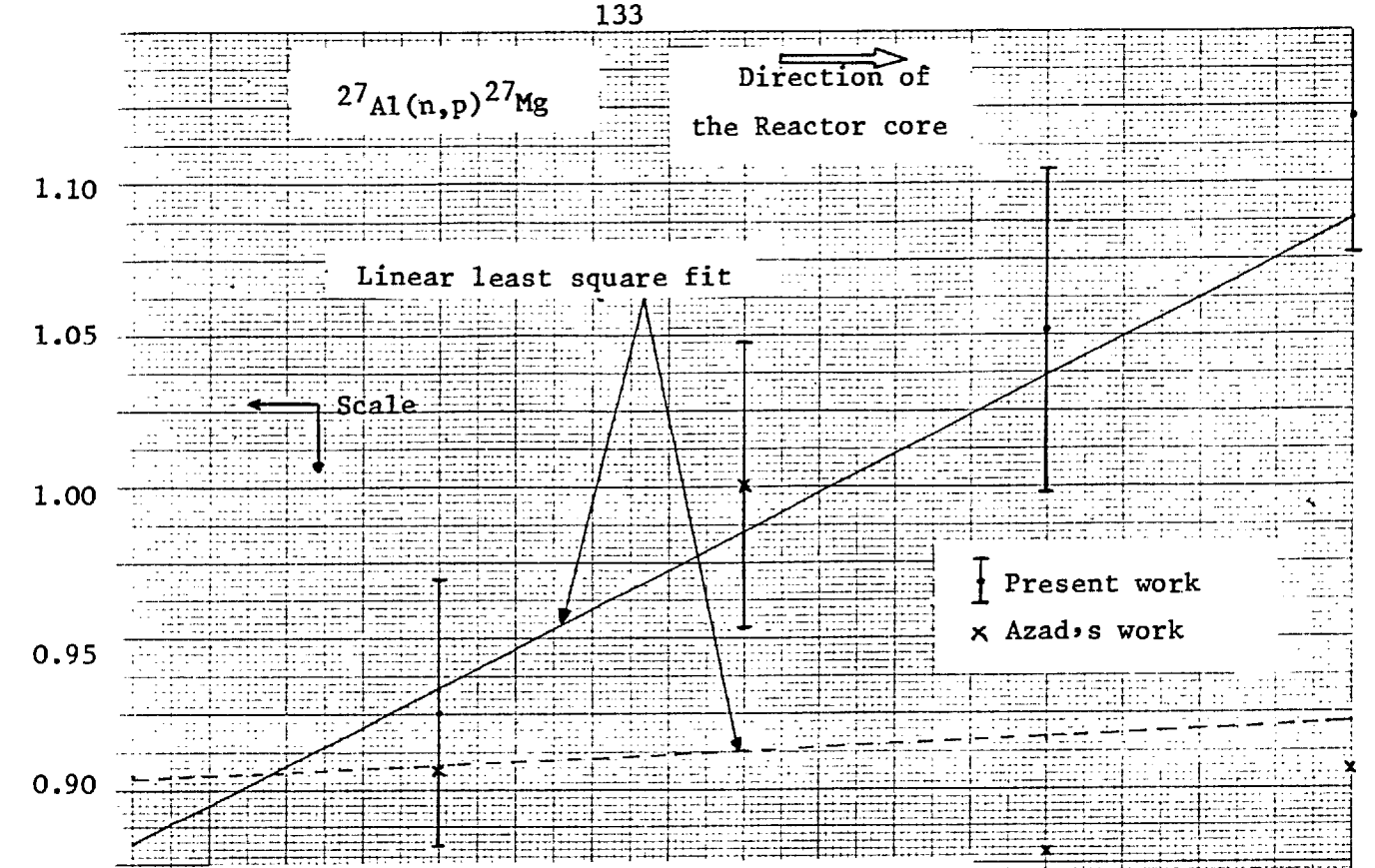


Fig.4.13(a). Reaction rate traverses in NISUS for $^{27}Al(n,p)^{27}Mg$ reaction.

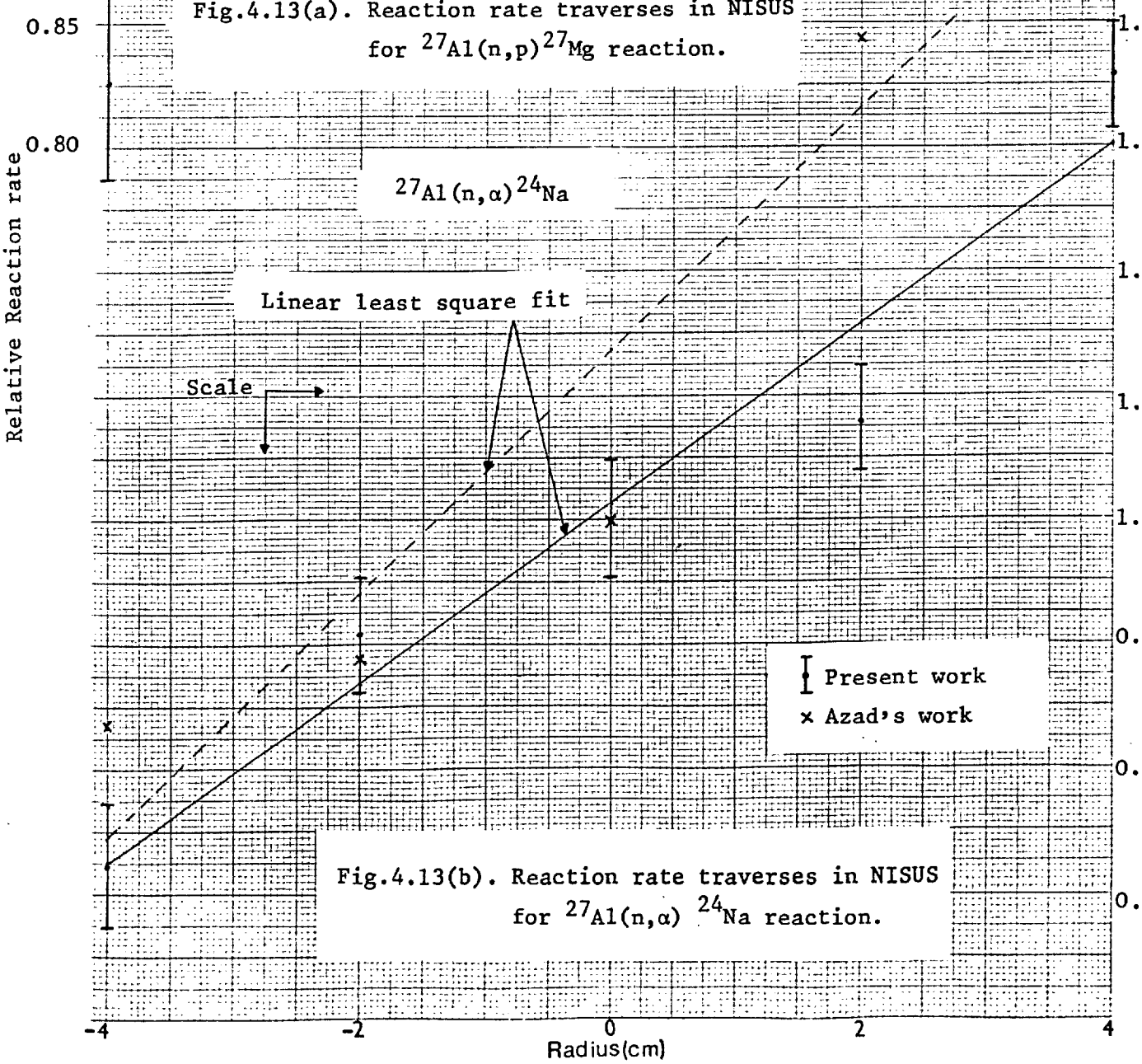


Fig.4.13(b). Reaction rate traverses in NISUS for $^{27}Al(n,\alpha)\ ^{24}Na$ reaction.

TABLE 4.22

^{24}Mg (n,p) ^{24}Na Absolute reaction rates

Position (cm)	Reaction-rate/atom [(a)] x 10^{-3}	Error [(b)] (%)
4	0.0543	± 6.0
2	0.0495	± 6.8
0	0.0467	± 4.9
-2	0.0428	± 8.0
-4	0.0394	± 9.4

(a) Normalised to monitor ^{197}Au (n,γ) reaction rate per atom.

(b) All uncertainties are 1 σ estimates.

TABLE 4.23

^{27}Al (n,α) ^{24}Na Absolute reaction rates

Position (cm)	Reaction-rate/atom [(a)] x 10^{-3}	Error [(b)] (%)
4	0.0232	± 3.3
2	0.0204	± 3.5
0	0.0197	± 3.6
-2	0.0188	± 3.7
-4	0.0169	± 4.0

(a) Normalised to monitor ^{197}Au (n,γ) reaction rate per atom.

(b) All uncertainties are 1 σ estimates.

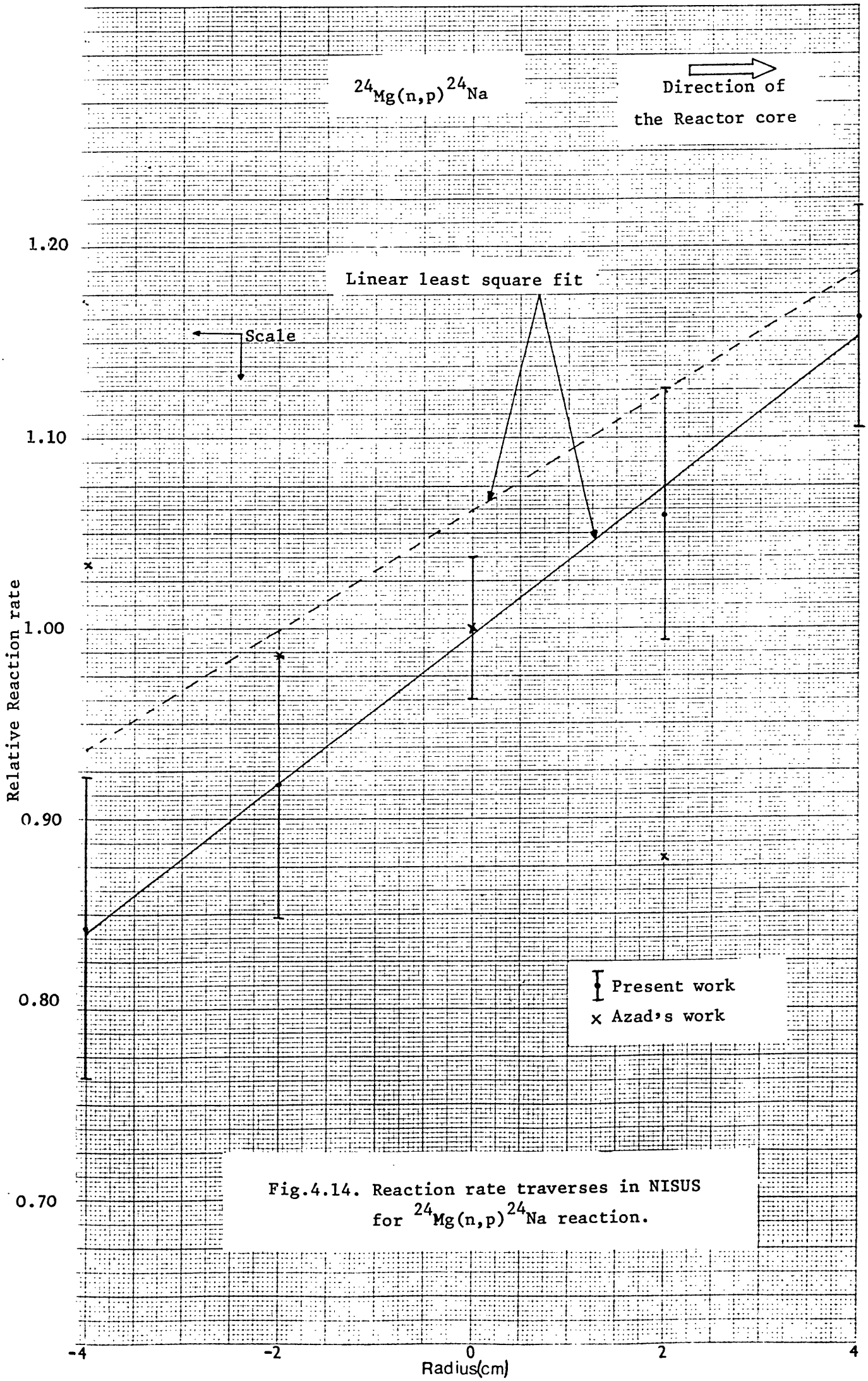


Fig.4.14. Reaction rate traverses in NISUS for $^{24}Mg(n,p)^{24}Na$ reaction.

(9) $^{27}Al(n, \alpha)^{24}Na$ reaction

Thick Al foils as in $^{27}Al(n,p)$ reaction were used for this reaction. Gamma self absorption correction is done for each foil according to section 4.3.1. Reaction rates are given in Table 4.23. Reaction rate traverses are shown in Fig. 4.13(b). The reaction rate decreases by ∿30%. The reaction rate decrease in this reaction is found higher than those of other threshold detectors measured (∿20%) in this work and also it is higher than the reaction rate traverses for high energy reactions in ΣΣ [10]. The reaction rate decrease measured by Azad is ∿40%. This value is higher than the value in the present work and also the value obtained from ΣΣ.

(10) $^{24}Mg(n,p)^{24}Na$ reaction

Reaction rates inside NISUS are given in Table 4.22. The experimental errors are very high. Thin foils of 0.127 mm thickness were used for reaction rate measurements and this reaction has a high threshold of ∿ 6.50 MeV so the number of interactions with neutrons in this material is very low which gives very poor counting statistics. Reaction rate traverses are given in Fig. 4.14. Reaction rate decreases by ∿30%. The decrease in reaction rate traverses is also found higher than the other threshold reactions (∿ 20%). Reaction rate traverses by Azad have been shown in Fig. 4.14 but did not show systematic decrease. The fitted reaction rate decrease is ∿25%.

By comparing the reaction rate traverses for non threshold and threshold activation detectors in NISUS (present and previous work) and in ΣΣ, it can be concluded that

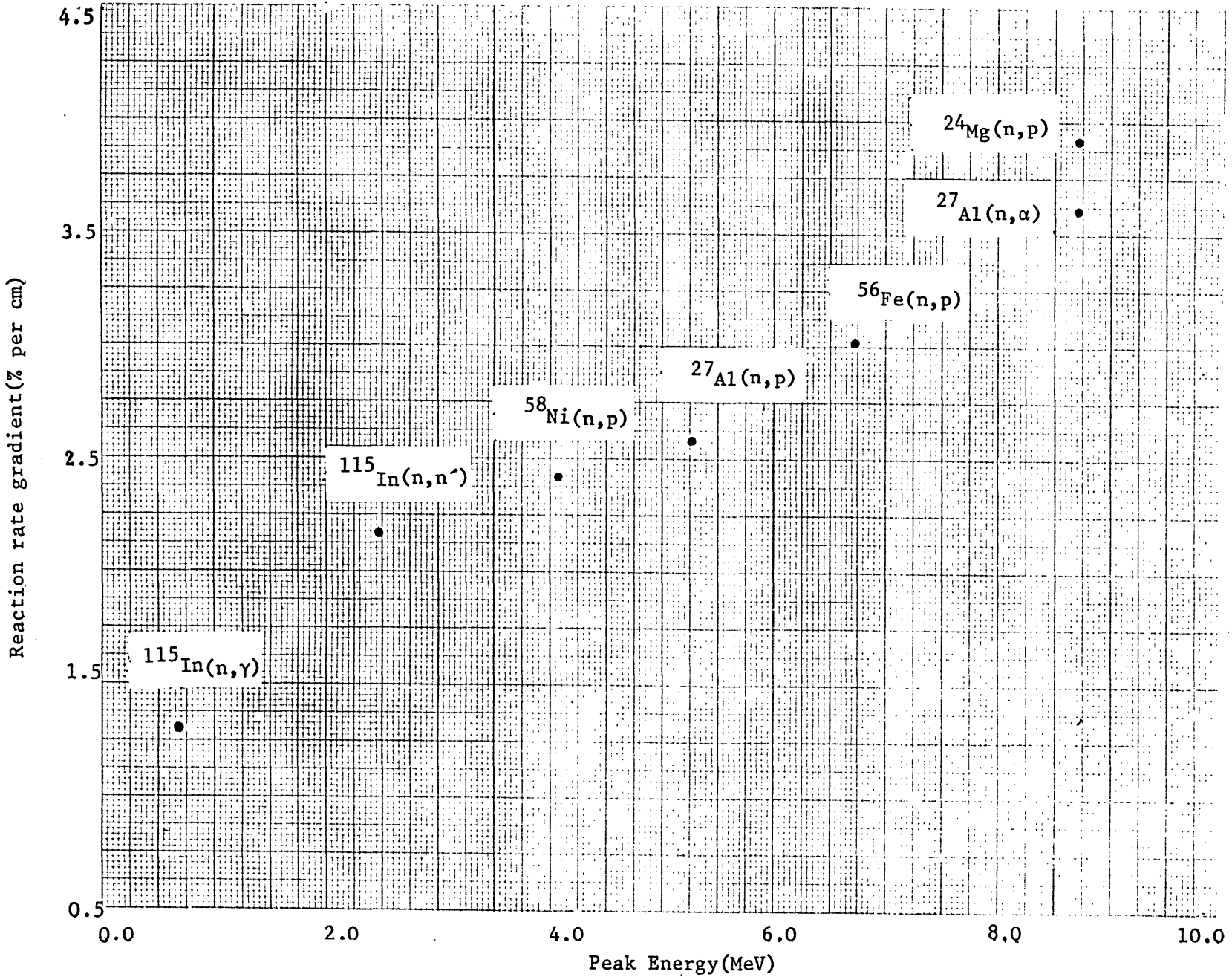


Fig. 4.15. Most proble energy response of multiple foil detectors in the NISUS central neutron spectrum.

the reaction rate traverses for different detectors in NISUS in the present work agree well within the statistical errors with both theoretical and experimental reaction rate traverses in ΣΣ[10]. The reaction rate decrease across the distance of 8 cm inside NISUS from the direction of core is ∿ 20% except $^{27}Al(n,\alpha)$ and $^{24}Mg(n,p)$ reactions and agrees with the ∿ 18% decrease for a distance of 10 cm through the centre of ΣΣ observed by Fabry for high energy reaction rate traverses. The reaction rate traverses for different activation detectors in Azad's work[42] cannot be compared properly because in some reactions the reaction rate did not show systematic decrease across the diameter of the cavity and the random error for each reaction is not available. Reaction rate gradient obtained from reaction rate traverses has been plotted as a function of most probable response energy of different activation detectors in the NISUS central neutron spectrum in Fig. 4.15. It can be seen from Fig. 4.15 that the flux gradient in NISUS is increasing as the response energy of the activation detectors is increased.

4.8 Fission rate and fission ratio measurements at the centre of NISUS

Accurate measurement of fission rates are necessary for fast reactor fuels and materials dosimetry. In fast reactors fission ratios such as $^{238}U/^{235}U$, $^{239}Pu/^{235}U$ etc., are important since in fast reactors the neutron spectrum is hard and the majority of

fissions occur with high energy neutrons. In fast reactors because of poor knowledge on differential cross section data these kinds of measurement are very valuable in predicting the neutron behaviour in a hard spectrum.

Three techniques have been applied, namely fission chamber, La-140 and total integral gamma counting in this work to measure the central fission rates and fission ratios of ^{235}U, ^{239}Pu, ^{238}U and ^{237}Np for the NISUS fast neutron field.

4.8.1 Fission rates and fission ratio by fission chamber technique

Measurements of absolute fission rates were performed by D. Azimi[34] using NBS type fission chambers during the visit of A. Fabry of CEN/SCK, MOL, Belgium to the University of London Reactor Centre with collaboration of J.G. Williams and myself. The absolute fission rates were derived from the absolute counting of fissions occurring in a known quantity of fissile material. A set of ^{235}U, ^{239}Pu, ^{238}U and ^{237}Np fissionable deposits obtained from NBS, Washington (specifications of the deposits given in Table 4.3 section 4.4) was used to measure absolute fission rates at the centre of NISUS. Corrections have been applied to the observed number of fission fragments to find the absolute fission rates. These corrections include the number of fission fragments lost due to alpha discrimination, absorption of fission fragments in the fissile material, fission in other isotopes than the principal one, dead time loss, perturbation for the introduction of fission chamber material such as

neutron scattering and absorption and also due to access hole for electronic cables and gas tubing. Table 4.24 presents an inventory of all corrections applied to the raw counting results in order to define absolute isotopic fission rates per nucleus. Correction values have been taken from Ref. 34 except for ULRC-6 ^{235}U fissionable deposit where correction has been made for epicadmium access hole perturbation as (0.995 ± 0.005) experimentally determined for non threshold fission detectors in NISUS (given in Table 4.8). Fabry determined experimentally the same correction (0.995 ± 0.005) for epicadmium access hole perturbation in ΣΣ for NBS ^{239}Pu and ^{235}U deposits[44] so the same corrections were applied to NBS ^{239}Pu and ^{235}U deposits for fission rate measurements in NISUS. Fission rates in ΣΣ were corrected for 1.006 for chamber perturbation on ^{237}Np and ^{238}U. The same corrections were applied for NBS chamber data in NISUS because the ΣΣ, NISUS and CFRMF neutron spectra are close to each other[43].

The dual triple counting system for fission chamber measurement originally developed at NBS[16] and modified at MOL[44] was reproduced for the present fission rate measurements in NISUS. A charge sensitive preamplifier, three integral discriminators and three scalers constitute the main pulse processing system. A high precision pulse generator, an oscilloscope and a multichannel analyser were used both for setting up the amplifier gains and discriminators as well as to provide additional and continuous control of chamber

TABLE 4.24

Corrections of the pulse rates to isotopic unperturbed fission rates of NBS and ULRC fission chambers

Foil identification and Principal Isotope	Extrapolation to zero	Dead time loss	Absorption in deposit	Fission in other Isotopes	Neutron Scattering and absorption	Access hole perturbation
NBS 49 I-1-1 ^{239}Pu	1.0078 ± 0.007	Negligible	1.0055 ± 0.0035	0.997	1.000	0.995 ±0.005
NBS 28 N-5-2 ^{238}U (natural)	1.0514 ± 0.0039	Negligible	1.0375 ± 0.0095	0.885	1.006± 0.003	1.000 ± 0.000
NBS 25 S-2-3 ^{235}U	1.0114 ± 0.0009	Negligible	1.0121 ± 0.0035	0.9995	1.000	0.995 ± 0.005
NBS 37 S-5-2 ^{237}NP	1.0240 ± 0.0014	Negligible	1.0343 ± 0.0080	0.980	1.006 ± 0.003	1.000 ± 0.000
NBS 28 HD-5-1 ^{238}U (depleted)	1.0303 ± 0.0032	Negligible	1.0355 ± 0.0090	1.000	1.006 ± 0.003	1.000 ± 0.000
ULRC - 3 ^{238}U	1.0318 ± 0.0023	Negligible	1.0166 ± 0.0042	0.994	1.011±0.004	1.000 ± 0.000
ULRC - 6 ^{235}U	1.0224 ± 0.0032	Negligible	1.0071 ± 0.0035	0.996	1.000	0.995 ± 0.005

performance. The fission chamber performance and operation are described in Ref. 34. A block diagram of dual triple-scaler counting system is reproduced in Fig. 4.16 from Ref. 34.

Two independent monitoring systems have been used for reactor power monitoring (described in section 4.7).

The average isotopic fission/monitor ratio for NBS deposits exposed at the centre of NISUS is given in Table 4.25[34].

4.8.2 Absolute fission rates and fission ratio by fission foils(^{140}La technique)

Absolute fission rates of ^{238}U and ^{235}U are determined by counting a particular fission product. Then, knowing the fission yield of this fission product, the number of fissions which have occurred in the sample can be calculated. One of the uranium fission products is ^{140}Xe and it decays to a stable isotope $^{140}_{58}Ce$ through a sequence of decay as follows:

$$^{140}Xe_{54} \xrightarrow[16s]{\beta^-} {}^{140}Cs_{55} \xrightarrow[66s]{\beta^-} {}^{140}Ba_{56} \xrightarrow[12.79d]{\beta^-} {}^{140}La_{57} \xrightarrow[40.26h]{\beta^-} {}^{140}Ce_{58}(\text{stable}) \qquad (4.8.1)$$

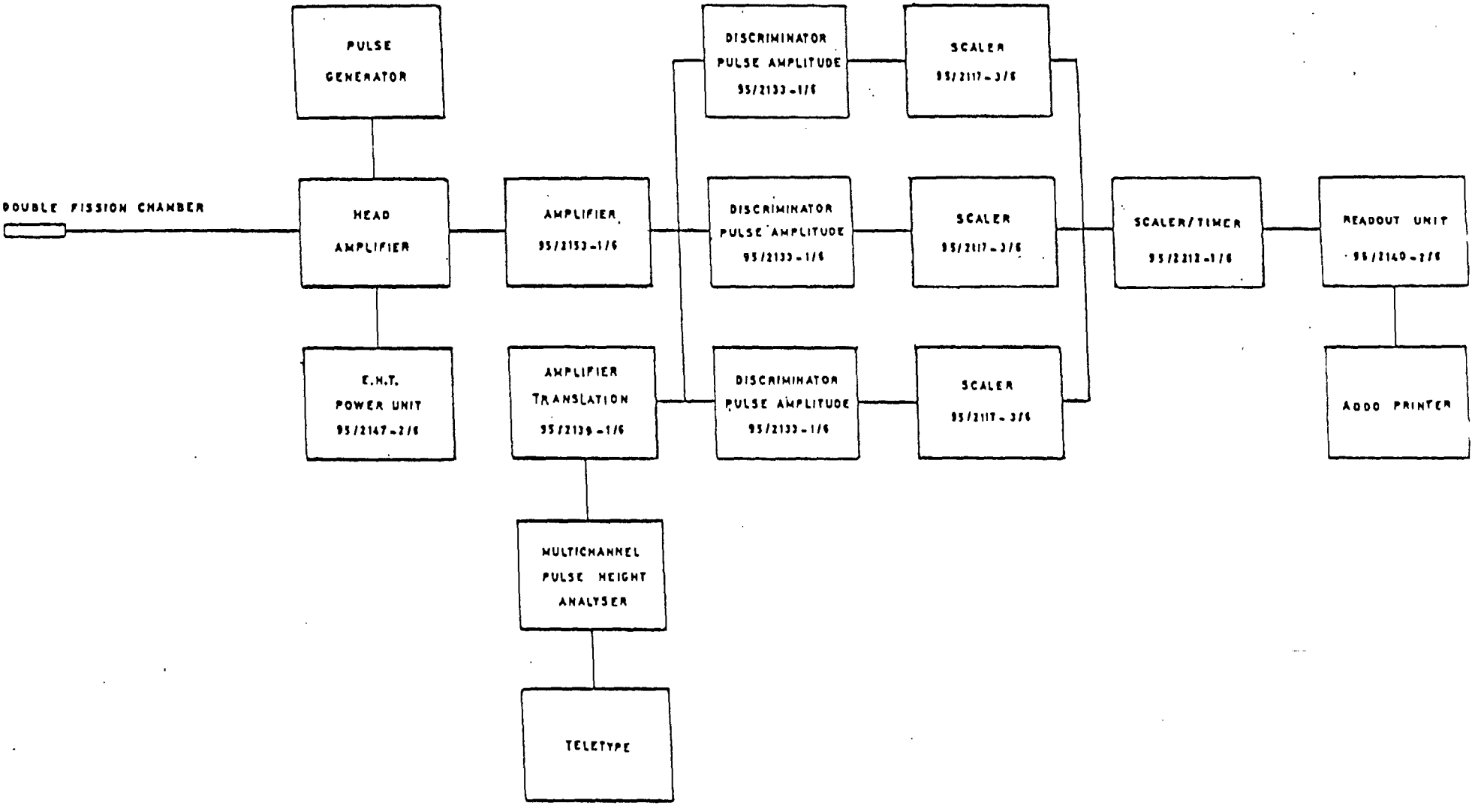


Fig.4.16. Block diagram of one side of the dual triple-scaler counting system.

TABLE 4.25

Average isotopic fission/monitor ratio for the exposure of NBS fission chambers at NISUS centre

Fission chamber	Foil identification	Principal Isotope	Fission/Monitor [(a)]	
			Fission rate per atom / Chamber monitor 1 x 10^{-20}	Fission rate per atom [(b)] / Au monitor A x 10^{-3}
NBS	NBS	^{239}Pu	17.50 ± 1.5%	222.02 ± 1.6%
		^{237}NP	5.681 ± 2.0%	70.62 ± 2.0%
		^{235}U	14.87 ± 1.4%	188.48 ± 1.4%
		^{238}U	0.8528 ± 1.8%	10.650 ± 1.8%

(a) Total error at 1σ confidence level.

(b) Errors due to monitor consistency and counting stability are not included.

In this decay scheme Barium builds up very rapidly because of its long half life (12.79d)[39] in comparison to the short half life of its precursor ^{140}Cs (66s). Usually fission product ^{140}La is used to measure the gamma activity. ^{140}La emits several gamma rays of which 1.596 MeV photopeak brings 95.33%[39] of the dissipated energy of the excited nucleus to the ground state. The decay scheme of ^{140}La is shown in Fig. 4.17. The contribution from other gamma rays (2.52 and 3.00 MeV) is only a few per cent to the energy release of the excited nucleus. The half life of ^{140}La is 40.26 hours, but because of 12.79 days half life of its parent, ^{140}Ba, the effective half life of ^{140}La is virtually 12.79 days.

96% enriched and 0.0356% depleted uranium foils were used to measure F5 and F8. Each foil wrapped by 0.0254 mm aluminium foil in order to catch escaping fission fragments was mounted on the aluminium foil holder and fixed to the access plug (described in chapter 3). The access plug was loaded inside NISUS in such a way that the foils were placed exactly at the centre of NISUS. After the irradiation of enriched and depleted foils, the activity was allowed to decay for ten days so that the 1.596 MeV photopeak from 12.79 days ^{140}La was essentially free from any other fission product γ-activity and ^{140}La was in equilibrium with the parent ^{140}Ba. The counting was performed on Ge(Li) detection system and the 1.596 MeV photopeak of sample was counted several times.

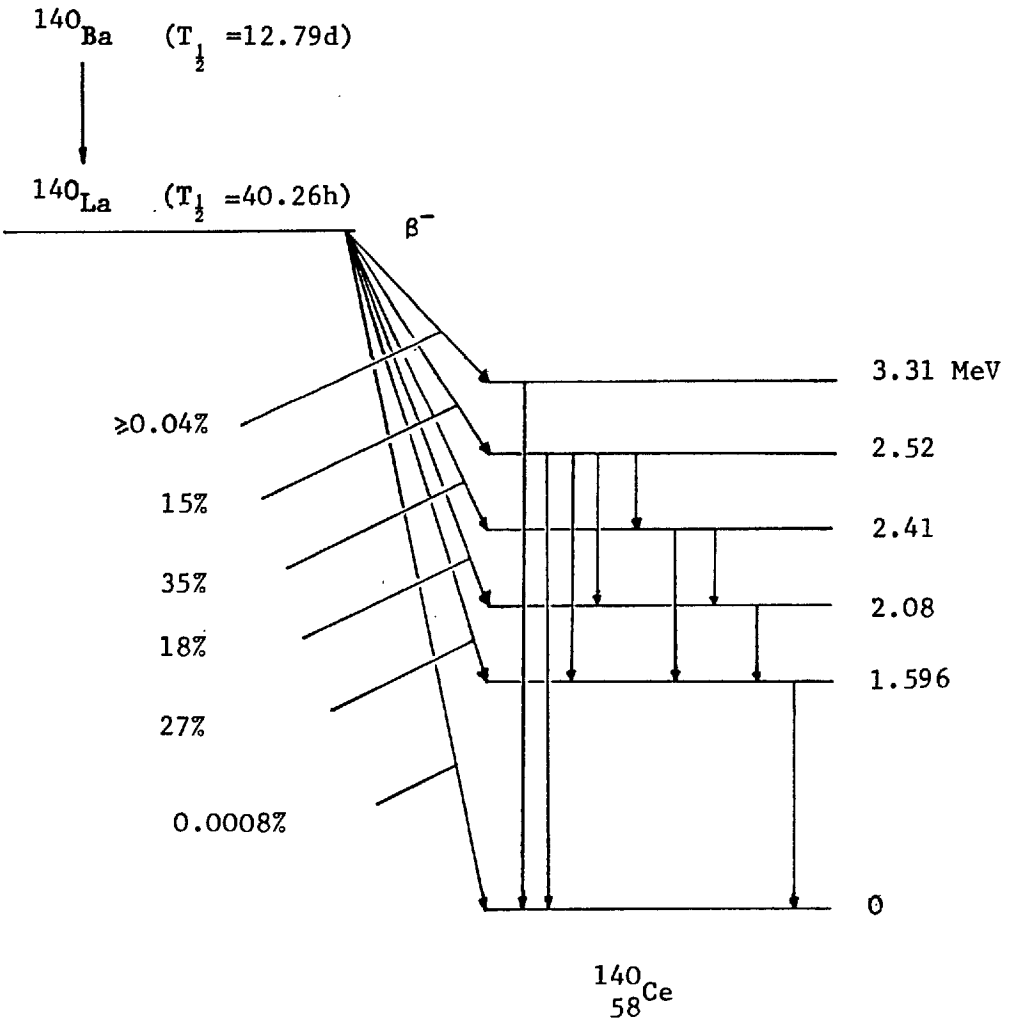


Fig.4.17. Decay scheme of ^{140}La.

At the time of counting the isotopes ^{140}Ba and ^{140}La had reached equilibrium, so the number of ^{140}Ba nuclei produced in fissioning is given by:

$$N_{o_{Ba}} = \frac{\lambda_{La} - \lambda_{Ba}}{\lambda_{Ba}} N_{La}(t_d) e^{\lambda_{Ba} t_d} \qquad (4.8.2)$$

Where λ_{La} and λ_{Ba} are the decay constants of ^{140}La and ^{140}Ba

$N_{La}(t_d)$ is the number of ^{140}La in the sample at decay time t_d.

The fission yields for ^{140}Ba for NISUS was used from revised fission yield values given by Fabry for $\Sigma\Sigma$[51]. (Fission yield values for $\Sigma\Sigma$ are used because NISUS and $\Sigma\Sigma$ are similar spectrum).

$y = 0.058 \pm 3.4\%$ for 96% enriched uranium

$y = 0.060 \pm 3.3\%$ for 0.0356% depleted uranium.

Thus knowing the fission yields for ^{140}Ba, the total fission events occurring in each foil is calculated:

$$F = \frac{N_{o_{Ba}}}{Y} \qquad (4.8.3)$$

The total fissions occurring in each sample results from the fission in ^{235}U and ^{238}U so to calculate the values of F5 and F8 the following set of equations is solved:

$$\left.\begin{aligned} FE/T_{aE} &= N_{5E} \times F5 + N_{8E} \times F8 \\ FD/T_{DE} &= N_{5D} \times F5 + N_{8D} \times F8 \end{aligned}\right) \qquad (4.8.4)$$

Where FE and FD are the total number of fissions in enriched and depleted foils.

T_{aE} and T_{aD} are the irradition times for the enriched and depleted foils.

N_{5E} and N_{5D} are the number of ^{235}U atoms in enriched and depleted foils.

N_{8E} and N_{8D} are the number of ^{238}U atoms in enriched and depleted foils.

A computer program "LANABS"[42] is used to calculate the values of F5 and F8 with their errors. The results of calculation of F5 and F8 for centre position of NISUS are given in Table 4.26.

TABLE 4.26

NISUS central fission rates of ^{235}U and ^{238}U by fission activation detectors

Position in NISUS	^{235}U			^{238}U		
	(a) Fission rate/atom $\times 10^{-18}$	(b) Au monitor A activity $\times 10^{-15}$	Fission rate/atom / Au monitor A $\times 10^{-3}$	(a) Fission rate/atom $\times 10^{-18}$	(b) Au monitor A activity $\times 10^{-15}$	Fission rate/atom / Au monitor A $\times 10^{-3}$
Centre	197.57±4.5%	1.0631±0.18%	185.84±4.5%	11.685±5.1%	1.0796±0.15%	10.823±5.1%

(a) Total error at 1σ confidence level.

(b) Random error at 1σ confidence level.

4.8.3 Weighted average of fission rates and fission ratio of ^{235}U and ^{238}U

Absolute fission rates of ^{235}U and ^{238}U measured by fission chamber and ^{140}La techniques are given in Table 4.25 and 4.26. It can be seen from these tables that the fission rates of ^{235}U and ^{238}U agree very well within $\sim$ ±1.5% by both these two techniques. In determining final absolute fission rates of ^{235}U and ^{238}U for NISUS, a weighted average of fission rate values of ^{235}U and ^{238}U obtained by these two techniques is used. Absolute fission rates and fission ratio of ^{235}U and ^{238}U is given in Table 4.27.

4.8.4 Fast fission ratio ($^{238}U/^{235}U$) measurement by total integral counting technique

The method consists of irradiating simultaneously two uranium foils of different enrichments located at the centre of NISUS and then comparing their fission product γ-activities at energies above 1.28 MeV with a NaI spectrometer. A calibration factor P(t) required to relate the measured γ-activity ratio to the true fission ratio F.R. is obtained in a separate experiment.

4.8.4 Irradiation of foils and counting procedure

(a) Two uranium foils of different enrichments (356 ppm ^{235}U and 96% ^{235}U enriched ^{235}U) were wrapped separately by 0.0254 mm thick aluminium foil in order to catch escaping fission fragments. These wrapped uranium foils were mounted on the aluminium foil holder

TABLE 4.27

Weighted average of Fission rates and fission ratio of ^{235}U and ^{238}U by fission chamber and ^{140}La technique in NISUS centre[a]

^{235}U			^{238}U			Fission ratio $\frac{F8}{F5}$
Fission rate per atom/Au monitor A		Weighted mean of Fission rate per atom/Au monitor A (F5) $\times10^{-3}$	Fission rate per atom/Au monitor A		Weighted mean of Fission rate per atom/Au monitor A (F8) $\times10^{-3}$	
Fission chamber technique[b] $\times10^{-3}$	^{140}La technique $\times10^{-3}$		Fission chamber technique[b] $\times10^{-3}$	^{140}La technique $\times10^{-3}$		
188.48± 2.1%	185.84±4.5%	188.00±1.9%	10.650±2.3%	10.823±5.1%	10.684±2.1%	0.05683±2.8%

(a) Error quoted is the total error both for fission chamber measurement and activation foil measurement (^{140}La technique).

(b) Fission rate per atom/Au monitor is considered for fission chamber measurement because fission rate per atom by activation foil normalised by Au monitor activity only. Errors due to monitor consistency and counting stability are included.

(∿ 0.4 mm thick) and loaded inside NISUS via the access plug in such a way that the foils were placed at the centre of NISUS. The γ-activity ratio from the samples of different enrichment is a function of the duration of irradiation and of the time after shut down. Brown and Skillings[48] have shown decay curves of γ-activity ratio for two different irradiations. So a standard duration for the irradiation was adopted and to carry out at the subsequent calibration experiment to relate fission product γ-activity to fission rate under the same conditions. The time chosen for these irradiations was 7 hours in order to get good statistics from the counts of the foils specially from depleted uranium foils. The irradiated uranium foils were counted on the NaI(Tl) spectrometer. A block diagram of the counting system is shown in Fig. 2.6 in chapter 2. The discriminator bias level was fixed at 1.28 MeV, this being greater than the bremsstrahlung associated with ^{238}U capture products (the maximum β-energy of ^{239}U is 1.2 MeV). Setting up this level was accomplished by observing an accurate differential bias curve of the 1.28 MeV ^{22}Na-Peak and then calibrating this bias level in terms of count rate from a ^{60}Co source (1.332 MeV). The count rate calibration was subsequently used to set up the bias level and to check the stability of the counting system, allowance being made for the ^{60}Co decay. Identical unirradiated uranium foils were also counted, to measure the background plus natural activity of the foils. Fission chamber and Au monitors were used for reactor power monitoring.

4.8.4 Determination of the γ-activity ratio

(b) The gamma activity of each foil results from fission product activity resulting from the fast fission in ^{235}U and ^{238}U. Two simultaneous equations can be written for the activity from each foil. The activity of each foil is due to fission process both in ^{235}U and ^{238}U. Therefore each equation consists of two parts:

$$\left.\begin{aligned} CD(t) &= N5D \times F5(t) + N8D \times F8(t) \\ CE(t) &= N5E \times F5(t) + N8E \times F8(t) \end{aligned}\right) \qquad (4.8.4)$$

Where CD(t) and CE(t) are depleted and enriched uranium foil count rates at time t corrected for weight and background.

N5D and N5E are number densities of ^{235}U in depleted and enriched foils.

N8D and N8E are number densities of ^{238}U in depleted and enriched foils.

F5(t) and F8(t) are gamma activities of fission products of ^{235}U and ^{238}U per atom.

By solving the equations in (4.8.4):

$$\frac{CD(t)}{CE(t)} = \frac{N5D + N8D \dfrac{F8(t)}{F5(t)}}{N5E + N8E \dfrac{F8(t)}{F5(t)}}$$

$$\left|\frac{F8(t)}{F5(t)}\right|_{\gamma} = \frac{N5E \left|\dfrac{CD(t)}{CE(t)} - \dfrac{N5D}{N5E}\right|}{N8E \left|\dfrac{N8D}{N8E} - \dfrac{CD(t)}{CE(t)}\right|} \qquad (4.8.5)$$

In equation (4.8.5), $\frac{F8(t)}{F5(t)}$ is the gamma activity fission ratio. The irradiated foils were counted alternately. Therefore a delay counting correction was applied to CD(t) and CE(t) in equation (4.8.5). The delay counting correction was performed by linear interpolation between two successive counts of each foil and calculating the count rate corresponding to the other counting time. The assumption that the decay is sufficiently linear over the corresponding time interval has been verified empirically[49].

The fission product gamma activity of depleted and enriched uranium foils and their ratio $(F8/F5)_{\gamma}$ as a function of time for each counting together with the expected error due to counting statistics are given in Table 4.28. The variation of the gamma activity ratio with time is shown in Fig. 4.18. The gamma activity ratio is fitted with the least squares exponential function. The solid line as shown in Fig. 4.18 is drawn through the fitted points.

TABLE 4.28

Result of gamma activity fission ratio (F8/F5)γ as a function of time with uranium foils without fission chamber.

Run	Decay time (mins.)	Depleted ^{235}U counts/sec/gm. (F8)γ	Enriched ^{235}U counts/sec/gm. (F5)γ	Fission chamber monitor (CPS)	Gamma activity fission ratio (F8/F5)γ (a)
1	70.50	136.56	2799.00		0.04879±1.67%
2	80.83	119.74	2577.60		0.04646±1.78%
3	91.17	111.20	2356.20		0.04719±1.84%
4	101.50	102.66	2152.26		0.04770±1.92%
5	111.84	93.75	1948.31		0.04812±2.01%
6	122.17	84.84	1837.02	1329.40	0.04618±2.11%
7	132.50	79.65	1725.73		0.04615±2.2%
8	142.83	74.45	1613.29		0.04615±2.3%
9	153.17	71.45	1500.85		0.04761±2.3%
10	163.50	68.45	1415.45		0.04836±2.4%
11	173.84	63.78	1330.04		0.04795±2.4%
12	184.17	59.10	1258.17		0.04697±2.5%
13	194.50	55.82	1186.30		0.04705±2.6%
14	204.84	52.54	1130.95		0.04644±2.7%
15	215.17	49.27	1075.60		0.04576±2.8%
16	225.50	46.00	1027.78		0.04473±2.9%
17	235.84	45.03	979.96		0.04593±2.9%
18	246.17	44.06	932.55		0.04725±2.9%
19	256.50	40.69	885.14		0.04597±3.0%
20	266.83	37.32	837.23		0.04458±3.2%
21	277.17	36.00	789.32		0.04561±3.2%
22	287.50	34.68	757.01		0.04581±3.3%

(a) Random error with 1 σ confidence level.

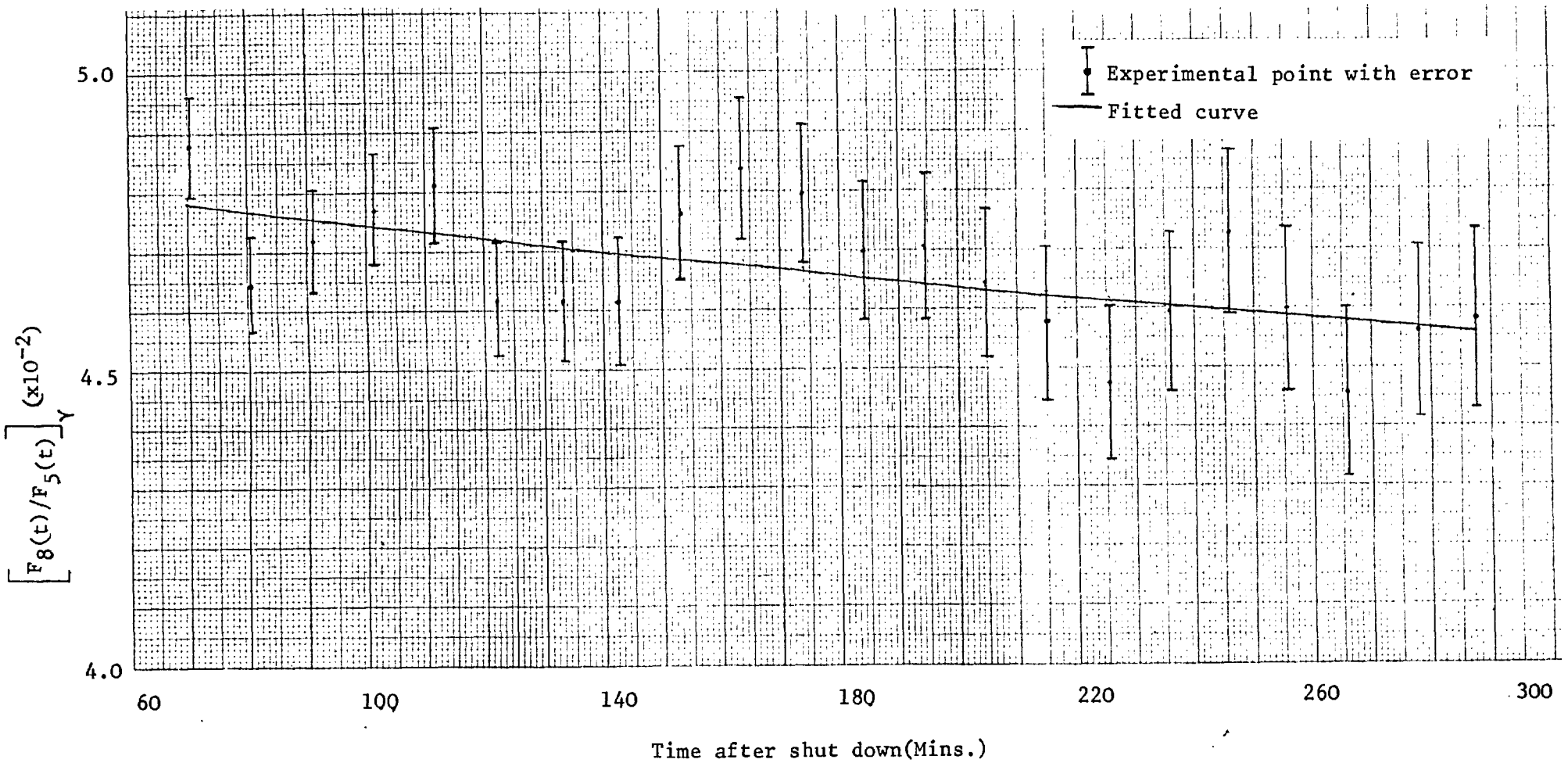


Fig.4.18. Variation of γ activity ratio with time measured by two Uranium foils without Fission chamber.

4.8.4 Measurement of calibration factor P(t) in NISUS

(c) P(t) is a factor required to convert the gamma activity fission ratio to true fission ratio and is given by:

$$P(t) = |F8/F5| \; / |F8(t)/F5(t)|_{\gamma} \qquad (4.8.6)$$

The true fission ratio is a constant quantity and the gamma activity fission ratio $(F8/F5)_{\gamma}$ is a time dependent function (decay time). The gamma activity fission ratio obtained from equation (4.8.5) depends on the ratio of $\frac{CD}{CE}$. $(F8/F5)_{\gamma}$ decreases with time as (CD/CE) does. Therefore P(t) is a time dependent parameter. P(t) also depends on several factors such as bias energy, detector geometry, irradiation length and size of foils. However, foils of same size and same counting systems were used in the P(t) measurement as those used in gamma activity fission ratio measurement. So the dependence of P(t) on bias level, detector geometry, etc., cancels.

A double fission ionisation chamber was used to measure P(t) in the NISUS spectrum. This double chamber was designed and constructed at the University of London Reactor Centre as shown in Fig. 4.19[34]. The P(t) measurement was performed in collaboration with D. Azimi. In the experiment two uranium foils (one ^{235}U and the other one ^{238}U)

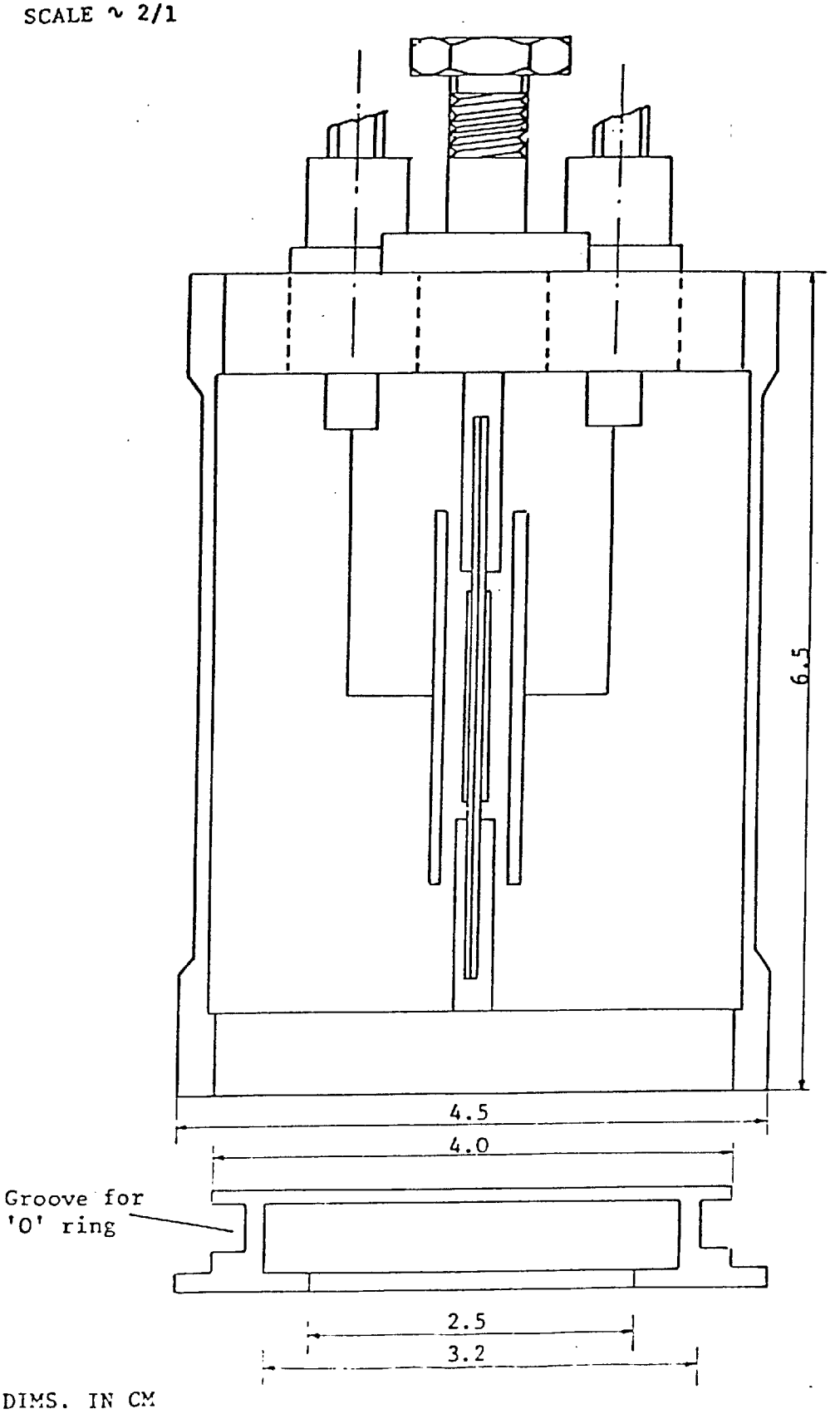


Fig.4.19. The enlarged cross-sectional view of the ULRC double Fission chamber.

wrapped by 0.0254 mm thick aluminium foil were sandwiched between the two back-to-back ULRC fissile deposits (Table 4.3) and loaded inside the ULRC chamber. The fission chamber was then inserted into the NISUS spectrum and irradiated for the same length of time as the two uranium foils irradiated without fission chamber for the gamma activity fission ratio measurement.

Knowing the ^{235}U and ^{238}U number ratios in the two deposits, the true fission ratio (F8/F5) is obtained and shown in Table 4.29 after applying all necessary corrections for fission chamber measurements (this fission ratio value is the Run 25 of Table 6.8 of Ref. 34). Assuming the same neutron flux and spectrum at the foils as at the fission chamber deposits, the corresponding gamma activity ratio $(F8/F5)_\gamma$ is obtained as a function of time, t , from the end of irradiation. Both fission chamber and Au monitor were used for reactor power monitoring. The fission product gamma activities and their ratio $|F8(t)/F5(t)|_\gamma$ calculated from the foil measurement with fission chamber in the usual way. The calibration factor P(t) is calculated simply by dividing the true fission (F8/F5) by gamma activity fission ratio.

Fission activity gamma ratio $|F8(t)/F5(t)|_\gamma$, true fission ratio (F8/F5) and the calibration factor P(t) are given in Table 4.30. The variation of gamma activity ratio with time is shown in Fig. 4.20.

TABLE 4.29

Absolute fission ratio (F8/F5) measurement by ULRC chamber in NISUS centre[(a)]

(Run 25 Table 6.8 Ref. 34)

^{235}U fission rate per atom/monitor		^{238}U fission rate per atom/monitor		True fission ratio (F8/F5)	
F.C. monitor 1	Au (n,γ) monitor A	F.C. monitor 1	Au (n,γ) monitor A	F.C. monitor 1	Au (n,γ) monitor A
15.116±1.4%	0.19597±1.4%	0.82852±2.0%	0.01074±2.0%	0.05481±2.5%	0.05480±2.5%

(a) Errors due to monitor consistency and counting stability are not included.

TABLE 4.30

Result of the calibration factor P(t) obtained from fission chamber and Uranium foils measurement for NISUS

Run	Decay time (mins)	Depleted ^{235}U counts/sec/gm. $(F8)_\gamma$	Enriched ^{235}U counts/sec/gm. $(F5)_\gamma$	Fission chamber monitor (cps)	(a) Gamma activity fission ratio $(F8/F5)_\gamma$	(b) True fission ratio (F8/F5) (Table 4.29)	(c) Calibration factor $P(t) = \frac{F8/F5}{F8(t)/F5(t)^\gamma}$
1	70.50	132.66	2822.36		0.04700±1.6%		1.166 ± 3.0%
2	80.83	117.48	2578.24		0.04557±1.7%		1.203 ± 3.0%
3	91.17	108.64	2334.12		0.04654±1.8%		1.178 ± 3.1%
4	101.50	99.80	2189.87		0.04557±1.9%		1.203 ± 3.1%
5	111.84	92.22	2045.61		0.04508±1.9%		1.216 ± 3.1%
6	122.17	84.63	1882.88		0.04495±2.0%		1.220 ± 3.2%
7	132.50	80.52	1720.15		0.04681±2.1%		1.171 ± 3.3%
8	142.83	76.51	1605.32		0.04766±2.1%		1.150 ± 3.3%
9	153.17	70.94	1490.48		0.04760±2.2%		1.151 ± 3.3%
10	163.50	65.35	1424.59		0.04587±2.3%		1.195 ± 3.4%
11	173.84	61.86	1358.69	1323.33	0.04553±2.4%	0.05481±2.5%	1.204 ± 3.5%
12	184.17	58.35	1265.27		0.04612±2.4%		1.188 ± 3.5%

TABLE 4.30 (continued)

13	194.50	54.73	1175.26		0.04657± 2.5%		1.177 ± 3.5%
14	204.83	51.11	1120.30		0.04562±2.6%		1.201 ± 3.6%
15	215.17	48.95	1065.35		0.04595±2.7%		1.193 ± 3.4%
16	225.50	46.79	1018.79		0.04593±2.7%		1.193 ± 3.7%
17	235.84	44.06	972.27		0.04532±2.8%		1.210 ± 3.8%
18	246.17	41.33	924.69		0.04470±2.9%		1.226 ± 3.8%
19	256.50	39.76	877.18		0.04533±3.0%		1.209 ± 3.9%
20	266.83	38.18	828.95		0.04606±3.0%		1.190 ± 3.9%
21	277.17	36.65	780.72		0.04694±3.1%		1.168 ± 4.0%
22	287.50	35.12	759.29		0.04625±3.1%		1.185 ± 4.0%

(a) Random error with 1σ confidence level.

(b) Total error in fission chamber measurement.

(c) Total error in fission chamber measurement and random error in foil measurement.

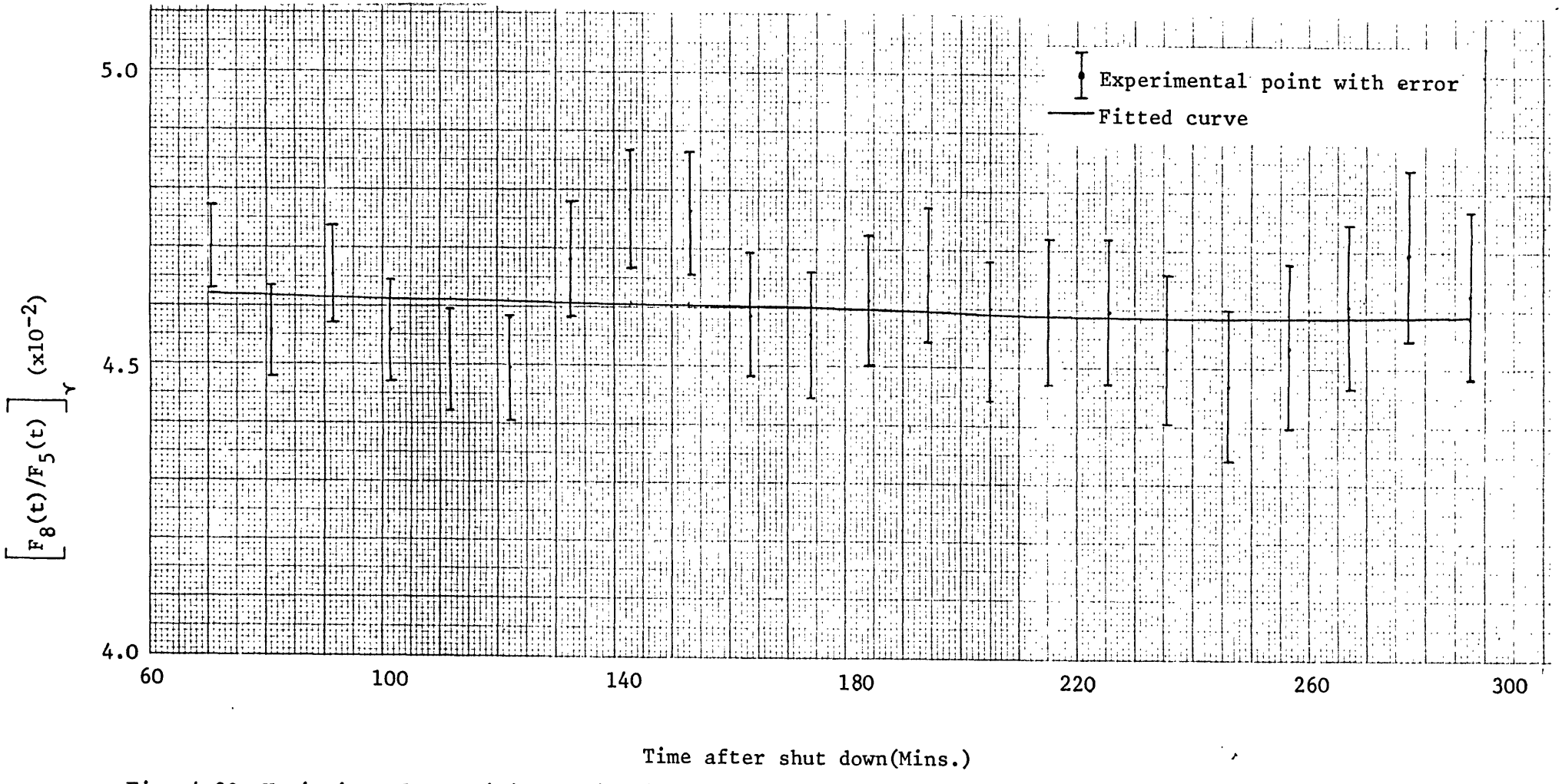


Fig. 4.20. Variation of γ activity ratio with time measured by two Uranium foils with Fission chamber.

The calibration factor P(t) is shown in Fig. 4.21.

Solid lines drawn in Figs. 4.20 and 4.21 are the least squares fitted points using an exponential function. True fission ratios are obtained by multiplying the calibration factor P(t) (Fig. 4.21) with gamma activity ratio (Fig. 4.18) as a function of time from the fitted lines and are given in Table 4.31. Calibration factor at 240 minutes in the present work is evaluated as

$$P(240) = 1.192 \pm 3.8\%$$

The calibration factor at 240 minutes measured by Pazirandeh[50] in a fission plate is

$$P(240) = 1.24 \pm 1.1\%$$

Present value of P(240) for NISUS agrees with the value given by Paziranedh but with poor precision.

It can be seen from Figs. 4.18, 4.20 and 4.21 that the solid lines do not fit the data well at all points. This is due to the fluctuation in count rate caused by instabilities in the counting system. The stability of the counting system is important to reduce the count rate fluctuation. Generally the counting heads and head amplifiers are housed in a constant temperature box. In the present

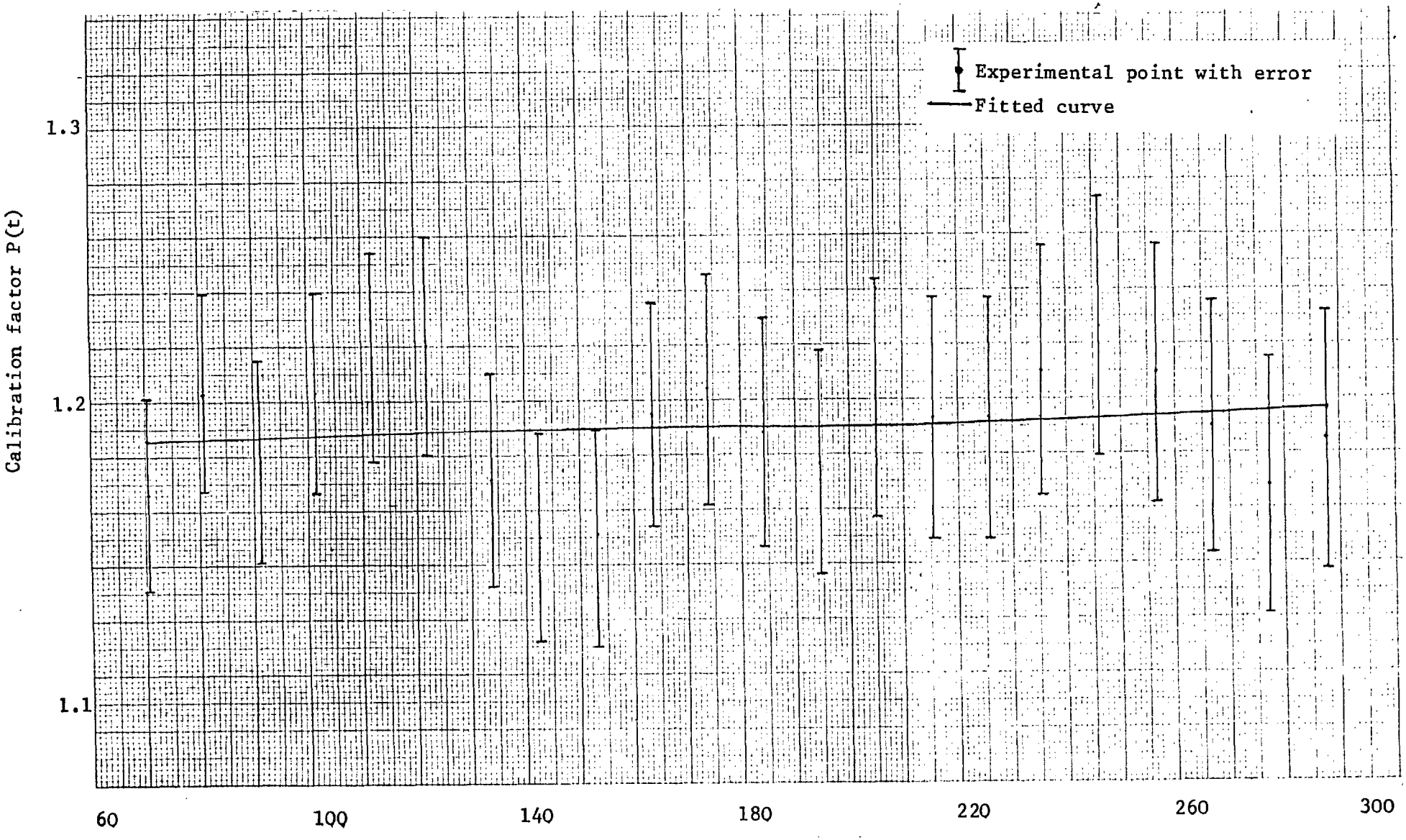


Fig.4.21. Calibration factor as a function of time P(t) measured by Fission chamber and Uranium foils for the NISUS neutron spectrum.

TABLE 4.31

Result of true fission ratios (F8/F5) obtained from calibration factor P(t) and gamma activity fission ratio F8/F5 and the weighted mean of true fission ratio

Decay time (mins.)	Calibration factor[(a)] $P(t) = \frac{F8/F5}{\left\|\overline{F8/F5}\right\|_\gamma}$ (Fig. 4.21)	Gamma activity[(b)] fission ratio $\left\|F8/F5\right\|_\gamma$ (Fig. 4.18)	True fission ratio[(c)] $\frac{F8}{F5} = P(t) \times \left\|\frac{F8(t)}{F5(t)}\right\|_\gamma$	Weighted mean of fission ratio F8/F5
100	1.187 ± 3.1%	0.04743 ± 1.9%	0.05630 ± 3.6%	
150	1.189 ± 3.3%	0.04690 ± 2.3%	0.05576 ± 4.0%	
				0.05561 ± 2.1%
200	1.190 ± 3.6%	0.04635 ± 2.7%	0.05516 ± 4.5%	
240	1.192 ± 3.8%	0.04600 ± 2.9%	0.05483 ± 4.8%	

(a) Total uncertainties are estimated by the combination of errors from absolute fission ratio measurement by fission chamber and random error for gamma activity fission ratio measurement by foil measurement with fission chamber.

(b) Random error is estimated only.

(c) Total error is due to the error in P(t) measurement and statistical error in $\left|F8/F5\right|_\gamma$ measurement by foil only.

work the counting system was not housed in a constant temperature box.

Table 4.32 shows the fission ratio (F8/F5) obtained by total integral technique and the fission ratio by fission chamber and ^{140}La technique (Table 4.27). It is found from Table 4.32 that the fission ratio (F8/F5) agrees within experimental errors in both cases.

In evaluating fast fission ratio (F8/F5) for NISUS, the fission ratio by total integral technique is not considered. The recommended fission ratio (F8/F5) for NISUS is that obtained from the absolute fission rates of ^{235}U and ^{238}U by fission chamber and ^{140}La techniques (Table 4.27).

4.8.5 Final fission rate and fission ratio measurements at the centre of NISUS

Absolute fission rates of ^{235}U, ^{239}Pu, ^{238}U and ^{237}Np were determined by NBS fission chambers (Table 4.25). Absolute fission rates of ^{235}U and ^{238}U were measured by fission foils (^{140}La technique) (Table 4.26). So the weighted mean values of fission rates of ^{235}U and ^{238}U were determined (Table 4.27). Fission rates ^{235}U, ^{239}Pu, ^{238}U and ^{237}Np are given in Tables 4.25 and 4.27. Table 4.33 gives the final result of absolute fission rates of ^{235}U, ^{239}Pu, ^{238}U and ^{237}Np and also fission ratios are formed relative to ^{235}U fission rates.

TABLE 4.32

Result of fast fission ratio (F8/F5) measurement by total integral technique and weighted mean of fission chamber and ^{140}La technique

Position in NISUS	Fast fission ratio (F8/F5)	
	Total Integral technique	Fission chamber and ^{140}La technique
Centre	0.05561 ± 2.1%	0.05683 ± 2.8%

TABLE 4.33

Final result of fission rates and fission ratios of ^{235}U, ^{239}Pu, ^{238}U and ^{237}NP at the centre of NISUS[a]

Reaction	Fission rate per atom/Au monitor A $\times 10^{-3}$	Fission ratio	Fission ratio
^{235}U (n,f) F.P.	188.00 ± 1.9%	$\frac{^{235}U\ (n,f)}{^{235}U\ (n,f)}$	1.000 Ref.
^{239}Pu (n,f) F.P.	222.02 ± 2.3%	$\frac{^{239}Pu\ (n,f)}{^{235}U\ (n,f)}$	1.17933 ± 3.0%
^{237}NP(n,f) F.P.	70.62 ± 2.6%	$\frac{^{237}NP\ (n,f)}{^{235}U\ (n,f)}$	0.37512 ± 3.2%
^{238}U (n,f) F.P.	10.684 ± 2.1%	$\frac{^{238}U\ (n,f)}{^{235}U\ (n,f)}$	0.05683 ± 2.8%

(a) Total error at 1 σ confidence level.

(Errors due to monitor consistency and counting stability are included).

4.9 NISUS central reaction rate measurements

NISUS central reaction rate for non fission and fission detectors were determined during reaction rate traversing (Tables 4.14 - 4.23 in section 4.7) and fission rate measurements (Table 4.33 in section 4.8) in NISUS during the period of February - June, 1975.

NISUS central reaction rates were measured again for all non fission detectors to check the reproducibility of central reaction rate only during the period of December, 1975 and February - May, 1976. NISUS central reaction rates were measured three times for some reactions. These absolute central reaction rates are given in column 2 in Table 4.34 together with their dates of measurement and all other information. The latest central reaction rate measurement of each reaction in the NISUS neutron field was used for interlaboratory comparison and the evaluation of the calculated reaction rate.

Fission rates due to ^{235}U and ^{238}U foils were not measured again because these fission rates were determined by both fission chambers and activation foils (^{140}La technique). Fission rates of ^{235}U and ^{238}U by these two techniques agree very well within $\sim \pm 1.5\%$ (Tables 4.25 and 4.26). The weighted average of fission rates of ^{235}U and ^{238}U by these two techniques is considered (Table 4.27). Fission rates of ^{239}Pu and ^{237}Np were determined by NBS fission chambers only because other ^{239}Pu and ^{237}Np fission foils were not available.

TABLE 4.34

Results of NISUS Central Reaction - rate measurement of various neutron dosimeters

Reaction	Reaction-rate[a,b] x 10^{-3}	Date of measurement	Comments
$^{55}Mn\ (n,\gamma)^{56}Mn$[e]	3.7408 ± 2.8%	Feb,1975	0.127-mm foil with four other similar foils measured for spatial scanning across 8 cm diameter of NISUS through the centre.
	3.8010 ± 2.8%	Feb,1976	0.127-mm foil alone measured at the centre of NISUS.
$^{115}In\ (n,\gamma)\ ^{116m}In$	29.688 ± 2.8%	Feb,1975	0.254 foil with four other similar foils measured for spatial scanning of NISUS.
	30.645 ± 3.0%	Feb,1976	0.254-mm foil alone measured at the centre of NISUS.
$^{197}Au\ (n,\gamma)\ ^{198}Au$[f]	50.355 ± 2.8%	Feb,1975	0.0508-mm foil with four other similar foils measured for reaction rate traversing in NISUS.
	50.373 ± 2.8%	Feb,1976	0.0508-mm foil alone measured at the centre of NISUS.
$^{235}U\ (n,f)$[c]	188.00 ± 1.9%	April and June,1975	0.0635-mm foil alone measured at the centre of NISUS in April, 1975 175.2 $\mu g/cm^2$-thick NBS foil measured by NBS fission chamber at the centre of NISUS in June, 1975.

TABLE 4.34 (continued)

^{239}Pu (n,f) (d)	222.02 ± 2.3%	June,1975	83.0 μg/cm^2 thick NBS foil measured by NBS fission chamber at the centre of NISUS in June, 1975.
^{237}Np (n,f) (d)	70.620 ± 2.6%	June,1975	497.3 μg/cm^2 thick NBS foil measured by NBS fission chamber at the centre of NISUS in June, 1975.
^{115}In (n,n')^{115m}In	6.8803 ± 2.8%	April,1975	0.254-mm foil with four other similar foils measured for reaction rate traversing in NISUS.
	7.0189 ± 2.8%	March,1976	0.254-mm foil alone measured at the centre of NISUS.
^{238}U (n,f) (c)	10.684 ± 2.1%	May and June,1975	0.0381-mm foil alone measured at the centre of NISUS in May, 1975. 541.5- and 513.9- μg/cm^2 thick foils measured by NBS fission chamber at the centre of NISUS in June, 1975.
^{58}Ni (n,p) ^{58}Co	3.3250 ± 3.6%	March,1975	0.254-mm foil with four other similar foils measured for reaction rate traversing in NISUS.
	3.3082 ± 3.2%	March,1976	0.254-mm foil alone measured at the centre of NISUS.
^{64}Zn (n,p) ^{64}Cu	0.9462 ± 3.2%	April,1975	0.254-mm foil with four other similar foils measured for spatial scanning of NISUS.
	1.0000 ± 2.7%	March,1976	0.254-mm foil alone measured at the centre of NISUS.

TABLE 4.34 (continued)

^{27}Al (n,p) ^{27}Mg	0.1178 ± 5.6%	June,1975	1.170-mm foil alone measured at the centre of NISUS.
	0.1190 ± 5.4%	March,1976	1.170-mm foil alone measured at the centre of NISUS.
	0.1194 ± 5.0%	May, 1976	1.170-mm foil alone measured at the centre of NISUS.
^{56}Fe (n,p) ^{56}Mn	0.0275 ± 2.8%	May, 1975	2.997-mm foil with four other similar foils measured for reaction rate traversing in NISUS. (Value rejected).
	0.0307 ± 2.7%	Dec,1975	2.997-mm foil alone measured at the centre of NISUS.
	0.0317 ± 3.2%	April,1976	0.381-mm foil alone measured at the centre of NISUS.
^{24}Mg (n,p) ^{24}Na	0.0467 ± 4.9%	April,1975	0.127-mm foil with four other similar foils measured for reaction rate traversing in NISUS.
	0.0465 ± 4.5%	March,1976	0.127-mm foil alone measured at the centre of NISUS.
	0.0444 ± 3.5%	May,1976	0.381-mm foil alone measured at the centre of NISUS.
^{27}Al (n,α) ^{24}Na	0.0197 ± 3.6%	May,1975	1.170-mm foil with four other similar foils measured for spatial scanning of NISUS.
	0.0196 ± 3.0%	April,1976	1.170-mm foil alone measured at the centre of NISUS.

(a) Absolute central reaction rate for nuclide normalised to gold monitor activity.

(b) All uncertainties are estimated at 1 σ confidence level.

(c) Weighted average of fission chamber and foil activation measurements.

(d) Measured by fission chambers only.

(e) No self shielding correction has been applied as no correction is available.

(f) Self shielding correction has been applied from Ref.10.

It is found from Table 4.34 that the reproducibility of central reaction rates is good. For capture and threshold detectors they agree within ± 1σ level except $^{64}Zn(n,p)^{64}Cu$ and $^{56}Fe(n,p)^{56}Mn$ reactions. An Fe foil of similar thickness (∿ 3 mm) used in spatial scanning of NISUS was measured for central reaction rate only in December, 1975 and the reaction rate increased by ∿ 12%. To check the reproducibility and consistency of the $^{56}Fe(n,p)^{56}Mn$ reaction rate measurement, an Fe foil of thickness (∿ 0.38 mm) was measured alone at the centre of NISUS in April, 1976 and the reaction rate agrees within ∿ 3% with the reaction rate measured in December, 1975 (shown in Table 4.34). Moreover it is observed that the $^{56}Fe(n,p)^{56}Mn$ central reaction rate measured in NISUS in December, 1975 and April, 1976 agrees with the $^{56}Fe(n,p)^{56}Mn$ measured central reaction rate in ΣΣ during inter-laboratory comparison of reaction rates and their ratios (Described in Section 5.2 in Chapter 5). So the $^{56}Fe(n,p)^{56}Mn$ central reaction rate measured in May, 1975 has been rejected. The variation in $^{64}Zn(n,p)^{64}Cu$ reaction measured in April, 1975 and March, 1976 is ∿ 6% (2σ level).

Thus it can be concluded that the reaction rate measured at the centre of NISUS of various neutron dosimeters are reproduced within ∿ ± 1σ confidence level except the $^{64}Zn(n,p)^{64}Cu$ reaction (Table 4.34).

5. MEASUREMENT OF REACTION RATES IN MOL-ΣΣ AND $\chi_{25}(E)$ AND COMPARISON OF REACTION RATE RATIOS IN NISUS, MOL-ΣΣ AND $\chi_{25}(E)$ NEUTRON FIELDS

5.1 Reaction rate measurements in MOL-ΣΣ and $\chi_{25}(E)$ neutron fields at MOL

Integral reaction rate measurements were performed at ΣΣ secondary standard and U-235 thermal neutron induced fission neutron spectrum ($\chi_{25}(E)$) fields at MOL, Belgium in collaboration of J.G. Williams (ULRC) and F. Cops (MOL) at the advice of A. Fabry (MOL) in April 1976. Activation foils of various materials were irradiated in ΣΣ and $\chi_{25}(E)$ neutron fields. These foils were the same foils used in the NISUS standard neutron field for reaction rate measurements. The specifications of the foils are given in Table 4.1 in Chapter 4.

A set of foils of different materials was placed in a flanged tube type aluminium foil holder. Aluminium spacer foils ($\sim$ 0.127 mm diameter X $\sim$0.04 mm thickness) were used to provide separation between each foil. This is shown in Fig. 5.1(a). The aluminium foil holder was then positioned inside an aluminium tube shown in Fig. 5.1(b). The dimensions of the aluminium foil holder and the aluminium tube are shown in Figs. 5.1(a) and 5.1(b).

The ΣΣ-assembly was pulled out of the graphite cavity and transferred through a roller path to an elementary hot cell. The aluminium tube with activation foils inside the aluminium foil holder was mounted

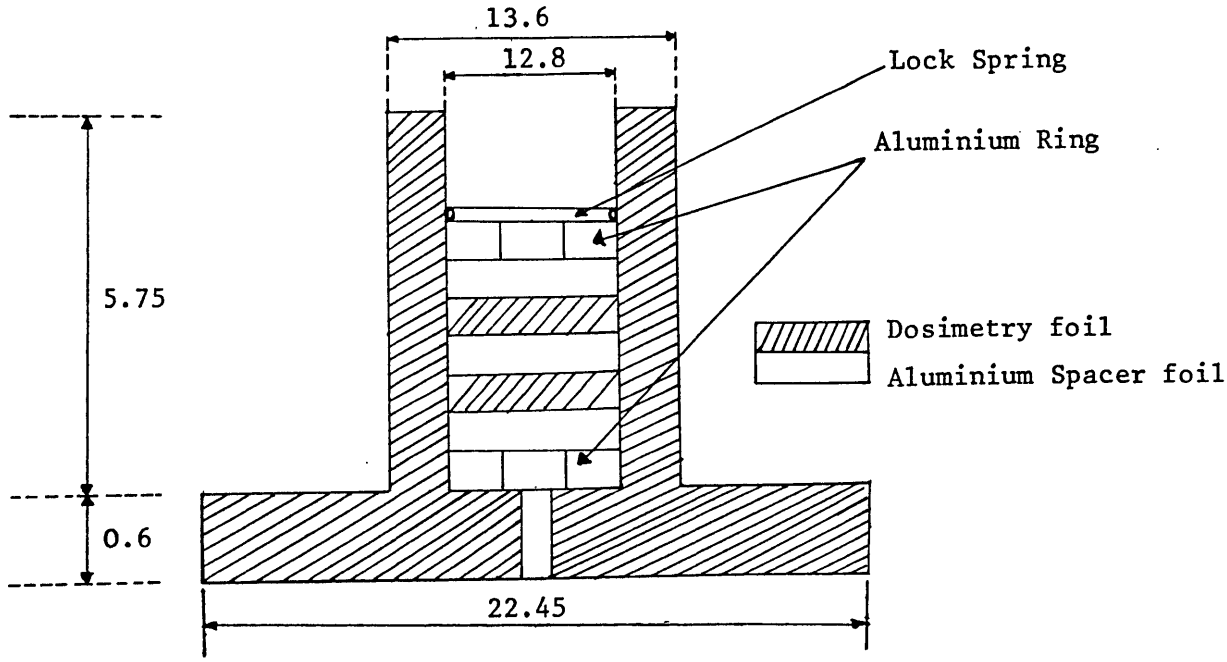


Fig.5.1(a). Schematic diagram of an Aluminium foil holder with Activation foils positioned inside.

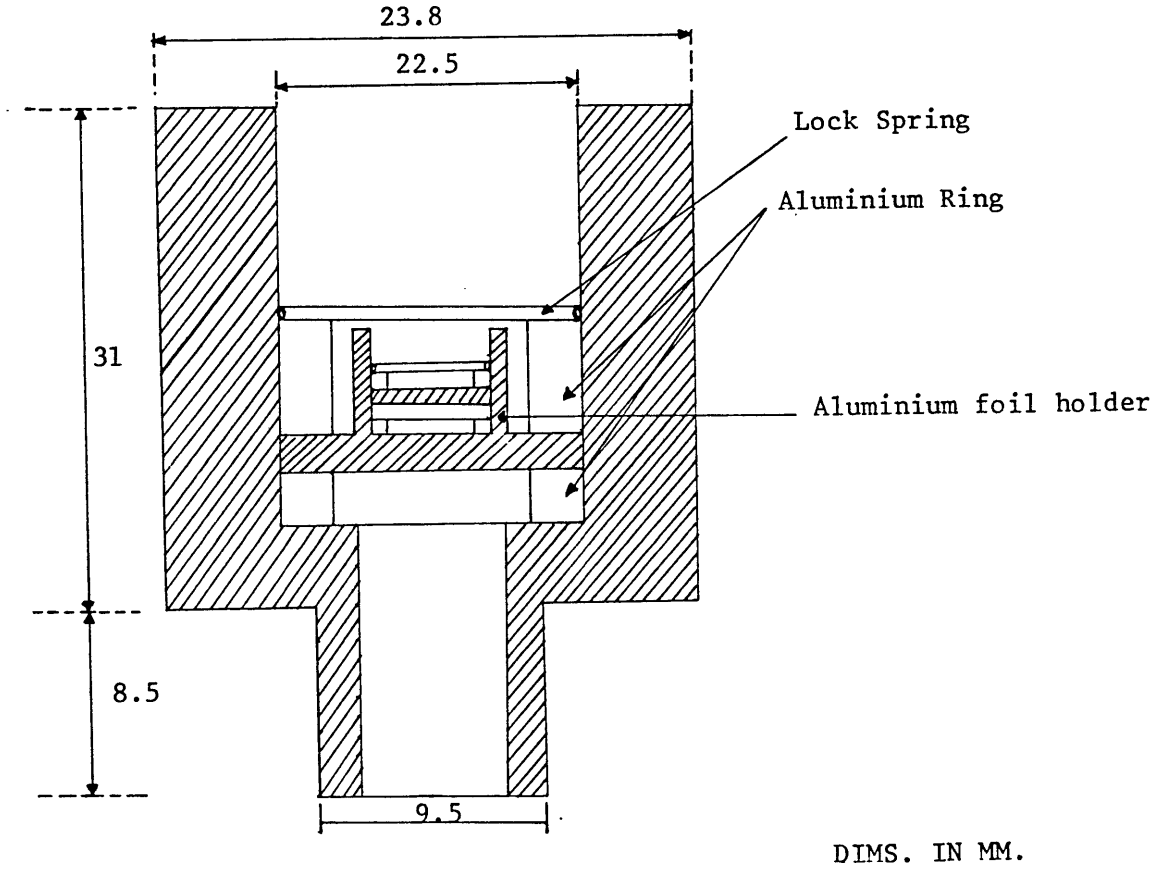


Fig.5.1(b). Schematic diagram of an Aluminium tube with Aluminium foil holder positioned inside.

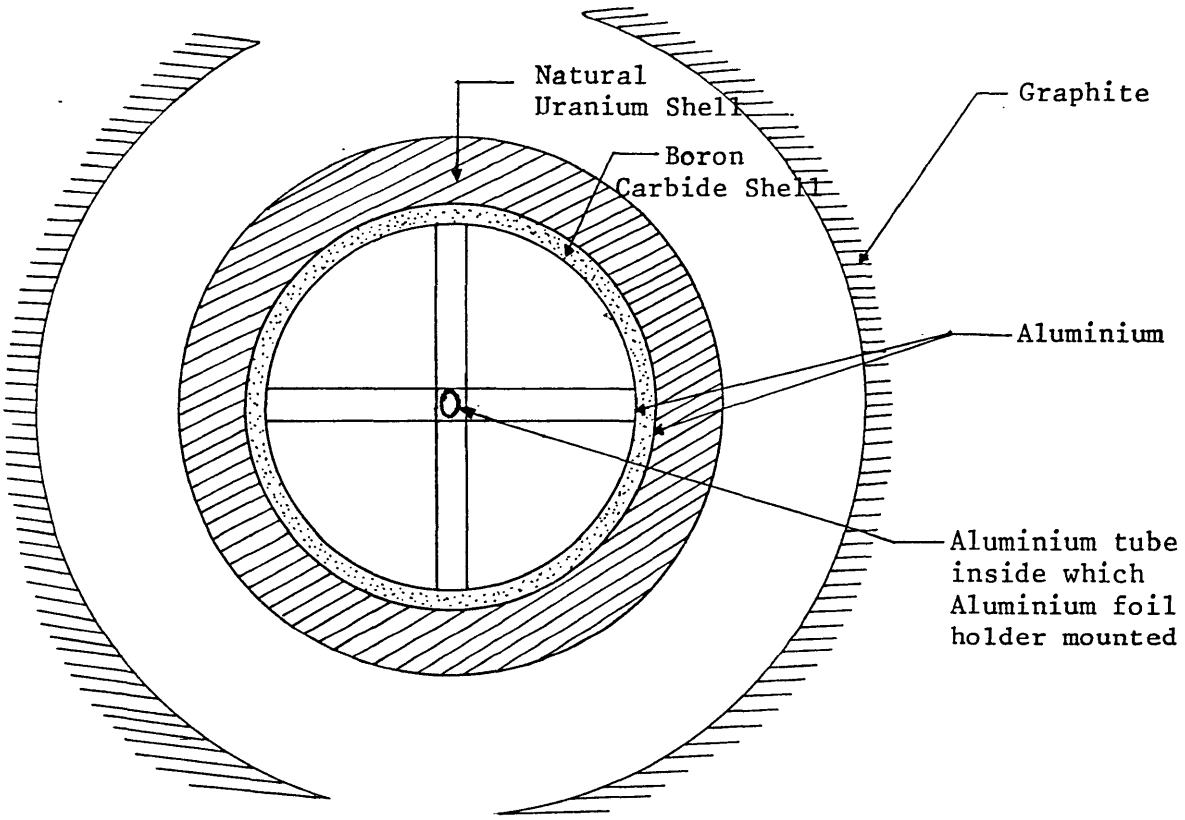


Fig.5.2(a). Cross-sectional in-pile view of the ΣΣ facility with Activation foils mounted at the centre.

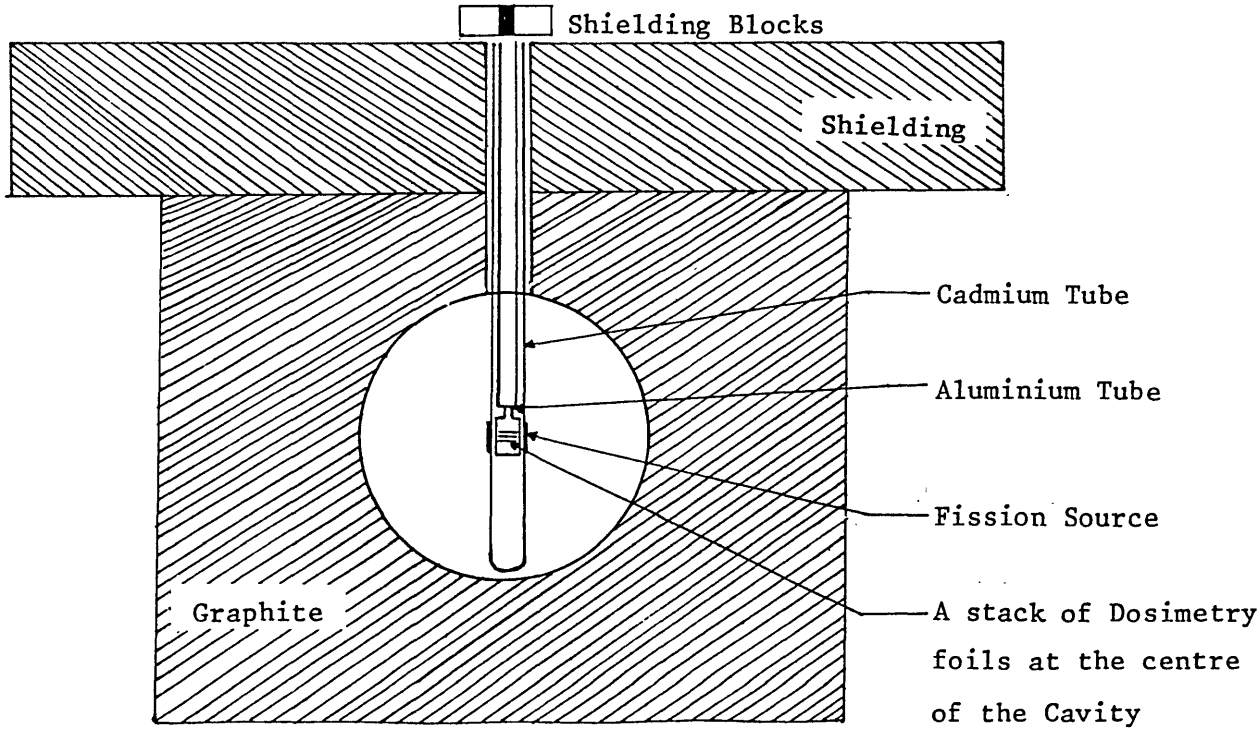


Fig.5.2(b). Schematic diagram of ^{235}U fission spectrum Cavity with Activation foils mounted at the centre.

by removing the upper hemisphere of the natural uranium and boron carbide shells. An in-pile view of the ΣΣ facility with activation foils at the centre is shown in Fig. 5.2(a).

A similar stack of non fissile threshold foils was mounted inside the small aluminium tube (Fig. 5.1(b)). This small tube was then connected to a long aluminium tube by an aluminium stem and inserted vertically inside the cadmium tube in such a way that the foils were positioned at the centre of the 1 meter spherical fission cavity. The positioning of the foils inside the U-235 fission cavity field is shown in Fig. 5.2(b).

The foils were irradiated at a power of 600 kW. Table 5.1 summarises the effective irradiation times and BR1 reactor power levels for 3 runs and 2 runs respectively performed in ΣΣ and fission spectrum neutron fields in order to obtain reaction rate of various activation foils. The effective irradiation time was supplied by F. Cops from MOL, Belgium[53]. The effective irradiation time $\overline{T}(\lambda)$ for activation of a radioisotope with half life $T_{\frac{1}{2}} = \ln 2/\lambda$, exposed to a time-dependent neutron flux specified by the power level profile function f(t), is deduced[46] from the relationship

$$1-e^{-\lambda T(\lambda)} = \frac{\lambda e^{-\lambda T}\int_0^T f(t)e^{\lambda t}dt}{\overline{f}} \qquad (5.1.1)$$

TABLE 5.1

Data relative to joint irradiations in ΣΣ and the fission spectrum at MOL.

Neutron fields		Reaction	Effective irradiation time (sec)	Reactor Power Level (KW)
ΣΣ	$\chi_{25}(E)$			
Run 1	-	$^{197}Au(n,\gamma)^{198}Au$	29219	600
Run 2	Run 2	$^{64}Zn(n,p)^{64}Cu$	28973	"
		$^{56}Fe(n,p)^{56}Mn$	26031	"
		$^{22}Al(n,\alpha)^{24}Na$	29021	"
Run 3	Run 3	$^{115}In(n,\gamma)^{116m}In$ (a)	12135	"
		$^{115}In(n,n')^{115m}In$	28370	"
		$^{58}Ni(n,p)^{58}Co$	29235	"
		$^{24}Mg(n,p)^{24}Na$	29021	"

(a) Reaction rate of $^{115}In(n,\gamma)^{116m}In$ for $\chi_{25}(E)$ was not evaluated.

TABLE 5.2

Day-to-day Reactor Power monitoring by means of Indium activation detector (Reactor Power 600 KW)

$^{115}In(n,n')^{115m}In$ (a) reaction (12.7 mm diam x 0.127 mm thick)

Date	Run	Neutron fields	
		ΣΣ	$\chi_{25}(E)$
12.4.76.	1	11795127 ± 0.35%	-
13.4.76.	2	11896834 ± 0.29%	12868310 ± 0.26%
14.4.76.	3	12020599 ± 0.18%	12963641 ± 0.45%

(a) $^{115}In(n,n')^{115m}In$ monitor reaction data was supplied by F. Cops of Belgium.

in which T is the true, total irradiation duration

$\overline{f}$ is some appropriately selected time-averaging of f(t), e.g.

$$\overline{f} = \int_{\Delta t} f(t)dt$$

where Δt is taken here as the true exposure duration at the nominal reactor power.

After irradiation of each foil in $\Sigma\Sigma$ and fission spectrum fields at BR1 reactor in Belgium, the foils were brought to London immediately. The foils were then counted in the Ge(Li) detector system at the University of London Reactor Centre. The Ge(Li) detecting system was the same which was used for reaction rate measurements of different foils in the NISUS neutron field. The same procedure was applied (Described in detail in section 4.7 in Chapter 4) to compute absolute reaction rate of various materials from $\Sigma\Sigma$ and $\chi_{25}(E)$ neutron fields.

The central reaction rates for $\Sigma\Sigma$ and $\chi_{25}(E)$ neutron fields were measured relatively to a day-to-day reactor power monitoring scheme at MOL based on the activation reaction $^{115}In(n,n')^{115m}In$. Three monitor indium foils were placed along with the activation foils inside the aluminium foil holder and mounted at the centre of $\Sigma\Sigma$ and $\chi_{25}(E)$ neutron fields. The saturated activity of monitor foils was

determined by F. Cops at MOL, Belgium for each run. Table 5.2 shows day-to-day reactor power monitoring for ΣΣ and $\chi_{25}(E)$ benchmark neutron fields at MOL.

Central reaction rates of various materials measured in ΣΣ and $\chi_{25}(E)$ neutron fields are given in Table 5.3. The errors are estimated at 1σ confidence level.

5.2 Comparison of experimental reaction rate ratios in NISUS, ΣΣ and $\chi_{25}(E)$ neutron fields

Spectral indices are defined as the ratio of two reaction rates:

$$S_{ij} = Ri/Rj$$

Where S_{ij} is the spectral index of reaction i to j.

Ri and Rj are the reaction rate of reactions i and j respecively.

Spectral indices are sensitive to spectrum variations and are therefore a means of comparing different spectra since these indices are the ratio of two reaction rates, it is not necessary to normalise the two spectra.

Comparison of experimental reaction rate ratios has been made for NISUS, ΣΣ and $\chi_{25}(E)$ neutron fields. These reaction rate ratios

TABLE 5.3

Central reaction rate measurements in ΣΣ and $\chi_{25}(E)$ benchmark neutron fields at MOL, Belgium.

Reaction	Reaction rate x 10^{-25} (a)	
	Neutron fields	
	ΣΣ (Present)	$\chi_{25}(E)$ (Present)
$^{115}In(n,\gamma)^{116m}In$	74.441 ± 2.5% (b)	-
$^{197}Au(n,\gamma)^{198}Au$	123.59 ± 2.3% (b)	-
$^{115}In(n,n')^{115m}In$	17.143 ± 2.3% (b)	16.98 ± 2.1% (b)
$^{58}Ni(n,p)^{58}Co$	8.0216 ± 2.7% (b,d)	9.4325 ± 2.5% (b,d)
$^{64}Zn(n,p)^{64}Cu$	2.4263 ± 2.5% (b)	2.9382 ± 2.4% (b)
$^{56}Fe(n,p)^{56}Mn$	0.0799 ± 3.3% (c)	0.0929 ± 3.3%
$^{24}Mg(n,p)^{24}Na$	0.1045 ± 3.1% (b)	0.1333 ± 3.0% (b)
$^{24}Al(n,\alpha)^{24}Na$	0.0470 ± 2.8% (b)	0.0623 ± 2.6% (b)

(a) Reaction rate per nucleus are normalised to $^{115}In(n,n')^{115m}In$ monitor saturated activity. Total uncertainties are estimated at 1σ confidence level.

(b) Half life and γ-ray intensity are quoted from Ref. 39.

(c) Half life and γ-ray intensity are quoted from Ref. 37.

(d) 2.9% correction has been made for coincidence summing effect according to Ref. 74.

are formed relative to $^{115}In(n,n')^{115m}In$ reaction in the denominator and are shown in Tables 5.4 and 5.5. Reaction rate ratios for NISUS are obtained from column 2 of Table 4.34 in Chapter 4 (NISUS central reaction rate measurements are considered only). For ΣΣ, these ratios are obtained from the measurement of Fabry[31 and 44] and also from Table 5.3 in the present work, The same foils and the same counting system were used to measure reaction rates of several reactions in the ΣΣ neutron field (Table 5.3) as those which were used in the determination of reaction rates in the NISUS neutron field. So the comparison between reaction rate ratios for these reactions in NISUS and ΣΣ fields will give direct information about the variation of spectrum in these two standard neutron fields because the bias due to measurer and the counting system are eliminated by using the same foils and same counting system.

Threshold reaction rates were measured in the $\chi_{25}(E)$ neutron field and are compared with the evaluated reaction rates of Fabry in $\chi_{25}(E)$[31] and these are shown in Table 5.5 (columns 4 and 5).

Comparing the reaction rate ratios of NISUS (present) and ΣΣ (present) when the same foils and same counting system were used (column 6 in Table 5.4) it can be seen that these reaction rate ratios agree very well within ± 1σ random error for all reactions except $^{24}Mg(n,p)^{24}Na$ reaction which agrees within ± 2σ random error. Random

TABLE 5.4

Comparison of experimental reaction rate ratios in NISUS and ΣΣ neutron fields between present measurements in NISUS and ΣΣ and Fabry's measurement in ΣΣ.

Reaction	Effective threshold energy (MeV) (a)	Reaction rate ratio[b] Neutron fields: NISUS (Present)	ΣΣ(Present)	ΣΣ(Fabry)	NISUS(Present) Ratio[f] ΣΣ(Present) Ratio (Cols. 3&4)	NISUS(Present) Ratio ΣΣ(Fabry) Ratio (Cols. 3&5)	ΣΣ(Present) Ratio ΣΣ(Fabry) Ratio (Cols. 4&5)
$^{55}Mn(n,\gamma)^{56}Mn$	-	0.5415 ± 3.8%	-	0.678 ±3.6%[d,e]	-	0.800 ± 5.2%	-
$^{115}In(n,\gamma)^{116m}In$	-	4.366 ± 4.0%	4.342 ± 3.4%	4.228 ±4.0%	1.005 ± 1.0%	1.033 ± 5.7%	1.027 ± 5.3%
$^{197}Au(n,\gamma)^{198}Au$	-	7.1768 ± 3.9%	7.209 ± 3.3%	7.148 ± 2.8%	0.995 ± 0.5%	1.004 ± 4.8%	1.009 ± 4.3%
^{235} (n,f)	-	26.785 ± 3.3%	-	27.00 ± 2.8%[c]	-	0.992 ± 4.3%	-
$^{239}Pu(n,f)$	-	31.632 ± 3.5%	-	31.75 ± 2.1%[c]	-	0.996 ± 4.1%	-
$^{237}Np(n,f)$	0.6	10.06 ± 3.7%	-	10.25 ± 2.5%[c]	-	0.981 ± 4.5%	-
$^{115}In(n,n')^{115m}In$	1.2	1.000 Ref.± 2.8%[g]	1.000 Ref.±2.3%[g]	1.000 Ref.±2%[g]	1.000 Ref.± 0.3% (g)	1.000 Ref.±3.4%(g)	1.000 Ref.±3.1%[g]
$^{238}U(n,f)$	1.5	1.522 ± 3.2%	-	1.522 ± 2.0%[c]	-	1.000 ± 3.8%	-
$^{58}Ni(n,p)^{58}Co$[h]	2.8	0.4713 ± 4.1%	0.4679 ± 3.5%	0.474 ± 3.2%	1.007 ± 1.7%	0.994 ± 5.2%	0.987 ± 4.7%
$^{64}Zn(n,p)^{64}Cu$	2.8	0.1425 ± 4.0%	0.1415 ± 3.4%	-	1.007 ± 0.8%	-	-
$^{27}Al(n,p)^{27}Mg$	4.4	0.0170 ± 5.6%	-	0.0175 ± 1o%	-	0.971 ± 11.5%	-
$^{56}Fe(n,p)^{56}Mn$	6.0	0.00452 ± 4.2%	0.00466 ± 4.0%	0.00464 ± 3.6%	0.970 ± 2.9%	0.974 ± 5.5%	1.004 ± 5.4%
$^{24}Mg(n,p)^{24}Na$	6.8	0.00633 ± 4.3%	0.00610 ± 3.9%	-	1.038 ± 2.9%	-	-
^{27}Al $(n,\alpha)^{24}Na$	7.2	0.00279 ± 4.1%	0.00274 ± 3.6%	0.00309 ± 3.6%	1.018 ± 1.9%	0.903 ± 5.5%	0.887 ± 5.1%

(a) Effective threshold energy values are quoted from Ref. 31.

(b) Reaction rate ratio formed relative to $^{115}In(n,n')^{115m}In$ reaction in the denominator.

(c) $^{235}U(n,f)$, $^{239}Pu(n,f)$, $^{238}U(n,f)$ and $^{237}Np(n,f)$ fission rate relative to $^{115}In(n,n')$ reaction rate are quoted from Ref. 44.

(d) Reaction rates relative to $^{115}In(n,n')^{115m}In$ reaction in the denominator are quoted from Ref. 31.

(e) Errors are quoted from Ref. 10.

(f) Uncertainties are estimated for random errors only at 1σ confidence level.

(g) This is the original total error assigned to $^{115}In(n,n')^{115m}In$ reaction rate measurement. It was used with other individual reaction rate error assignments to obtain the error assignments for this table.

(h) 2.9% correction has been made for coincidence summing effect according to Ref. 74 (Explained in Appendix C.)

TABLE 5.5

Comparison of experimental reaction rate ratios in $\chi_{25}(E)$ neutron field at MOL between present measurement and Fabry's measurement

Reaction	Effective[a] threshold energy (MeV)	Reaction rate ratio [b]		$\frac{\chi_{25}(E)\ \text{(Present)}}{\chi_{25}(E)\ \text{(Fabry)}}$ Ratio
		$\chi_{25}(E)$ (Present)	$\chi_{25}(E)$ (Fabry)[c]	
$^{115}In(n,n')^{115m}In$	1.2	1.000 Ref.±2.1%[e]	1.000 Ref.±3.1%[e]	1.000 Ref.±3.7%
$^{58}Ni(n,p)^{58}Co$[d]	2.8	0.556 ± 3.3%	0.574 ± 5.2%	0.969 ± 6.2%
$^{64}Zn(n,p)^{64}Cu$	2.8	0.173 ± 3.2%	0.158 ± 5.9%	1.095 ± 6.7%
$^{56}Fe(n,p)^{56}Mn$	6.0	0.00547 ± 3.9%	0.00548 ± 7.4%	0.998 ± 8.4%
$^{24}Mg(n,p)^{24}Na$	6.8	0.00785 ± 3.7%	0.00783 ± 5.8%	1.003 ± 6.9%
$^{27}Al(n,\alpha)^{24}Na$	7.2	0.00367 ± 3.3%	0.00373 ± 5.8%	0.984 ± 6.7%

(a) Effective threshold energy values are quoted from Ref1. 31.

(b) Reaction rate ratio formed relative to $^{115}In(n,n')^{115m}In$ reaction in the denominator.

(c) Reaction rates relative to $^{115}In(n,n')^{115m}In$ reaction are the evaluated values quoted from Ref. 31.

(d) 2.9% correction has been made for coincidence summing effect according to Ref. 74 (Explained in Appendix C).

(e) This is the original total error assigned to $^{115}In(n,n')^{115m}In$ reaction rate measurement. It was used with other individual reaction rate error assignments to obtain the error assignments for this table.

errors are considered only in these reaction rate ratio comparison because systematic errors are cancelled when same foils and same counting system were used. This comparison shows that the NISUS and ΣΣ neutron fields are identical.

Comparison has been made between the reaction rate ratios of NISUS (present) and ΣΣ (Fabry) (column 7 in Table 5.4), it is found that the reaction rate ratios for these two fields agree very well within their total uncertainties except $^{55}Mn(n,\gamma)^{56}Mn$ and $^{27}Al(n,\alpha)^{24}Na$ reactions. The reaction rate for $^{55}Mn(n,\gamma)^{56}Mn$ reaction was not corrected for self shielding effect in case of NISUS neutron field as no self shielding correction is available. The 20% discrepancy will be reduced if a self shielding correction is made. The NISUS $^{27}Al(n,\alpha)$ reaction rate is $\sim$ 10% lower than ΣΣ $^{27}Al(n,\alpha)$ reaction rate. The reason for this is not known but Fabry is currently checking his value.

By making comparison of reaction rate ratios of ΣΣ(present) and ΣΣ(Fabry) (column 8 in Table 5.4), it is observed that the reaction rate ratios agree well within their $\pm$ 1 σ total uncertainties in all reactions except $^{27}Al(n,\alpha)^{24}Na$ reaction. ΣΣ (present) $^{27}Al(n,\alpha)^{24}Na$ reaction rate ratio is lower $\sim$ 11% than that of ΣΣ(Fabry). Nearly the same discrepancy is obtained for $^{27}Al(n,\alpha)^{24}Na$ reaction rate for NISUS (present) and ΣΣ(Fabry) comparison (column 7 in Table 5.4).

So ∿ 10% higher value for $^{27}Al(n,\alpha)^{24}Na$ reaction rate in ΣΣ(Fabry) can be attributable to reaction rate measurement of $^{27}Al(n,\alpha)^{24}Na$ reaction at MOL. This is supplemented in a recent paper[31] by Fabry that the measured integral data for $^{27}Al(n,p)^{27}Mg$, $^{56}Fe(n,p)^{56}Mn$ and $^{27}Al(n,\alpha)^{24}Na$ may be high for ΣΣ.

Comparing the reaction rate ratios of $\chi_{25}(E)$ (present) and $\chi_{25}(E)$ (Fabry) (Column 5 in Table 5.5) it can be seen that the measured reaction rate ratios agree well except $^{64}Zn(n,p)^{64}Cu$ reaction which is ∿ 10% higher in case of $\chi_{25}(E)$ (present) than $\chi_{25}(E)$ (Fabry). No suitable explanation can be found for this discrepancy yet.

Comparison of measured spectral indices in NISUS and ΣΣ relative to the ^{235}U fission spectrum is made in Table 5.6 and shown in Fig. 5.3. It is found that the reaction rate ratios in NISUS and ΣΣ relative to the ^{235}U fission spectrum are agreeing well within ± 1σ total uncertainties. This shows that the high energy spectral tail (above ∿2 MeV) of NISUS and ΣΣ neutron fields is close to a pure ^{235}U fission spectrum. It is observed in most fission driven systems that the high energy spectral shape above ∿2.5 MeV is nearly fission spectrum shape[31 and 7].

Thus by interlaboratory comparisons of measured reaction rate ratios in NISUS and ΣΣ and also relative to $\chi_{25}(E)$ neutron field, it can be concluded that NISUS and ΣΣ are the two almost identical standard fast neutron fields and the high energy spectral tail of these two neutron fields (NISUS and ΣΣ) is close to a pure U-235 fission spectrum shape (above ∿ 2.5 MeV).

TABLE 5.6

Comparison of reaction rate ratios in NISUS, ΣΣ and $\chi_{25}(E)$ neutron fields between present measurements.

Reaction	Effective threshold energy (Mev)	Reaction rate ratio[a]			NISUS (Present) Ratio	ΣΣ(Present) Ratio
		NISUS (Present) (Col. 3 in Table 5.4)	ΣΣ (Present) (Col. 4 in Table 5.4)	$\chi_{25}(E)$ (Present) (Col. 5 in Table 5.5)	$\chi_{25}(E)$ (Present) Ratio (Cols. 3 & 5)	$\chi_{25}(E)$ (Present) Ratio (Cols. 4 & 5)
$^{115}In(n,n')^{115m}In$	1.2	1.000 Ref. ± 2.8%[b]	1.000 Ref. ± 2.3%[b]	1.000 Ref. ± 3.1%[b]	1.000 Ref. ± 4.1%	1.000 Ref. ± 3.9%
$^{58}Ni(n,p)^{58}Co$	2.8	0.4713±4.1%	0.4679 ±3.5%	0.556 ±5.2%	0.849±6.6%	0.843±6.3%
$^{56}Fe(n,p)^{56}Mn$	6.0	0.00452±4.2%	0.00466±4.0%	0.00547±3.9%	0.826±5.7%	0.852±5.6%
$^{24}Mg(n,p)^{24}Na$	6.8	0.00633±4.3%	0.00610±3.9%	0.00785±3.7%	0.806±5.7%	0.777±5.4%
$^{27}Al(n,\alpha)^{24}Na$	7.2	0.00279±4.1%	0.00274±3.6%	0.00367±3.3%	0.760±5.3%	0.747±4.9%

(a) $^{64}Zn(n,p)^{64}Cu$ reaction rate has not been considered because the present measurement of $^{64}Zn(n,p)^{64}Cu$ has a discrepancy of ~10% with Fabry's $^{64}Zn(n,p)^{64}Cu$ evaluation in $\chi_{25}(E)$ neutron field (shown in Table 5.5).

(b) This is the original total error assigned to $^{115}In(n,n')^{115m}In$ reaction rate measurement. It was used with other individual reaction rate error assignments to obtain the error assignments for this table.

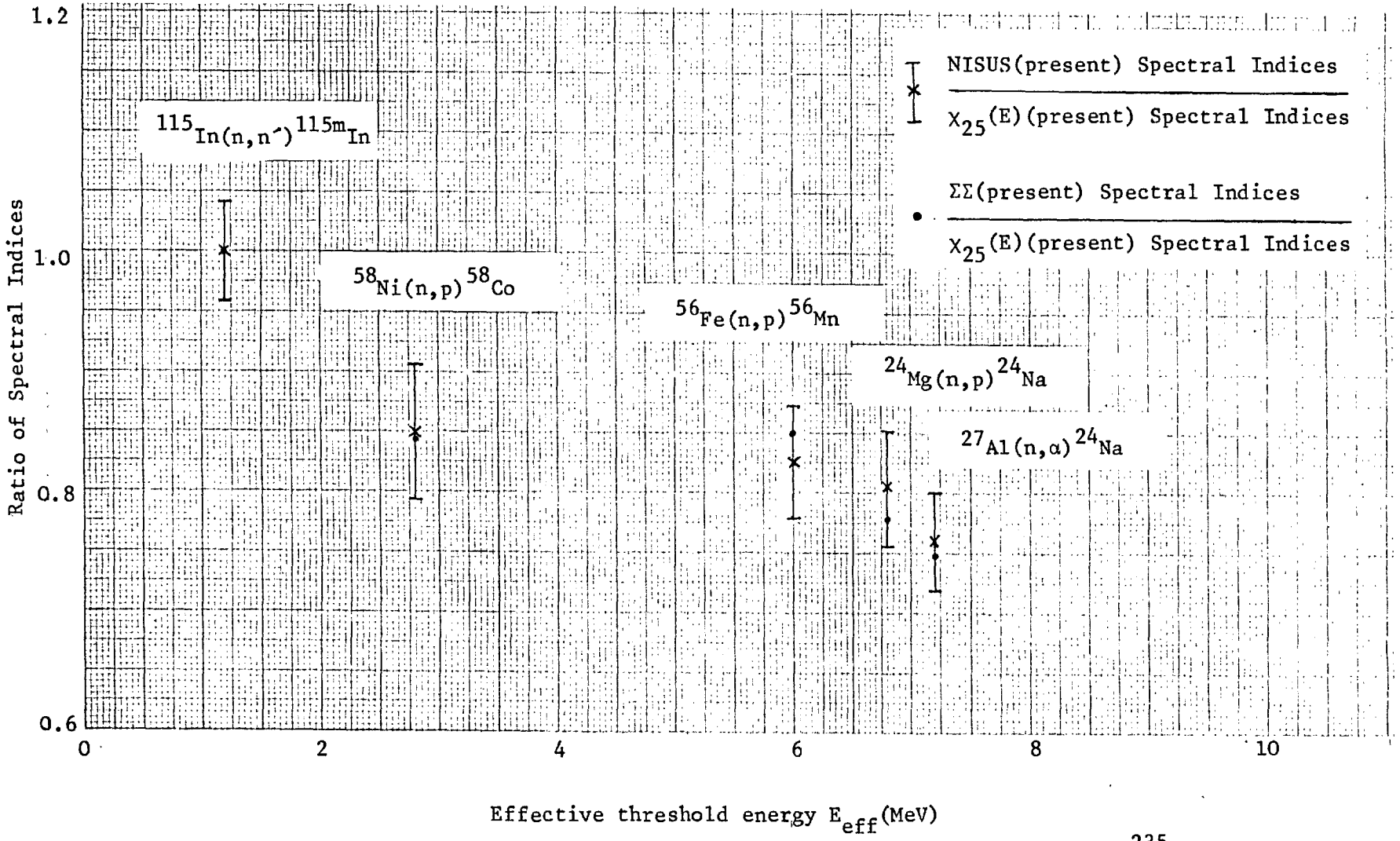


Fig.5.3. Measured Spectral indices for NISUS and ΣΣ neutron fields relative to the ^{235}U fission neutron spectrum in the present work.

6. CROSS SECTION DATA

The relation between the absolute reaction rate per atom of a material and the neutron spectrum $\phi(E)$ is

$$A = \int_0^\infty \sigma(E)\ \phi(E)dE \qquad (6.1.1)$$

Where $\sigma(E)$ is the energy dependent cross section of the material for the reaction measured and A is the reaction rate per atom of the material determined experimentally. Appropriate emphasis has to be and is increasingly placed onto the establishment of consistent and reliable dosimetry cross section files [54 & 55] for activation foils used to monitor or calibrate material testing experiments and to yield consistent fluxes and spectra. A basic requirement for these nuclear data files is their ability to reproduce integral reaction rates observed in neutron flux spectra. Standard neutron fields are particularly ideal benchmarks[54] for the integral consistency testing of the dosimetry reactions featuring the best known differential energy dependent cross sections[46].

6.1 Evaluated energy dependent cross sections

Energy dependent cross sections for different dosimetry reactions have been used in conjunction with the SIMMM code (a code for neutron spectrum analysis explained in detail in Chapter 7) to determine the

integral reaction rates and central neutron spectrum of NISUS.

Table 6.1 lists the energy dependent cross sections for different dosimetry reactions used in this work and the source of cross section data for each reaction.

TABLE 6.1

Dosimetry reactions and source and specification of cross section data set used

Reaction	Data file for $\sigma_i(E)$	Specification	Category
$^{55}Mn(n,\gamma)^{56}Mn$	SAND II Library	McElroy(1967)(Ref. 59)	II
$^{115}In(n,\gamma)^{116m}In$	CEN-SCK "	Fabry (1970) (Ref. 62)	II
$^{197}Au(n,\gamma)^{198}Au$	ENDF/BIII "	Material 1166	I
$^{235}U(n,f)F.P.$	ENDF/BIII "	Material 1157	I
$^{239}Pu(n,f)F.P.$	ENDF/BIII "	Material 1159	I
$^{237}Np(n,f)F.P.$	SAND-II "	BNWL-1312 (Ref. 58)	I
$^{238}U(n,f)F.P.$	ENDF/BIII "	Material 1158	I
$^{115}In(n,n')^{115m}In$	SAND-II "	BNWL-1312 (Ref. 58)	I
$^{58}Ni(n,p)^{58}Co$	SAND-II "	BNWL-1312 (Ref. 58)	I
$^{64}Zn(n,p)^{64}Cu$	SAND-II "	McElroy(1967)(Ref. 59)	II
$^{27}Al(n,p)^{27}Mg$	SAND-II "	BNWL-1312 (Ref. 58)	II
$^{56}Fe(n,p)^{56}Mn$	SAND-II "	BNWL-1312 (Ref. 58)	II
$^{24}Mg(n,p)^{24}Na$	SAND-II "	McElroy(1967)(Ref. 59)	II
$^{27}Al(n,\alpha)^{24}Na$	SAND-II "	BNWL-1312 (Ref. 58)	I

To improve the evaluated cross sections by benchmark experiments, two categories of neutron dosimetry reactions have been recognised[54]. In category I are those reactions with the best known cross sections i.e. $^{235}U(n,f)$, $^{238}U(n,f)$, $^{239}Pu(n,f)$, $^{237}Np(n,f)$, $^{197}Au(n,\gamma)^{198}Au$, $^{115}In(n,n')^{115m}In$, $^{58}Ni(n,p)^{58}Co$ and $^{27}Al(n,\alpha)^{24}Na$, and a few others. Most other useful dosimetry reactions are placed in category II. Some of category I and II reactions used in this work are shown in Table 6.1. In determining flux spectra for CFRMF and ΣΣ by SAND II (a code for neutron spectrum unfolding), McElroy[7] used evaluated energy dependent cross sections for different dosimetry reactions as listed in Table 6. except $^{55}Mn(n,\gamma)^{56}Mn$, $^{115}In(n,\gamma)^{116m}In$, $^{64}Zn(n,p)^{64}Cu$ and $^{24}Mg(n,p)^{24}Na$.

ENDF/B cross section data library

ENDF/B III cross sections were converted into DLC-2/99 energy group structure from pointwise cross sections by applying SUPERTOG[56]. ENDF/BIII cross sections converted into DLC-2/99 energy group structure were obtained from Ref. 57. DLC-2/99 group structure covers the energy range from 4×10^{-1} eV to 15.0 MeV.

SAND-II cross section data library

A tabular listing of energy interval averaged cross sections is given by McElroy for different neutron induced reactions[58 & 59] in a 620 group structure. The energy range for the 620 group structure covers from 1.0×10^{-4} eV to 18 MeV. These cross sections[58] were

evaluated from McElroy's previous work[59], by the unfolding technique and by modifying his previous work[59] to agree with Grundl[60] and Liskien and Paulsen[61].

CEN-SCK cross section data library

Fabry recommended a set of cross section data for several dosimetry reactions in the energy range 10 KeV to 20 MeV[62].

The energy dependent cross sections for different reactions from SAND-II and CEN-SCK cross section libraries were in different group structures from the ENDF/B DLC-2/99 group structure. These cross sections were converted into the 99 group structure after being weighted by a fission spectrum. These cross sections in the 99 group structure were weighted by the NISUS spectrum shape and subsequently collapsed into a 20 group structure.

6.2.1 Fission spectrum averaged cross section

For any condensation a neutron spectrum must either be determined or assumed to obtain a spectral averaged cross section. As a first approximation a fission spectrum is assumed to obtain a spectral averaged cross section in 99 groups.

Cranberg's fission spectrum of ^{235}U[63] was used to average the cross sections. The Cranberg equation is

$$\phi(E) = C \exp(-E/0.965) \text{ Sinh } (2.29E)^{\frac{1}{2}} \qquad (6.2.1)$$

$$C = 0.453$$

The integral value of $\phi(E)$ between two energy boundaries using Simpson's rule (shown in Fig. 6.1) is

$$\int_{Ei+1}^{Ei} \phi(E)dE = \frac{1}{3}\left(\frac{E_i - E_{i+1}}{2}\right) \left|\phi(E_i) + 4\phi(E_m) + \phi(E_{i+1})\right|, (i = 1,2,3....g) \qquad (6.2.2)$$

Where $\phi(E)$ = Cranberg fission spectrum as given in equation (6.2.1)

E_i = upper energy boundary of group i

E_{i+1} = lower energy boundary of group i

$\phi(E_i)$ = fission spectrum at boundary i

$= 0.453 \ (-E_i/0.965) \ \sinh(2.29E_i)^{\frac{1}{2}}$

$\phi(E_{i+1})$ = fission spectrum at boundary (i+1)

$= 0.453 \ (-E_{i+1}/0.965) \ \sinh(2.29 \ E_{i+1})^{\frac{1}{2}}$

$$\phi(E_m) = 0.453 \left|\frac{-(E_i + E_{i+1})}{2 \times 0.965}\right| \sinh \left|2.29 \ \frac{(E_i + E_{i+1})}{2}\right|^{\frac{1}{2}}$$

A computer program FISSION was used to obtain fission spectrum for different energy groups.

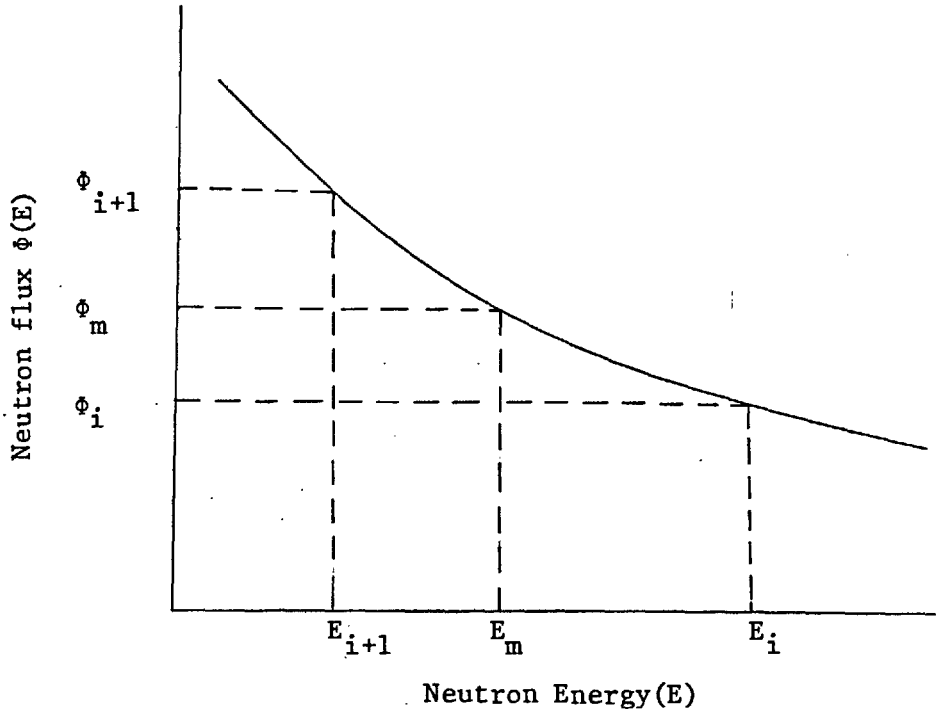


Fig.6.1. Simpson's rule.

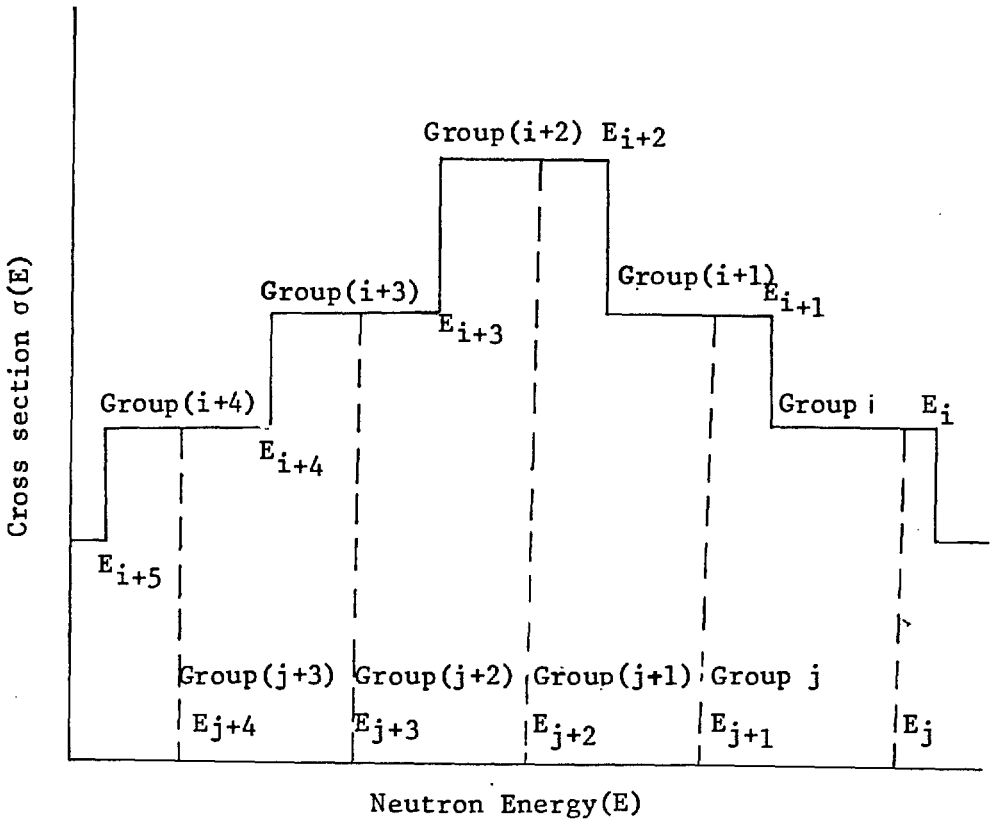


Fig.6.2. Group conversion for Cross section data.

6.2.2 Group collapsing

The fission spectrum obtained for different energy groups (620 groups in case of McElroy's data and 55 groups in case of Fabry's data) was collapsed into DLC-2/99 group structure. As the energy boundaries are different for old and new energy groups, it is necessary to consider what fraction of the fission spectrum of each old group (620 group) is contributing to each new group (99 groups). This is obtained by taking the ratio of the lethargy width of old energy group i within the new energy group j to the total lethargy of group i (shown in Fig. 6.2). Thus the spectrum for a new energy group j can be defined as

$$\phi_j(E) = \phi_i(E)\left(\frac{U_{i,j}}{U_i}\right) + \phi_{i+1}(E)\left(\frac{U_{i+1,j}}{U_{i+1}}\right) \qquad (6.2.3)$$

where $\phi_j(E)$ = fission spectrum of new energy group j

$\phi_i(E)$ = fission spectrum of old energy group i

$\phi_{i+1}(E)$ = fission spectrum of old group (i+1)

$U_{i,j}$ = lethargy width of old energy group i within new group j

U_i = total lethargy width of group i

$\left(\frac{U_{i,j}}{U_i}\right)$ = ratio of the lethargy width of group i within group j to the total lethargy width of group i

$\left(\frac{U_{i+1,j}}{U_{i+1}}\right)$ = ratio of the lethargy width of group (i+1) within group j to the total lethargy width of group (i+1)

Equation (6.2.3) can be written as

$$\phi_j(E) = \phi_i(E) \frac{\ln(\frac{E_j}{E_{i+1}})}{\ln(\frac{E_i}{E_{i+1}})} + \phi_{i+1}(E) \frac{\ln(\frac{E_{i+1}}{E_{j+1}})}{\ln(\frac{E_{i+1}}{E_{i+2}})} \qquad (6.2.4)$$

where E_i, E_{i+1}, E_{i+2} are the upper energy boundaries of old groups i, (i+1), (i+2) respectively.

E_j and E_{j+1} are the upper energy boundaries of new groups j and (j+1) respectively.

The fission spectrum averaged cross section for new energy group j can be evaluated as

$$\bar{\sigma}_j = \frac{\sum_j^{j+1} \sigma_i(E)\, \phi_j(E)}{\sum_j^{j+1} \phi_j(E)} , \quad (j=1,2,.....G) \qquad (6.2.5)$$

A computer program SIGMA was used to obtain fission spectrum averaged cross section for the new energy groups.

6.3 NISUS spectrum weighted cross sections

The energy dependent cross sections were all converted into the 99 group structure in order to weight these cross sections by the NISUS 1 spectrum. NISUS 1 central neutron spectrum was evaluated into the 99 group structure using the ANISN code (A one dimensional discrete ordinates transport code with Anisotropic scattering) by J. Petr[47]. NISUS 1 assembly is the same as NISUS 1b. The only difference between these two configurations is that NISUS 1 had Belgian B_4C shell in its assembly and NISUS 1b has American B_4C shell in its assembly.

The evaluated cross sections for different dosimetry reactions in 99 groups were weighted by the NISUS 1 spectrum and collapsed into a 20 group structure.

The present accuracy of these evaluated cross sections was at the 10-20% level (1σ)[7] although for some reactions, such as $^{235}U(n,f)$ it is much better. Error in the evaluated cross sections was taken from Ref. 7 which lists the current updated SAND-II-evaluated cross section tape error assignments based on the 15-group energy structure used with the SAND-II Monte Carlo error analysis code.

The evaluated energy dependent cross section for different dosimetry reactions with their errors are given in Appendix B in Tables B1-B6 as unadjusted cross sections and the energy dependent

cross sections are plotted in Figures 6.3 - 6.9.

Values are possibly subject to bias due to the collapsing scheme documented above, but these biases are thought to be small. Rigorous checks of any collapsing scheme should be applied before data are used in any comprehensive adjustment scheme.

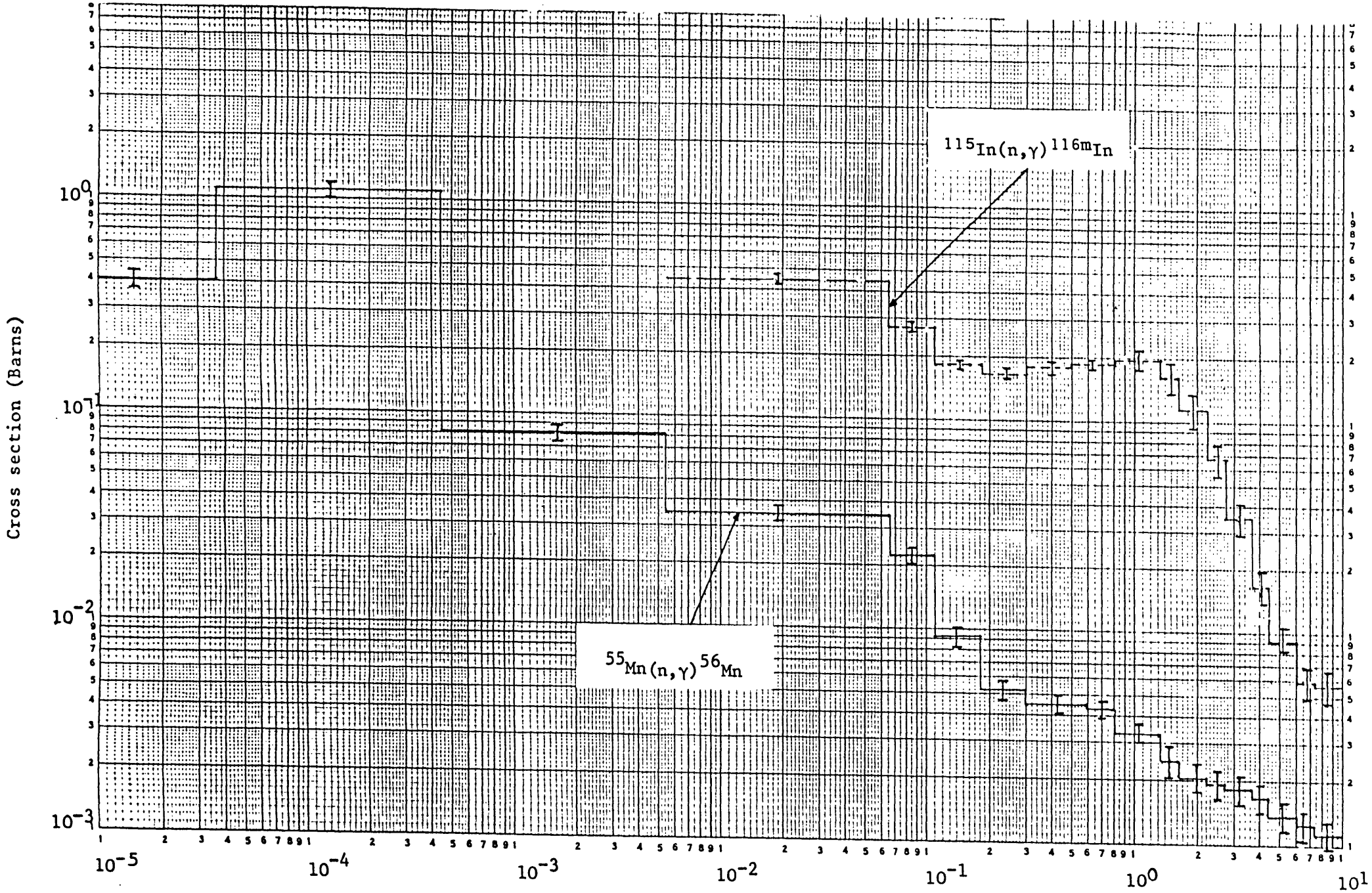


Fig.6.3. $^{55}Mn(n,\gamma)^{56}Mn$ and $^{115}In(n,\gamma)^{116m}In$ cross sections.

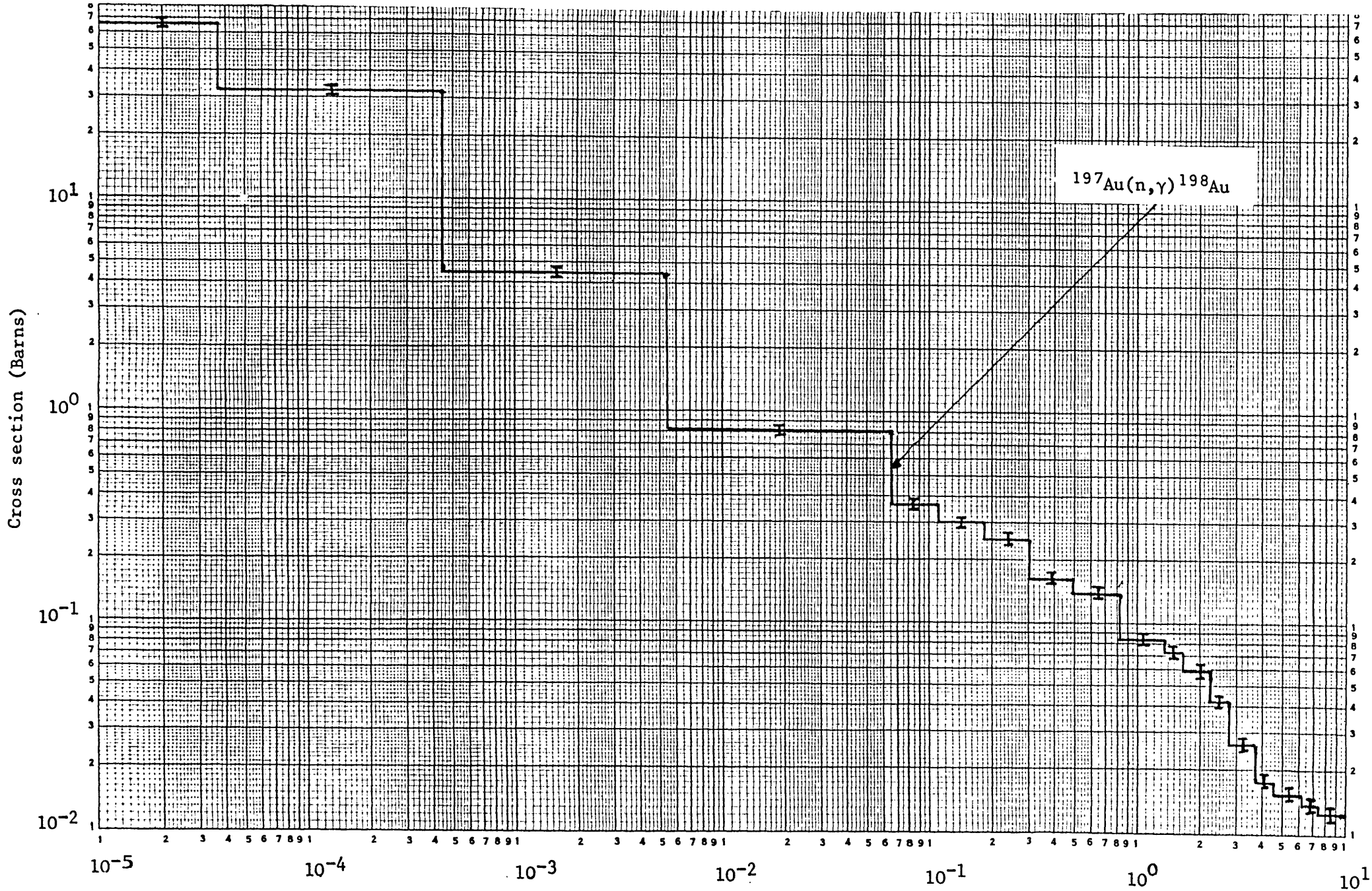


Fig. 6.4. $^{197}Au(n,\gamma)^{198}Au$ cross section.

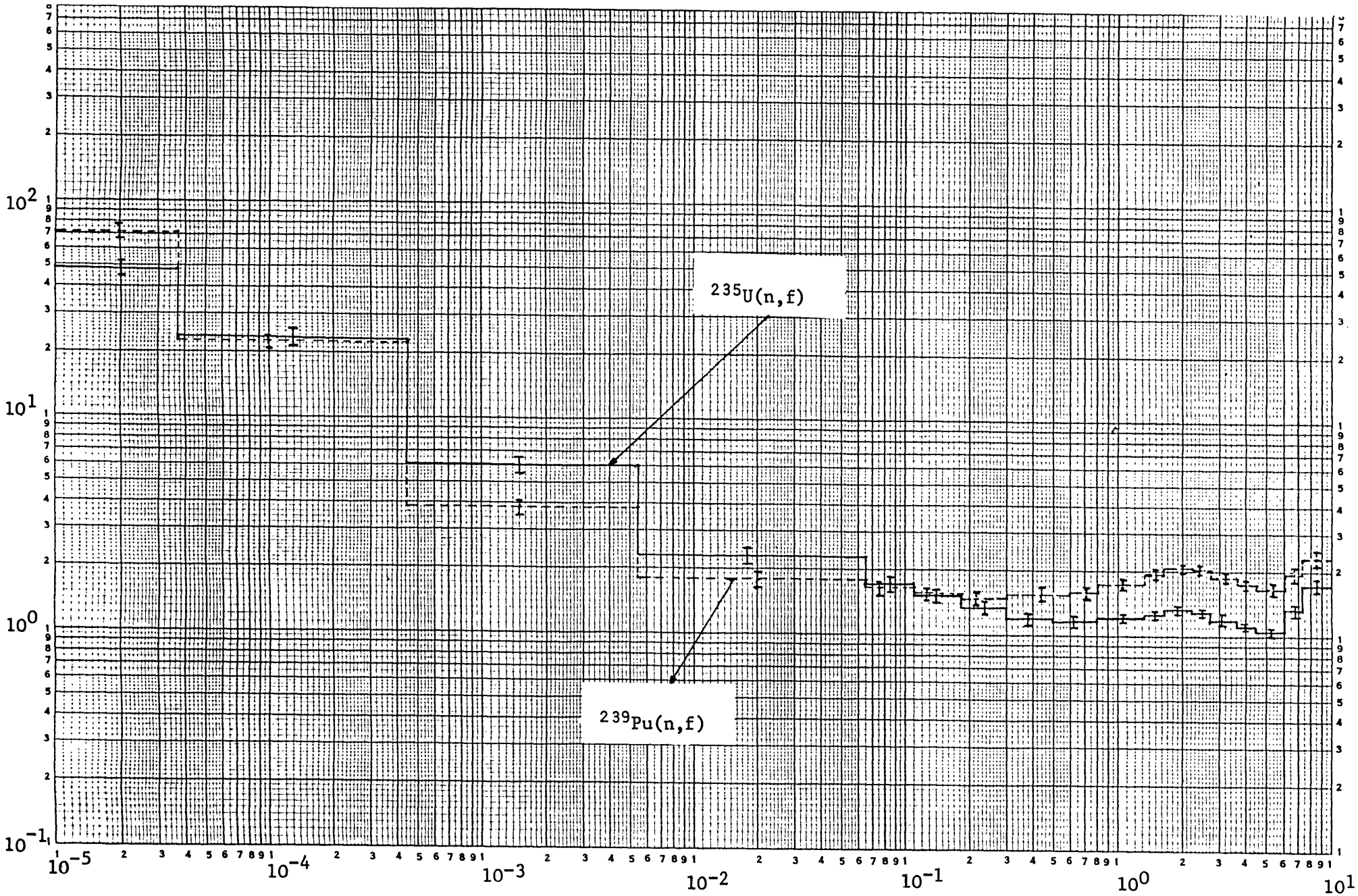


Fig. 6.5. $^{235}U(n,f)$ and $^{239}Pu(n,f)$ cross sections.

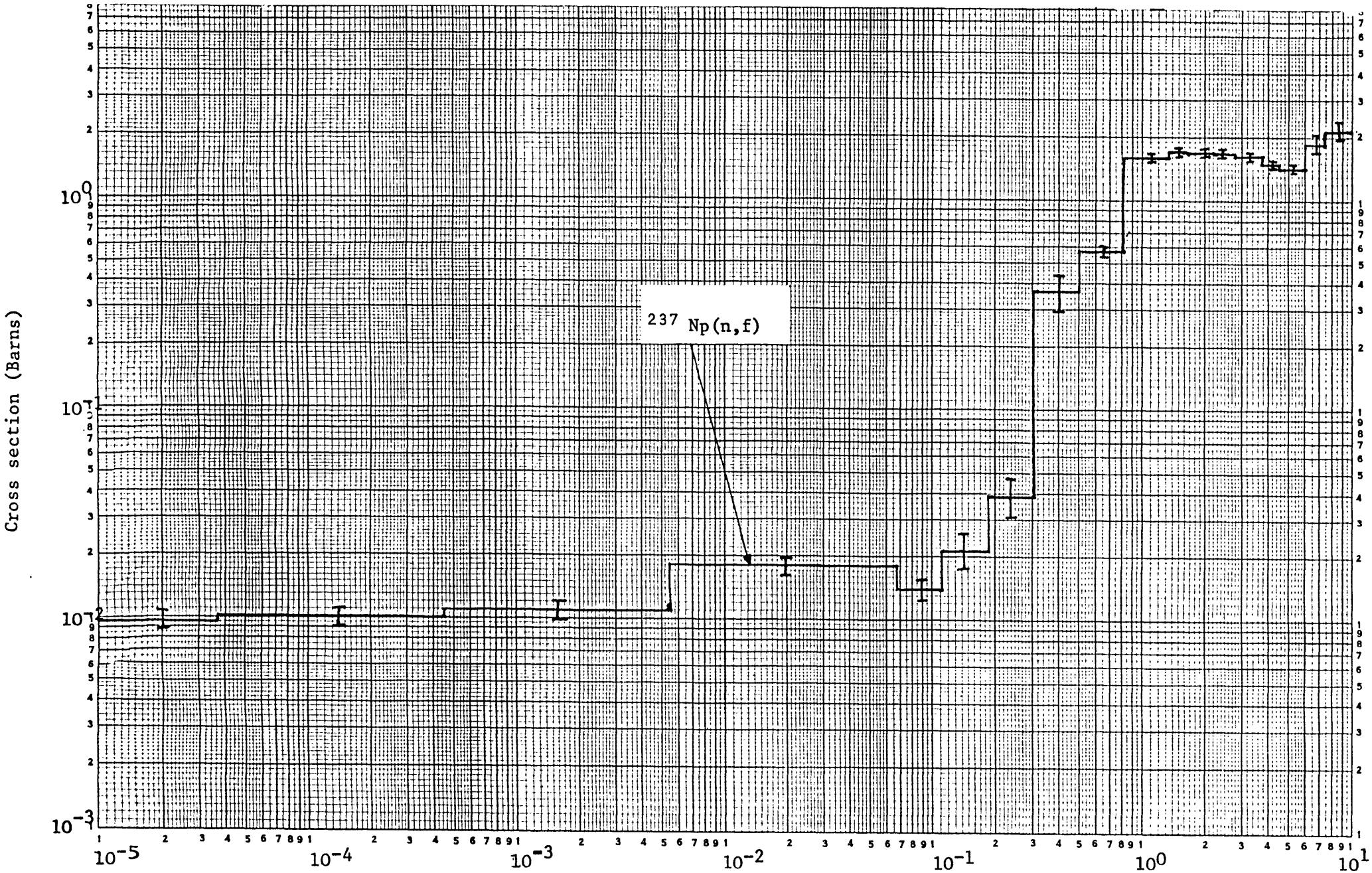


Fig.6.6. $^{237}Np(n,f)$ cross section

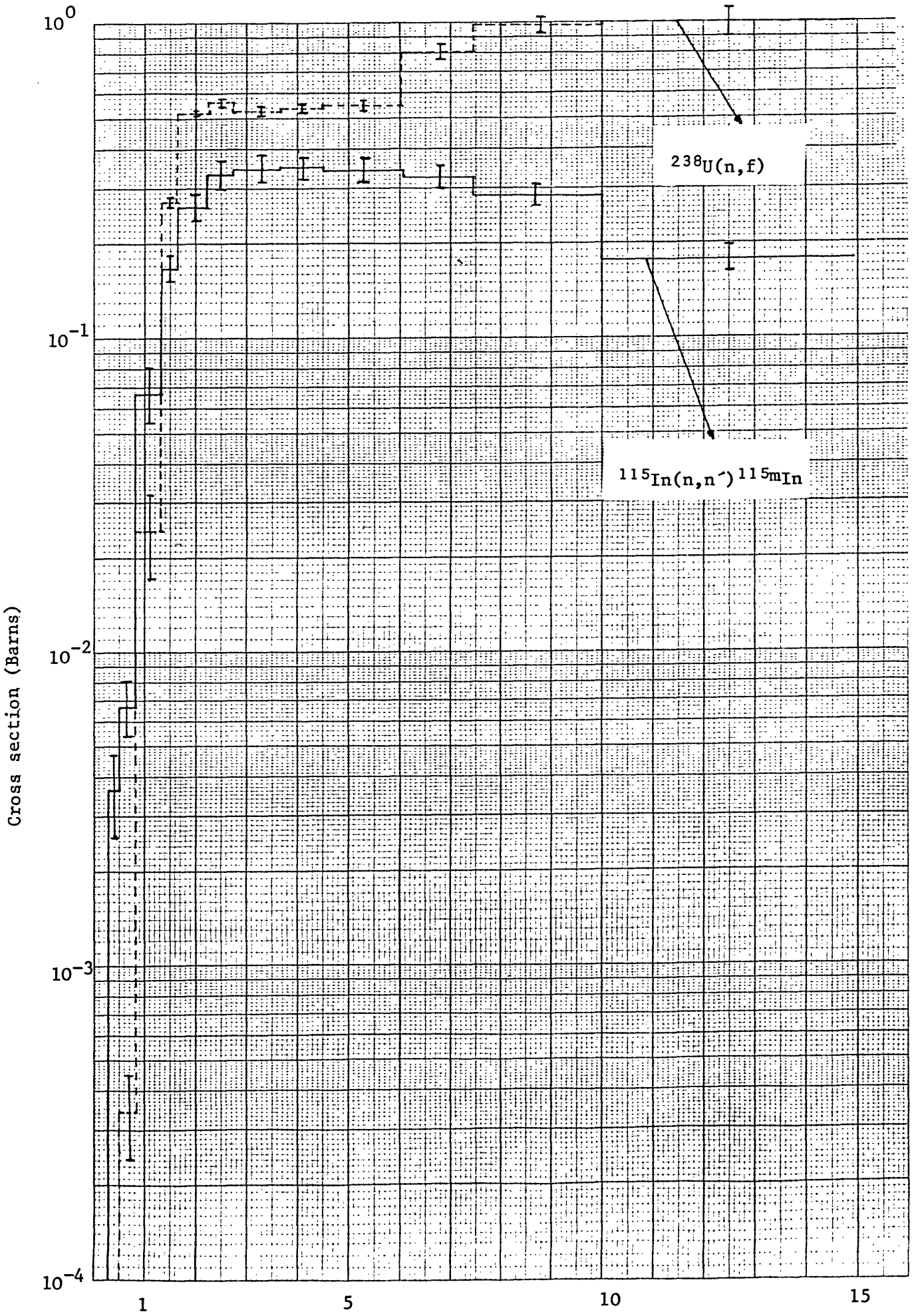


Fig.6.7. $^{115}In(n,n')^{115m}In$ and $^{238}U(n,f)$ cross sections.

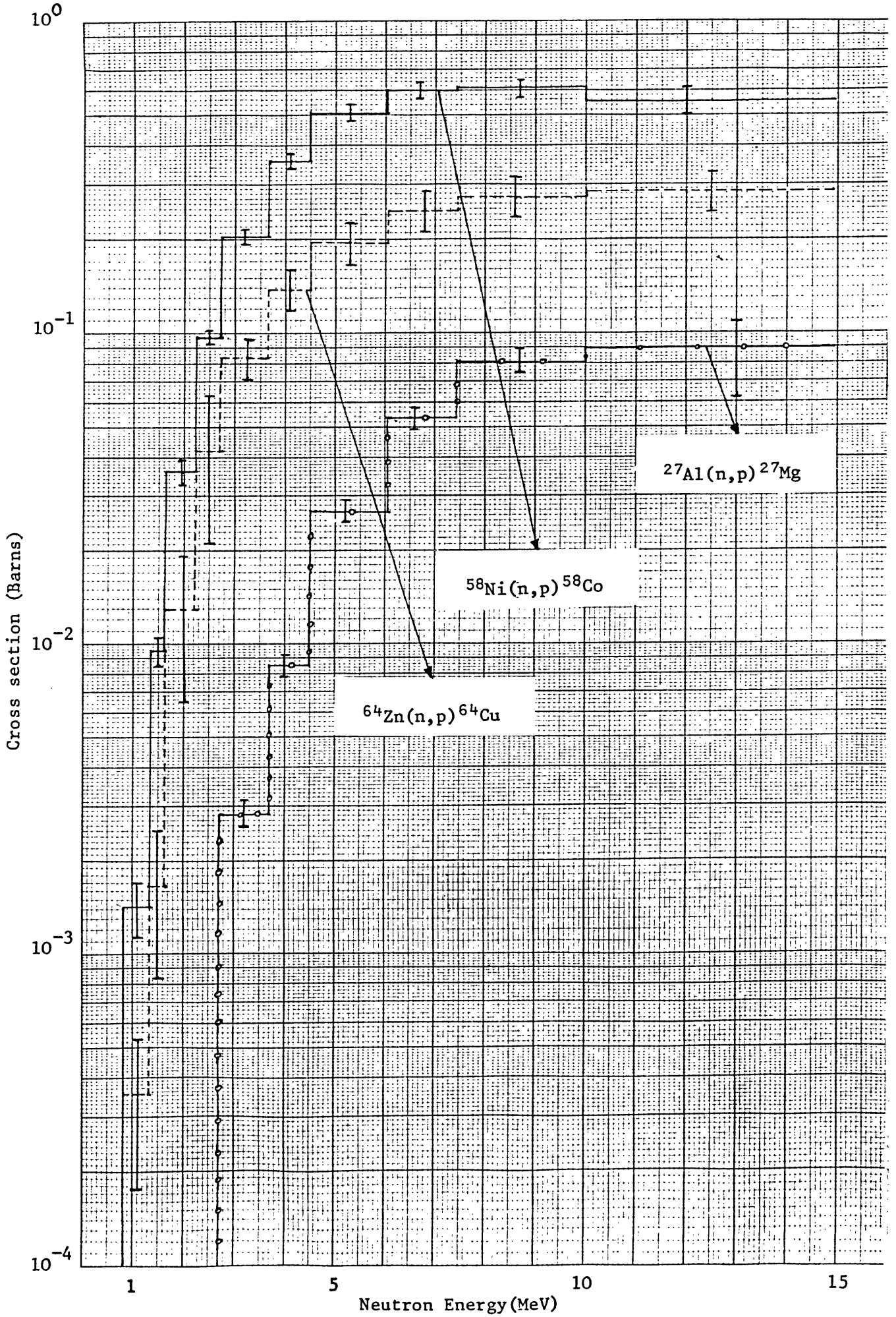


Fig.6.8. $^{58}Ni(n,p)^{58}Co$, $^{64}Zn(n,p)^{64}Cu$ and $^{27}Al(n,p)^{27}Mg$ cross sections.

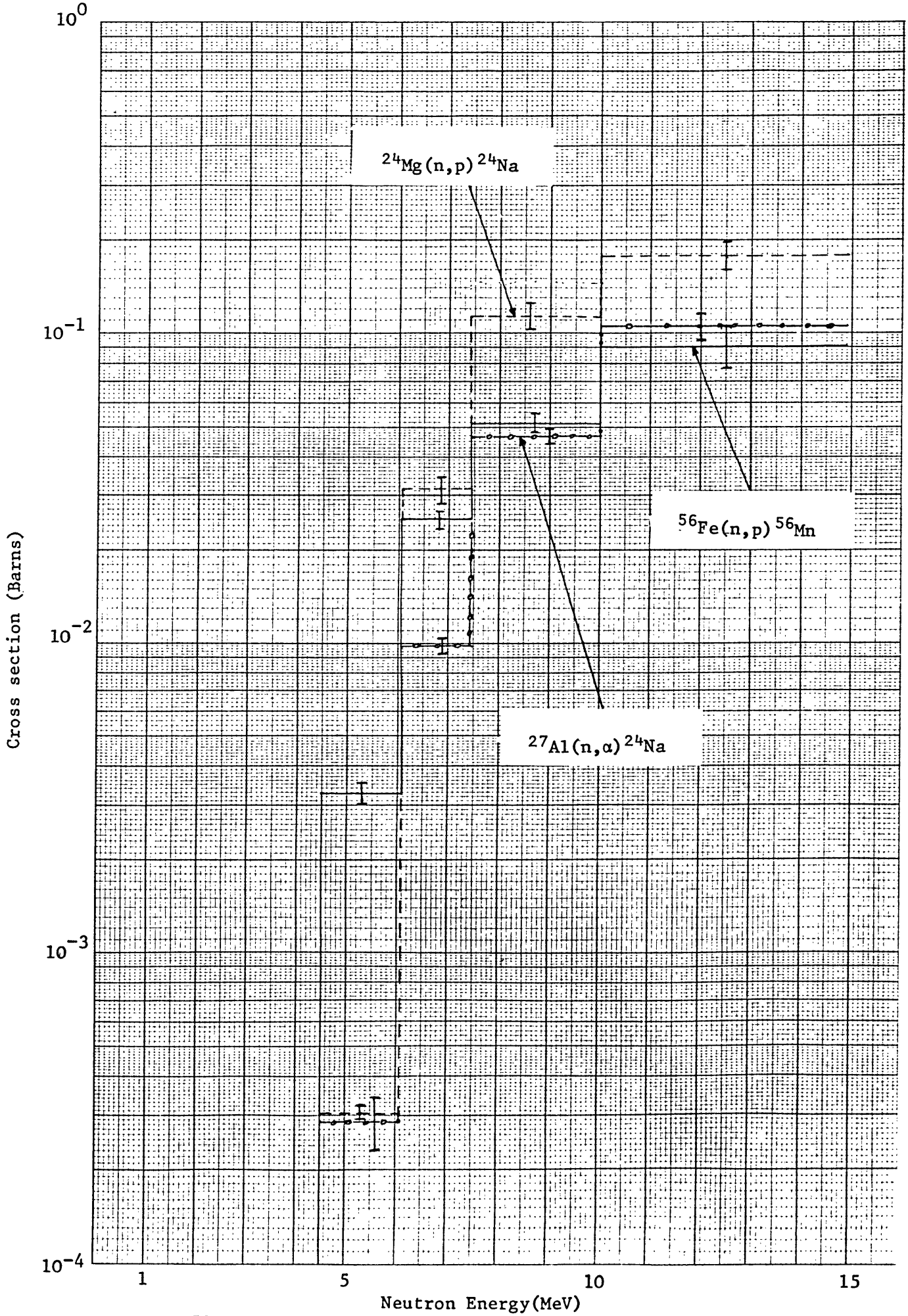


Fig.6.9. $^{56}Fe(n,p)^{56}Mn$, $^{24}Mg(n,p)^{24}Na$ and $^{27}Al(n,\alpha)^{24}Na$ cross sections.

7. COMPARISON OF MEASURED AND CALCULATED REACTION RATES IN NISUS AND INTERLABORATORY COMPARISON OF THE EVALUATED CENTRAL NEUTRON SPECTRUM (NISUS AND ΣΣ)

7.1 Comparison of measured and calculated reaction rates in NISUS

Integral reaction rates were measured in standard fast neutron fields and their expected values were calculated from evaluated differential data. Reaction rates are evaluated by satisfying the relationship:

$$R_{i,j} = \int_0^\infty \sigma_i(E)\phi_j(E)dE \qquad (7.1.1)$$

Where $R_{i,j}$ = is the reaction rate per nucleus for reaction i, in neutron field j.

$\sigma_i(E)$ = is the evaluated differential energy cross section of reaction i and $\phi_j(E)$ is the evaluated spectral shape of the neutron field j.

This relationship in multigroup form for K energy groups is:

$$R_{i,j} = \sum_{k=1}^{K} (\sigma_{i,j,k} \cdot \phi_{j,k}) \qquad (7.1.2)$$

Where the multigroup fluxes and cross sections are defined in such a way as to preserve the relationship (7.1.1).

If $R_{i,j}$, $\sigma_{i,j,k}$ and $\phi_{j,k}$ are the measured reaction rates, cross sections and fluxes respectively then inevitably

$$R_{i,j} \neq \sum_{k=1}^{K} (\sigma_{i,j,k} \cdot \phi_{j,k}) \qquad (7.1.3)$$

because of experimental uncertainties in all measured quantities.

In order to resolve this difficulty a nuclear data adjustment technique has been applied. Methods of nuclear data adjustment to fit fast reactor integral experiments have been described by Cecchini[64], Hemment and Pendlebury[65], Pazy et al[66], Barne and Ravier[67], Rowlands and MacDougall[28] and Campbell and Rowlands[5]. In references 5, 28, 65 and 66, the cross section adjustments are obtained by minimising the sum of the squares of the cross section adjustments and the residual discrepancies between the calculation using adjusted cross sections and the integral measurements (all relative to their estimated standard deviations).

In this work we define a set of evaluated quantities $R^*_{i,j}$, $\sigma^*_{i,j,k}$, and $\phi^*_{j,k}$ as those which minimise the quantity

$$F = \sum_{i,j} \left| \frac{R^*_{i,j} - R_{i,j}}{\Delta R_{i,j}} \right|^2 + \sum_{i,j,k} \left| \frac{\sigma^*_{i,j,k} - \sigma_{i,j,k}}{\Delta \sigma_{i,j,k}} \right|^2 + \sum_{j,k} \left| \frac{\phi^*_{j,k} - \phi_{j,k}}{\Delta \phi_{j,k}} \right|^2 \qquad (7.1.4)$$

subject to the constraint that

$$R^*_{i,j} = \sum_{k=1}^{K} (\sigma^*_{i,j,k} \cdot \phi^*_{j,k}) \qquad (7.1.5)$$

Where $R^*_{i,j}$ = is the calculated reaction rate per nucleus for reaction i, in neutron field j.

$\sigma^*_{i,j,k}$ = is the calculated cross section for reaction i, in neutron field j for energy group k.

$\phi^*_{j,k}$ = is the calculated flux for neutron field j for energy group k.

$R_{i,j}$ = is the measured reaction rate per nucleus for reaction i, in neutron field j.

$\sigma_{i,j,k}$ = is the cross section evaluated from differential measurements for reaction i, in neutron field j for energy group j.

$\phi_{j,k}$ = is the flux evaluated from spectrometry measurements for neutron field j for energy group k.

$\Delta R_{i,j}$, $\Delta\sigma_{i,j,k}$ and $\Delta\phi_{j,k}$ are the errors on the corresponding measured quantities[68]

A modified form of equation (7.1.4) is used in this work to minimise the quantity:

$$F = \sum_{i,j} \left| \frac{(XK)R^*_{i,j} - R_{i,j}}{\Delta R_{i,j}} \right|^2 + \sum_{i,j,k} \left| \frac{\sigma^*_{i,j,k} - \sigma_{i,j,k}}{\Delta \sigma_{i,j,k}} \right|^2 +$$

$$+ \sum_{j,k} \left| \frac{\phi^*_{j,k} - \phi_{j,k}}{\Delta \phi_{j,k}} \right|^2 \qquad (7.1.6)$$

Where XK is an arbitrary normalisation constant.

Before using equation (7.1.6) for minimising the descrepancies of reaction rates, cross sections and flux spectrum after adjustment of cross sections and fluxes, it is necessary to normalise the input flux spectrum. The flux normalisation constant can be evaluated if equation (7.1.6) is used in the following modified form:

$$F = \sum_{i,j} \left| \frac{(XK)\ R^*_{i,j} - R_{i,j}}{\Delta R_{i,j}} \right|^2 \qquad (7.1.7)$$

$$\text{Where } R^*_{i,j} = \sum_{k=1}^{K} (\sigma_{i,j,k} \cdot \phi_{j,k}) \qquad (7.1.8)$$

In equation (7.1.8), the calculated reaction rates are obtained using unadjusted cross sections ($\sigma_{i,j,k}$) and flux spectrum ($\phi_{j,k}$). The constant XK in equation (7.1.7) normalises the calculated reaction rates to minimise the discrepancy between the calculated and measured reaction rates. Virtually the constant XK in equation (7.1.7) normalises

the input flux spectrum ($\phi_{j,k}$).

So the flux normalisation constant XK is obtained by minimising F in equation (7.1.7).

This value is used as a starting guess for XK when the function F in (7.1.6) is minimised, but XK remains an unconstrained parameter which is able to change during the minimisation.

A computer program SIMMM (Simultaneous Minimisation Method)[69] has been written to perform the evaluation. This program is based on a minimisation program MINROS[70] and the method is described by Rosenbrock[71]. Solution of the problem depends on a non-linear minimisation method capable of dealing with (I x J x K) + (J x K) unknown parameters where I is the number of reactions, J is the number of spectra and K is the number of energy groups. Due to limitation of the core memory of M7600 computer (100 K words), the parameters I, J, K are chosen as 8, 1, and 20 respectively for evaluation in the present work. A list of the SIMMM program is presented in Appendix D.

Input to the program were integral measured reaction rates, evaluated differential energy cross sections and evaluated neutron spectrum and the errors due to all these measured quantities. The program calculates values of reaction rates, fluxes and cross sections which minimise the function F (equation 7.1.6).

Reaction rates measured in the NISUS standard neutron field were considered in this work. The evaluated cross section data in 20 energy groups for different reactions were obtained from Appendix B. The evaluated flux spectrum for NISUS in 20 energy groups was obtained from the recommended central neutron flux spectrum for MOL-ΣΣ secondary standard neutron field[10] because MOL-ΣΣ standard nuetron field is similar to the NISUS standard neutron field. (The similarity of MOL-ΣΣ and NISUS facilities is described in sections 3.2 and 3.3, Chapter 3).

7.2 Comparison of unadjusted and adjusted cross sections and spectrum in NISUS

The SIMMM program was run first with measured reaction rates in NISUS to evaluate calculated reaction rates before adjustment of cross section and spectrum data (Equation 7.1.7). Then the SIMMM program was run to obtain calculated reaction rates after adjustment of data (Equation 7.1.6).

Initially 8 threshold reactions were chosen to cover the energy range of 15 MeV - 60 Kev in 15 energy groups.

Subsequently 6 threshold reactions out of the 8 threshold reactions used initially ($^{115}In(n,n')^{115m}In$ and $^{24}Mg(n,p)^{24}Na$ reactions are excluded because the energy response of these two detectors are almost similar to $^{238}U(n,f)$ and $^{27}Al(n,\alpha)^{24}Na$ reactions) and 2 non threshold reactions ($^{197}Au(n,\gamma)^{198}Au$ and $^{235}U(n,f)$ reactions) were

chosen to cover the energy range of 15 MeV - 50 eV in 20 energy groups. Details of reaction rates used in nuclear data unadjustment and adjustment runs are given in Table 7.1.

Calculated threshold reaction rates without adjustment of data were evaluated in run 1. The residual discrepancy between measured reaction rate and calculated reaction rate without adjustment of data relative to the standard deviation in measured integral reaction rate is given as

$$A = \left| \frac{(XK)R^{*}_{i,j} - R_{i,j}}{\Delta R_{i,j}} \right|$$

The value of A indicates the fitting of unadjusted cross section and spectrum to the measured integral value relative to the standard deviation in measured integral reaction rate. This is shown in Fig. 7.1. In run 2, the calculated threshold reaction rates were obtained after adjustment of data. The value of A is obtained in similar way. This is also shown in Fig. 7.1. It can be seen from Fig. 7.1 that the value of A is within $\sim\pm 1\sigma$ level for adjusted data and varies within $\sim\pm 4\sigma$ level for all threshold reaction rates with unadjusted data. The calculated reaction rates before and after adjustment of data relative to measured reaction rates are shown in Fig. 7.2 and given in Table 7.2. The ratio of calculated reaction

TABLE 7.1

Details of measured reaction rates used in nuclear data unadjustment and adjustment runs.

Reaction	Nuclear data and spectrum		Reaction	Nuclear data & spectrum	
	Without Adjustment	With Adjustment		Without Adjustment	With Adjustment
$^{237}NP(n,f)$	Run 1	Run 2	$^{197}Au(n,\gamma)^{198}Au$	Run 3	Run 4
$^{115}In(n,n')^{115m}In$			$^{235}U(n,f)$		
$^{238}U(n,f)$			$^{237}Np(n,f)$		
$^{58}Ni(n,p)^{58}Co$			$^{238}U(n,f)$		
$^{27}Al(n,p)^{27}Mg$			$^{58}Ni(n,p)^{58}Co$		
$^{56}Fe(n,p)^{56}Mn$			$^{27}Al(n,p)^{27}Mg$		
$^{24}Mg(n,p)^{24}Na$			$^{56}Fe(n,p)^{56}Mn$		
$^{22}Al\ (n,\alpha)^{24}Na$			$^{27}Al(n,\alpha)^{24}Na$		

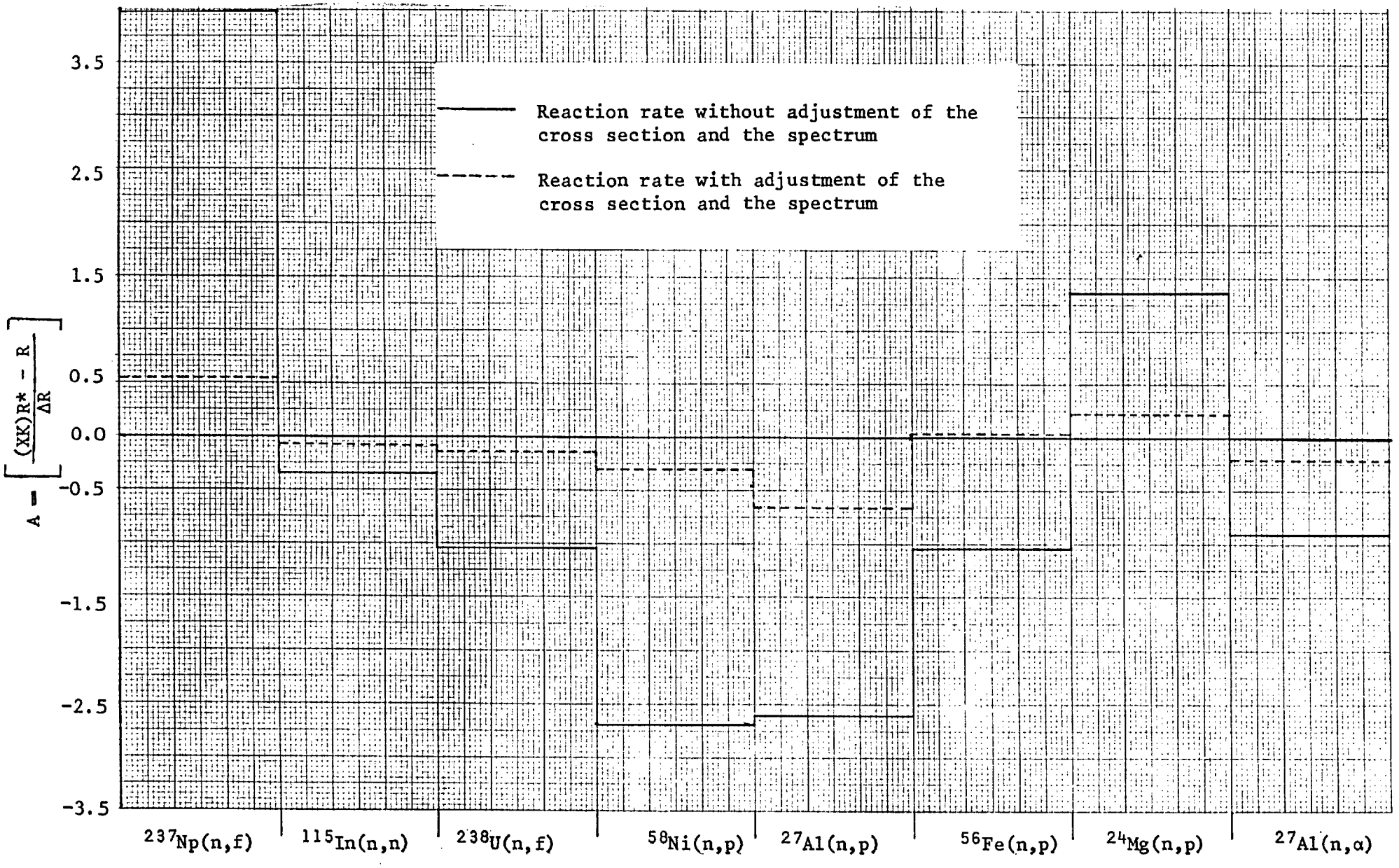


Fig.7.1. Residual discrepancy between calculated and measured reaction-rate relative to the uncertainty in the measurement without and with adjustment of the data of threshold reactions.

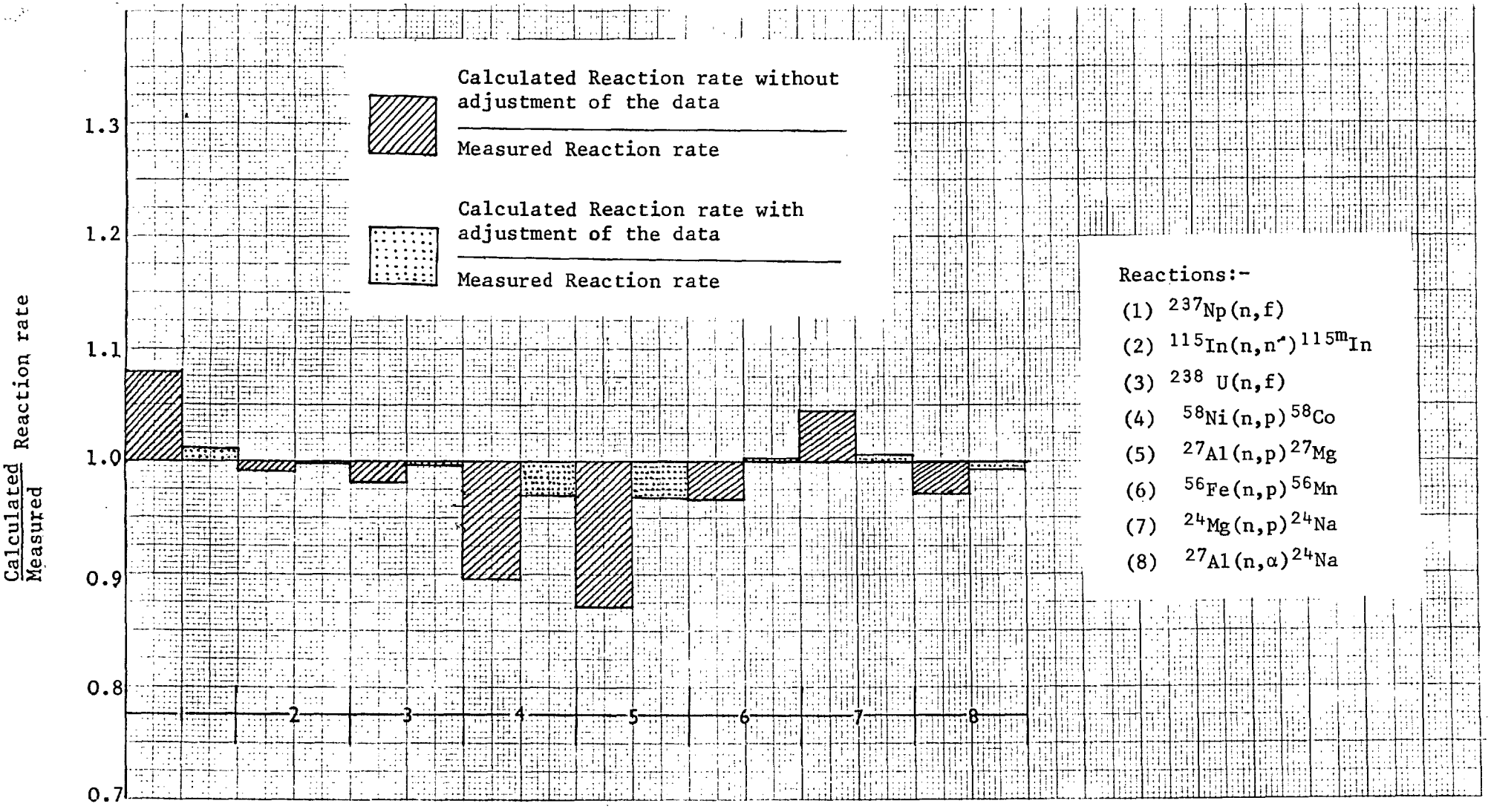


Fig.7.2. Comparison of calculated and measured reaction-rate ratios of threshold rections in the NISUS central-neutron field.

TABLE 7.2

Calculated reaction rates (threshold) without and with adjustment of data and measured reaction rates and their ratios. The value of the minimisation function F.

Reaction	Measured Reaction rate x 10^{-3}	Calculated reaction rate x10^{-3}		Calculated reaction rate before adjustment of data	Calculated reaction rate after adjustment of data	Minimisation function F	
		Without adjustment of data	With adjustment of data	Measured reaction rate (cols.2&3)	Measured reaction rate (cols. 2&4)	Without adjustment of data	With adjustment of data
$^{237}NP(n,f)$	$70.620 \pm 2.6\%$ (a)	76.246	71.388	1.08	1.011		
$^{115}In(n,n')^{115m}In$	$7.0189 \pm 2.8\%$	6.9566	7.0073	0.991	0.998		
$^{238}U(n,f)$	$10.684 \pm 2.1\%$	10.480	10.643	0.981	0.996	34.87	5.49
$^{58}Ni(n,p)^{58}Co$	$3.3082 \pm 3.2\%$	2.9650	3.2042	0.896	0.969		
$^{27}Al(n,p)^{27}Mg$	$0.11940 \pm 5.0\%$	0.10417	0.11557	0.872	0.968		
$^{56}Fe(n,p)^{56}Mn$	$0.03170 \pm 3.2\%$	0.03064	0.03176	0.967	1.002		
$^{24}Mg(n,p)^{24}Na$	$0.04440 \pm 3.5\%$	0.04641	0.04467	1.045	1.006		
$^{27}Al(n,\alpha)^{24}Na$	$0.01960 \pm 3.0\%$	0.01904	0.01947	0.971	0.993		

(a) The total error estimated at 1σ confidence level.

rate after adjustment of data and measured reaction rate agrees within $\sim\pm3\%$ and whereas the ratio of calculated reaction rate before adjustment of data and measured reaction rate agrees within $\sim\pm13\%$ for all threshold reactions.

Similarly 8 non threshold and threshold reaction rates were used to evaluate calculated reaction rates before and after adjustment of data in run 3 and 4 respectively. The value of A is shown in Fig. 7.3. It is found from Fig. 7.3 that the value of A is within $\sim\pm1\sigma$ level for adjusted data and within $\sim\pm4\sigma$ level for unadjusted data for all non threshold and threshold reaction rates. The calculated reaction rates without and with adjustment of data relative to measured reaction rates are shown in Fig. 7.4 and given in Table 7.3. It can be seen from Fig. 7.4 and Table 7.3 that the ratio of calculated reaction rate after adjustment of data and the measured reaction rate agrees within $\sim \pm$ 2.5% and $\sim \pm$ 15% for the ratio of unadjusted calculated reaction rates and measured reaction rates for all non-threshold and threshold reaction rates.

It can be concluded that the calculated reaction rates with adjustment of data are agreeing very well with the measured reaction rates. The value of the minimisation quantity F is within the number of degrees of freedom for both cases (threshold reaction rates and non threshold reaction rates). The value of F is given in Table 7.2 and 7.3.

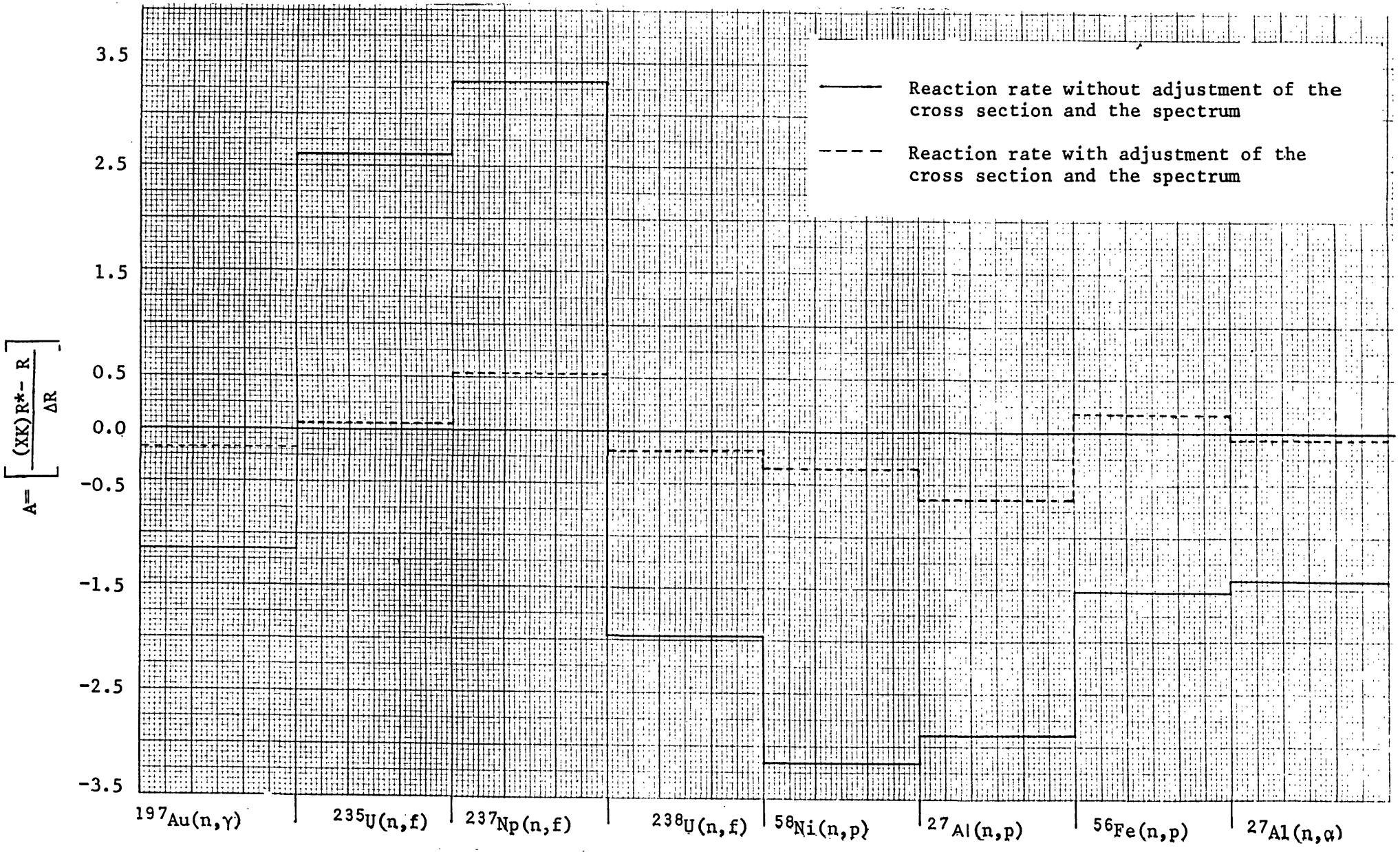


Fig. 7.3. Residual discrepancy between calculated and measured reaction-rate relative to the uncertainty in the measurement without and with adjustment of the data of non-threshold and threshold reactions.

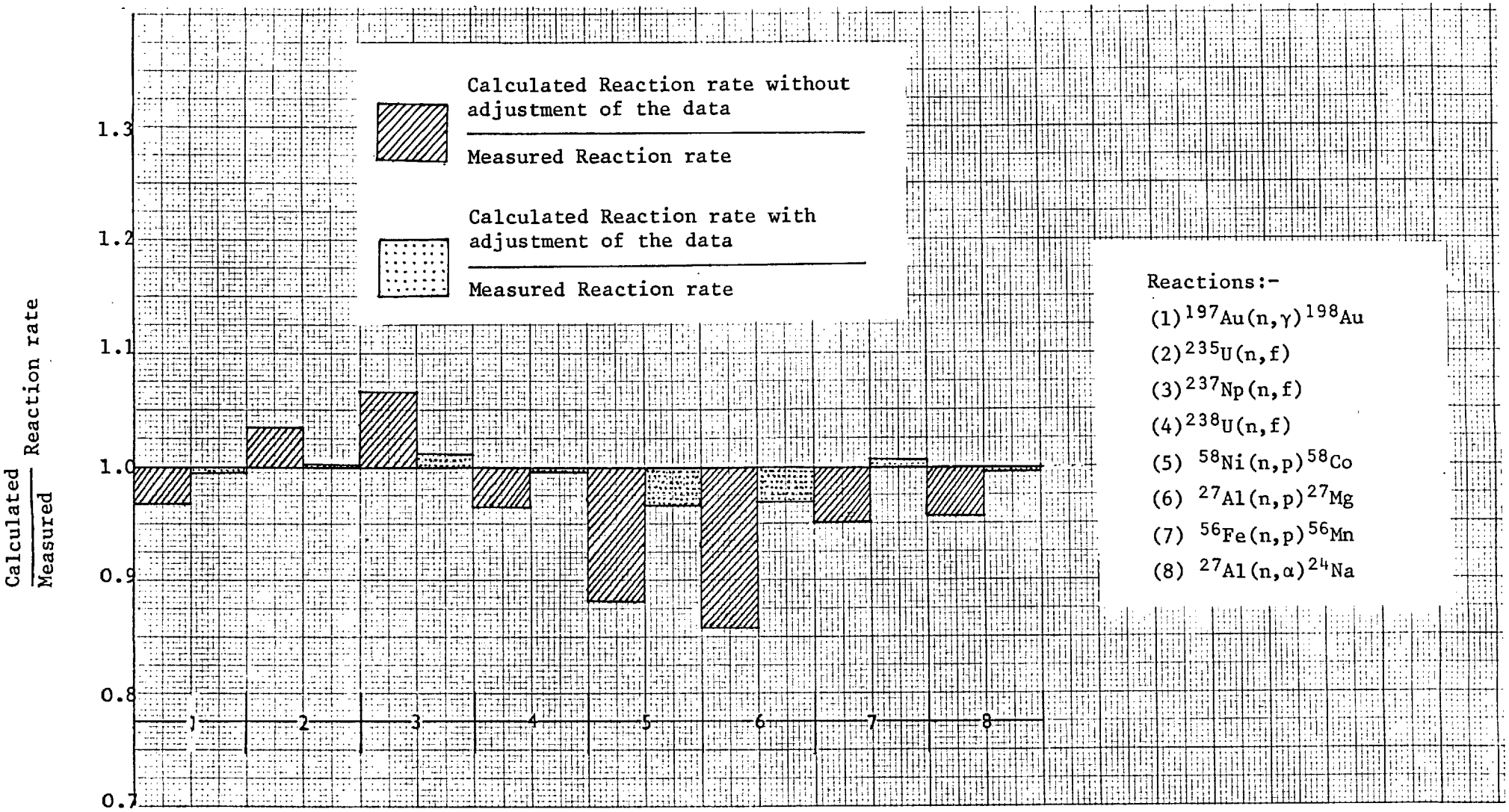


Fig.7.4. Comparison of calculated and measured reaction-rate ratios of non-threshold and threshold reactions in the NISUS central-neutron field.

TABLE 7.3

Calculated reaction rates (non-threshold and threshold) without and with adjustment of data and measured reaction rates and their ratios. The value of the minimisation function F.

Reaction	Measured reaction rate x 10^{-3}	Calculated reaction rate x10^{-3}		Calculated reaction rate before adjustment of data	Calculated reaction rate after adjustment of data	Minimisation function F	
		Without adjustment of data	With adjustment of data	Measured reaction rate (Cols. 2&3)	Measured reaction rate (Cols. 2&4)	Without adjustment of data	With adjustment of data
$^{197}Au(n,\gamma)\,^{198}Au$	50.373±2.8% (a)	48.741	50.126	0.968	0.995	45.79	5.26
$^{235}U(n,f)$	188.00± 1.9%	194.66	188.38	1.035	1.002		
$^{237}Np(n,f)$	70.620±2.6%	75.292	71.396	1.066	1.011		
$^{238}U(n,f)$	10.684±2.1%	10.311	10.636	0.965	0.996		
$^{58}Ni(n,p)^{58}\,Co$	3.3082±3.2%	2.9172	3.1986	0.882	0.967		
$^{27}Al(n,p)\,^{27}Mg$	0.11940±5.0%	0.10249	0.11566	0.858	0.969		
$^{56}Fe(n,p)^{56}\,Mn$	0.03170±3.2%	0.03014	0.03188	0.951	1.006		
$^{27}Al(n,\alpha)\,^{24}Na$	0.01960±3.1%	0.01874	0.01956	0.956	0.998		

(a) The total error estimated at 1σ confidence level.

The adjusted and unadjusted cross section data for threshold(8) reactions (Run 2) and for non-threshold and threshold(8) reactions (Run 4) are presented in Appendix B in Tables B1 - B5 respectively. The adjustments made by SIMMM are generally much smaller than the assigned uncertainties.

The unadjusted cross section data for other reactions which are not used in the SIMMM program are presented in Table B6.

7.3 NISUS unfolded spectrum

The program SIMMM is simultaneously evaluating reaction rates, cross sections and flux spectrum. In Run 2, the program evaluated reaction rates, cross sections and neutron spectrum for 8 threshold reactions. The NISUS central neutron spectrum after adjustment of data was unfolded for the energy range 15 MeV - 60 KeV in 15 energy groups. The $\Sigma\Sigma$ reference central neutron spectrum with its error was the starting spectral approximation for NISUS. The uncertainties assigned to $\Sigma\Sigma$ input spectrum were $\pm$ 20% for the energy range 15 MeV - 2 MeV (energy groups 1 - 7) because few fission neutrons are available above 5 MeV and $\Sigma\Sigma$ spectral shape is erroneous above 4 MeV[31], $\pm$ 10% for the energy range 2 MeV - 60 KeV (energy groups 8 - 15) though $\Sigma\Sigma$ spectrometry data are claimed to be accurate within $\pm$ 5%[31] and $\pm$ 50% for the energy range interval 60 KeV - 0.4 eV (energy groups 16 - 20) because broad energy groups were considered in this work and below 6 KeV the $\Sigma\Sigma$ input spectrum is not reliable[10].

The NISUS unfolded spectrum and ΣΣ input spectrum are shown in Fig. 7.5. Flux ratio $(\frac{\text{NISUS unfolded flux}}{\text{input flux}})$ for 15 energy intervals is shown in Fig. 7.6. NISUS unfolded spectrum and ΣΣ input spectrum and flux ratios are given in Table 7.4.

Comparing Figs. 7.5 and 7.6 and Table 7.4, it is found that the ΣΣ input spectrometry fluxes fall below those of the NISUS unfolded fluxes by ∿ 7% above 6 MeV though within 20% error. The ΣΣ input spectrum above 5 MeV was defined by the ENDF/BIII calculation[10]. The NISUS unfolded spectrum are 23% and 12% higher than the spectrum for the energy intervals 6 - 4.5 MeV and 4.5 - 2.7 MeV respectively. Fabry also observed discrepancies of the ratio of measured and calculated cross section data for ΣΣ using ΣΣ evaluated spectrum and ENDF/BIV data file (Table VI in Ref. 31). In the 6 - 4 MeV range, the ΣΣ evaluated spectrum relied on three experimental points obtained with the GFK ^{3}He(n,p) neutron spectrometer. It is concluded that the ΣΣ reference spectral shape is erroneous above 4 MeV and requires updating[31]. For ΣΣ, the multiple foil results by SANDII also observed the fall of the ΣΣ spectrometry and calculated fluxes above ∿ 2 MeV[7].

The agreement between the NISUS unfolded spectrum and the ΣΣ evaluated spectrum is very good (within ∿ ± 5%) in the ∿ 2.7 MeV - ∿ 60 KeV region except the energy interval 1.35 - 0.82 MeV. The ΣΣ spectrometry data are accurate to within ∿ ± 5% from ∿ 1.5 MeV to ∿ 20 KeV and are satisfactorily reproduced by SANDII, using the ENDF/BIV dosimetry file[31]. NISUS neutron fluxes are lower ∿ 8%

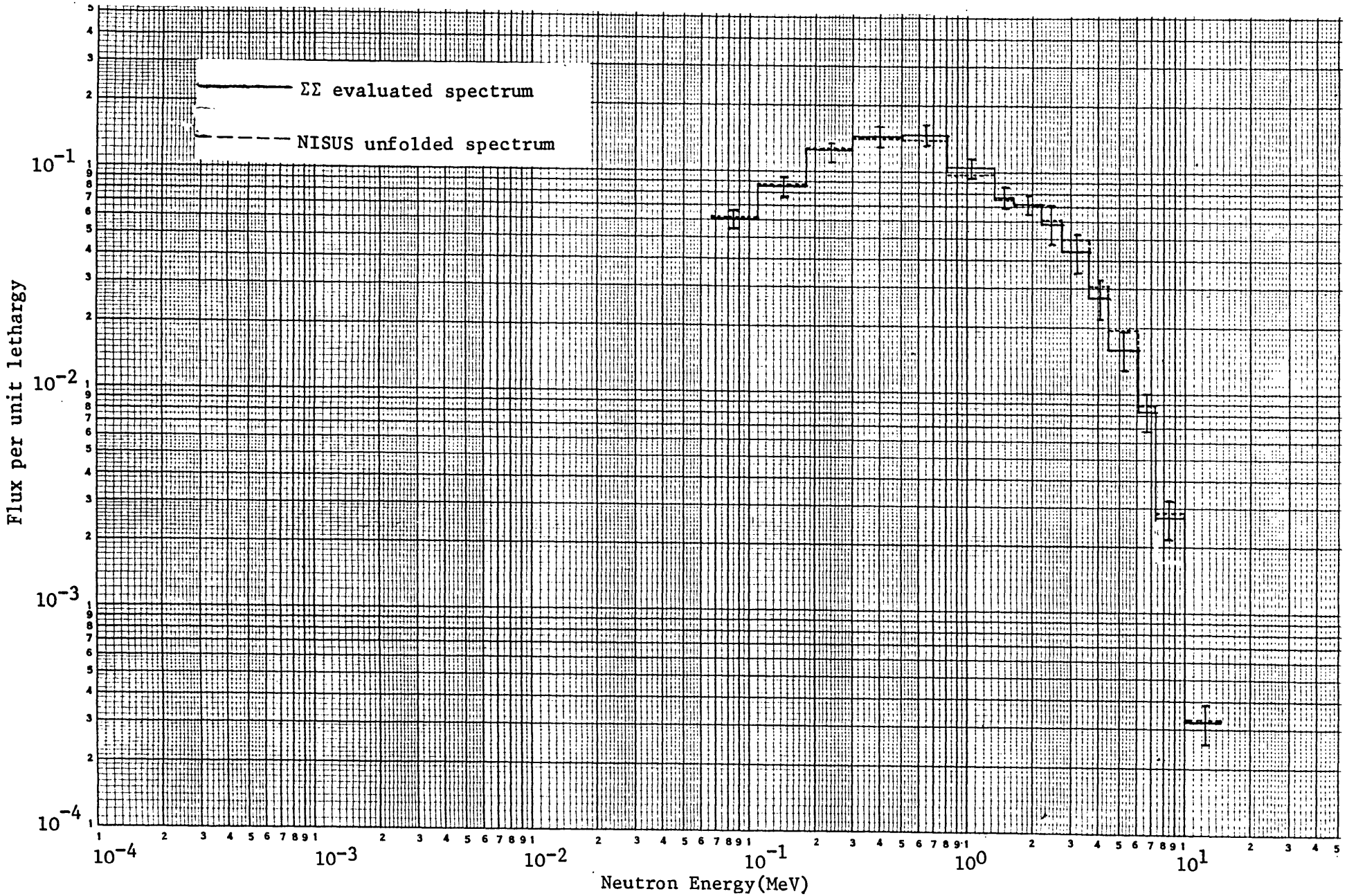


Fig.7.5. The NISUS central neutron spectrum unfolded by multiple-foil (threshold reactions) spectrometry (using the ΣΣ spectrometry evaluated central neutron spectrum as the starting spectral form).

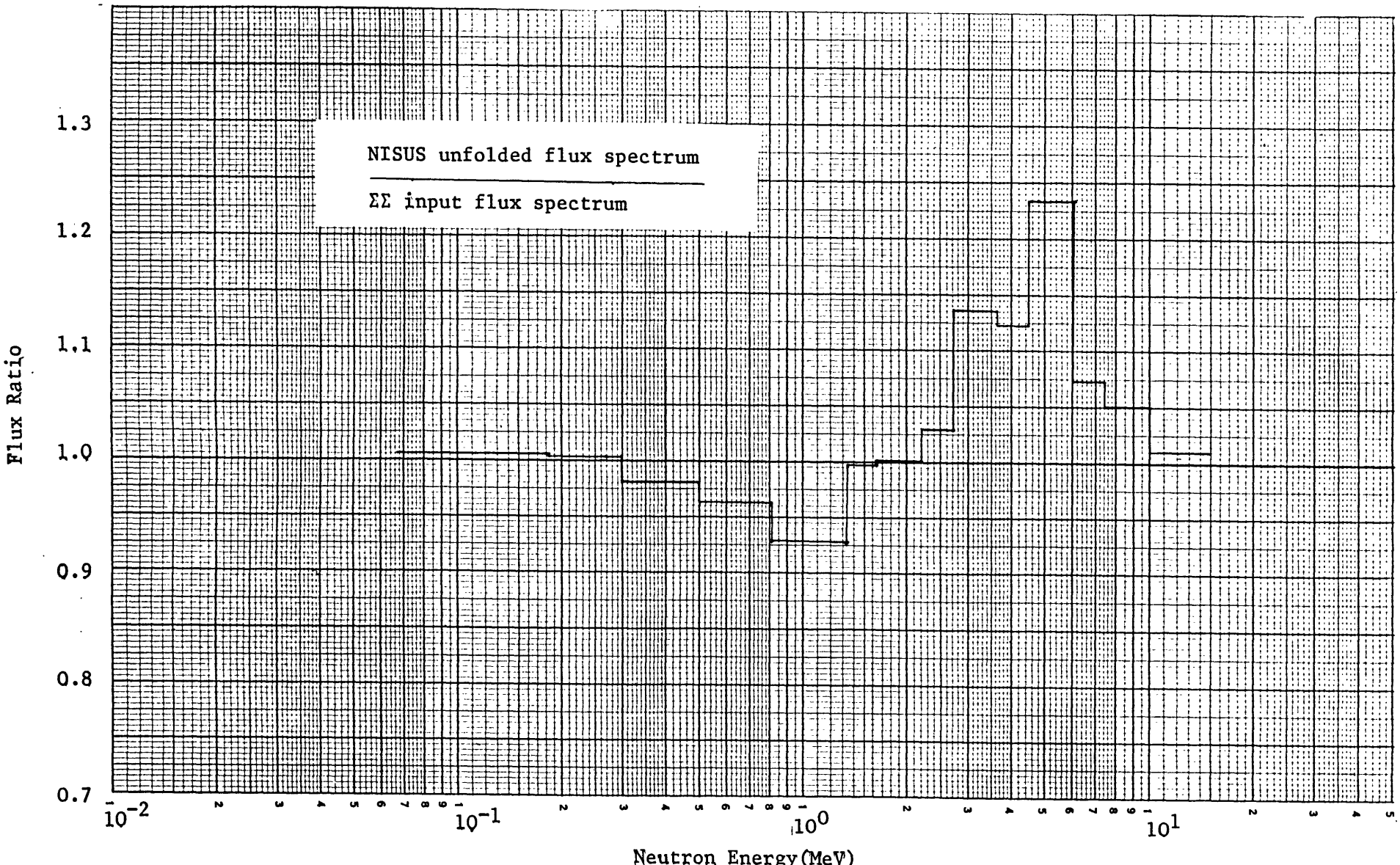


Fig. 7.6. Comparison of the NISUS central neutron flux spectrum unfolded by threshold foil detectors and the ΣΣ spectrometry evaluated central neutron flux spectrum for the energy range ∿15MeV- ∿60KeV.

TABLE 7.4

NISUS unfolded neutron fluxes and ΣΣ input neutron fluxes and their ratios over energy ranges for threshold reactions.

Group Number	Energy Range (MeV)	Lethargy Width	NISUS unfolded flux per unit lethargy	ΣΣ input flux per unit lethargy	Error in ΣΣ input flux (%)	$\frac{\text{NISUS unfolded flux}}{\Sigma\Sigma \text{ input flux}}$
1	10.0000 E+00 - 14.9180 E+00	0.4	3.2389 E-04	3.2063 E-04	20	1.010
2	7.4082 E+00 - 10.0000 E+00	0.3	2.8658 E-03	2.7274 E-03	20	1.051
3	6.0653 E+00 - 7.4082 E+00	0.2	8.9827 E-03	8.3678 E-03	20	1.073
4	4.4933 E+00 - 6.0653 E+00	0.3	1.9651 E-02	1.5938 E-02	20	1.233
5	3.6788 E+00 - 4.4933 E+00	0.2	3.0655 E-02	2.7311 E-02	20	1.122
6	2.7253 E+00 - 3.6788 E+00	0.3	4.9994 E-02	4.4004 E-02	20	1.136
7	2.2313 E+00 - 2.7253 E+00	0.2	6.0445 E-02	5.8748 E-02	20	1.029
8	1.6530 E+00 - 2.2313 E+00	0.3	7.1834 E-02	7.1726 E-02	10	1.002
9	1.3534 E+00 - 1.6530 E+00	0.2	7.6648 E-02	7.7384 E-02	10	0.990
10	8.2085 E-01 - 1.3534 E+00	0.5	9.7316 E-02	1.0483 E-01	10	0.928
11	4.9789 E-01 - 8.2085 E-01	0.5	1.4290 E-01	1.4832 E-01	10	0.963
12	3.0197 E-01 - 4.9787 E-01	0.5	1.4338 E-01	1.4606 E-01	10	0.982
13	1.8316 E-01 - 3.0197 E-01	0.5	1.2320 E-01	1.2276 E-01	10	1.004
14	1.1109 E-01 - 1.8316 E-01	0.5	8.6619 E-02	8.6204 E-02	10	1.005
15	6.7379 E-02 - 1.1109 E-01	0.5	6.0939 E-02	6.0611 E-02	10	1.005

($\sim \pm$ 10% error was assigned in the energy range 1.35 - 0.82 MeV) than $\Sigma\Sigma$ input fluxes in 1.35 - 0.82 MeV region. The presence of $^{237}Np(n,f)$ foil (with significance response 0.5 to 2 MeV region) contributes to the poorer agreement in this energy interval.

Similarly 8 reactions (2 non-threshold and 6 threshold reactions mentioned in Table 7.1) were used in Run 4. Two non-threshold reactions were used to unfold the NISUS spectrum for the energy range $\sim$ 15 MeV - 50 eV and to observe whether there is any impact on the NISUS unfolded spectrum obtained by only threshold reactions (Fig. 7.5) due to the inclusion of non-threshold reactions.

NISUS unfolded spectrum and $\Sigma\Sigma$ evaluated input spectrum with its errors and the flux ratio in 20 energy groups are shown in Figs. 7.7 and 7.8 and in Table 7.5. Both NISUS and $\Sigma\Sigma$ neutron fluxes were normalised to integrals $\int \phi(u)du = 1$. As can be seen from Figs. 7.7 and 7.8 and Table 7.5 that NISUS unfolded spectrum and flux ratios were reproduced quite satisfactorily in Run 4 for the energy ranges 15 MeV - 60 KeV as obtained in Run 2. So it confirms that there is no effect on the NISUS unfolded spectrum for the energy range 15 MeV - 60 KeV region for the inclusion of non-threshold reactions.

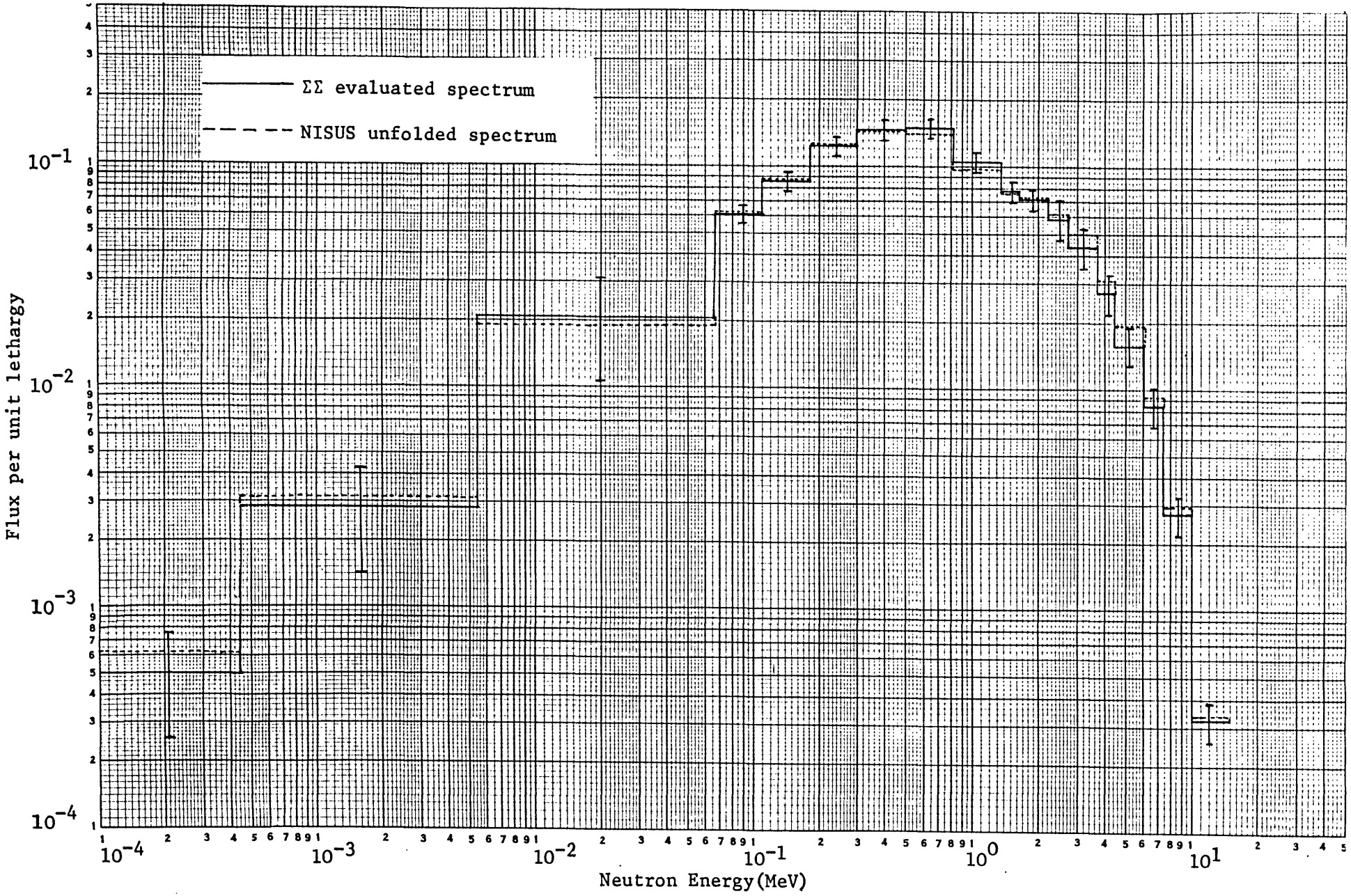


Fig. 7.7. The NISUS central neutron spectrum unfolded by multiple foil(nonthreshold and threshold reactions) spectrometry (using the ΣΣ spectrometry evaluated central neutron spectrum as the starting spectral form).

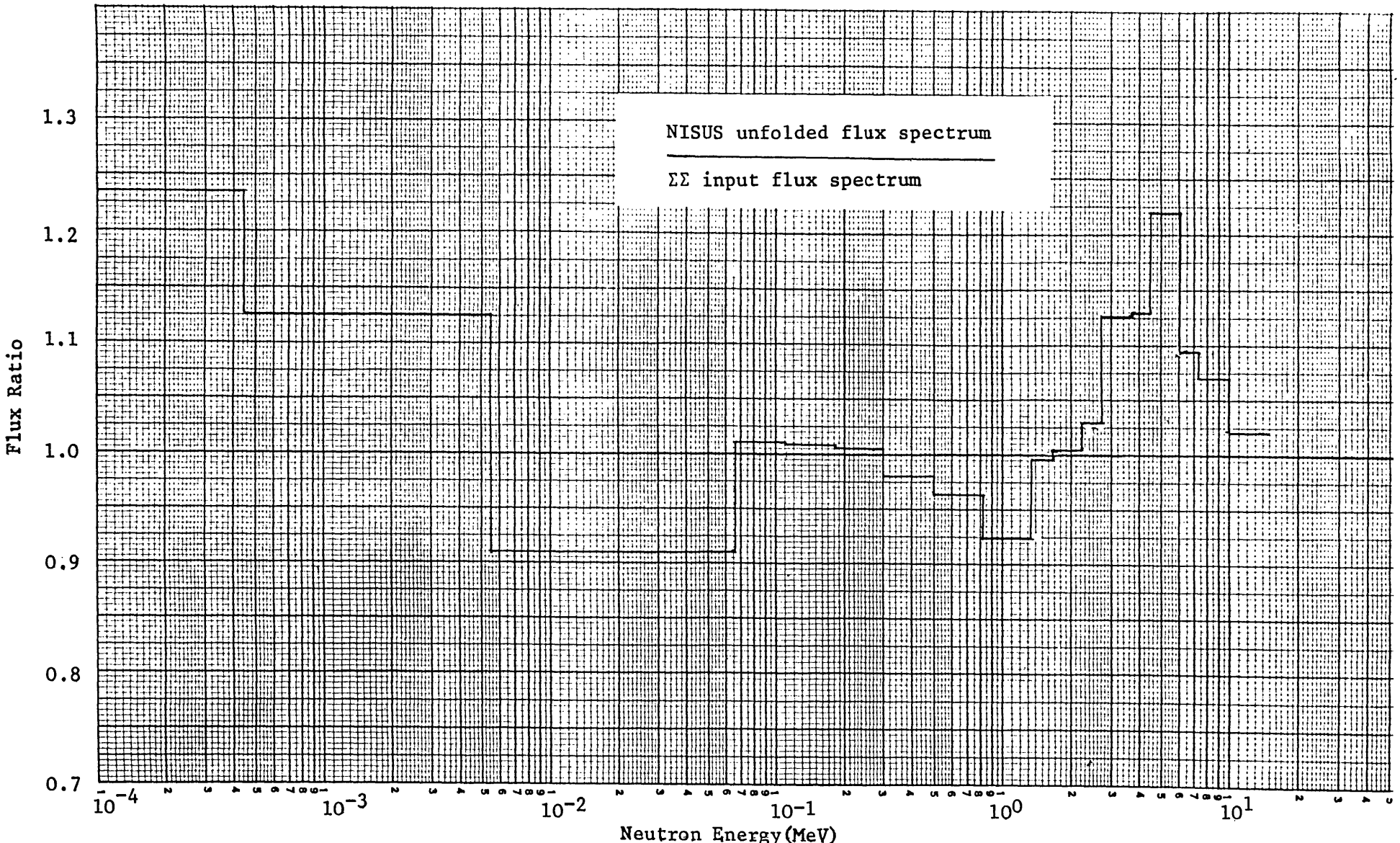


Fig.7.8. Comparison of the NISUS central neutron flux spectrum unfolded by non threshold and threshold detectors and the ΣΣ spectrometry evaluated central neutron flux spectrum for the energy range ∿15 MeV-∿50eV.

TABLE 7.5.

NISUS unfolded neutron fluxes and ΣΣ input neutron fluxes and their ratios over energy ranges for non-threshold and threshold reactions.

Group Number	Energy Range (MeV)	Lethargy width	NISUS unfolded flux per unit lethargy	ΣΣ input flux per unit lethargy	Error in ΣΣ input neutron flux (%)	NISUS unfolded flux / ΣΣ input flux
1	10.0000 E+00 - 14.9180 E+00	0.4	3.2737 E-04	3.2063 E-04	20	1.021
2	7.4082 E+00 - 10.0000 E+00	0.3	2.9184 E-03	2.7274 E-03	20	1.070
3	6.0653 E+00 - 7.4082 E+00	0.2	9.1484 E-03	8.3678 E-03	20	1.093
4	4.4933 E+00 - 6.0653 E+00	0.3	1.9447 E-02	1.5938 E-02	20	1.220
5	3.6788 E+00 - 4.4933 E+00	0.2	3.0857 E-02	2.7311 E-02	20	1.130
6	2.7253 E+00 - 3.6788 E+00	0.3	5.0007 E-02	4.4004 E-02	20	1.126
7	2.2313 E+00 - 2.7253 E+00	0.2	6.0371 E-02	5.8748 E-02	20	1.028
8	1.6530 E+00 - 2.2313 E+00	0.3	7.2067 E-02	7.1726 E-02	10	1.005
9	1.3534 E+00 - 1.6530 E+00	0.2	7.7049 E-02	7.7384 E-02	10	0.996
10	8.2085 E-01 - 1.3534 E+00	0.5	9.6884 E-02	1.0483 E-01	10	0.924
11	4.9787 E-01 - 8.2085 E-01	0.5	1.4283 E-01	1.4832 E-01	10	0.963
12	3.0197 E-01 - 4.9787 E-01	0.5	1.4345 E-01	1.4606 E-01	10	0.982
13	1.8316 E-01 - 3.0197 E-01	0.5	1.2355 E-01	1.2276 E-01	10	1.006
14	1.1109 E-01 - 1.8316 E-01	0.5	8.6987 E-02	8.6204 E-02	10	1.009
15	6.7379 E-02 - 1.1109 E-01	0.5	6.1258 E-02	6.0611 E-02	10	1.011
16	5.5308 E-03 - 6.7379 E-02	2.5	1.9039 E-02	2.0925 E-02	50	0.910
17	4.5400 E-04 - 5.5308 E-03	2.5	3.1708 E-03	2.8147 E-03	50	1.127
18	3.7267 E-05 - 4.5400 E-04	2.5	6.2246 E-04	5.0414 E-04	50	1.235
19	3.0590 E-06 - 3.7267 E-05	2.5	1.6157 E-05	1.5713 E-05	50	1.028
20	4.1399 E-07 - 3.0590 E-06	2.0	0.0	0.0	50	0.0

NISUS unfolded neutron fluxes fall 10% below ΣΣ evaluated input neutron fluxes in the ∿ 60 - ∿ 5 KeV region. The multiple foil results by SANDII shows that the neutron fluxes fall below those of the spectrometry for ΣΣ for the energy range ∿ 100 - ∿ 5 KeV energy region[7].

NISUS unfolded fluxes are higher ∿ 10% and ∿ 20% in the energy intervals ∿ 5 - ∿ 0.5 KeV and ∿ 0.5 KeV - ∿ 50 eV respectively than those of the ΣΣ evaluated spectrum. Below 6 KeV, the presently recommended ΣΣ spectrum is obtained by the ENDF/BIII calculation. The low energy tail below 6 KeV for ΣΣ evaluated spectrum is believed to be somewhat unreliable. Multiple foil results by SANDII for ΣΣ show that activation detectors (with significant response in low energy spectrum such as $^{197}Au(n,\gamma)$ reaction) with broad energy groups can produce uncertainties in the low energy spectrum and also too little flux is considered in the low energy tail of the calculated ΣΣ spectrum.

Thus it can be concluded that the NISUS unfolded spectrum is in very good agreement (∿ ± 5%) with the ΣΣ evaluated spectrum in the ∿ 2.7 MeV - ∿ 60 KeV region except 1.35 - 0.82 MeV energy interval (NISUS fluxes fall by ∿ 8% in this energy region). Above 2.7 MeV, NISUS spectrum is higher by up to 20% but within ± 20% assigned uncertainties. NISUS spectrum falls ∿ 10% in the energy interval

$\sim$ 60 KeV - $\sim$ 5 KeV and rises $\sim$ 10% and $\sim$ 20% in the energy ranges $\sim$ 5 - 0.5 KeV and $\sim$ 0.5 KeV - $\sim$ 50 eV. The deviations of NISUS unfolded spectrum are within the assigned errors with the $\Sigma\Sigma$ evaluated spectrum.

The normalisation of the NISUS flux spectrum on an absolute scale is obtained from SIMMM. The total flux at a reactor power of 100 kW corresponding to a $^{197}Au(n,\gamma)$ reaction rate for monitor A of 1.0669×10^{-15} reaction $atom^{-1}$ sec^{-1} was found to be 1.348×10^{8} from Run No. 3 in which threshold and non-threshold reactions were included without adjustment of the cross section and spectrum and 1.288×10^{8} from Run No. 4 in which adjustment of the cross section and spectrum occurred.

NISUS absolute flux at a reactor power of 100 kW is considered as 1.288×10^{8} $ncm^{-2}sec^{-1}$ because Run No. 4 was obtained after the adjustment of the cross section and spectrum.

8. COMPARISON OF NISUS SPECTRUM UNFOLDED BY MULTIPLE FOIL SPECTROMETRY WITH OTHER SPECTROMETER TECHNIQUES

The NISUS central neutron unfolded spectrum $\phi(u)$ in NISUS 1b assembly obtained by the program SIMMM was compared to the central neutron spectra measured by the proton recoil proportional counter for the energy range $\sim$ 1.7 MeV - $\sim$ 60 KeV[47] (energy groups 9 - 15 in the present work) and ^{6}Li sandwich spectrometer for the energy region $\sim$ 7.5 MeV - $\sim$ 60 KeV[72] (energy groups 3 - 15 in this work). The measured pointwise NISUS neutron flux per unit lethargy from Refs. 47 and 72 was normalised to the measured pointwise $\Sigma\Sigma$ neutron flux per unit lethargy at $\sim$ 0.5 MeV. The $\Sigma\Sigma$ evaluated central neutron spectrum[10] is used as the reference spectrum in this work.

The NISUS spectra from proton recoil counter and ^{6}Li spectrmeter were collapsed in the energy groups of the present work (20 energy groups) and $\phi(u)$ was normalised to equal integrals $\int\phi(u)du$ of the $\Sigma\Sigma$ spectrum within the energy limits $\sim$ 1.7 MeV - $\sim$ 60 KeV and $\sim$ 7.5 MeV - $\sim$ 60 KeV respectively.

The NISUS spectra measured by multiple foil, proton recoil and ^{6}Li spectrometers are given in Table 8.1 and shown in Fig. 8.1 together with the $\Sigma\Sigma$ evaluated spectrum. NISUS neutron group fluxes obtained by these three techniques are formed relative to $\Sigma\Sigma$ neutron group fluxes and are also given in Table 8.1 and Fig. 8.2.

TABLE 8.1

NISUS spectrum unfolded by multiple foil spectrometry and comparison with other experimental results.

Energy group	Energy Range (MeV)	Flux per unit lethargy				SIMMM / ΣΣ	PRC / ΣΣ	^{6}Li / ΣΣ
		ΣΣ Spectrometry	Multiple foil Spectrometry (SIMMM)	Proton Recoil Counter	^{6}Li Spectrometer			
1	10.0000 E+00 - 14.9180 E+00	3.2063 E-04	3.2737 E-04	-	-	1.021	-	-
2	7.4082 E+00 - 10.0000 E+00	2.7274 E-03	2.9184 E-03	-	-	1.070	-	-
3	6.0653 E+00 - 7.4082 E+00	8.3678 E-03	9.1484 E-03	-	8.6886 E-03	1.093	-	1.038
4	4.4933 E+00 - 6.0653 E+00	1.5938 E-02	1.9447 E-02	-	2.0440 E-02	1.220	-	1.282
5	3.6788 E+00 - 4.4933 E+00	2.7311 E-02	3.0857 E-02	-	3.1050 E-02	1.130	-	1.137
6	2.7253 E+00 - 3.6788 E+00	4.4004 E-02	5.0007 E-02	-	4.8172 E-02	1.126	-	1.085
7	2.2313 E+00 - 2.7253 E+00	5.8748 E-02	6.0371 E-02	-	6.4745 E-02	1.028	-	1.102
8	1.6530 E+00 - 2.2313 E+00	7.1726 E-02	7.2067 E-02	-	6.7573 E-02	1.005	-	0.942
9	1.3534 E+00 - 1.6530 E+00	7.7384 E-02	7.7049 E-02	7.3271 E-02	7.2492 E-02	0.996	0.946	0.937
10	8.2085 E-01 - 1.3534 E+00	1.0483 E-01	9.6884 E-02	1.0638 E-01	1.0811 E-01	0.924	1.015	1.031
11	4.9787 E-01 - 8.2085 E-01	1.4832 E-01	1.4283 E-01	1.4201 E-01	1.4429 E-01	0.963	0.957	0.973
12	3.0197 E-01 - 4.9787 E-01	1.4606 E-01	1.4345 E-01	1.4059 E-01	1.3726 E-01	0.982	0.963	0.942
13	1.8316 E-01 - 3.0197 E-01	1.2276 E-01	1.2355 E-01	1.2263 E-01	1.1159 E-01	1.006	1.000	0.909
14	1.1109 E-01 - 1.8316 E-01	8.6204 E-02	8.6987 E-02	9.4384 E-02	8.9936 E-02	1.009	1.095	1.043
15	6.7379 E-02 - 1.1109 E-01	6.0611 E-02	6.1258 E-02	6.6942 E-02	6.8943 E-02	1.011	1.104	1.137
16	5.5308 E-03 - 6.7379 E-02	2.0925 E-02	1.9039 E-02	-	-	0.910	-	-
17	4.5400 E-04 - 5.5308 E-03	2.8147 E-03	3.1708 E-03	-	-	1.127	-	-
18	3.7267 E-05 - 4.5400 E-04	5.0414 E-04	6.2246 E-04	-	-	1.235	-	-
19	3.0509 E-06 - 3.7267 E-05	1.5713 E-05	1.6157 E-05	-	-	1.028	-	-
20	4.1399 E-07 - 3.0509 E-06	0.0	0.0	-	-	-	-	-

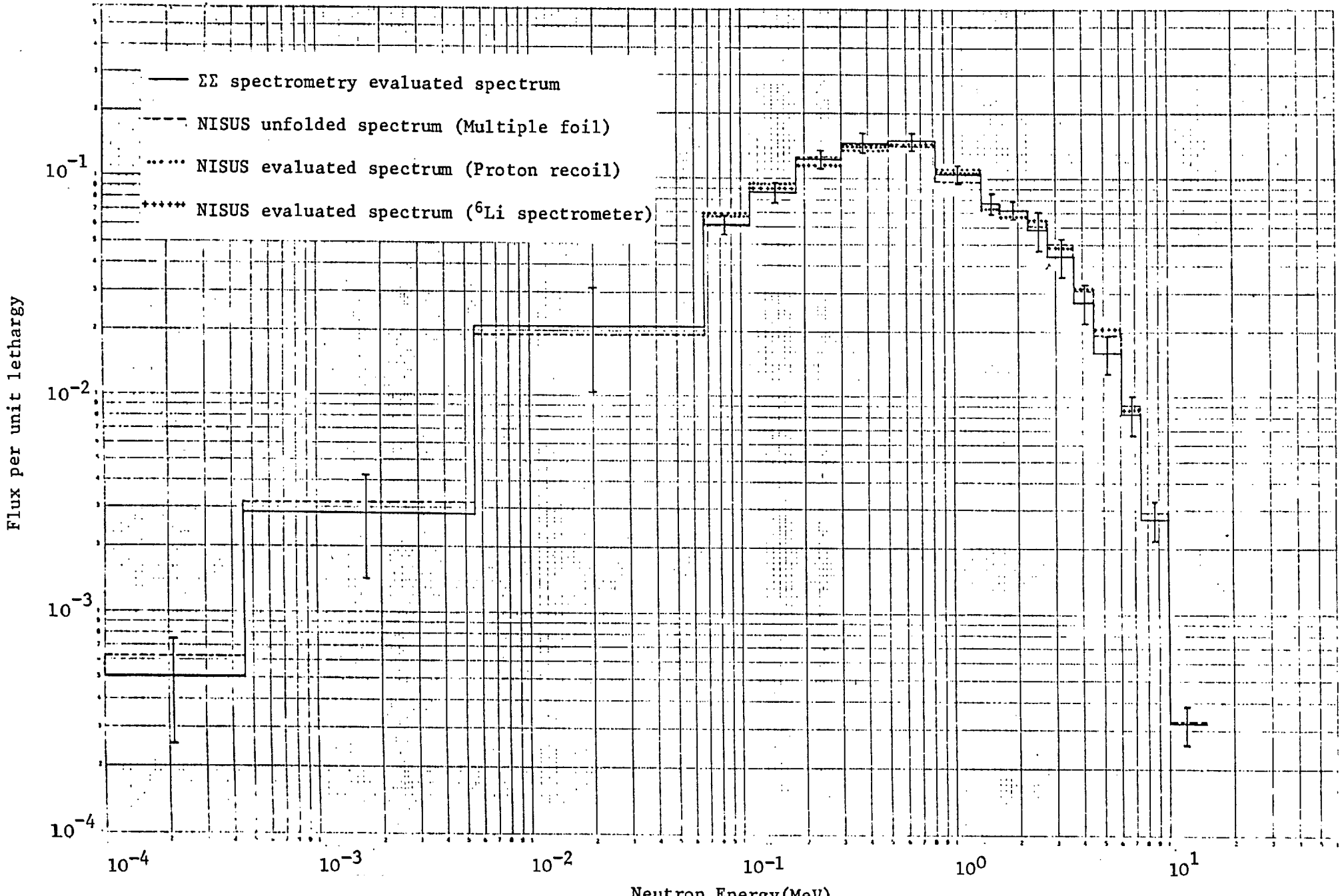


Fig.8.1. Comparison of the NISUS central neutron spectrum unfolded by multiple foil spectrometry and measured by Proton recoil and ^{6}Li spectrometers. The ΣΣ evaluated central neutron spectrum is used as the reference spectrum.

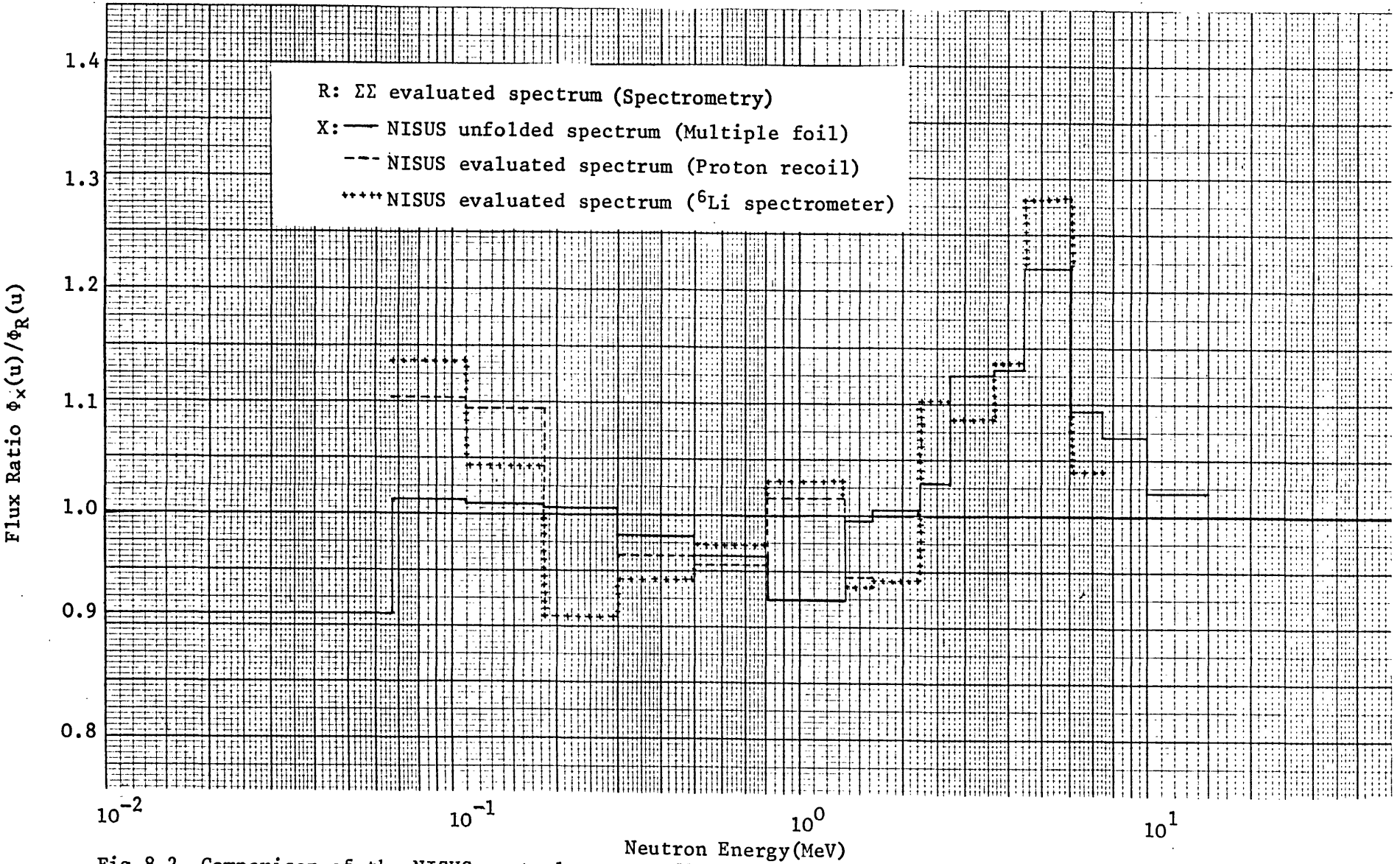


Fig.8.2. Comparison of the NISUS central neutron flux spectrum unfolded by multiple foil spectrometry and measured by Proton recoil and ^{6}Li spectrometers. The ΣΣ spectrometry evaluated central neutron flux spectrum is used as the refernce spectrum.

It can be seen from Table 8.1 and Fig. 8.2. that the NISUS neutron fluxes measured by ^{6}Li spectrometer are higher $\sim$ 4% than the $\Sigma\Sigma$ neutron fluxes over the energy region $\sim$ 7.4 - 6.0 MeV but the NISUS neutron fluxes by multiple foil is $\sim$ 9% higher than the $\Sigma\Sigma$ neutron fluxes over the same energy region. The NISUS spectra measured by ^{6}Li spectrometer and multiple foil method are higher $\sim$ 28%, $\sim$ 14% and $\sim$ 22%, 13% respectively than the $\Sigma\Sigma$ spectra in the energy regions $\sim$ 6.0 - 4.5 MeV and $\sim$ 4.5 - 3.7 MeV. It is found that the NISUS spectrum determined by ^{6}Li and multiple foil spectrometers agrees within $\sim \pm$ 6% in the energy region $\sim$ 7.4 - $\sim$ 4 MeV. No uncertainty has been estimated for the neutron fluxes in different energy groups in the NISUS unfolded spectrum in the present work. But the $\sim \pm$ 6% variation is within the $\sim$ 10% uncertainty in the $^{6}Li(n,\alpha)$ cross section data above 4 MeV[73]. It is worth mentioning that the $\Sigma\Sigma$ neutron spectrum is erroneous in the energy range 6 - 4 MeV (Explained in Section 7.3). So a large discrepancy is observed between the evaluated NISUS and $\Sigma\Sigma$ spectra in this energy range. This discrepancy is certainly not attributable to real differences between the two fields.

NISUS neutron fluxes by multiple foil are higher $\sim$ 13% and $\sim$ 3% than the $\Sigma\Sigma$ neutron fluxes in the energy regions $\sim$ 3.7 - 2.7 MeV and $\sim$ 2.7 - 2.2 MeV and neutron fluxes by ^{6}Li spectrometer are higher $\sim$ 9% and $\sim$ 10% than the $\Sigma\Sigma$ neutron fluxes for the same energy regions.

Flux ratio between multiple foil technique and ΣΣ spectrometry agrees very well in the energy range ∿ 2.2 - ∿ 1.7 MeV but neutron fluxes determined by ^{6}Li spectrometer fall below ∿ 6% those of ΣΣ spectrum in the same energy region. The error assigned in the neutron spectrum by ^{6}Li measurement is ∿ 8.5% for the energy range ∿ 2.9 - 1.7 MeV[72].

The NISUS spectra measured by multiple foil, proton recoil and ^{6}Li spectrometers agree very well within ∿ ± 5% with the ΣΣ spectrum over the energy range ∿ 1.7 MeV - ∿ 180 KeV except the NISUS neutron fluxes by multiple foil fall ∿ 8% below the ΣΣneutron fluxes at ∿ 1.3 MeV - ∿ 800 KeV and the NISUS neutron fluxes by ^{6}Li spectrometer fall ∿ 9% below the ΣΣ neutron fluxes at ∿ 300 - ∿180 KeV. The discrepancy at ∿ 1.3 MeV - ∿ 800 KeV is due to the presence of $^{237}Np(n,f)$ reaction rate in SIMMM to unfold the NISUS spectrum (Explained in Section 7.3). The variation in ^{6}Li spectrum measurement at ∿ 300 - ∿ 180 KeV may be attributed to the ∿ ± 15% uncertainty in the spectrum measurement by ^{6}Li spectrometer for ∿ 600 - ∿ 10 KeV[73].

NISUS neutron fluxes determined by multiple foil agree very well with the ΣΣ neutron fluxes for the energy range ∿ 180 - ∿ 60 KeV. But the NISUS fluxes measured by proton recoil counter are ∿ 10% higher than the ΣΣ neutron fluxes in this energy region. An accuracy of ∿ ± 3% has been claimed by J. Petr for NISUS spectrum measurement by proton recoil counter over the energy range ∿ 2 MeV - ∿ 40 KeV[47]

ΣΣ spectrometry data are claimed to be accurate within ∿ ± 5% for the energy range ∿ 2 MeV - ∿ 20 KeV[31]. Part of the discrepancy may be attributed to the normalisation procedure. NISUS neutron fluxes by ^{6}Li spectrometer are also higher ∿ 4% and ∿ 14% in the energy region ∿ 180 - ∿ 110 KeV and ∿ 110 - ∿ 60 KeV respectively. This variation may be due to the uncertainty (∿ ± 15%) in the spectrum measurement by ^{6}Li spectrometer and also due to the normalisation procedure because the NISUS spectrum measured by proton recoil and ^{6}Li spectrometers agree within ∿ ± 5% over the energy range ∿ 2 MeV - ∿ 40 KeV[47 & 72].

Thus it can be concluded that the NISUS spectrum measured by multiple foil and proton recoil spectrometers agrees within ∿ ± 5% for the energy region ∿ 1.7 MeV - ∿180 KeV except ∿1.35 MeV - ∿800 KeV but agrees within ∿ ± 10% for the energy range ∿ 1.7 MeV - ∿60 KeV. The NISUS spectrum measured by ^{6}Li spectrometer agrees within ∿ ± 6% with the spectrum measured by multiple foil over the energy range ∿ 7.5 MeV - ∿ 300 KeV except ∿ 1.35 MeV - ∿ 800 KeV. The discrepancy observed in the NISUS spectrum measured by ^{6}Li and multiple foil spectrometers are ∿±10%, ∿±4% and ∿±14% in the energy ranges ∿ 300 - ∿ 180 KeV, ∿ 180 - ∿ 110 KeV and ∿ 110 - ∿ 60 KeV respectively.

The present accuracy of the evaluated energy dependent cross section data used in unfolding the spectrum is at the 10 - 20% level (1σ) although for some reactions it is much better[7].

It may be concluded from the forgoing comparisons that the spectrum obtained using SIMMM with the multiple foil technique is in general consistent within ± 10% with the values from ^{6}Li and proton recoil neutron spectrometers used in NISUS, but not with the ΣΣ evaluated spectrum. It should be noted that the ΣΣ evaluated spectrum was included in the SIMMM evaluation, but that the NISUS spectrometry results were not.

9. SUMMARY AND CONCLUSIONS

The object of the research programme was to perform measurement of integral reaction rates induced in an appropriate number of selected neutron dosimeters, e.g. activation foils in well established benchmark and standard fast neutron fields. The standard fast neutron fields chosen in this work were: NISUS, MOL-ΣΣ and $\chi_{25}(E)$. Interlaboratory comparison of measured reaction rates and their ratios for the NISUS, ΣΣ and $\chi_{25}(E)$ neutron fields were performed to provide accurate integral reaction rates and their ratios, to investigate the variation of spectrum in these three fast neutron fields and also to identify any discrepancy in measurement techniques. Measured reaction rates in the NISUS neutron field only were used in a simultaneous evaluation of reaction rates, cross sections and spectrum using the SIMMM code. Comparison was made of the NISUS central neutron spectrum unfolded by multiple foil spectrometry with the results of other experimental techniques used in NISUS. Inter-laboratory comparison of spectra of fast neutron fields (NISUS and ΣΣ) was made.

At the first stage of the project integral reaction rates of non-fissile and fissile foils of various materials of importance in fast neutron dosimetry were measured in NISUS. The selection of activation foils was made in such a manner as to cover the entire energy range of the NISUS spectrum. The energy range covered by the neutron detectors for the central ∿ 90% response was ∿ 50 eV - ∿ 12.5 MeV which is essentially

the fast neutron energy response. A similar energy response for the same detectors was observed in the ΣΣ facility.

Absolute reaction rates of various materials in five positions inside NISUS were determined with the calibrated Ge(Li) detector after making all necessary corrections (external absorber, self absorption, dead time, self shielding and pulse pile up) where applicable. The reaction rate traverses for different neutron detectors inside NISUS in the present work agreed well within the statistical errors with both theoretical and experimental traverses in ΣΣ. The decrease of high energy reaction rate traverses across the distance of 8 cm. through the centre of NISUS is ∿ 20% from the direction of the reactor core which may be compared with ∿ 18% decrease across the distance of 10 cm for high energy reaction rate traverses in ΣΣ from the direction of the reactor core[10]. It is observed that the reaction rate gradient is dependent on the energy response of various neutron detectors in the NISUS spectrum. The reaction rate gradient increases as the energy response of the detectors is increased (shown in Fig. 4.15).

Absolute NISUS central fission rates of ^{235}U, ^{239}Pu, ^{238}U and ^{237}Np were determined by NBS absolute double fission chambers. Absolute fission rates of ^{235}U and ^{238}U were also measured by fission foils (^{140}La technique). Absolute fission rates of ^{235}U and ^{238}U determined by fission chambers and activation foils agreed within ∿ ± 1.5%. So the weighted mean values of absolute fission rates of ^{235}U and ^{238}U

were determined. Fission ratio of ^{235}U, ^{239}Pu, ^{238}U and ^{237}Np relative to ^{235}U were determined.

NISUS central reaction rates were measured again for all non-fission detectors in order to check the consistency and reproducibility of the central reaction rate measured during reaction rate traverse measurements. For capture and threshold detectors, NISUS central reaction rate agreed very well and the reproducibility is within $\sim \pm 1\sigma$ level except $^{64}Zn(n,p)^{64}Cu$ and $^{56}Fe(n,p)^{56}Mn$ reactions. The variation in $^{64}Zn(n,p)^{64}Cu$ reaction measured in April, 1975 and March, 1976 is $\sim$ 6% (2σ level). The $^{56}Fe(n,p)^{56}Mn$ reaction was measured again in December, 1975 and in April, 1976 and it was observed that the $^{56}Fe(n,p)^{56}Mn$ reaction measured in December, 1975 and April, 1976 was $\sim$ 12% and $\sim$ 15% higher than the $^{56}Fe(n,p)^{56}Mn$ reaction measured in May, 1975. When making inter-laboratory comparison of reaction rate ratios of NISUS and $\Sigma\Sigma$ neutron fields, the $^{56}Fe(n,p)^{56}Mn$ reaction measured in December 1975 and April 1976 agreed within $\sim \pm 5\%$. So the reaction rate of $^{56}Fe(n,p)^{56}Mn$ measured in May 1975 was rejected (Table 4.34). Absolute central fission rates of ^{235}U and ^{238}U were not measured again to check the reproducibility because the fission rates were measured by fission chamber and activation foil techniques and they agreed within $\sim \pm 1.5\%$. Fission rates of ^{239}Pu and ^{237}Np were measured by NBS fission chambers only because other ^{239}Pu and ^{237}Np fission foils were not available. It was found that the reproducibility of the NISUS central reaction rate for threshold and non-threshold foils was very good and agreed within the uncertainty of $\sim \pm 1\sigma$ confidence

level except the $^{64}Zn(n,p)^{64}Cu$ reaction (Table 4.34).

Day-to-day reactor power monitoring of each irradiation was performed by activation foil detectors and fission chambers. Activation detectors only were used as reactor power monitoring during the reaction rate traverse measurements in NISUS. Two fission chambers and two gold foils were used as monitors during the course of fission rate measurements by NBS fission chambers and subsequently used for the measurement of the NISUS central reaction rate of various materials. It was observed that the long term monitoring consistency was not achieved by fission chambers due to drifting in electronic system. The gold monitor in Position A was more consistent than any other monitor and was used for normalising of reactor power for each irradiation in the present work.

In the second stage of the project reaction rates were measured in MOL-$\Sigma\Sigma$ and $\chi_{25}(E)$ neutron fields. The same foils and the same counting system were used in reaction rate measurements which were previously used in NISUS reaction rate measurements. 8 reaction rates in $\Sigma\Sigma$ and 6 reaction rates in $\chi_{25}(E)$ neutron fields were measured. Comparisons were made between the reaction rate ratios measured in NISUS, $\Sigma\Sigma$ and $\chi_{25}(E)$ neutron fields in the present work and also with reaction rate ratios measured by Fabry in $\Sigma\Sigma$ and $\chi_{25}(E)$ neutron fields[31]. Reaction rate ratios agreed within their $\sim \pm$ 1σ random errors (except $^{24}Mg(n,p)^{24}Na$ reaction which agreed within $\sim \pm 2\sigma$ random error) for NISUS and $\Sigma\Sigma$ neutron

fields when using the same foils and same counting system |when considering NISUS (present work) and ΣΣ (present work) in Table 5.4|. The present reaction rate ratios agreed with Fabry's data within their total uncertainties (± 1σ level) for NISUS and ΣΣ except for $^{55}Mn(n,\gamma)^{56}Mn$ and $^{27}Al(n,\alpha)^{24}Na$ reactions |when considering NISUS (present work) and ΣΣ (Fabry) in Table 5.4|. A 20% discrepancy was observed in the $^{55}Mn(n,\gamma)^{56}Mn$ reaction. This discrepancy is attributable to the lack of any self shielding correction to the $^{55}Mn(n,\gamma)^{56}Mn$ reaction rate measured in NISUS. The $^{27}Al(n,\alpha)^{24}Na$ reaction measured in NISUS was ∿ 10% lower than that measured by Fabry in ΣΣ. The same discrepancy (∿ 10% lower than Fabry's data) was observed when $^{27}Al(n,\alpha)^{24}Na$ reaction was measured in ΣΣ |ΣΣ (present work) in Table 5.4| using the same foil and same counting system as was used in the NISUS $^{27}Al(n,\alpha)^{24}Na$ reaction measurement. The discrepancy in the $^{27}Al(n,\alpha)^{24}Na$ reaction for ΣΣ may be attributable to errors in Fabry's measurement at Mol, Belgium. In a recent paper Fabry states that the measured integral reaction rates of $^{27}Al(n,p)^{27}Mg$, $^{56}Fe(n,p)^{56}Mn$ and $^{27}Al(n,\alpha)^{24}Na$ may be too high[31]. The consistency of reaction rate measurements can be obtained by making interlaboratory comparison. So intercomparison of measurement technique will emerge as mandatory to provide proper confirmation of discrepancy in measurements, this is possible because the concept of standard neutron fields[10] allows valuable comparisons for detectors and instruments that are not transferable between laboratories[31].

Comparing the reaction rate ratios of the $\chi_{25}(E)$ neutron field from the present work with Fabry's data [$\chi_{25}(E)$ (present work) and $\chi_{25}(E)$ (Fabry) in Table 5.5 respectively], it was found that the measured reaction rate ratios agreed well within their total uncertainties (Table 5.5) except for the $^{64}Zn(n,p)^{64}Cu$ reaction rate which was $\sim$ 10% higher in the present work compared with that of Fabry. No suitable explanation can be found for this discrepancy yet. But it is thought that repeating the measurement in $\chi_{25}(E)$ neutron field for this reaction may resolve this discrepancy.

Comparison of reaction rate ratios in NISUS, ΣΣ and $\chi_{25}(E)$ neutron fields indicates that reaction rate ratios agreed well within their total uncertainties (± 1 σ level) in these three fast neutron fields (Tables 5.4 and 5.5). It is found that NISUS and ΣΣ are two almost identical fast neutron fields and they are standardised and are reproducible. The high energy spectral tail of these two neutron fields (NISUS and ΣΣ) is close to a fission spectrum shape because the high energy spectral shape above $\sim$ 2.5 MeV is nearly a fission spectrum shape in most fission driven systems [7 & 31].

A set of integral reaction rates measured in the NISUS neutron field together with a consistent set of evaluated energy-dependent cross section values σ(E) and an approximate input spectrum (the ΣΣ evaluated spectrum was used as input spectrum) were used to evaluate the reaction rates in NISUS by the SIMMM code. The SIMMM code simultaneously evaluated cross section data, reaction rates and spectrum by

adjustment of the cross section data and the input spectrum. Only 8 measured reaction rates could be used to evaluate calculated reaction rates due to the storage limitation in the core memory of the computer (M7600). The SIMMM code was run first with 8 threshold reactions only and in the second run the code was used for 8 non-threshold and threshold reactions. In both runs, the calculated reaction rates agreed very well with the measured reaction rates within $\sim \pm 3\%$ which are within the estimated errors of the measured reaction rates.

The SIMMM code evaluated the NISUS spectrum for the energy range $\sim$ 15 MeV - $\sim$ 60 KeV for threshold reactions and also for the energy range $\sim$ 15 MeV - $\sim$ 50 eV for non-threshold and threshold reactions. It was found that the neutron fluxes found in both runs was essentially the same for the energy range $\sim$ 15 MeV - $\sim$ 60 KeV and the reproducibility of the spectrum for this energy range is very good. This confirms that the inclusion of non-threshold reaction rates did not have any impact on the high energy tail of the NISUS spectrum.

NISUS spectrum unfolded by multiple foil spectrometry was compared with the NISUS spectra measured by proton recoil[47] and ^{6}Li spectrometers[72]. NISUS neutron group fluxes measured by the above mentioned three techniques were formed relative to the $\Sigma\Sigma$ evaluated spectrum and comparison has been made of flux ratios (Table 8.1 and Fig. 8.2). The $\Sigma\Sigma$ evaluated spectrum is considered as the reference spectrum in this work.

It was found that the NISUS spectrum evaluated using the multiple foil data agrees with data from proton recoil spectrometers within ∿ ±5% for the energy region ∿ 1.7 MeV - ∿ 180 KeV except for the ∿ 1.35 MeV - ∿ 800 KeV energy interval (the neutron fluxes by multiple foil method fall ∿ 10% below those of the proton recoil counter in this energy region). Agreement between the proton recoil and multiple foil results is within ∿ ±10% for the whole energy range, ∿ 1.7 MeV - ∿ 60 KeV, in which the comparison can be made. The NISUS spectrum measured by ^{6}Li spectometers agrees within ∿ ± 6% with the NISUS spectrum evaluated using the multiple foil data over the energy region ∿ 7.5 MeV - ∿300 KeV except for the 1.35 MeV - ∿ 800 KeV energy interval. Fluxes from the ^{6}Li spectrometers and evaluated from the multiple foil data differ by between 4% and 14% for the energy intervals ∿ 300 KeV - ∿60 KeV and this variation may in part be due to the uncertainty (∿ ± 15%) in the spectrum measurement by ^{6}Li spectrometers[73] and due to the normalisation procedure.

By making interlaboratory comparison of spectra of NISUS and ΣΣ neutron fields, it was observed that the NISUS spectrum evaluated using the multiple foil data was in agreement within ∿ ± 5% with the ΣΣ evaluated spectrum in the ∿ 3 MeV - ∿60 KeV region except in the ∿ 1.35 MeV - ∿ 800 KeV energy interval (NISUS neutron fluxes are lower by ∿ 8% in this energy region). The NISUS unfolded fluxes were found to be ∿10%-20% higher than the evaluated fluxes above

$\sim$ 3 MeV. It is mentioned by Fabry in a recent paper that the ΣΣ evaluated spectrum between 6-4 MeV is erroneous[31]. The NISUS spectrum was found to be lower by $\sim$ 10% in the energy interval $\sim$ 60 - $\sim$ 5 KeV than the ΣΣ spectrum. The ΣΣ evaluated spectrum was lower below $\sim$ 5 KeV than the NISUS unfolded spectrum. This deviation is due to the use of the activation detectors with broad energy response (as for example, $^{197}Au(n,\gamma)^{198}Au$ reaction) which can produce uncertainties in the low energy spectrum. Also it is reported that too little flux is considered in the low energy tail of the calculated ΣΣ spectrum[7].

The present accuracy of the evaluated energy dependent cross section data used in unfolding the spectrum is at the 10 to 20% level (1σ) although for some reactions it is much better[7]. The discrepancies observed in the comparison of spectrum by multiple foil spectrometry with the results of other experimental techniques and also in interlaboratory comparison of spectra can be improved if more accurate, consistent and updated evaluated cross section data sets (ENDF/BIV dosimetry cross section data) are used.

Finally the work performed in this research programme can be concluded briefly as:

(1) it has been established that integral reaction rates measured in the NISUS neutron field for non fissile materials have been obtained

with an accuracy of < ± 5% (1σ level) and are reproduced within the uncertainty of ± 1σ confidence level except the $^{64}Zn(n,p)^{64}Cu$ reaction rate. The $^{64}Zn(n,p)^{64}Cu$ reaction has been reproduced within ±2σ confidence level. Fission rates of fissile materials have been obtained with the estimated accuracy of < ± 2.5% (1σ level).

Reaction rates measured in ΣΣ and $\chi_{25}(E)$ neutron fields are obtained with an accuracy of < ± 5% (1σ level) for non fissile materials.

(2) by interlaboratory comparison of the measured reaction rates and their ratios in NISUS, ΣΣ and $\chi_{25}(E)$ neutron fields, it has been established that integral reaction rates and their ratios can be reproduced within ∿ ± 5% except for the $^{55}Mn(n,\gamma)^{56}Mn$ reaction in the NISUS neutron field and the $^{64}Zn(n,p)^{64}Cu$ reaction in the $\chi_{25}(E)$ neutron field in the present work. This confirms the consistency in the measurement techniques and also it proves that NISUS and ΣΣ are two almost identical, standard and reproducible fast neutron fields. The consistency of reaction rate ratios of NISUS and ΣΣ with the $\chi_{25}(E)$ neutron field also proves that the high energy spectral tail of NISUS and ΣΣ above ∿ 2.5 MeV is close to the fission spectrum shape.

(3) as consistency is being obtained in measured reaction rates in these three standard fast neutron fields, the measured integral reaction rates can be used for testing and evaluating dosimetry cross section data sets.

(4) the integral reaction rates predicted by the SIMMM code have agreed very well with the measured reaction rates in NISUS within $\sim \pm 3\%$ after making plausible adjustments of cross section data and the input spectrum. This proves the validity and reliability of the SIMMM code and the data used.

(5) the NISUS spectrum unfolded by the SIMMM code has agreed with the results of other experimental techniques (proton recoil and ^{6}Li spectrometers) for the energy range $\sim$ 1.7 MeV - $\sim$ 180 KeV in case of proton recoil counter and $\sim$ 7.5 MeV - $\sim$ 300 KeV in case of ^{6}Li spectrometers. The variation in spectrum in other energy intervals can be improved if the errors in the cross section data used by different techniques (multiple foil and ^{6}Li spectrometers) are reduced.

(6) interlaboratory comparison of spectra of NISUS and $\Sigma\Sigma$ has agreed within $\sim \pm 5\%$ for the energy range $\sim$ 3 MeV - $\sim$ 60 KeV. The discrepancy in spectrum in these two standard fast neutron fields for the other energy intervals can be minimised if the present accuracy of the evaluated cross section data at the 10-20% level (1σ) can be improved and also more accurate measurement by other spectrometry techniques.

REFERENCES

1. "Nuclear Energy and the Environment", Addendum to the Agency's report to the economic and social council of the United Nations for 1969-70, I.A.E.A., Vienna, INFCIRC/139/Add. 1.

2. STORRES, E., "Introduction to the Physics of Fast Power Reactors", Developments in the Physics of Nuclear Power Reactors. Tech. Rep. No. 143, 247, I.A.E.A., Vienna (1973).

3. HUNT, S.E., "Fission, Fusion and the energy Crisis". Pergamon Press, Oxford, U.K. 1st Edition, P 67 (1974).

4. SCHMIDT, J.J., "General Status of Nuclear Data Requirements", Nuclear Data for Reactors (Proc. 2nd Int. Conf., Helsinki 1970) Vol. I, 3, I.A.E.A., Vienna (1970).

5. CAMPBELL, C.G., and ROWLANDS, T.L., "The relationship of microscopic and integral data", Nuclear Data for Reactors (ibid 4), Vol. II, 391, I.A.E.A., Vienna (1970).

6. PAZY, A., RAKAVY, G., REISS, I., WAGSCHALL, J.J., YA'ARI, ATARA., and YEIVIN, Y., "The role of integral Data in Neutron Cross-section Evaluation", Nucl. Sci. & Eng., 55, 280 (1974).

7. McELROY, W.N., and KELLOGG, L.S., "Fuels and Materials Fast-Reactor dosimetry Data development and testing", Nucl. Tech., 25, 180 (1975).

8. DUDEY, N.D., POPEK, R.J., GREENWOOD, R.C., HELMER, R.G., ROGERS, J.W., KELLOGG, L.S., and ZIMMER, W.H., "Fission Product-rate Measurements and Yields". Nucl. Tech., 25, 294 (1975).

9. BESANT, C.B., EMMETT, J., CAMPBELL, C.G., KERRIDGE, M., and JONES, T.C., "Design and Construction of a Fast Reactor Neutron Spectrum Generator - NISUS", Nucl. Eng. Int., 18, 425, May (1973).

10. FABRY, A., DELEEUW, G., and DELEEUW, S., "The Secondary Intermediate Energy Standard Neutron Field at the MOL-ΣΣ Facility", Nucl. Tech., 25, 349 (1975).

11. FABRY, A., GRUNDL, J.A., and EISHENHAUER, C., "Fundamental Integral Cross Section Ratio Measurements in the Thermal-Neutron-Induced Uranium-235 Fission Neutron Spectrum", Conf. on Nucl. Cross Sections and Technology, Washington, D.C., March (1975).

12. GREENWOOD, R.C., HELMER, R.G., ROGERS, J.W., DUDEY, N.D., POPEK, R.J., KELLOGG, L.S., and ZIMMER, W.H., "Non-Fission Reaction Rate Measurements", Nucl. Tech., 25, 274 (1975).

13. ZIJP, W.L., "Review of Activation Methods for the Determination of Fast Neutron Spectra", RCN-37, Petten, May (1965).

14. BECKURTS, K.H., and WIRTZ, K., "Neutron Physics", Springer, Verlag (1964).

15. CARTER, P., and JONES, E.D., "Detectors and Counting Methods for Routine Flux Monitoring", AERE-R5491 (1967).

16. GRUNDL, J.A., and GILLIAM, D.M., "Measurement of Absolute Fission Rates", Nucl. Tech., 25, 237 (1975).

17. YULE, H.P., "Special Publ.", Nat. Bur. Stands., Vol. II, 312 (1969).

18. "Gamma Reference Source Data Sheet 11181, Source Specification", The Radiochemical Centre, Amersham, England, July (1975).

19. THEIN, M., "Decay Scheme of ^{110m}Ag, Private communication", University of London Reactor Centre (ULRC) (1976).

20. TOPPING, J., "Errors of Observation and their Treatment", Chapman and Hall Limited, London, 3rd Edition (1962).

21. NAG Library Manual, "E02ABF, Document No. 601, ICL 1900 System", Nottingham Algorithms Group.

22. LEDERER, C. M., HOLLANDER, J.M., and PERLMAN, I., "Table of Isotopes", John Wiley and Sons, Inc., London, 6th Edition (1967).

23. FABRY, A., and VANDEPLAS, P., "Generation of Intermediate Standard Neutron Spectra and their Application in Fast Reactor Physics", (Proc. of Symp. on Fast Reactor Physics, Karlsruhe, 1967), Vol. I, 389, I.A.E.A., Vienna (1968).

24. AZAD, S., BESANT, C.B., EMMETT, J., CAMPBELL, C.G., JONES, T.C., KERRIDGE, M., PETR, J., and WILLIAMS, J.G., "NISUS - A Neutron Intermediate Standard Uranium Source on Irradiation Facilities for Research Reactors", (Proc. of Symp., Tehran, 1972), 185, I.A.E.A., Vienna (1973).

25. GRANT, P.J., "The London University Nuclear Reactor CONSORT", Nature, 29, 911 (1965).

26. ZARTMAN, I.F., "The Future United States Fast Reactor Physics Program", Proc. of the Int. Conf. on Fast Critical Experiments and their Analysis, ANL-7320 (P 737), Argonne, October (1967).

27. BROOMFIELD, A.M., GEORGE, C.F., INGRAM, G., JAKEMAN, D., and SANDERS, J.E., "Measurements of k-infinity, Reaction Rates and Spectra in ZEBRA Plutonium Lattices", Proc. of Int. Conf. on Fast Reactor Physics, BNES, London, P.15 (1969).

28. ROWLANDS, J.L., and MACDOUGAL, J.D., "The use of Integral Measurements to Adjust Cross Sections and Predict Reactor Properties", ibid 27, P.180.

29. CAMPBELL, C.G., "United Kingdom Programme in Fast Reactor Physics", Proc. of Symp. on Fast Reactor Physics, Karlsruhe, 30 October - 3 November 1967, I.A.E.A., Vienna (1968).

30. Proceedings of Int. Conf. on Fast Reactor Physics, BNES, London, June (1969).

31. FABRY, A., CEULEMANS, H., VANDEPLAS, P. (SCK/CEN, MOL), McELROY, W.N., and LIPPINCOTT, E.P. (HEDL)., "Reactor Dosimetry Integral Reaction Rate Data in LMFBR Benchmark and Standard Neutron Fields : Status, Accuracy and Implications", First ASTM-EURATOM Symposium on Reactor Dosimetry, Petten, September 22 - 26 (1975).

32. GRUNDL. J.A., "Private Communication", (1974).

33. EMMETT, J., Ph.D. Thesis (In Preparation), University of London, I.C.

34. AZIMI, D., "Fission Rates in NISUS - A Fast Reactor Neutron Spectrum Generator", Ph.D. Thesis, University of London, I.C. (1975).

35. FABRY, A., and VANDEPLAS, P., "Computational Design and Major Aims of the C.E.N./S.C.K., Secondary Standard Neutron Spectrum Facility", I.A.E.A. Panel on Fast Reactor Spectrum Measurements and their Interpretation, Argonne, 10-15 November (1970).

36. Vendor Certificate, Reactor Experiments Inc., California, U.S.A.

37. SMITH, DONALD L., and MEADOWS, JAMES W., "Cross Section Measurement of (n,p) Reactions for ^{27}Al, $^{46,47,48}Ti$, $^{54,56}Fe$, ^{58}Ni, ^{59}Co and ^{64}Zn from Near Threshold to 10 MeV", Nucl. Sci. & Eng., 58, 314-20 (1975).

38. Handbook of Chemistry and Physics (CRC), "Table of Isotopes", 51st Edition (1970-71).

39. HELMER, R.G., and GREENWOOD, R.C., "Evaluated Decay Scheme Data", Nucl. Tech., 25, 258 (1975).

40. Reactor Physics Constant, ANL-5800, 1964 Edition.

41 ELERY, STORM., and HARVEY, I. ISRAELE., "Photon Cross Sections from 1 KeV - 100 MeV for Elements Z = 1 to Z = 100", Nucl. Data Tables, 7, No. 6, Academic Press, New York (1970).

42. AZAD, S., "Fast Neutron Reaction Rate and Spectrum Measurements", Ph.D. Thesis, University of London, I.C. (1973).

43. FABRY, A., WILLIAMS, J.G., HANNAN, A.H.M.A., and AZIMI, D., "Intercomparison of the Intermediate-Energy Standard Neutron Fields at the NISUS and MOL-ΣΣ Facilities by Means of NBS-type Absolute Fission Chambers", To be published (1976).

44. FABRY, A., COPS, F. (C.E.N./S.C.K.), GRUNDL, J.A., and GILLIAM, D. (NBS), "Fission Rate Measurements in the ΣΣ Standard Neutron Field by Means of NBS Absolute Fission Chamber", AF/Sa - 61 - 606/75 - 02/c/a. Reactor Study, Reactor Physics, MOL, May 16 (1975).

45. BARFORD, N.C., "Experimental Measurements: Precision, Error and Truth", Addison-Wesley Company, London, P63 (1967).

46. FABRY, A., and CZOCK, K.H., "Measurements of Integral Cross Section Ratios in Two Dosimetry Benchmark Neutron Fields", INDC(IAEA)-005/G, IAEA/RL/27, December (1974).

47. PETR, J., "Neutron Energy Spectrum Measurements in a Standard Fast Neutron Assembly", Ph.D. Thesis, University of London, I.C. (1973).

48. BROWN, W.A.V., SKILLINGS, D.J., BLACKMANN, T.E., and BURHOLT, G.D., "Measurement of Fast Fission Ratio", AEEW-R341, U.K.A.E.A. (1964).

49. CARDER, M.D., PERKS, A.J., and SANDERS, L.G., "The Measurement of ^{238}U : ^{235}U Fission Ratios", AERE-R3205, A.E.R.E., Harwell, U.K. (1960).

50. PAZIRANDEH, A., "Reaction Rates in Fissile Material", Ph.D. Thesis, University of London, I.C. (1969).

51. FABRY, A., "Private Communication", (1973).

52. FABRY, A., "Private Communication", (1976).

53. COPS, F., "Private Communication", C.E.N./S.C.K., MOL, Belgium (1976).

54. DUNFORD, C., and VLASOV, M., "Proceedings of a Consultants Meeting on Nuclear Data for Reactor Neutron Dosimetry", INDC(NDD)-56/U, I.A.E.A., Vienna (1973).

55. MAGURNO, B.A., and OZER, O., "ENDF/B File for Dosimetry Applications", Nucl. Tech., 25, 376 (1975).

56. WRIGHT, R.Q., GREEN, N.M., LUCINS, J.L., and CRAVAN, Jr., C.W., "SUPERTOG - A Program to Generate Fine Group Constants and P_n Scattering Matrices from ENDF/B", Report ORNL-TM-2679 (1969).

57. CURTIS, R., "Private Communication", Dept. of Physics, University of Birmingham (1975).

58. SIMONS, R.L., and McELROY, W.N., "Evaluated Reference Cross Section Library", BNWL-1312, Battle North West Laboratories (1970).

59. McELROY, W.N., and BERG, S., "Reference Cross Section Library for SANDII - A Computer-Automated Iterative Method for Neutron Flux Spectra Determination by Foil Activation", AFWL-TR-67-41, Vol. III, Air Force Weapons Laboratory, Kirtland, AFB, New Mexico, July (1967).

60. GRUNDL, J.A., "A Study of Fission Neutron Spectra with High Energy Activation Detectors - Part I. Detector Development and Excitation Measurements, Nucl. Sci. & Eng., 30, 39 (1967).

61. LISKIEN, H., and PAULSEN, A., "Cross Sections for the $^{63}Cu(n,\alpha)^{60}Co$, $^{60}Ni(n,p)^{60}Co$ and Some Other Threshold Reactions Using Neutrons from $^{9}Be(\alpha,n)^{12}C$ Reaction", Nucleonik, 8, 315 (1966).

62. FABRY, A., DECOSTER, M., MINSART, G., SCHEPERS, J.C., and VANDEPLAS, P., "Implications of Fundamental Integral Measurements on High Energy Nuclear Data for Reactor Physics", 2nd Int. Conf. on Nuclear Data for Reactors (Proc. of Conf., Helsinki, 15-19 June, 1970), I.A.E.A., Vienna, Vol. II, 535 (1970).

63. CRANBERG, L., FRYE, G., NERESON, N., and ROSEN, L., "Fission Neutron Spectrum of ^{235}U", Phys. Review, 103, 662 (1956).

64. CECCIHINI, G., GANDINI, A., DAL, BONO. I., and FALESCHINI, B., "Comparison between Experimental and Theoretical Integral Data on Fast Critical Facilities. CALI, a Program for Generating "Effective" Nuclear Group Constants by a Correlation Method", Proc. of the Int. Conf. on Fast Critical Experiments and their Analysis, ANL-7320 (P.107), Argonne, October (1966).

65. HEMMENT, P.C.E., and PENDELBURY, E.D., "The Optimisation of Neutron Cross Section Data Adjustments to give Agreement with Experimental Critical Sizes", Ibid 64, P.88.

66. PAZY, A., RAKAVY, G., REISS, Y., and YEIVIN, Y., "Use of Integral Measurements as Supplementary Data in Neutron Cross Section Evaluation", Ibid 64, P.270.

67. BARRE, J.Y., HEINDLER, N., LAPACELLE, T., and RAVIER, J., "Lessons Drawn from Integral Experiments on a set of Multi-Group Cross Sections", Proc. of Int. Conf. on Fast Reactor Physics, BNES, London, P.165 (1969).

68. CARDER, W., HANNAN, A.H.M.A., and WILLIAMS, J.G., "Simultaneous Evaluation of Cross Sections, Integral Reaction Rates and Spectra in Fast Neutron Dosimetry", Paper presented in Nuclear Data Forum 1975 at U.K.A.E.A., A.E.R.E., Harwell, U.K. December (1975).

69. SIMMM - "Simultaneous Minimisation Method to find Minima of General Functions of Many Variables", University of London Reactor Centre (ULRC), July (1976).

70. SHEPPEY, G.C., "MINROS - A Program to find Local Minima of General Functions of Many Variables", D504 CERN 6600 Computer Program Library.

71. ROSENBROCK, H.H., "An Automatic Method for Finding the Greatest or Least Value of a Function", Computer J., 3, 175-82 (1960).

72. KOUTZOUKOS, G., "Developments in Lithium Neutron Spectrometry for Measurements in Fast Neutron Spectra", Ph.D. Thesis, University of London, I.C. (1975).

73. RICKARD, I.C., "The use of the Lithium-6 Semiconductor Sandwich Spectrometer for the Measurement of Fast Neutron Spectra", Nucl. Inst. and Methods., 105, 397 (1972).

74. FABRY, A., "Private Communication", September (1976).

75. "Gamma Reference Source Data Sheet 11166, Source Specification", The Radiochemical Centre, Amersham, England, March (1973).

APPENDIX A

I. Standardisation of ^{110m}Ag gamma source.

II. Dead time and pulse pile up effect.

III. Correction for finite source area of activation foils.

APPENDIX AI

Standardisation of ^{110m}Ag gamma ray source made at ULRC

One ^{109}Ag point sample was irradiated in ICIS (In-core irradiation system) of "CONSORT" Reactor at the University of London Reactor Centre for 3 hours. After irradiation the sample contained ^{110m}Ag radioactive source. This source decayed with several gamma energies. Gamma rays, whose energies are within the range of $\sim$ 0.300 to $\sim$ 1.60 MeV (gamma rays used in reaction rate calculations are within these energy regions) and gamma ray branching ratios as appropriate, were considered. Table A.1 shows energies and branching ratios of gamma rays of ^{110m}Ag source used in this work. Energies and branching ratios of gamma ray in ^{110m}Ag decay were obtained from Ref. 19.

The activity of ^{110m}Ag source was not known, so relative efficiencies of Ge(Li) detector were determined. It was then tried to normalise these relative efficiencies to the experimental absolute efficiency values obtained from the calibrated gamma sources. There were not too many absolute experimental absolute efficiency values from the calibrated sources (only 7 experimental absolute efficiency values were available from standard sources) to normalise the relative efficiencies for the energy range $\sim$ 0.400 - $\sim$ 1.5 MeV. Gamma ray energies 0.658 -, 0.818 - and 0.885 - MeV of ^{110m}Ag source are close to the gamma ray energies of 0.662 -, 0.835 - and 0.898 - MeV of

standard gamma sources, so the absolute efficiencies determined by standard sources for the above energies (0.662 -, 0.835 - and 0.898 - MeV) were interpolated and extrapolated to determine the absolute efficiencies for energies 0.658 -, 0.818 - and 0.885 - MeV from Fig. A.1. Absolute efficiencies of 0.658 -, 0.818 - and 0.885 - MeV of ^{110m}Ag source was determined in the following way:

To determine the absolute efficiency at 0.658 - MeV, the slope ($\frac{\Delta\eta}{\Delta E}$ = Efficiency per MeV) was determined nearer to 0.658 - and 0.662 - MeV energy range from Fig. A.1.

Slope ($\frac{\Delta\eta}{\Delta E}$) nearer to 0.658 - and 0.662 - MeV = 0.01429 MeV^{-1}

Efficiency for the energy difference (0.662 - 0.658 MeV = 0.004 MeV)

$$= 0.005714 \times 10^{-2}$$

Efficiency (η) at 0.662 MeV = 1.027×10^{-2} from Fig. A.1.

η at 0.658 MeV $= 1.027 \times 10^{-2} - (-.005714 \times 10^{-2})$

$$= 1.033 \times 10^{-2}$$

Similarly the absolute efficiencies for 0.818 - and 0.885 - MeV which are close to 0.835 - and 0.898 - MeV were determined.

Absolute efficiencies of 0.658 -, 0.818 - and 0.885 - MeV are given in Table A.2. These absolute efficiencies were then used to determine the activities of ^{110m}Ag source at 0.658 -. 0.818 - and 0.885 - MeV and the weighted mean of the activity of ^{110m}Ag was obtained. The activities at 0.658 -, 0.818 - and 0.885 - MeV and the weighted mean of the activity of ^{110m}Ag source with their errors are given in Table A.3.

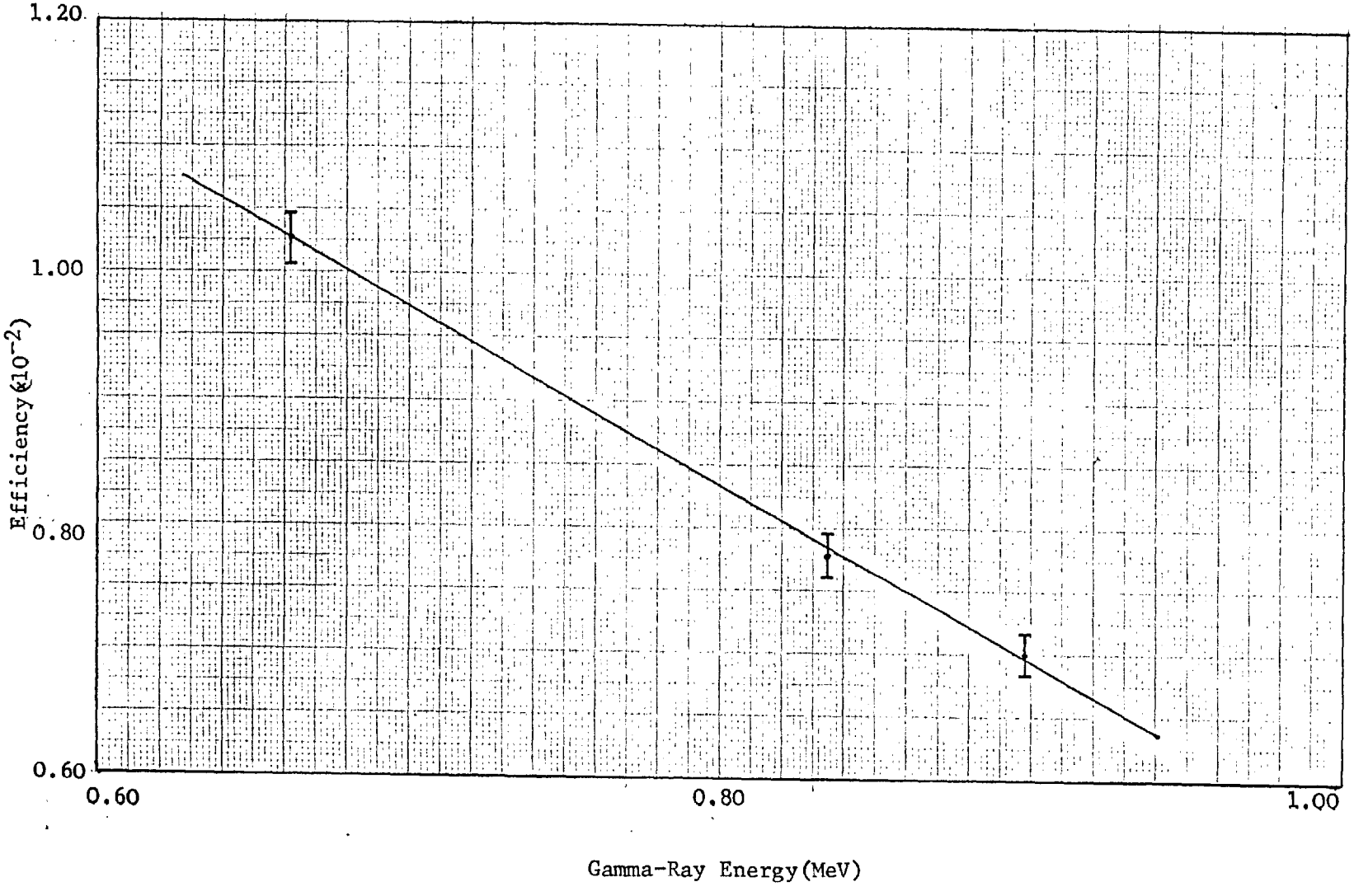


Fig.A.1. Absolute photopeak efficiency measured for the Ge(Li) detector at 0.662-, 0.835- and 0.898 MeV by standard gamma sources used to obtain absolute efficiency at 0.658-, 0.818- and 0.885 MeV. A hand-drawn line is shown through the experimental points.

This weighted mean of activity was used to determine the absolute efficiencies of Ge(Li) detector from ^{110m}Ag source. The activity and absolute efficiencies from ^{110m}Ag source are given in Tables 2.2 and 2.3 respectively in Section 2.2 in Chapter 2.

TABLE A.1

Gamma ray energy and branching ratio of ^{110m}Ag source

Gamma ray energy[a] (MeV)	Gamma ray branching ratio[a] and its error (%)
0.447	3.46 ± 0.13
0.620	2.81 ± 0.07
0.658	94.30 ± 2.33
0.707	16.57 ± 0.39
0.818	7.42 ± 0.21
0.885	73.98 ± 1.83
1.384	26.07 ± 0.60
1.475	4.38 ± 0.10

(a) Gamma energies and branching ratios are quoted from Ref. 19.

TABLE A.2

Absolute efficiencies of ^{110m}Ag source at 0.658 -, 0.818- and 0.885 MeV.

Isotope	Gamma energy (MeV)	Absolute efficiency in μCi and its error
^{110m}Ag	0.658	1.033×10^{-2} ± 1.9%
	0.818	8.027×10^{-3} ± 2.3%
	0.885	7.190×10^{-3} ± 2.4%

TABLE A.3

Activities of ^{110m}Ag source at 0.658 -, 0.818 -, 0.885 - MeV and the weighted mean of activity of ^{110m}Ag source.

Isotope	Gamma energy (MeV)	Activity in μCi and its error	Weighted mean of activity in μCi and its error
^{110m}Ag	0.658	0.1741 ± 3.0%	0.1700 ± 1.7%
	0.818	0.1660 ± 2.8%	
	0.885	0.1709 ± 3.0%	

APPENDIX AII

Dead time and pulse pile up effect

Standard gamma emitting sources were used for the calibration of Ge(Li) detector. It was observed that the dead time varied from $\sim$ 3 - 22% for different gamma sources in the analyser with conversion gain 8192. The dead time was corrected by the analyser itself when the source was counted in live time.

Pulse pile up is the loss of count from the photopeak that results when more than one pulse arrives during a time interval of the pulse duration and as a result produces a larger pulse. In order to determine whether there was any pulse pile up effect, the experiment was performed with standard gamma sources and a pulse generator. The pulser was adjusted so that the pulse shape was similar to the output pulse from Ge(Li) detector. The pulser and one gamma source were counted together for a specified period of time with conversion gain 8192 and the area under the pulser peak was determined from the spectrum (C_1). The gamma source was counted alone for the same time for the same region and the background under the pulser peak was determined (C_2). $C_o = C_1 - C_2$ was the observed peak are of the pulser. Then the pulser was counted alone for the same time and for the same region and the true peak area (C_t) was obtained. The relative peak areas $\frac{C_t}{C_o}$ gave the required correction

to the gamma count rate. In this way corrections were obtained for all standard gamma sources.

A similar experiment was performed with all gamma sources with conversion gain 1042. Dead time in the analyser varied from 3 - 12% for different gamma sources. Nearly the same corrections were obtained for gamma sources. If the corrections which have been obtained were due to dead time then the corrections for gamma count rate should be different for two conversion gains, but these were not obtained. So it can be concluded that the effect was due to pulse pile up. Corrections applied to the count rate of gamma sources are given in Table A.4.

The effect of pulse pile up was also considered for the activation foils (for $^{197}Au(n,\gamma)\ ^{197}Au$ and $^{115}In(n,n')$ reactions) and corrections were found to be < 0.4%.

Coincident gamma ray pile up is not accounted for by the above method.

TABLE A.4

Pulse pile up corrections applied to the count rate of standard gamma sources.

Isotope	Gamma energy (MeV)	Pulse pile up Correction factor	Analyser[(a)] dead time (%)
^{279}Hg	0.279	1.0013	3
^{110m}Ag	0.447	1.0116	10
^{110m}Ag	0.620	1.011	10
^{110m}Ag	0.658	1.011	10
^{137}Cs	0.662	1.0323	18
^{110m}Ag	0.707	1.0110	10
^{110m}Ag	0.818	1.0115	10
^{54}Mn	0.835	1.0097	9
^{110m}Ag	0.885	1.0115	10
^{88}Y	0.898	1.0127	11
^{60}Co	1.173	1.0299	22
^{60}Co	1.332	1.0323	22
^{110m}Ag	1.384	1.0115	10
^{110m}Ag	1.475	1.0116	10
^{88}Y	1.836	1.0126	11

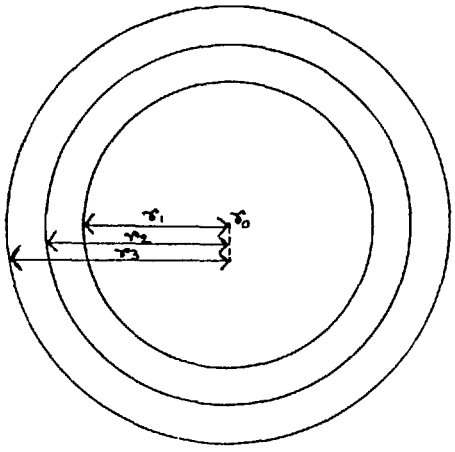
(a) The analyser dead time quoted is approximate with conversion gain 8192.

APPENDIX AIII

Correction for finite source area of activation foils

The efficiencies of the Ge(Li) detector as a function of energy were determined by standard point gamma sources and these efficiency values were used to compute the reaction rate of activation foils of diameter ∿ 12.7 mm. The foils are not point sources so it is necessary to find correction for efficiencies used in reaction rate measurements.

The experiment has been performed with ^{110m}Ag point source. The efficiency for 0.658 MeV gamma ray energy has been determined at distances 6.35 -, 4.24 -, 2.12 - and 0 - mm (centre of the foil) on either side of the centre position of the foil. The efficiencies corresponding to distances were shown in Fig. A.2 are given in Table A.5.



$r_0 = r'_0 = 0$ mm

$r_1 = r'_1 = 2.12$ mm

$r_2 = r'_2 = 4.24$ mm

$r_3 = r'_3 = 6.35$ mm

Fig. A.2 Dimensions of activation foil in mm.

As the distances were increased from the centre, the efficiencies were decreasing on either side of the centre. The average efficiency was obtained by considering $(\eta_{av})_{r_1} = \frac{\eta_{r_1} + \eta_{r_0} + \eta_{r'_0} + \eta_{r'_1}}{4}$ for radial distance r_1 from the centre. The average efficiency values were determined for r_2 and r_3 in a similar way and are given as follows:

$$\begin{aligned} (\eta_{av})_{r_1} &= 0.01038 \\ (\eta_{av})_{r_2} &= 0.01028 \\ (\eta_{av})_{r_3} &= 0.01015 \end{aligned} \qquad \text{(A.1)}$$

The weighted mean of the efficiency of 0.658 MeV gamma ray was determined using the equation:

$$(\eta)_{\text{weighted}} = \frac{\sum_{n=1}^{3} \pi(r_n^2 - r_{n-1}^2)\,(\eta_{av})_{rn}}{\sum_{n=1}^{3} \pi(r_n^2 - r_{n-1}^2)} \qquad \text{(A.2)}$$

where the area $\pi(r_n^2 - r_{n-1}^2)$ was taken as the weighting factor and $(\eta_{av})_{rn}$ as the average efficiency values for r_1, r_2 and r_3 respectively.

TABLE A.5

Absolute efficiency of Ge(Li) detector for 0.658 MeV at different radial distances.

Radial distance (mm)	Gamma ray energy (MeV)	Absolute efficiency and its error
6.35 (γ_3)	0.658	0.01011 ± 1.6%
4.24 (γ_2)	0.658	0.01024 ± 1.6%
2.12 (γ_1)	0.658	0.01037 ± 1.6%
0 (γ_0 & γ_0')	0.658	0.01042 ± 1.6%
-2.12 (γ_1')	0.658	0.01032 ± 1.6%
-4.24 (γ_2')	0.658	0.01019 ± 1.6%
-6.35 (γ_3')	0.658	0.01007 ± 1.6%

TABLE A.6

Absolute efficiency of Ge(Li) detector at 0.658 MeV.

Source radius (mm)	Absolute efficiency and its error	Discrepancy (%)
0	0.01042 ± 1.6%	∿ 1.9%
6.35	0.01022 ± 1.4%	

Thus $(\eta)_{weighted}$ is found as

$$(\eta)_{weighted} = 0.01022 \pm 1.4\%$$

The efficiency values obtained at the centre position and the weighted mean efficiency for radial distances are given in Table A.6. It can be seen from Table A.6 that the efficiency should be decreased by $\sim$ 1.9% for finite source area of the foil (radius 6.35 mm) for 0.658 MeV. The efficiencies are energy dependent and it is required to find the weighted mean efficiencies for all finite source areas used in reaction rate measurements. In this work only the weighted mean efficiency for 0.658 MeV was determined and the error assigned to the absolute efficiencies for gamma ray energies is 2.0% (Table 2.4, Chapter 2). Therefore, no correction has been applied to the absolute efficiencies used in reaction rate measurements. Of course, this correction must be made, but it is assumed that the energy dependence of the correction is a second order effect and can be ignored when only reaction rate ratios are considered.

APPENDIX B

Unadjusted and adjusted cross section data for threshold and non-threshold reactions.

TABLE B.1

Unadjusted and adjusted cross section data for $^{197}Au(n,\gamma)^{198}Au$ and $^{235}U(n,f)$ reactions.

Energy group	Energy Range (MeV)	$^{197}Au(n,\gamma)^{198}Au$ reaction				$^{235}U(n,f)$ reaction			
		Unadjusted cross section (Barn)	Error %	Adjusted/Unadjusted cross section		Unadjusted cross section (Barn)	Error %	Adjusted/Unadjusted cross section	
				Run 2	Run 4			Run 2	Run 4
1	10.0000 E+00 - 14.9180 E+00	1.1095 E-02	7	-	1.000	1.7520 E+00	10	-	1.000
2	7.4082 E+00 - 10.0000 E+00	1.2529 E-02	7	-	1.000	1.7078 E+00	6	-	1.000
3	6.0653 E+00 - 7.4082 E+00	1.3733 E-02	7	-	1.000	1.3208 E+00	6	-	1.000
4	4.4933 E+00 - 6.0653 E+00	1.5306 E-02	7	-	1.000	1.0548 E+00	4	-	1.000
5	3.6788 E+00 - 4.4933 E+00	1.7753 E-02	7	-	1.000	1.1029 E+00	3	-	1.000
6	2.7253 E+00 - 3.6788 E+00	2.6383 E-02	7	-	1.000	1.1937 E+00	3	-	1.000
7	2.2313 E+00 - 2.7253 E+00	4.2159 E-02	7	-	1.000	1.2927 E+00	3	-	1.000
8	1.6530 E+00 - 2.2313 E+00	5.9365 E-02	7	-	1.000	1.3059 E+00	3	-	0.999
9	1.3534 E+00 - 1.6530 E+00	7.2577 E-02	7	-	1.000	1.2514 E+00	4	-	0.999
10	8.2085 E-01 - 1.3534 E+00	8.3954 E-02	7	-	1.001	1.2139 E+00	4	-	0.999
11	4.9787 E-01 - 8.2085 E-01	1.3922 E-01	6	-	1.001	1.1636 E+00	6	-	0.997
12	3.0197 E-01 - 4.9787 E-01	1.6305 E-01	6	-	1.001	1.1946 E+00	7	-	0.996
13	1.8316 E-01 - 3.0197 E-01	2.5204 E-01	6	-	1.002	1.3329 E+00	7	-	0.995
14	1.1109 E-01 - 1.8316 E-01	3.0049 E-01	6	-	1.001	1.5064 E+00	7	-	0.996
15	6.7379 E-02 - 1.1109 E-01	3.6274 E-01	6	-	1.001	1.7238 E+00	8	-	0.996
16	5.5308 E-03 - 6.7379 E-02	7.1202 E-01	5	-	1.001	2.3056 E+00	8	-	0.993
17	4.5400 E-04 - 5.5308 E-03	4.4826 E+00	5	-	1.003	6.0480 E+00	8	-	0.996
18	3.7267 E-05 - 4.5400 E-04	3.2049 E+01	5	-	1.006	2.3369 E+01	8	-	0.997
19	3.0590 E-06 - 3.7267 E-05	6.6638 E+01	4	-	1.000	4.8408 E+01	8	-	0.999
20	4.1399 E-07 - 3.0590 E-06	4.1084 E+01	4	-	1.000	1.4779 E+01	8	-	1.000

TABLE B.2.

Unadjusted and adjusted cross section data for $^{237}NP(n,f)$ and $^{115}In(n,n')^{115m}In$ reactions.(a)

Energy Group	$^{237}NP(n,f)$ reaction				$^{115}In(n,n')^{115m}In$ reaction			
	Unadjusted cross section (Barn)	Error (%)	Adjusted / Unadjusted cross section		Unadjusted cross section (Barn)	Error (%)	Adjusted / Unadjusted cross section	
			Run 2	Run 4			Run 2	Run 4
1	2.4718 E+ 00	10	0.999	0.999	1.7822 E-01	10	1.000	-
2	2.1485 E+ 00	10	0.998	0.998	2.8644 E-01	8	1.000	-
3	1.8745 E+ 00	10	0.997	0.996	3.2859 E-01	8	1.000	-
4	1.4139 E+ 00	4	0.999	0.999	3.4648 E-01	8	1.002	-
5	1.4706 E+ 00	3	0.999	0.999	3.5050 E-01	8	1.001	-
6	1.6026 E+ 00	3	0.998	0.998	3.4906 E-01	10	1.005	-
7	1.6897 E+ 00	3	0.998	0.998	3.3298 E-01	10	1.005	-
8	1.6912 E+ 00	4	0.994	0.994	2.6116 E-01	10	1.006	-
9	1.6905 E+ 00	4	0.996	0.996	1.6750 E-01	10	1.003	-
10	1.5864 E+ 00	5	0.980	0.980	6.7601 E-02	20	1.015	-
11	5.6424 E- 01	5	0.990	0.990	6.7283 E-03	20	1.002	-
12	3.6376 E- 01	20	0.894	0.895	3.6304 E-03	30	1.003	-
13	3.8737 E-02	20	0.990	0.990	3.1549 E-06	30	1.000	-
14	2.1555 E-02	20	0.996	0.996	0.0	0.0	-	-
15	1.3933 E-02	10	0.999	0.999	0.0	0.0	-	-
16	1.7861 E-02	10	-	0.999	0.0	0.0	-	-
17	1.0905 E-02	10	-	1.000	0.0	0.0	-	-
18	1.0000 E-02	10	-	1.000	0.0	0.0	-	-
19	9.8507 E-03	10	-	1.000	0.0	0.0	-	-
20	4.0983 E-03	10	-	1.000	0.0	0.0	-	-

(a) Energy range for different groups mentioned in Table B.1.

TABLE B.3

Unadjusted and adjusted cross section data for $^{238}U(n,f)$ and $^{58}Ni(n,p)^{58}Co$ reactions.(a)

Energy Group	$^{238}U(n,f)$ reaction				$^{58}Ni\ (n,p)^{58}Co$ reaction			
	Unadjusted cross section (Barn)	Error (%)	Adjusted / Unadjusted cross section		Unadjusted cross section (Barn)	Error (%)	Adjusted / Unadjusted cross section	
			Run 2	Run 4			Run 2	Run 4
1	9.9686 E-01	10	1.000	1.000	5.5770 E-01	10	1.001	1.001
2	9.8780 E-01	6	1.001	1.001	6.1261 E-01	6	1.002	1.002
3	8.0976 E-01	6	1.001	1.001	6.0241 E-01	6	1.003	1.004
4	5.4990 E-01	4	1.001	1.001	5.1015 E-01	6	1.009	1.009
5	5.4253 E-01	3	1.001	1.001	3.5949 E-01	5	1.005	1.005
6	5.3569 E-01	3	1.001	1.002	2.0433 E-01	5	1.007	1.008
7	5.6194 E-01	3	1.001	1.002	9.7797 E-02	5	1.003	1.003
8	5.2041 E-01	4	1.003	1.004	3.6000 E-02	5	1.006	1.007
9	2.7178 E-01	4	1.001	1.002	9.5138 E-03	10	1.001	1.001
10	2.4463 E-02	30	1.019	1.023	1.4215 E-03	10	1.002	1.002
11	3.4514 E-04	30	1.000	1.000	0.0	0.0	-	-
12	1.7954 E-04	30	1.000	1.000	0.0	0.0	-	-
13	5.8324 E-05	30	1.000	1.000	0.0	0.0	-	-
14	4.9998 E-05	30	1.000	1.000	0.0	0.0	-	-
15	3.7236 E-05	30	1.000	1.000	0.0	0.0	-	-
16	2.3347 E-06	30	-	1.000	0.0	0.0	-	-
17	0.0	0.0	-	-	0.0	0.0	-	-
18	0.0	0.0	-	-	0.0	0.0	-	-
19	0.0	0.0	-	-	0.0	0.0	-	-
20	0.0	0.0	-	-	0.0	0.0	-	-

(a) Energy range for different groups mentioned in Table B.1.

TABLE B.4

Unadjusted and adjusted cross section data for $^{27}Al(n,p)^{27}Mg$ and $^{56}Fe(n,p)^{56}Mn$ reactions [a]

Energy Group	$^{27}Al(n,p)^{27}Mg$ reaction				$^{56}Fe(n,p)^{56}Mn$ reaction			
	Unadjusted cross section (Barn)	Error (%)	Adjusted / Unadjusted cross section		Unadjusted cross section (Barn)	Error (%)	Adjusted / Unadjusted cross section	
			Run 2	Run 4			Run 2	Run 4
1	8.9762 E-02	20	1.013	1.013	9.1196 E-02	15	0.997	0.989
2	8.1676 E-02	8	1.013	1.013	5.1827 E-02	6	0.998	0.992
3	5.3375 E-02	8	1.018	1.018	2.5069 E-02	6	0.998	0.992
4	2.6856 E-02	8	1.029	1.029	3.2836 E-03	8	0.998	0.995
5	8.4966 E-03	8	1.001	1.006	6.7104 E-05	8	1.000	1.000
6	2.8445 E-03	10	1.012	1.012	6.3511 E-07	8	1.000	1.000
7	7.3370 E-05	30	1.002	1.002	0.0	0.0	-	-
8	0.0	0.0	-	-	0.0	0.0	-	-
9	0.0	0.0	-	-	0.0	0.0	-	-
10	0.0	0.0	-	-	0.0	0.0	-	-
11	0.0	0.0	-	-	0.0	0.0	-	-
12	0.0	0.0	-	-	0.0	0.0	-	-
13	0.0	0.0	-	-	0.0	0.0	-	-
14	0.0	0.0	-	-	0.0	0.0	-	-
15	0.0	0.0	-	-	0.0	0.0	-	-
16	0.0	0.0	-	-	0.0	0.0	-	-
17	0.0	0.0	-	-	0.0	0.0	-	-
18	0.0	0.0	-	-	0.0	0.0	-	-
19	0.0	0.0	-	-	0.0	0.0	-	-
20	0.0	0.0	-	-	0.0	0.0	-	-

(a) Energy range for different groups mentioned in Table B.1.

TABLE B.5

Unadjusted and adjusted cross section data for $^{24}Mg(n,p)^{24}Na$ and $^{27}Al(n,\alpha)^{24}Na$ reactions[a]

Energy group	$^{24}Mg(n,p)^{24}Na$ reaction				$^{27}Al\ (n,\alpha)^{24}Na$ reaction			
	Unadjusted cross section (Barn)	Error (%)	Adjusted / Unadjusted cross section		Unadjusted cross section (Barn)	Error (%)	Adjusted / Unadjusted cross section	
			Run 2	Run 4			Run 2	Run 4
1	1.7778 E-01	10	0.987	-	1.0498 E-01	10	1.012	1.005
2	1.1445 E-01	10	0.935	-	4.7028 E-02	6	1.014	1.003
3	3.1047 E-02	10	0.962	-	9.7919 E-03	6	1.006	1.002
4	3.0557 E-04	5	0.976	-	2.8626 E-04	20	1.006	1.002
5	0.0	0.0	-	-	0.0	0.0	-	-
6	0.0	0.0	-	-	0.0	0.0	-	-
7	0.0	0.0	-	-	0.0	0.0	-	-
8	0.0	0.0	-	-	0.0	0.0	-	-
9	0.0	0.0	-	-	0.0	0.0	-	-
10	0.0	0.0	-	-	0.0	0.0	-	-
11	0.0	0.0	-	-	0.0	0.0	-	-
12	0.0	0.0	-	-	0.0	0.0	-	-
13	0.0	0.0	-	-	0.0	0.0	-	-
14	0.0	0.0	-	-	0.0	0.0	-	-
15	0.0	0.0	-	-	0.0	0.0	-	-
16	0.0	0.0	-	-	0.0	0.0	-	-
17	0.0	0.0	-	-	0.0	0.0	-	-
18	0.0	0.0	-	-	0.0	0.0	-	-
19	0.0	0.0	-	-	0.0	0.0	-	-
20	0.0	0.0	-	-	0.0	0.0	-	-

(a) Energy range for different groups mentioned in Table B.1.

TABLE B.6

Unadjusted cross section data for $^{55}Mn(n,\gamma)^{56}Mn$, $^{115}In(n,\gamma)^{116}In$, $^{239}Pu(n,f)$ and $^{64}Zn(n,p)^{64}Cu$ reactions(a)

Energy Group	$^{55}Mn(n,\gamma)^{56}Mn$ reaction		$^{115}In(n,\gamma)^{116}In$ reaction		$^{239}Pu(n,f)$ reaction		$^{64}Zn(n,p)^{64}Cu$ reaction	
	Unadjusted cross section (Barn)	Error (%)	Unadjusted cross section (Barn)	Error (%)	Unadjusted cross section (Barn)	Error (%)	Unadjusted cross section (Barn)	Error (%)
1	9.3246 E-04	15	5.9151 E-03	17	2.2001 E+00	10	2.8604 E-01	15
2	1.1256 E-03	15	5.6229 E-03	17	2.3224 E+00	8	2.7659 E-01	15
3	1.2393 E-03	15	5.8796 E-03	17	1.9468 E+00	8	2.4807 E-01	15
4	1.3746 E-03	15	9.0855 E-03	17	1.6751 E+00	6	1.9471 E-01	15
5	1.6676 E-03	15	1.6705 E-02	17	1.7407 E+00	5	1.3820 E-01	15
6	1.8282 E-03	15	3.5027 E-02	17	1.8756 E+00	5	8.3659 E-02	15
7	1.9304 E-03	15	6.6843 E-02	17	2.0408 E+00	5	4.2150 E-02	50
8	2.0659 E-03	15	1.1302 E-01	17	2.0496 E+00	5	1.2843 E-02	50
9	2.4389 E-03	15	1.6162 E-01	17	1.9390 E+00	5	1.6683 E-03	50
10	3.3406 E-03	10	1.9669 E-01	10	1.7445 E+00	6	3.5383 E-04	50
11	4.3183 E-03	10	1.8416 E-01	5	1.5853 E+00	7	5.8455 E-05	50
12	4.4895 E-03	10	1.8408 E-01	5	1.5721 E+00	7	4.4986 E-05	50
13	5.2233 E-03	10	1.6838 E-01	5	1.4940 E+00	7	1.9163 E-06	50
14	9.1990 E-03	10	1.8438 E-01	5	1.5383 E+00	7	0.0	0.0
15	2.2496 E-02	8	2.7387 E-01	5	1.6314 E+00	8	0.0	0.0
16	3.4919 E-02	8	4.5413 E-01	5	1.7858 E+00	8	0.0	0.0
17	8.0751 E-02	8	0.0	0.0	3.8082 E+00	8	0.0	0.0
18	1.1000 E+00	8	0.0	0.0	2.2543 E+01	8	0.0	0.0
19	4.0913 E-01	8	0.0	0.0	7.2225 E+01	8	0.0	0.0
20	1.0197 E+00	2	0.0	0.0	1.4064 E+01	8	0.0	0.0

(a) Energy range for different groups mentioned in Table B.1.

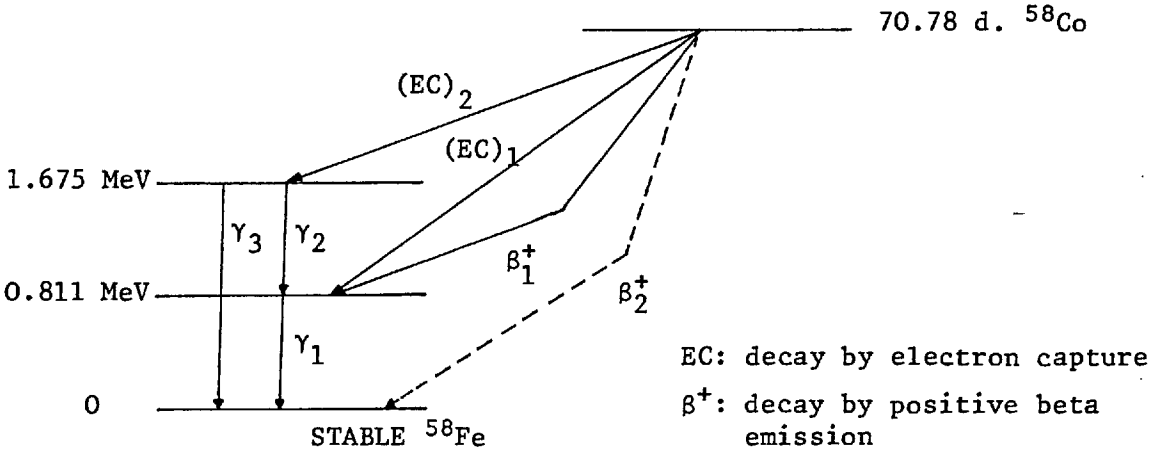
APPENDIX C

Correction for coincidence summation effects in ^{58}Co absolute activity measurement.

APPENDIX C

Correction for coincidence summation effects in Cobalt-58 absolute activity measurement

Real coincidence summing effects depend on the source-detector distance and the radioisotopic decay scheme. The coincidence summing effect increases rapidly with decreasing source-detector distance. The source-crystal separation distance is 1.772 cm (Table 2.1). Correction for coincidence summing effects in Cobalt-58 absolute activity measurement only was determined in this work according to Ref. 74. The decay level scheme of Cobalt-58 is as follows:



Ge(Li) spectrometer resolves the lines ∿ 0.811 and 0.864 MeV of Cobalt-58. The disintegration rate of the source is given by the equation:

$$\frac{S_{\gamma 1}}{A} = \eta_{\gamma 1} I_{\gamma 1} - \eta_{\gamma 1} \frac{\eta_{\gamma 2}}{P^*_{\gamma 2}} I_{\gamma 1} I_{\gamma 2} - 2\eta_{\gamma 1} \frac{\eta_{511}}{P^*_{511}} I_{\beta_1^+} I_{\gamma 1} \qquad (C.1)$$

(Loss due to coincidence summing between γ^1 and γ^2) (Loss due to coincidence summing between γ^1 and the two 0.511 MeV annihilation quanta associated to β_1^+)

$$= (1 - \frac{\eta_{\gamma 2}}{P^*_{\gamma 2}} I_{\gamma 2} - 2 \frac{\eta_{511}}{P^*_{511}} I_{\beta_1^+})$$

$$A = \frac{S_{\gamma 1}}{(1 - \frac{\eta_{\gamma 2}}{P^*_{\gamma 2}} I_{\gamma 2} - 2 \frac{\eta_{511}}{P^*_{511}} I_{\beta_1^+})} \qquad (C.2)$$

$\eta_{\gamma i}$: Photopeak efficiency for gamma ray of energy $E_{\gamma i}$

$P^*_{\gamma i}$: Effective Photofraction for gamma ray of energy $E_{\gamma i}$ (Peak to total count rate ratio including back scattered radiation from shield walls and adjacent structural supports).

$I_{\gamma i}$, $I_{\beta i}$: Emission intensities per decay.

$S_{\gamma i}$: Photopeak area for gamma ray of energy $E_{\gamma i}$.

A : Absolute disintegration rate of the source (dps).

The data pertinent to the present corrections is as follows according to Ref. 74:

$E_{\gamma 1}$	:	0.811 MeV	$I_{\gamma 1}$	:	0.9945 ± 0.0001
$E_{\gamma 2}$	:	0.864 MeV	$I_{\gamma 2}$	:	0.0069 ± 0.0002
($E_{\gamma 3}$	:	1.675 MeV	$I_{\gamma 3}$	:	0.00519 ± 0.00009)
			$I_{\beta^+_1}$	:	0.1500 ± 0.0005

The photopeak efficiencies for gamma ray of energies (0.511, 0.811 and 0.864 MeV) were obtained from the photopeak efficiency curve Fig. 2.5. The effective photo fractions for gamma ray of energies (0.511 and 0.864 MeV) were determined from the extrapolation of the effective photo fractions for standard gamma source of energies 0.662 MeV (^{137}Cs gamma source) and 0.835 MeV (^{54}Mn gamma source). The photo peak efficiency and the effective photo fraction for the gamma ray of energy E_{γ_i} are given in Table C.1.

TABLE C.1

The photopeak efficiency and the photofraction for the gamma ray of Energy E_{γ_i}

Gamma Energy (MeV) ($E_{\gamma i}$)	Photopeak Efficiency ($\eta_{\gamma i}$)	Effective Photofraction ($P^*_{\gamma i}$)
0.511	0.0140	0.15
0.811	0.00790	0.1082
0.864	0.00728	0.102
0.835	0.00778	0.1073
0.662	0.01027	0.1248

The correction factor obtained using equation (C.2) is:

$$1.029 \pm 0.0003$$

2.9% correction has been applied to the Cobalt-58 activity measurement. The correction is dominated by losses due to coincidence between the 0.811 MeV line and the 0.511 MeV annihilation quanta.

APPENDIX D

List of the SIMMM program

APPENDIX D

List of the SIMMM program

PROGRAM SIMMM(INPUT,OUTPUT,PUNCH,TAPE 1=INPUT,TAPE 2=OUTPUT)

PURPOSE

SIMULTANEOUS EVALUATION OF CROSS SECTION, INTEGRAL REACTION RATES AND SPECTRA BY MINIMISING THE DISCREPANCIES BETWEEN EVALUATED AND MEASURED VALUES.

SPECIFICATION OF THE VARIABLES USED IN THE PROGRAM:

NPAR	- NUMBER OF PARAMETERS
I	- NUMBER OF ENERGY GROUPS
J	- NUMBER OF REACTIONS
K	- NUMBER OF SPECTRUM
SIGMA	- INPUT CROSS SECTION
FSIGMA	- FRACTIONAL ERROR IN THE INPUT CROSS SECTION
DELSIG	- ERROR IN THE INPUT CROSS SECTION
XSIGMA	- ADJUSTED CROSS SECTION
PHI	- DIFFERENTIAL NEUTRON SPECTRUM AS THE INPUT SPECTRUM
FPHI	- FRACTIONAL ERROR IN THE DIFFERENTIAL NEUTRON SPECTRUM
DELPHI	- ERROR IN THE DIFFERENTIAL NEUTRON SPECTRUM
XPHI	- ADJUSTED DIFFERENTIAL NEUTRON SPECTRUM
RATE	- MEASURED REACTION RATE PER ATOM PER MONITOR SATURATED ACTIVITY
FRATE	- FRACTIONAL ERROR IN THE MEASURED REACTION RATE
DELRATE	- ERROR IN THE MEASURED REACTION RATE
XRATE	- CALCULATED REACTION RATE
XK	- NORMALISATION CONSTANT
A	- EVALUATES THE SQUARE OF THE DIFFERENCE BETWEEN CALCULATED AND MEASURED REACTION RATE RELATIVE TO THE ERROR IN THE MEASURED REACTION RATE
B	- EVALUATES THE SQUARE OF THE DIFFERENCE BETWEEN ADJUSTED AND MEASURED NEUTRON SPECTRUM RELATIVE TO THE ERROR IN THE MEASURED NEUTRON SPECTRUM
C	- EVALUATES THE SQUARE OF THE DIFFERENCE BETWEEN ADJUSTED AND MEASURED CROSS SECTION RELATIVE TO THE ERROR IN THE INPUT CROSS SECTION
F	- SUMMATION OF A, B AND C

```
      SUBROUTINE FCN(NPAR,G,F,X,IFLAG)
      DIMENSION X(NPAR),SIGMA(20,13),FSIGMA(20,13),DELSIG(20,13),
     1PHI(20,1),FPHI(20,1),DELPHI(20,1),RATE(13,1),FRATE(13.1),
     2DELRATE(13,1),XSIGMA(20,13),XPHI(20,1),XRATE(13,1),BOUND(40)
      DATA BOUND/14.9180E+00,10.0000E+00,7.4082E+00,6.0653E+00,
     14.4933E+00,3.6788E+00,2.7253E+00,2.2313E+00,1.6530E+00,
     21.3534E+00,0.8205E+00,0.49787E+00,0.30197E+00,0.18316E+00,
     30.11109E+00,0.67379E-01,0.55308E-02,0.45400E-03,0.37267E-04,
     40.30590E-05,10.0000E+00,7.4082E+00,6.0653E+00,4.4933E+00,
     53.6788E+00,2.7253E+00,2.2313E+00,1.6530E+00,1.3534E+00,
     60.82085E+00,0.49787E+00,0.30197E+00,0.18316E+00,0.11109E+00,
     70.67379E-01,0.55308E-02,0.45400E-03,0.37267E-04,0.30590E-05,
     80.41399E-06/

      IF(IFLAG.NE.1) GO TO 99
      READ(1,1)NI,NJ,NK
    1 FORMAT(3I10)
    2 FORMAT(5(E15.5))
      DO 27 J=1,NJ
   27 READ(1,2) (SIGMA(I,J),I=1,NI)
      DO 28 J=1,NJ
   28 READ(1,2) (FSIGMA(I,J),I=1,NI)
      DO 29 K=1,NK
   29 READ(1,2) (PHI(I,K),I=1,NI)
      DO 31 K=1,NK
   31 READ(1,2) (FPHI(I,K),I=1,NI)
      DO 32 K=1,NK
   32 READ(1,2) (RATE(J,K),J=1,NJ)
      DO 33 K=1,NK
   33 READ(1,2) (FRATE(J,K),J=1,NJ)
      WRITE(2,21)
   21 FORMAT(//,10X,*DATA CHECK*)
      DO 22 J=1,NJ
      WRITE(2,24) J
   24 FORMAT(/5X,*REACTION*,I5,5X,*VALUES FOR SIGMA*//)
   22 WRITE(2,2)(SIGMA(I,J),I=1,NI)
      DO 34 J=1,NJ
      WRITE(2,36) J
   36 FORMAT(/5X,*REACTION*,I5,5X,*VALUES FOR FRACTION OF SIGMS*//)
   34 WRITE(2,2) (FSIGMA(I,J),I=1,NI)
      DO 38 K=1,NK
      WRITE(2,39) K
   39 FORMAT(/5X,*SPECTRA*.I5,5X,*VALUES FOR MOL-SIGMA SPECTRA*//)
   38 WRITE(2,2) (PHI(I,K),I=1,NI)
      DO 42 K=1,NK
      WRITE(2,43) K
   43 FORMAT(/5X,*SPECTRA*,I5,5X,*VALUES FOR FRACTION OF MOL-SIGMASPECT
     1RA*//)
   42 WRITE(2,2) (FPHI(I,K),I=1,NI)
      DO 46 K=1,NK
      WRITE(2,47) K
   47 FORMAT(/5X,*SPECTRA*,I5,5X,*VALUES FOR NISUS MEASURED REACTION RAT
     1E*//)
   46 WRITE(2,2) (RATE(J,K),J=1,NJ)
```

```
      DO 49 K=1,NK
      WRITE(2,51) K
   51 FORMAT(/5X,*SPECTRA*,I5,5X,*VALUES FOR FRACTION OF NISUS MEASURED
     1 REACTION RATE*//)
   49 WRITE(2,2) (FRATE(J,K),J=1,NJ)
      DO 26 I=1,NI
      DO 26 K=1,NK
      IF(PHI(I,K)EQ.0.0) PHI(I,K)=1E-10
   26 PHI(I,K)=PHI(I,K)*0.12841
      DO 100 J=1,NJ
      DO 100 I=1,NI
      L=I+(J-1)*NI
      IF(SIGMA(I,J).EQ.0.0) SIGMA(I,J)=0.00000001
      X(L)=SIGMA(I,J)
      IF(FSIGMA(I,J).EQ.0.0) FSIGMA(I,J)=0.0005
      DELSIG(I,J)=(FSIGMA(I,J)*SIGMA(I,J))
  100 CONTINUE
      DO 120 K=1,NK
      DO 120 I=1,NI
      DELPHI(I,K)=(FPHI(I,K)*PHI(I,K))
      L=NI*NJ+I+(K-1)*NI
      X(L)=PHI(I,K)
  120 CONTINUE
      DO 130 K=1,NK
      DO 130 J=1,NJ
      DELRATE(J,K)=(FRATE(J,K)*RATE(J,K))
  130 CONTINUE
      L=NI*NJ+NI*NK+1
      X(L)=1.
   99 CONTINUE
      DO 10 J=1,NJ
      DO 10 I=1,NI
      L=I+(J-1)*NI
      XSIGMA(I,J)=X(L)
   10 CONTINUE
      DO 12 K=1,NK
      DO 12 I=1,NI
      L=NI*NJ+I+(K-1)*NI
      XPHI(I,K)=X(L)
   12 CONTINUE
      DO 25 K=1,NK
      DO 25 J=1,NJ
   25 XRATE(J,K)=0.
      DO 30 K=1,NK
      DO 30 J=1,NJ
      DO 30 I=1,NI
   30 XRATE(J,K)=XSIGMA(I,J)*XPHI(I,K)+XRATE(J,K)
      L=NI*NJ+NI*NK+1
      XK=X(L)
      A=0.
      DO 40 K=1,NK
      DO 40 J=1,NJ
   40 A= A+(XK*XRATE(J,K)-RATE(J,K))/DELRATE(J,K)*(XK*XRATE(J,K)-RATE(J,K
     1))/DELRATE(J,K)
      B=0.
      DO 50 K=1,NK
      DO 50 I=1,NI
```

```
 50 B=B+((XPHI(I,K)-PHI(I,K))/DELPHI(I,K))*((XPHI(I,K)-PHI(I,K))/DELPH
   1I(I,K))
    C=0.
    DO 60 J=1,NJ
    DO 60 I=1,NI
    C=C+((XSIGMA(I,J)-SIGMA(I,J))/DELSIG(I,J))*((XSIGMA(I,J)-SIGMA(I,J
   1))/DELSIG(I,J))
 60 CONTINUE
    F=A+B+C
    IF(IFLAG.EQ.3) GO TO 999
    RETURN
999 DO 105 J=1,NJ
    WRITE(2.106) J
106 FORMAT(/5X,*REACTION*I5)
    WRITE(2,107)
107 FORMAT(10x,*GROUP*,5X,*ENERGY BOUNDARY*,14X,*XSIGMA*,10X,*SIGMA*,6
   1X,*C=((XSIGMA-SIGMA)/DELSIG)*,5X,*CSQD*/26X,*(MEV)*/)
    DO 110 I=1.NI
    C=(XSIGMA(I,J)-SIGMA(I,J))/DELSIG(I,J)
    CSQD=C**2
    WRITE(2,108) I,BOUND(I+NI),XSIGMA(I,J),SIGMA(I,J),C,CSQD
108 FORMAT(10X,I5,E12.5,2H -,E12.5,3(5X,E12.5),15X,E12.5)
110 CONTINUE
105 CONTINUE
    WRITE(2,111) XK
111 FORMAT(//10X,*VALUE OF XK FOR THIS RUN*,5X,E12.5)
    DO 112 K=1,NK
    WRITE(2,113)
113 FORMAT(//10X,*GROUP*,5X,*ENERGY BOUNDARY*,15X,*XPHI*,17X,*PHI*,10X
   1,*B=(XPHI-PHI)/DELPHI*,10X,*BSQD*/26X,*(MEV)*)
    DO 114 I=1,NI
    B=(XPHI(I,K)-PHI(I,K))/DELPHI(I,K)
    BSQD=B**2
    WRITE(2,108)I,BOUND(I),BOUND(I+NI),XPHI(I,K),PHI(I,K),B,BSQD
114 CONTINUE
112 CONTINUE
    DO 116 K=1,NK
    WRITE(2,117)
117 FORMAT(//49X,*XRATE*,13X,*RATE*,5X,26H A=(XK*XRATE-RATE)/DELRATE,8
   1X,*ASQD*)
    DO 118 J=1,NJ
    A=(XK*XRATE(J,K)-RATE(J,K))/DELRATE(J,K)
    ASQD=A**2
    WRITE(2,119) XRATE(J,K),RATE(J,K),A,ASQD
119 FORMAT(38X,2(5X,E12.5),10X,E12.5,15X,E12.5)
118 CONTINUE
116 CONTINUE
    WRITE(2,140)
140 FORMAT(///50X,*VALUE OF F*)
    WRITE(2,121) F
121 FORMAT(50X,E12.5)
    RETURN
    END
```